DEVELOPMENT AND APPRAISAL OF MRI CONTRAST AGENTS FOR THE *IN VIVO* ANALYSIS OF STEM CELL GRAFTS

This thesis is submitted for the degree of Doctor of Philosophy at Cardiff University

Susannah Jane Williams

Supervisors:

Nicholas Allen

Stephen Paisey

Anne Rosser

June 2012

Abstract

The work reported in this thesis deals with the need for efficient *in vivo* tracking and monitoring of grafted cells and their subsequent survival. It is considered in the context of cell transplantation for neurodegenerative disorders, particularly Huntington's and Parkinson's disease, although the scope for a good contrast agent to monitor cells *in vivo* goes far beyond this. There is currently no routine method used to follow cells *in vivo* and it is crucial for the advancement of cell transplantation studies, both in terms of providing powerful longitudinal analysis and for decreasing the number of animals necessary per experiment. MRI allows good contrast resolution and provides details on soft tissue anatomy without being harmful to the subject. By labeling cells with an MRI contrast agent the labeled cells can be distinguished from the surroundings and information on location is attained. A good MRI contrast agent can provide more information than this though, but to date there hasn't been an MRI contrast agent developed that can simultaneously provide good signal and be reflective of the graft changes, while not affecting the cell's viability. The feasibility for *in vivo* MRI scanning of three MRI contrast agents were tested and detailed below. In **Chapter 3** we looked to utilise SPIOs as contrast agents. Since SPIOs are the most widely used of contrast agents they were tested in mouse ES cells, expanded whole ganglionic eminence and rat ventral mesencephalon and successfully labeled all cell types. Problems were discovered in reference to the needle track leaving an MRI visible track that eclipsed the area of graft deposition, and while SPIOs did not hamper graft survival, only large grafts extending out from the needle track could be reliably measured. **Chapter 4** examined the generation of ferritin constructs for use as contrast agents. Transgenes based on the ferritin subunits provide MRI contrast by increasing the iron content of a cell. Both subunits, heavy and light, were transfected into mouse ES cells and expressed to improve signal compared to overexpressing the ferritin heavy transgene alone, which has been done in the literature. The expected change in T_2 relaxation compared to control cell lines was observed *in vitro*. In **Chapter 5** the applicability for *in vivo* use of Chemical Exchange Saturation Transfer (CEST) was tested. CEST involves the selective saturation of protons of particular compounds that are then indirectly detected through the water signal. Current 2D RARE scans to pick up CEST are slow and not really transferable to animal studies, due to the large increase in scan time for each extra image slice required, here alternative 3D FLASH scans were developed that still allowed the CEST contrast change to be observed over a whole sample in a reasonable time frame. A transgene based on CEST was tested *in vivo* and expression was lost even under antibiotic selection. Work in this thesis contributes some understanding towards the promises and pitfalls of three MRI contrast agents, two of which may ultimately be used more routinely for cell tracking in the future.

Disclaimer:

The grafting of rat ventral mesencephalon and perfusions in Chapter 3 were carried out by Ludivine Breger.

The ventral mesencephalon graft into a Lister Hooded rat sections used for Perls' staining in Figure 3.9.A, Chapter 3, were from a previous experiment by Andreas Heuer.

Acknowledgements

I would like to thank my supervisors, Nicholas Allen for his molecular biology advice, Anne Rosser for her *in vivo* guidance and Stephen Paisey for his MRI knowledge, and all of them for their support and encouragement over the last few years. It has been great working with you all.

Thanks go to Pawel who worked the MRI machine and showed me how to use it.

All the members of the NDA lab have made the night shifts (as well as day shifts) good fun and our component club couldn't have been done without you. From those who were there when I joined: Shun Ming, Shona, Susie, Andrew, Sarah, Alysia, and Amanda, to those who came later: Emma, Sali, Katrin, Stephen, Rachel, Charlie, Dave, Joao and Jess.

Everyone in the BRG has been great to work alongside: Claire, Sophie, Ellen, Andi, Jane, Vicky and Ngoc Nga, who were there in times of need, thank you. Not to mention everyone else; Amy, Ludivine, Yat, Zubeyde, Anne Marie, Nan, Harri, Claris, Marija, Kate, Rike, Emma, Gaynor, Steve, Eduardo, Simon, Mariah, Hanna, and Alex.

I would also like to say it has been great getting to know everyone else in the wider environment for science chats, and encouragement. Vlad and his group, Ros, Boris, James, Val, Mark, and at the risk of writing too long a list I will stop because you all know who you are anyway!

All of the above have provided much food for thought and good debate in terms of science, as well as extracurricular activities. You're all great.

Also, thank you for your love and support over the years to my Mum, Dad, Jonathan and Matthew and all my family and friends and of course Michal.

It's been fun.

Glossary

Antiferromagnetism

A material in which the magnetic moments alternate such that there is no net moment in the absence of a externally applied magnetic field below the Néel temperature, above which it is typically a paramagnet.

Arrhenius' Law

For many common chemical reactions at room temperature, the reaction rate doubles for every 10°C increase in temperature

Brownian Motion

The random motion of particles suspended in a liquid or gas

Boltzman Distribution

A certain distribution function or probability measure for the distribution of the states of a system

Ferromagnetism

A physical phenomenom in which certain electrically uncharged materials strongly attract others.

FLASH

FLASH (Fast Low Angle Shot) is a fast gradient echo MRI sequence that can achieve extremely high T_1 contrast.

Magnetic Susceptibility

A dimensionless proportionality constant that indicates the degree of magnetization of a material in response to an applied magnetic field.

Néel Temperature:

The temperature above which an antiferromagnetic material becomes paramagnetic—that is, the thermal energy becomes ES large enough to destroy the macroscopic magnetic ordering within the material

Paramagnetism

A form of magnetism whereby the material is drawn in to a magnetic field, (as opposed to diamagnetic materials that are repelled), that is only evident when under the influence of an externally applied magnetic field.

RARE

RARE (Rapid Acquisition with Relaxation Enhancement) is an enhanced spin echo MRI sequence where multiple echoes are used and contribute to the same image.

Relaxivity

The ability of magnetic compounds to increase the relaxation rates of surrounding water proton spins

Superparamagnetism

A type of magnetism seen in ferromagnetic and ferrimagnetic nanoparticles, where magnetization can randomly flip direction, depending on temperature. In the absence of an external magnetic field the magnetization appears to average at zero and once an external magnetic field is applied the nanoparticles are magnetized with a larger magnetic susceptibility than a paramagnet.

TE / Echo Time

The TE, also called the echo time, is the time in milliseconds between the 90° pulse and the peak of the echo signal in spin echo pulse sequences.

TR / Repetition Time

The TR, also called the repetition time, represents the time between successive RF pulse sequences applied to the same slice. It is an important effect in controlling image contrast characteristics and contributes to total scan time

Zeta Potential

In a colloidal system it is the potential difference between the dispersion medium and the stationary layer of fluid attached to the dispersed particle

Zwitterion

A dipole with both a positive and negative charge at different positions in the molecule

Abbreviations

6-Hydroxydopamine	6-OHDA
Anterior-Posterior	AP
β-galactosidase neomycin fusion gene	β-geo
Base Pairs	bp
Central Nervous System	CNS
Chemical Exchange Saturation Transfer	CEST
Cresyl Violet	CV
Detection Solution	DS
Dorsal-Ventral	DV
Dulbecco's Modified Eagle Medium	DMEM
Dopamine Receptors	DR
Embryonic Day 14	*E14*
Embryonic Stem	ES
Ferric Ammonium Citrate	FAC
Ferritin	Ft
Field Dependent R2 Increase	FDRI
Field of View	FOV
Foetal Neural Precursors	FNP
Food and Drug Administration	FDA
Fast Low Angle Shot	FLASH
Flip Angle	FA
Gamma-Aminobutyric Acid	GABA
Gene of Interest	GOI
Good Manufacturing Practice	GMP
Graft Induced Dyskinesia's	GID
Green Fluorescent Protein	GFP
Hank's Balanced Salt Solution	HBSS
Height	H

Human	h
Hematopoietic Stem Cells	HSC
Horseradish peroxidase	HRP
Huntington's Disease	HD
Hydrodynamic Diameter	HDD
Internal Ribosome Entry Site	IRES
Immunocytochemistry	ICC
Immunohistochemistry	IHC
Induced Pluripotent Stem	iPS
Intravenous	IV
Iron	Fe
Luria-Bertani	LB
Magnetic Resonance Imaging	MRI
Medium Spiny Neurons	MSN
Mesenchymal Stem Cells	MSC
Medial Lateral	ML
Mouse Embryonic Fibroblasts	MEFs
Multiplicity of Infection	MOI
Multi-Slice-Multi-Echo	MSME
Nuclear Magnetic Resonance	NMR
Parkinson's Disease	PD
pIRES2-EGFP-CAG	PEC
Positron Emission Tomography	PET
Poly l Arginine	PLR
Poly l Lysine	PLL/PLK
Poly l Threonine	PLT
Polyadenylation Signals x 3	3xpA
Polyethylene Glycol	PEG
Prussian Blue	PB

Quinolinic Acid	QA
Radio Frequency	RF
Rapid Acquisition with Refocused Echoes	RARE
Reticuloendothelial System	RES
Sprague Dawley	SD
Super Paramagnetic Iron Oxide Particles	SPIOs
Tesla	T
Transfection Agent	TA
Transferrin	Tf
Transferrin Receptor	Tfrc
Transmission Electron Microscopy	TEM
Tumour Necrosis Factor	TNF
Ventral mesencephalon	VM
Volts	V
Whole Ganglionic Eminence	WGE

Contents

1 Introduction

Robust non-invasive monitoring of specific cell populations or gene expression *in vivo* would provide huge benefit when analysing results in the fields of stem cell research to follow transplantation of differentiated cell types, cancer biology to track metastasis, and monitoring the efficacy of gene therapy. In the field of regenerative medicine longitudinal analyses would allow the visualisation of development and growth of specific cells and tissues in an *in vivo* context. Transplantation of primary foetal cells has taken place for neurodegenerative diseases like Parkinson's and Huntington's disease, and the use of stem cell derived neurons as donor cells for these conditions is at a fairly advanced stage, but there are very few tools available to follow cell fate after surgery. The inability to successfully image and monitor these *in vivo* events is a rate limiting step. Current techniques used to try and address this can suffer from low penetrance, poor resolution, and limited specificity. Thus, further research is required to optimise and validate more robust methods. Magnetic resonance imaging (MRI) is one such imaging modality that is non-invasive and can provide detailed anatomical images with high resolution, excellent contrast, and is widely accessible.

1.1 Current Methods of *in vivo* imaging

Uncovering *in vivo* events and the consequences they may have on human health has played on the minds of people for centuries. It was the 1500's when Leonardo Da Vinci produced over 200 anatomical drawings of dissected cadavers, some of which were the first *ex vivo* events to ever be captured (O'Malley and Sounders 1952). Since then methods of visualising our inner workings have improved dramatically, with a myriad of techniques allowing non-invasive imaging. We have progressed from distinguishing between different organs, to more informative imaging providing functional information and details of gene expression. It is within the last 80 years that the different imaging technologies have taken off and regardless of the huge volume of work done to improve the technologies much potential remains to be harnessed.

1.1.1 Optical Imaging

One of the first non-invasive imaging methods came from the discovery of green fluorescent protein (GFP) from the jellyfish *Aequorea Victoria* in the 1950s (Shimomura 2009). Since then wild type GFP has been mutated to increase expression and enhance fluorescence, the most striking example being the brainbow mouse which exhibits almost 90 distinguishable colours (Livet *et al.* 2007). Although primarily used for *in vitro* culture and post mortem analysis, a GFP reporter has been used to visualise metastasis in a lymphoma mouse model *in vivo* (Troy *et al.* 2004). However, this fluorescence is severely limited by the optical properties of tissue that strongly absorb the wavelength (395nm) where GFP is excited, as such GFP is attenuated as a function of depth. Increasing the wavelength into the red and far red range, above 600nm, can circumvent this problem (Shaner *et al.* 2004) and engineering markers with wavelengths in the infrared range could help negate the limitations of depth further still (Shaner *et al.* 2007). Another optical reporter is based on bioluminescence and the luciferases began being characterised in the late 1960s (Greer III *et al.* 2002). The bioluminescence reporters typically take advantage of the luciferase enzyme from the firefly, *Photinus pyralis,* but require a substrate, luciferin, to generate light. Once again depth is a limiting factor and a million cells are needed to be seen at a 2cm depth (Rice *et al.* 2001). Unless looking subcutaneously, such light emitting probes have limited use *in vivo* at this time.

1.1.2 Positron Emission Tomography

To date tracking grafted cells *in vivo* has relied mainly on positron emission tomography (PET). A positron-emitting radionuclide (tracer) is introduced into the body on a biologically active molecule that emits pairs of gamma rays that are detected by the PET scanner. The specificity of PET imaging relies upon the biological specificity of the tracer compound used. Tracers can be either nonspecific metabolic activity reporters such as 2-fluoro-2-deoxy-D-glucose (FDG) or specific to receptors of interest, for example Raclopride, an antagonist for D2 dopamine receptors (Köhler *et al.* 1985): FDG has been used to provide information on grafted tissue over a two year period in the striatum of Huntington's disease (HD) patients, where an increase in FDG signal was observed in an area with low signal pretransplantation (Gaura *et al.* 2004). Raclopride is radio labeled with the carbon 11 radioisotope and competes for D_2/D_3 dopamine receptor occupancy whilst reporting on the release of endogenous dopamine (Hume *et al.* 1992). Raclopride has been

used reliably to track cells expressing D_2/D_3 receptors indicating the presence of striatal tissue in HD patients that received bilateral grafts of tissue from foetal whole ganglionic eminence (Reuter *et al.* 2008) and in patients with PD to look at the depletion of endogenous dopamine (Ishibashi *et al*. 2010). Another marker used in conjunction with PET is fluorodopa, F18, a radiolabelled compound of fluorinated L-DOPA that is an indirect marker of synaptic dopamine fluxes in the brain and used to examine changes in dopamine neurotransmission. While it does not discriminate between endogenous and exogenous dopaminergic activity it can give an indication of a surviving and functioning graft in the brain of Parkinson's disease (PD) patients (Remy *et al.* 1995).

Unfortunately due to a lack of compounds with appropriate biological specificity PET has been unable to target only donor cells *in vivo,* making it impossible to differentiate donor from host tissue with only application of radioactive compounds. Introducing reporter genes to a specific population of cells can allow them to be visualised using PET, for example mutant herpes simplex virus type 1 thymidine kinase increases the uptake of radioactively labelled substrates giving specific PET signal *in vivo* (Blasberg 2002; Gambhir *et al.* 2000). PET has excellent sensitivity compared to MRI and pica molar concentrations of the tracer can be imaged, allowing tracking and monitoring of small numbers of cells. The reporter genes still require administration of exogenous radioactive substrates and in addition these positron emitting radioligands limit the number of scans undertaken in an individual over the course of a given year to minimise exposure to the ionizing radiation (Based on calculations by the Health Protection Agency). The anatomical resolution is improving with newer models, but on the whole remains poor compared to MRI.

1.1.3 Magnetic Resonance Imaging

MRI allows *in vivo* imaging of the soft tissue anatomy and function; however to distinguish graft from host cells and follow the graft's fate or monitor gene expression contrast agents must be recruited. A cell must be labelled with an agent that generates significant MRI contrast (the contrast agent) prior to transplantation so labelled cells can be differentiated from host tissue in MRI images. Contrast agents can be detected directly, on addition of a substrate or from the product of an enzymatic reaction. There are a number of contrast agents available, one of the most common and most sensitive MRI reporters to date are the superparamagnetic

iron oxide particles (SPIOs) (see section 1.2). A second approach to develop MRI contrast agents combines MRI with transgenes, and shows much potential. The first use of a reporter gene was with nuclear magnetic resonance (NMR) spectroscopy, which detected over-expressed creatine kinase in the rodent liver using ^{31}P to measure the product (phosphocreatine) of the creatine kinase catalysed reaction (Koretsky *et al.* 1990). One of the earliest examples of enzyme based reporters for MRI takes advantage of the β-galactosidase enzyme and uses an exogenous substrate, EgadMe, for significant contrast. Thomas J. Meade and colleagues have worked on various 'smart' contrast agents such as EgadMe, a chelated gadolinium caged within a galactopyranose molecule, there are two isomers one with high and one with low relaxivity (Consentino *et al.* 2009). Only when the galactose group of the EgadMe substrate comes into contact with β-galactosidase is the cage door removed exposing gadolinium to water, causing a change in MRI contrast (Urbanczyk-Pearson and Meade 2008). Current work is based on designing a contrast agent whose cage doors can open and close reversibly. The substrate has to be administered before any signal is given out, requiring extra optimisation of administration and deciding the method by which the substrate can get to the area of interest. The concentration of substrate at particular areas in these cases may not be even, making signal analysis difficult to interpret. In brain grafts, substrates have the additional predicament of either successfully getting through the blood brain barrier, a notoriously difficult task, or being administered directly into the brain. Development of various MRI reporter genes has been advancing but none of these methods have really taken off into the main stream, partly due to the difficulties involved in generating strong contrast and because many require the use of additional substrates. The lack of development can partly be attributed to the separation between the fields of MRI and molecular biology (Gilad *et al.*, 2007a). Approaching the task while considering both, an MRI perspective and a biological one, should help the development of suitable MRI reporters, allowing long term monitoring of grafted cells in live animals.

1.1.4 Combining Imaging Modalities

Methods of *in vivo* cell monitoring have been used in tandem to try and encompass the above criteria. Johanna Jackson and colleagues have combined both MRI and PET imaging modalities to follow bone marrow derived stem cells after implantation into the striatum of a PD rat model (Jackson *et al.* 2009). The cells were labelled with

SPIOs to distinguish grafted tissue from host using MRI and the radioligand [^{11}C] raclopride to monitor dopamine release using PET to distinguish their functional efficacy (Jackson *et al.* 2009). These techniques are combined to get around (i) the persistence of signal from the SPIOs even after cell death, making it possible to tell whether the contrast seen on MRI is from live cells and (ii) the inability of PET to distinguish between host and grafted tissue. Although this approach overcomes some of the deficiencies of imaging transplanted cells, it does not overcome deleterious effects of SPIOs or the dilution of signal on cell division and the effects of radiation. PET is not a cheap option and the cost is increased by the combined use of MRI imaging. However, the use of radioactive ligands and its cost is often outweighed by the benefits and clinical necessity meaning PET is often used in Phase I and II clinical trials.

Current histological methods to analyse grafted tissue in a host lack the means for true temporal analysis to monitor graft formation and change in individual animals, thus *in vivo* imaging has a central role in shaping the future of cell transplantation therapies. Presently, there is not a single approach that can provide all the information required. An ideal system would boast the following characteristics: (i) the ability to distinguish between graft and host; (ii) the capacity to follow migratory cells with high sensitivity; (iii) tracking cells throughout their existence without dilution following cell division; (iv) allowing confirmation of cell type, be it neuron or astrocyte; (v) and the ability to correspond markers with anatomy. All with the pre requisite that normal cell behaviour remains unperturbed. Of course immunohistological verification will still be necessary, not only to confirm *in vivo* imaging results but for further analysis. It is unlikely any imaging modality will allow the full complement of genes expressed to be viewed *in vivo*, especially imaging at an individual cell level. There are a number of non-invasive imaging modalities available, of these MRI reporter constructs are still in their infancy, and yet have the most potential. The most sensitive and widely used MRI contrast agent to date are SPIOs, (Chambon *et al.* 1993; Johnson *et al.* 1996; Magnitsky *et al.* 2008), however these are associated with a number of problems which are detailed below. Development of a transgene based contrast agent has many advantages over SPIOs and can provide a neat complement to histological analysis through longitudinal, *in vivo* monitoring with all the benefits of MRI. Here we discuss SPIO's as contrast agents and two other transgene based contrast agents that have shown promise in the literature.

1.2   Superparamagnetic Iron Oxide Particles

Super paramagnetic iron oxide particles (SPIOs) are the most widely used agents for MRI imaging of transplanted cells in biomedical research. They are characterised by an iron oxide core and a coating, which varies from inorganic materials such as silica to synthetic or natural organic materials like phospholipids, fatty acids, natural polymer; dextran and biodegradable polymer; polyethylglycol (PEG). The SPIOs come in a variety of sizes comparable to that of cells (10-100µm), viruses (20-450nm), proteins (5-50nm) and genes (2nm width and 10-100nm length) (Pankhurst *et al.* 2003). They are often classified by size, measured by the hydrodynamic diameter (HDD), ranging from the ultra-small; 10-40 nm HDD, which are typically used for gene delivery, by using a biocompatible material genes of interest can be attached to the SPIOs allowing them to be transported to a specific cohort of cells both *in vitro* and *in vivo* (Neuberger *et al.* 2005); to those that reach up to 300 nm-3.5 µm that are administered orally, for example when detecting abnormal abdominal pathology (Johnson *et al.* 1996). The most commonly used SPIOs range from 60–150nm and are used as MRI contrast agents. They are also in development for use in drug delivery systems to carry cytotoxic drugs or therapeutic DNA to target a specific location using an external magnet (McBain *et al.* 2008). It is this size range that is most useful for labelling cells *in vitro* for *in vivo* monitoring after transplantation.

1.2.1   What are SPIOs

SPIOs are generally made from insoluble crystals of magnetite (Fe_3O_4) or maghemite (γ-Fe_2O_3) and each crystal contains thousands of Fe ions (Fe^{2+} and Fe^{3+}). The superparamagnetic part comes in when these ions are magnetically ordered within the crystal so that the net magnetic moment of the particle is so large it exceeds that of a typical paramagnetic ion. The effect is characterized by no remnant magnetic moment, unless it is in the presence of a magnetic field like that of an MRI machine, contrary to ferromagnets responsible for the common magnetism that one experiences in everyday life. SPIOs exist in a colloidal suspension because of their size: the energy of Brownian motion largely exceeds gravity (Einstein *et al.* 1926; Hawrylak *et al.* 1993). On intraperitoneal or intravenous administration SPIO's can be described as biodegradable, in that they are metabolized by cells and enter normal iron metabolism and are ultimately incorporated into haemoglobin or used in other metabolic processes (Schoepf *et al.* 1998; Weissleder *et al.* 1989)

1.2.2 MRI Properties of SPIOs

The most important characteristic of a contrast agent is the longitudinal and transverse relaxivities, the higher these are the smaller the volume necessary for discernable MRI contrast. Longitudinal relaxation rate is referred to by R1 or $1/T_1$, and transverse relaxation rate by R2 or $1/T_2$ in spin echo scans, and R2* in gradient echo scans. The R2 measurement, but not the R2*, depends on the diameter of the iron oxide particle, the diffusion coefficient and the echo spacing (Gillis *et al.* 2002). SPIOs shorten T_1, T_2 and T_2* relaxation, and due to the T_2 of SPIOs being far greater than the T_1 it explains why they are used primarily as negative contrast agents for T_2 weighted images (Gossuin *et al.* 2009). In MRI an increase in T_1 gives an increase in MR signal intensity, whereas an increase in T_2 decreases the signal, hence the loss of both signal and anatomical information when collecting T_2 weighted images of SPIO labelled samples. However, the most appropriate weighting of the image, whether it be T_1, T_2 or T_2*, is dependent on the distribution of SPIOs and the surrounding material. While SPIOs typically give a strong T_2 effect when internalized by cells, in a monodisperse and non-aggregated form the T_1 relaxation effect can be appropriately used to study vascular morphology (Allkemper *et al.* 2002).

In homogenous media the SPIO's proton relaxation rate increases linearly with contrast agent concentration. *In vivo* this does not hold true due to the tissue presenting additional factors that influence the contrast agent's relaxivity (Bjornerud and Johansson 2004). The lack of a linear relationship in this environment is unfortunate seeing as it would allow the observed effect to provide direct information on contrast agent concentration. Instead changes in MR signal in biological systems depend on the effect the contrast agent has on the magnetization of water in that particular tissue. The compartmentalization of SPIOs *in vivo* has a profound effect on T_1 and T_2 relaxivity, in general the result is a decrease in T_1 and an increase in T_2 relaxivity. In such a scenario the enhanced T_2 is due to susceptibility effects which are a consequence of the magnetization differences within a given voxel. The non-homogenous distribution of magnetized material *in vivo* causes local field gradients which speed up the loss of phase coherence of the spins contributing to the MR signal. Some paramagnetic contrast agent can be based on their ability to cause

local magnetization inhomogeneities, disrupting the proton's phase coherence as it passes through the magnetic field (Chu *et al.* 1990)

The effect on T_1 is a result of the tissue barriers imposing limitations on the water's access to the contrast agent compared to the fast exchange experienced if the water protons had unrestricted access. The proton exchange rate varies substantially between different tissues from $100sec^{-1}$ to as low as $1sec^{-1}$ in intra extracellular and vascular extravascular situations respectively, changing the T_1 relaxation rate *in vivo* (Donahue *et al.* 1997).

The detection threshold of SPIO labelled cells is influenced by signal to noise ratio and pulse sequence, and to an extent, field strength (Heyn *et al.* 2005). Different pulse sequences in the MRI programme change the T_2 relaxation rate which subsequently alters the sensitivity of the SPIO signal by up to two fold, (Majumdar *et al.* 1989) so the choice of programme should be taken into account during experiment preparation and analyses. Field strength generally will not increase the contrast because SPIOs reach a saturation of magnetization at 1-2T (Shen *et al.* 1993), once an external magnetic field is applied (i.e. the MRI machine) the magnetic fields around the SPIO very quickly align to give signal and higher field strength cannot improve what is already almost complete alignment. Scan type can be altered to reduce blooming effects to an extent, enabling more precise anatomical location in a T_2-weighted image or for increased sensitivity a T_2^*-weighted image can be used which also has a shorter acquisition time and higher spatial resolution but increased blooming of SPIO signal.

1.2.3 SPIOs as MRI contrast agents

Iron oxide particles have been used in medicine alongside MRI type apparatus for over 50 years, when Gilchrist and co-workers first injected a suspension of iron oxide particles into cancerous lymph nodes to differentially heat and destroy the nodes with an RF pulse (Gilchrist *et al.* 1957). SPIOs are taken up primarily by one of two major pathways, phagocytosis by phagocytes or endocytosis/pinocytosis in non-phagocytic cells then stored intracellularly in tubular lysozymes (Weissleder *et al.* 1997). Intravenous injection results in the SPIOs becoming covered in plasma membrane (opsonisation), which is critical to their uptake by the reticuloendothelial cell system (RES) that functions to remove foreign substances from the blood stream.

Biologically inactive substances are processed via the liver and the accumulation of SPIOs by the RES in the liver was taken advantage of for their first use as an MRI contrast agent. This began when they were used to facilitate the detection of liver tumours due to the preferential phagocytosis of SPIOs by normal hepatic Kupffer cells but not by the tumour tissue (Arnold *et al.* 2003). By the same reasoning this also allowed the efficient imaging of the spleen to diagnose tumours which remain SPIO negative (Kreft *et al.* 1994). In fact dextran coated SPIOs were the first organ specific MRI contrast agent approved for imaging liver and spleen pathology in clinical applications (Hamm *et al.* 1994). They can also aid differentiation between metastatic and benign lymph nodes (Anzai *et al.* 1994). Taken orally compounds like FDA approved SPIO Gastromark[tm] provide clear visualization of the loops of the bowel and surrounding gastrointestinal tract. They accumulate nonspecifically in gastrointestinal tumours which rely on the enhanced permeation, with fenestrae up to 700nm, and retention defined by a typically leaky vasculature and poor lymphatic drainage (Maeda *et al.* 2000; Moghimi *et al.* 2001).

The first studies imaging transplants of SPIO labelled neural cells into the adult rat brain were reported in 1992 (Hawrylak *et al.* 1993; Norman *et al.* 1992). The initial study demonstrated an association between the location of the cells and superparamagnetic particles using MRI and histology but the SPIOs aggregated and many remained outside the cells (Norman *et al.* 1992), possibly a result of the aggregation of large SPIO size, (1µm particles) and the choice of lectin wheat germ agglutinin acting as a transfection agent (TA). At about the same time a related piece of work was published using foetal rat cortical tissue labelled with dextran coated SPIOs of approximately 11nm enveloped in reconstituted Sendai virus envelopes and grafted into rat cerebral cortex. Signal was observed as late as 2 months post grafting but there was poor cell survival and numerous astrocytes and macrophages labelled around the grafting site, making the cell specificity dubious (Hawrylak *et al.* 1993). The MRI contrast was localized to the injection site in these studies making it questionable how much of the signal was from SPIOs and not from remaining hemosiderin. In the following years progress was achieved with the use of SPIOs coated with dextran, which has been shown to be a responsive method to dynamically track labelled cells *in vivo*, subsequently rat T cells were labelled *in vitro* (Yeh *et al.* 1995). *In vivo* MRI has been successfully used to track the fate of rat

MSCs co-labelled with SPIOs (Endorem) and bromodeoxyuridine for up to 50 days (Jendelova *et al.* 2003).

Many studies have focused on determining ways to track single SPIO labelled cells by MRI and at the same time using the minimum possible number of SPIO particles per cell (Heyn *et al.* 2005; Shapiro *et al.* 2004). This has been achieved but usually at the cost of decreasing the voxel size resulting in longer scan times – not ideal when scanning live specimens. Yet most *in vivo* work reports higher detection limits dependent on strength of the field which can improve detection limits by two fold (Verdijk *et al.* 2007). In some cases the minimum cell number observed has been 1,000 cells in a highly concentrated *in vitro* environment (Guzman *et al.* 2007). Using the highest magnetic field available for imaging rodents (17.6 T) Stroh observed 100 labelled cells grafted into the striatum but lesser numbers resulted in incomplete loss of signal and could not be unambiguously distinguished from the possible presence of blood, in addition the MRI could not be confirmed histologically due to the small numbers of cells used (Stroh *et al.* 2005). Another method to increase sensitivity to T_2^* effects uses steady state free precession (SSFP) sequences to allow detection of single labelled cells, *in vitro,* on a 1.5T clinical scanner (Foster-Gareau *et al.* 2003) While this is achievable in motionless, inhomogeneous media SSFP are problematic in live animals where they suffer from being extremely prone to motion and local magnetic field inhomogeneities.

1.2.4 Long term SPIOs analyses

The longevity of SPIO signal *in vivo* has been studied numerous times giving contradictory results. SPIO signal can last for several weeks *in vivo* and contrast was observed 18 weeks following transplantation of SPIO labelled human CNS stem cells grown as neurospheres into the mouse brain (Guzman *et al.* 2007). In Guzman's work a control group of cells that were killed prior to transplantation by freeze thawing showed reduced MRI signal loss over the first 35 days while imaging of live cells successfully depicted the cell's positions. Meanwhile another study found that one week following transplantation of SPIO labelled rat neural stem cells into a rat brain of SPIO labelled cells, T_2 and T_2^* weighted images showed obvious signal change but signal diminished and blurred at 7 weeks (Zhu *et al.* 2007).

There are a number of things that could happen to the SPIOs once they have been grafted *in vivo* other than remain within live cells. To determine whether SPIOs are

taken up by endogenous cells they have been injected alone into the rat brain: incorporation of nanoparticles into the cytoplasm of neurons, astrocytes or oligodendrocytes was not observed (Jendelova *et al.* 2004). In another study direct injection of SPIOs into the mouse brain to label endogenous NPCs have highlighted cause for concern when analysing results because contrast relocation could be interpreted as cellular recruitment when in fact it may be background migration of extracellular SPIOs (Vreys *et al.* 2010). Importantly SPIO contrast, especially in long term studies, needs to be interpreted with caution. Bernan and colleagues evaluated the factors contributing to MRI contrast change over time using a mNSC line that expressed firefly luciferase to provide information on cell viability and labelling with SPIOs. The cells were transplanted into either immunocompetent, graft-rejecting mice or immunodeficient, graft-accepting mice (Berman *et al.* 2011). The results were unexpected, the MRI hypointensity decreased in all animals over time but while the bioluciferase signal in graft-accepting mice increased, indicating graft survival and proliferation, and the bioluminescence signal in graft-rejecting mice dropped below background level, the MRI images were opposite to what the bioluminescence results and to what previous studies would suggest. The mice that accepted the graft lost SPIO contrast at a faster rate than those that rejected it, the latter showing increased intensity of SPIO contrast over the entire time course. These results suggest that SPIO contrast clearance is dominated by live cell proliferation as opposed to clearance provoked by cell death and their subsequent removal via phagocytes. The results were contrary to previous studies (Zhang *et al.* 2003a; Zhang *et al.* 2004) which reported that the hypointense signal was cleared when SPIO labelled NSCs were killed prior to transplantation. The differing result when compared with Zhang's work may be accounted for by the cell type used: Bernan used an immortalized cell line, which divided more rapidly than progenitor cells (Zhang *et al.* 2003a). In addition, Zhang et al injected cells into the cerebrospinal fluid which could clean away free SPIOs more efficiently than in the brain parenchyma. Either way it emphasises that SPIO signal can not be simply interpreted. Another point of analysis that may be important to note is that over time the dextran coat will degrade and the iron oxide particles will be released and freely interact with water protons providing a T1 effect (Chambon *et al.* 1993).

Other factors affecting signal diminishment result from asymmetrical cell division, causing the SPIOs to be unequally distributed between the daughter cells, and those cells which received a smaller payload, or none at all, becoming immediately undetectable (Walczak *et al.* 2007), or in proliferative cells the SPIOs are diluted out and only a negligible amount of iron remains in each cell, below the threshold of MRI sensitivity. It was shown SPIOs can be used to accurately locate grafted cells unless they were highly proliferative (Lepore *et al.* 2006). An abrupt cut off in signal was observed after 6 weeks when monitoring the limitations of SPIO tracking in highly proliferative cells *in vivo,* though this study fell short of investigating the occurrence of this fully (Lepore *et al.* 2006). Building on the signal loss, the first demonstration of the inadequacies of SPIOs to track highly proliferative cells after widespread distribution in the mouse brain *in vivo* was carried out by Walczak et al in 2007. They showed the hypointense signal remained strong at the site of injection of mouse neural stem cells and didn't accurately portray the cell's movement into the outer layers of the cortex which ameliorated the shiverer phenotype in *shi/shi* mice. The loss of signal happened in an extremely short space of time, approximately 6 days, and was thought to be a result of differentiation leading to increased asymmetrical partition of SPIOs between daughter cells, an essential part of embryogenesis and stem cell development (Lin and Schagat 1997), which isn't the case in undifferentiated stem cells. MRI was only really reflective of the graft in the very initial stages and casts a dark shadow on using SPIOs for long-term experiments. The impact of cell proliferation on SPIO labelling was reiterated the following year: after three subculture passages, SPIOs were almost completely cleared from a culture of human neural progenitor cells (Neri *et al.*, 2008). Neri *et al* determined that SPIO labelling is not applicable for use in rapidly dividing cells or long-term studies (Neri *et al.* 2008). An advantage of transplantation into the CNS is that the cell types used are generally slow dividing, differentiated neurons and glia. There was an increase in cell proliferation in Neri's cultures which could be attributed to the presence of iron, an essential element in metabolism, however, ultimately intracellular free iron leads to functional impairment and death (Knobel *et al.* 2006). While no toxicity after optimization of labelling an *in vitro* culture with SPIO and PLK was noted, this environment may not have been as challenging as *in vivo* environments, so while tolerance seemed fair *in vitro* stress models are warranted to fully analyse this (Neri *et al.* 2008).

1.2.5 SPIOs and Differentiation

The potential toxic effects of SPIOs in cells remain a troublesome quandary to most who are considering their use. Although some studies have demonstrated iron oxide particles are tolerated well *in vivo* (Kim *et al.* 2006) and with no cytotoxicity, others found more detrimental effects. SPIOs affect actin cytoskeleton formation which may have a knock on effect on differentiation down various lineages and migration (Soenen *et al.* 2010a). SPIOs were shown to inhibit differentiation in a number of cell types including inhibition of mesenchymal stem cells (MSC) into chondrocytes (Kostura *et al.* 2004). Kostura found that while neither osteogenesis nor adipogenesis were grossly affected, Feridex blocked chondrogenesis from MSCs. In a combination of SPIO labelled, and unlabelled cells, MSCs segregated into distinct groups with collagen II positive areas, a chondrogenic marker, mutually exclusive from PB staining. This is at odds to Arbab's work, which determined that there was no effect on the differentiation of hHSC and hMSC down a chondrogenic lineage nor differentiation to adipocytes or osteoblasts. After Bulte questioned their chondrogenic differentiation results (Bulte *et al.* 2004), Arbab duplicated Bulte's experiment demonstrating that incompletely washing extracellular SPIOs off cell cultures could prevent differentiation, in this case chondrogenesis (Arbab *et al.* 2004b).

Human foetal neural precursor cells exposed to high levels of SPIOs (800ug/ml) for extended time periods (72 hours) display a severe drop in survival and a reduced capacity to form neurospheres (Neri *et al.* 2008). Pisanic II and colleagues developed a quantifiable model cell system in which they showed that even moderate levels of iron oxide nanoparticles could adversely affect cell function, with cells exhibiting diminished ability to form mature neurites in a dose dependent manner (Pisanic *et al.* 2007). The niche the grafts inhabit may also be affected. SPIO labelled cells seem to induce an influx of microglia in the brain, while unlabelled controls did not (Lepore *et al.* 2006). However, further examination of the *in vitro* PB staining suggests that this could be a result of the SPIOs not being washed completely off the cells.

1.2.6 Altering SPIO Properties

The physiochemical properties, size, morphology, coating, charge and surface chemistry are fundamental to SPIOS behaviour and the way in which they can be used, and will be covered below. The initial view was that dextran coated SPIOs are

fully biocompatible as an MR contrast agent as demonstrated in the initial animal trials, where SPIOs were monitored for their impact on anaemia reversal, toxicity and removal from the body of Sprague Dawley rats and Beagle dogs (Weissleder *et al.* 1989). This assumed safety of SPIOs has since been thrown into question by findings that they possess certain traits standing them apart from bulk material or free ions, concerning their surface reactivity for one (Soenen *et al.* 2010). The cells normal homeostasis is at risk from both the physio chemico properties of the nanoparticles (Verma and Stellacci 2010) and the high intracellular concentration required to visualise in MRI.

1.2.6.1 SPIO coatings

Unmodified SPIOs are prone to aggregation and can flood the cell causing massive cell death. To prevent this aggregation they are typically coated with dextran (Berry *et al.* 2004). Other coatings are used, such as Gold, which can prevent SPIO aggregation, reduce the toxicity of the iron oxide core, and possesses optical properties that provides a second method of imaging at the near infrared region (Melancon *et al.* 2009). Starch coating assists generic cellular uptake and has been successful for imaging lymph nodes (Anzai *et al.* 1994).   There have also been attempts to develop new coatings that confer useful properties in addition to location information such as diagnostic and therapeutic. For example: The dextran coat can be impregnated with fluorescent particles that allow confirmation of MRI by subsequent fluorescence microscopy of post mortem sections (Shapiro *et al.* 2004). Magnetoliposomes (ML) are SPIOs with a phospholipid bilayer coating, allowing alteration to the surface properties for specific purposes, such as PEG mentioned earlier, which increases the blood half-life. As well as accumulating in the liver, spleen and kidneys SPIOs conjugated to the protein Annexin V recognizes cells by binding phosphatidyl serine in outer leaflets of cell membranes and binds plaque in hyperlipidemic rabbits, allowing evaluation of cardiovascular lesions. (Smith *et al.* 2007)

Clinical trials have been set up to monitor cells labelled with dextran coated SPIOs produced under the product name Endorem *in vitro* and injected into healthy human patients (US National Institutes of Health, 2009). As the use of SPIOs for cell labelling is increasing it is becoming more apparent that we lack information on

interactions between the SPIOs and cells, as the debate concerning their effects on cells continues (Soenen *et al.* 2010)

1.2.6.2 Transfection agents

A few cell types, e.g. Kuppfer cells and microglia, exhibit spontaneous uptake of iron oxide which is useful for diagnosing liver tumours by MRI after IV injection (Fleige *et al.* 2001). However, the vast majority, particularly non dividing and differentiated cells, have a very low uptake (Lewin *et al.* 2000), therefore a TA is required to adequately SPIO label cells. The TA must bind to the dextran coat via electrostatic interactions, altering the highly negative <u>zeta potential</u> of SPIOs, so that they can adhere to the membrane (Arbab *et al.* 2004a) and be taken up through endocytosis. Surface coatings with a positive charge tend to stick to cells (Fujita *et al.* 1994) and the zeta potential of SPIOs of approximately -32.24 ±0.67 mV can be increased when combined with protamine sulphate, 7.07±0.01 mV, giving a final zeta potential of 20.26±0.34 mV, appropriate for internalization by cells (Arbab *et al.* 2005)

The ability to complex TAs to SPIOs has been well studied (Arbab *et al.* 2004c; Hoehn *et al.* 2002; Kraitchman *et al.* 2003) However, many TAs are toxic to cells when used alone (Matuszewski *et al.* 2005). PLK is another often used TA but it is not clinical grade and has a low upper threshold of 10µg/ml outside of which it causes significant cell death (Himes *et al.* 2004; Matuszewski *et al.* 2005) compared to protamine sulphate's therapeutic window of 50mg/ml (Hinds *et al.* 2003). PLK has been shown to be 100x less efficient at transfection than protamine sulphate (Hinds *et al.* 2003). Protamine sulphate is a principle component in condensing DNA for lipofection which can also be used to change the surface charge of SPIOs (Matuszewski *et al.* 2005). Two benefits of using protamine sulphate are that it is FDA approved to reverse the anticoagulant effects of Heparin, so the SPIO – protamine sulphate complex system is feasible for clinical use. Also heparin can be used in the wash phase to help remove extracellular SPIOs from the cell surface after labelling.

To avoid the use of TAs, a number of protocols have been developed. Cells have been successfully labelled with a dextran coated SPIO, brand name Feridex, using electroporation, termed magnetoelectroporation (Walczak *et al.* 2005). Another method using SPIOs with additional carboxyl groups, called Ferubcarbotron, was

developed that provides higher affinity to the cell membrane, negating the need for additional TA when labelling non-phagocytic cells and successfully used to label hMSCs with no supplementary TA (Hsiao *et al.* 2007). In a comparison study between Ferucarbotron and a dextran coated SPIO, Fermoxide, plus protamine sulphate, both of which are clinically applicable approaches, Fermoxides showed a slight but significant increase in labelling human bone marrow stromal cell with more intracellular and less extracellular SPIOs (van Buul *et al.* 2009). This may be because the complexing of SPIOs to protamine sulphate forms larger particles (Montet-Abou *et al.* 2005), which can have a positive influence driving intracellular uptake as has been previously documented (Ogris *et al.* 1998) (Das *et al.* 2008). Micro sized particles have been successfully used to label hematopoietic CD34 cells and MSCs allowing detection of single cells (Hinds *et al.* 2003). When using a TA protamine sulphate has a number of benefits, already mentioned, compared to PLK and PLR if not carefully monitored can form complexes with SPIOs that are macroscopically visible and can't be taken up by endosomes in cells (Arbab *et al.* 2004a); . This is supported by studies determining protamine sulphate is comparable or superior to other SPIO-TA complexes (Matuszewski *et al.* 2005) (Kraitchman *et al.* 2003)

1.2.6.3 Size

A study using gold nanoparticles showed their *in vivo* distribution was size dependent, with the majority ending up in the liver and spleen and only the smaller 10nm group being detected in a wider variety of organs (kidney, testis, thymus, heart, lung, brain), after IV injection, corroborating what is seen with SPIO distribution (De Jong *et al.* 2008). Ultrasmall SPIOs (USPIOs) (approximate hydrodynamic diameter (HDD) 18nm) are not immediately recognised by the hepatic and splenic monocytic phagocytic system (recticuloendothelial cells) resulting in an increased half-life in the blood stream (Weissleder *et al.* 1990). They can then be taken up by the lymph nodes (Tanoura *et al.* 1992), bone marrow and extravasate through tight capillary pores permitting RES uptake throughout the body. For instance, the increased blood half-life of USPIOs leads to them being phagocytosed by macrophages within active areas of plaque formation, assisting with the detection of atherosclerotic plaques in the aortic wall of hyperlipidemic rabbits (Ruehm *et al.* 2001). Standard SPIOs are administered intraveneously, and to a lesser extent orally for gastrointestinal imaging

in whole animals. It is the *in vitro* labeling we are interested in here to follow grafted cells.

The 5-6nm HDD of a globular protein is recognised as the deciding factor being accountable for the ability of the renal and urinary systems to clear them extremely rapidly (Choi *et al.* 2007). The HDD of metal based nanoparticles like SPIOs can change *in vivo* by 15nm depending on the surface charge of the organic surface coating, For instance, <u>zwitterionic</u> coatings prevent the absorption of surface proteins so the final HDD will not increase size to the same extent as cationic or anionic ones (Choi *et al.* 2007).

Thus we have agents to increase blood half-life by avoiding the RES. For instance embedding PEG-ylated phospholipids into the lipid coating of SPIOs allows prolonged circulation after intravenous (IV) injection by suppressing uptake through RES, a result of decreased opsonisation because surface proteins cannot bind (Bulte *et al.* 1999). But the increase in HDD ultimately makes it harder to eliminate them from the body which becomes a problem in clinical applications due to the increased likelihood of toxicity. The most efficient size for cell labelling are particles of 100-150nm HDD (Daldrup-Link *et al.* 2003). The continued use of increasingly small SPIOs should be proceeded with caution as oxidative stress and calcium changes in macrophages in the alveolar have been associated with particles under 100nm, although these typically result from overload exposure when rodents are exposed to high concentrations of airborne particles (Donaldson *et al.* 2001). Various forms of nanoparticles have been shown to mobilize to the mitochondria, a redox active organelle, with the possibility of creating reactive oxygen species and so interfering with antioxidant defences (Oberdorster *et al.* 2005). In summary the physicochemical properties, size, morphology, coating, charge and surface chemistry are likely to modify responses and cell interactions and should be tested on a case by case basis.

SPIOs may have their drawbacks but, in the face of few alternatives, they remain the most frequently used method of MRI based cell labelling. As such, any new contrast agent needs to have their benefits and shortcomings compared against them. In the absence of a better contrast agent the necessity for *in vivo* monitoring of transplanted cells has left SPIOs as the only option and thus their effects on human neural stem cells (Guzman *et al.* 2007) and the immunological effects of iron

clearance (Janic *et al.* 2008) are being explored in preparation for clinical use following transplantation. *In vivo* MRI tracking of magnetically labelled cells in patients, such as transplanting SPIO labelled immature dendritic cells into lymph nodes to stimulate the immune system, which don't require a TA, has already begun (de Vries *et al.* 2005). The clinical applications have so far been used in the periphery and SPIOs have not been used in the CNS.

1.3   MRI Reporter Genes

MRI reporter genes could potentially non-invasively monitor transgene expression both in real time and at high resolution (the ability to distinguish two points that are in close proximity). The construction of transgenes allows the researcher's gene of choice to be introduced into the cell and to report on expression of a specific promoter if so required. The signal from MRI reporter genes can be overlaid with MRI images of soft tissue, adding functional information to high resolution anatomical images and thus increasing scientific interest in this area. A number of strategies are available for generating MRI contrast including those based on enzyme-catalysed chemical modification of metal based contrast agents, iron binding and storage proteins and artificial proteins for imaging based on chemical exchange saturation transfer (CEST).

1.3.1   Chemical Exchange Saturation Transfer (CEST)

One approach of particular interest that circumvents the limitations associated with PET and iron oxide particles is a new breed of endogenous reporter genes that work in conjunction with CEST. CEST exploits the ability of Nuclear Magnetic Resonance to resolve signals arising from the exchangeable protons of different molecules indirectly through the bulk water signal. A detailed account of the physics and theory behind CEST can be found in McMahon, et al, 2008 (McMahon *et al.* 2008) and will be discussed briefly here.

First we need to understand the basic principles of MRI. MRI relies on the spinning motion of specific nuclei present in biological tissues and unlike PET it uses no ionising radiation but an extremely powerful magnetic field. This field, B_0, causes alignment of the nuclei's axis of rotation, for instance in clinical applications the hydrogen nucleus is monitored. This single proton spins and, according to the laws

of electromagnetism (which state a magnetic field is created when a charged particle moves) this single positively charged proton thus acts as a small magnet. The north/south axis of each nucleus (represented by a small magnetic moment) is in a random orientation. When a strong magnetic field is applied all the nuclei align their axis of rotation to B_0, following a circular path around B_0 called precession (Figure 1.1). When a radiofrequency (RF) pulse is applied it causes excitation and the net magnetic moment moves out of alignment with B_0. Faraday's law of induction states that if a receiver coil or conductive loop is placed in the area of a moving magnetic field – for instance the net magnetic moment whose precession has now been 'flipped' by the RF pulse into the transverse plane where the receiver coil is – a voltage is induced in the receiver coil. This voltage represents the MR signal (further reading see (Harris 1986).
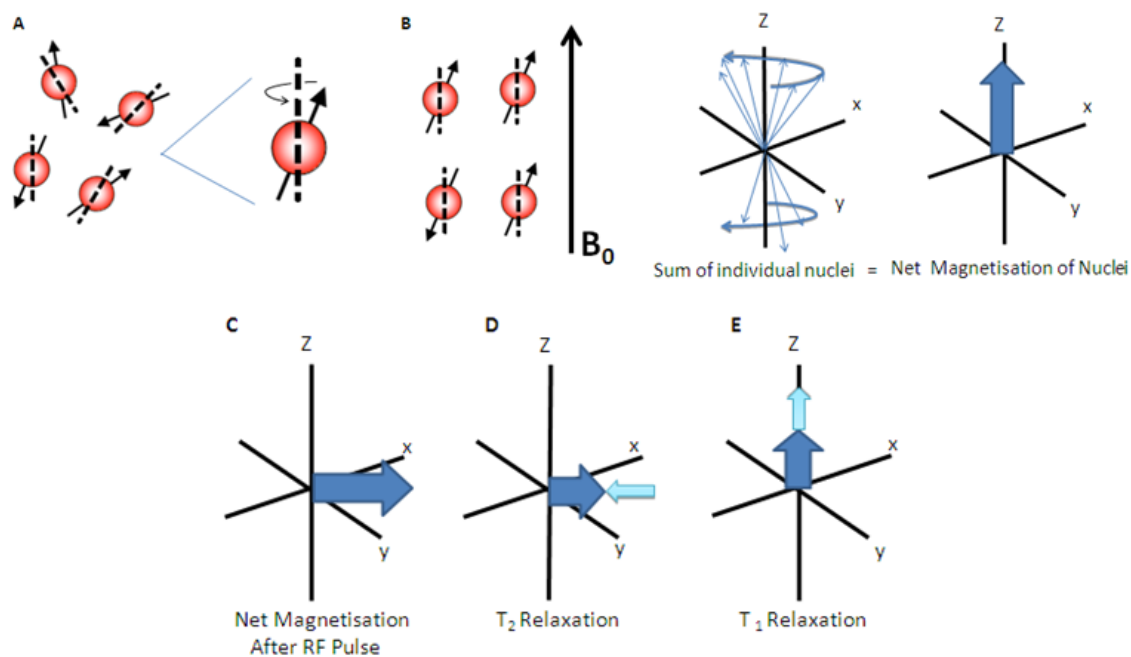
Figure 1.1: Hydrogen nuclei are randomly orientated and precess around their axis (A). In the presence of an externally applied magnetic field, B0, they align either parallel or antiparallel, with the majority in the lower energy, antiparallel, orientation leading to a net magnetisation (B). After addition of an RF pulse the spins are aligned and orientation states equalise in the XY plane (C) Relaxation from this excited state occurs in two ways; the fastest is T2 relaxation that decreases magnetisation in the XY plane (D) and the slower form, T1 relaxation, restores net magnetization in the Z plane (E). Adapted from EMRIC's web site: http://www.cardiff.ac.uk/biosi/researchsites/emric/basics.html

The behaviour of the energy received by the protons from the radiofrequency pulse is described by two relaxation constants: longitudinal relaxation time (T_1) and the transverse relaxation time (T_2). The inherent differences in relaxation times of tissues are what gives rise to MRI contrast. These differences can be enhanced by the action of exogenous contrast agents selectively adjusting the T_1, T_2 or T_2^*.

CEST requires a system be in constant chemical exchange, be it kinase enzymes catalysing exchange of the γ phosphate of ATP with the phosphate group of creatine phosphate (Mora *et al.* 1991) or, and for the purposes of this work, an intrinsic metabolite with an exchangeable proton that transfers between the metabolite and that of the solvent water. The MRI aspect of CEST is based on the targeted saturation by an RF pulse of a specific pool of exchangeable protons. Saturation is achieved through perturbation by a low power irradiation pulse, set at the resonance frequency of the nucleus in question, of the Boltzmann distribution of nuclear spins, conveying alignment either with or against the magnetic field. The spins that were aligned with the field flip so that the number of spins against the field increases at the expense of the spins aligned with the magnetic field. The field is said to become saturated once there is an equal number of spins aligned with and against the field, at this point the net magnetization is zero and no signal is observed in the NMR spectrum. If we call this saturated pool, pool A and the nuclei are in constant exchange with nuclei in pool B, we see that the exchange is transferring spins aligned against the field from pool A to pool B and vice versa. This results in a transfer of saturation from Pool A to Pool B and an associated decrease of Pool B's signal intensity, because the chemical exchange is usually much faster than the NMR relaxation process this results in an amplification of the saturation effect in Pool B. The signal intensity change of Pool B can be measured and this gives the CEST signal.

As we can see in Figure 1.2 the chemical shift of the two exchanging proton pools must be positioned far enough away so one is independent of the effects of the other's resonance frequency. To avoid miscellaneously recording the direct effects of the RF saturation pulse on the outer edge of the bulk water peak, rather than that due to proton exchange, it is necessary to compare the saturation effect of a correctly targeted saturation pulse to that of an equivalent saturation pulse applied with an identical offset on the opposite side of the bulk water signal (Figure 1.2). A

three point scan is commonly used, combining a) the scan with an RF irradiation on targeting the contrast agent, b) the scan with an RF pulse irradiating a position symmetrically around the water peak from the contrast agent and c) the control scan with no irradiation pulse. In regards to this, the saturation can be switched on and off by whether the scan has used the RF irradiation pulse or not to confirm whether the signal is real or artefact.

The resonance frequency of the protons is dictated by the surrounding chemical environment, and the differing resonance frequencies of the specific proton types allows "multi-colour" imaging (McMahon *et al.* 2008). For instance, the chemical exchange rates of exchangeable amide-, amine-, and hydroxyl protons of different polypeptides were predicted and 33 polypeptides were screened as contrast agents that are distinguishable from one and other (McMahon *et al.* 2008). McMahon choose Poly-L-lysine (PLK), poly-L-arginine (PLR) and poly-L-threonine (PLT) with contrast maximas at saturation frequency offsets from water of approximately 3.7ppm, 1.8ppm and 0.6ppm respectively. They likened each characteristic frequency to a colour channel in fluorescence imaging, with PLR's guanidyl giving the highest CEST sensitivity due in part to the number of exchangeable protons present on the side chain. While they developed three distinct groups of peptide labels based on the predominant exchangeable protons in proteins, they also recognised that there is a lot of room for improvement in the design and testing of alternative peptides, including which sequence will have the best imaging capacity *in vivo*.

Different types of CEST images are possible due to the nuclear magnetization of amide-, guanidyl-, and hydroxyl-protons being saturated at different and specific positions on a saturation frequency scale measured in parts per million and dictated by the chemical environment around the proton. Selective saturation using a radiofrequency pulse of a particular proton signal that is in exchange with surrounding water molecules (Figure 1.3) attenuates the MRI signal from the surrounding bulk water molecules as well as the original molecule. The subtraction of CEST images from normal MRI contrast images reveals bright spots where CEST agents are and this saturation can be switched on and off to confirm whether the signal is real or artefacts.

Before Saturation. Protons in constant rapid exchange

H_2O
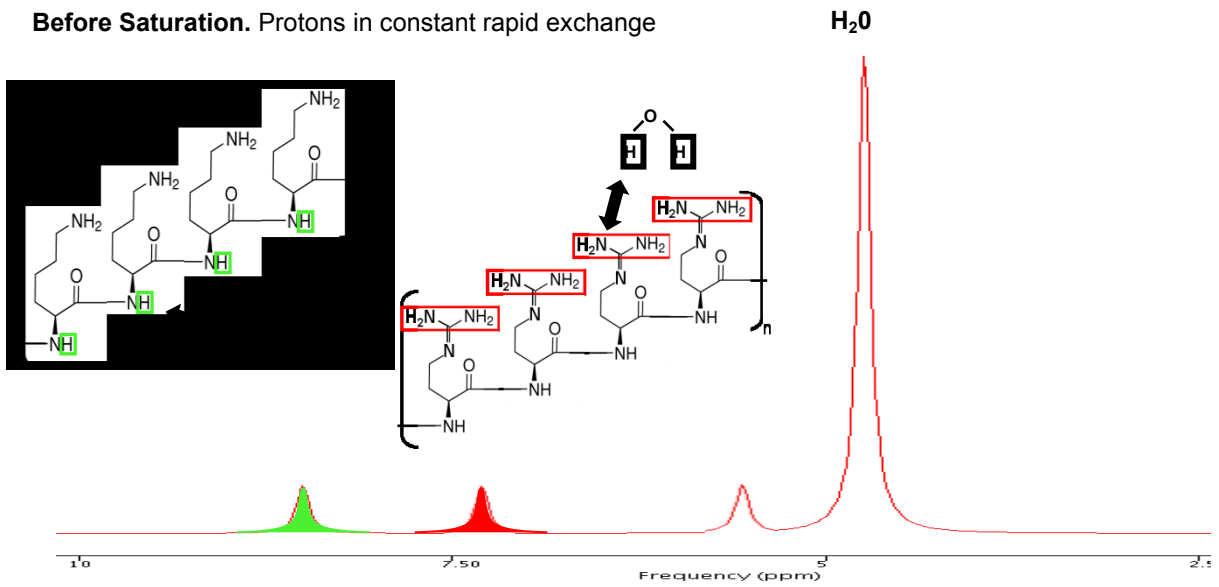
During Irradiation Pulses targeting lysine

H_2O

Offset RF field (B)

Targeting
RF field (A)
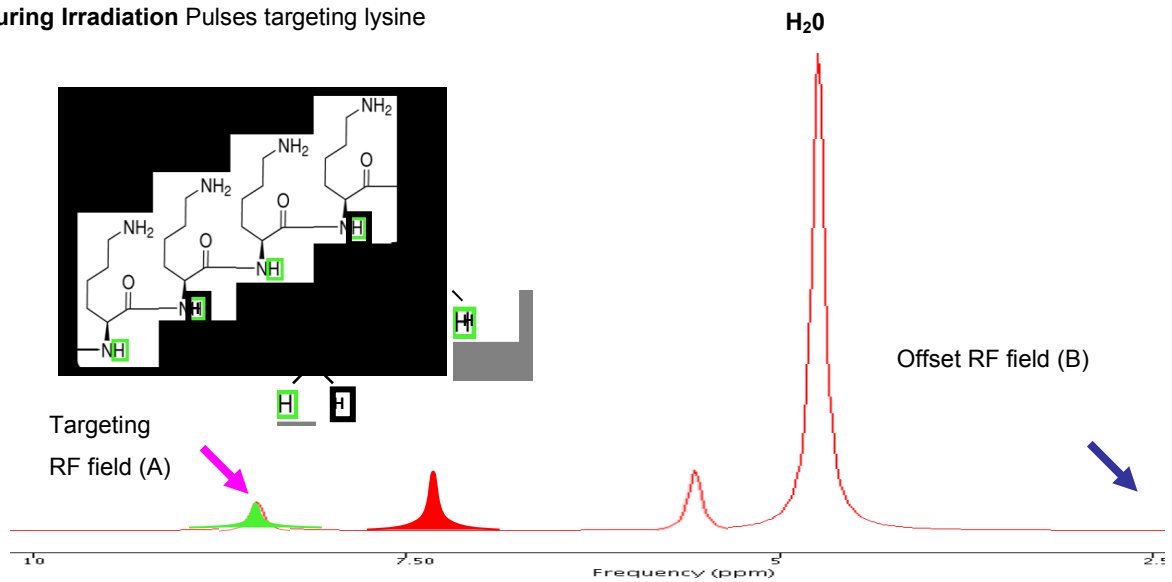
After Saturation of PLK protons

H_2O
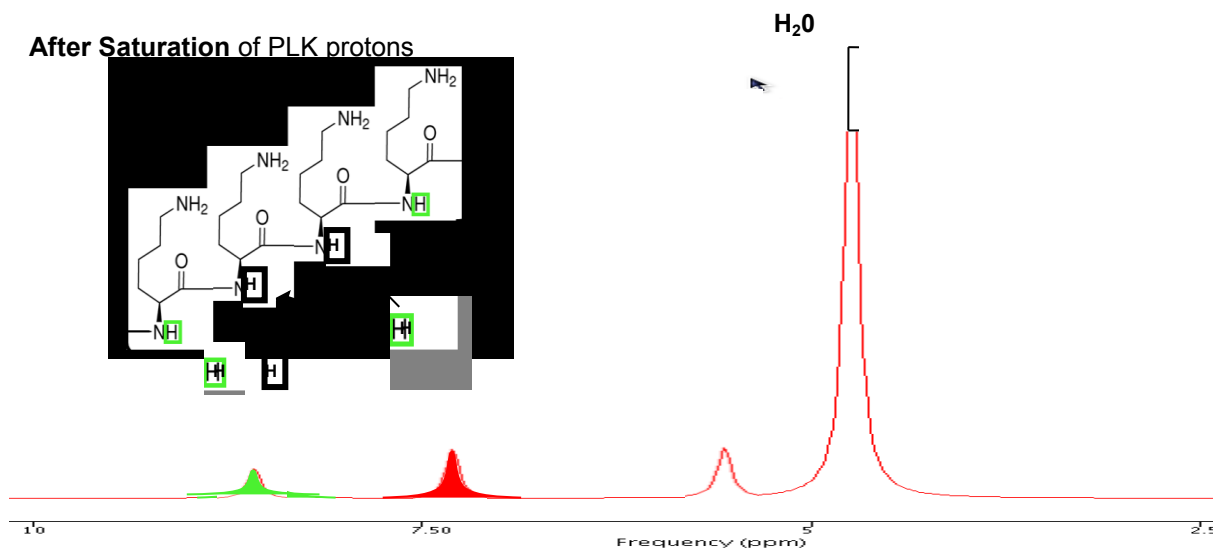
Figure 1.2: for legend see over
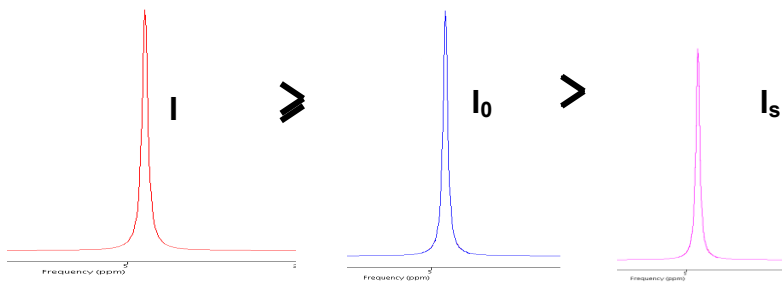
Figure 1.2: The basis of radiofrequency transfer. The rapid proton exchange between that of the PLK and water is indicated by black arrows. A given irradiation pulse is targeted, in this case to the amide proton's of lysine and during application of the RF pulse the irradiated PLK protons continue exchanging between those of water. The effect on PLK's protons is carried over with the protons when they become part of the water molecule. Now that they constitute the water peak signal there is an amplified decrease in the water peak. This decrease is measured after saturation to give the CEST signal. The RF field may perturb the intensity of the signal of water protons, and therefore the same RF field is applied at a frequency symmetrically opposite to that of the CEST agent (Blue arrow).
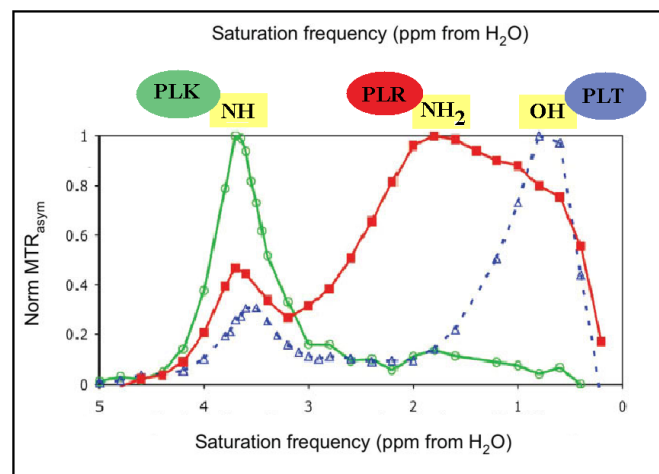
Figure 1.3: Positions of a saturation frequency scale that these poly amino acids dictating the radiofrequency needed to saturate the specific proton. PLK = poly l lysine, PLR = poly l arginine, PLT = poly l threonine. (Adapted from McMahon *et al.,* 2008)

The disadvantages of previous metal based contrast agents do not apply to this new faction of contrast agents. Noteworthy benefits, including those associated with transgenes:

1) The opportunity to dual label a single cell. The amide/hydroxyl/guanidyl proton of each different polypeptide represents a different position on a scale where Trimethylsilane is an arbitrary solution chosen as a reference point. Any of these positions can be irradiated with a distinct radiofrequency pulse varying between different polypeptides (Figure 1.3).

2) Any ambiguous bright spots on the screen can be verified as to whether they are real or not by running a second scan with omission of the RF pulse.

3) Preservation of signal throughout multiple cell divisions, allowing long term tracking of implanted cells and their progeny.

4) There will be no persistence of the contrast agents after cell death.

MR spectra have been used to study chemical exchange between species since the 1950s (McConnell and Thompson 1959), and the earliest example relating directly to today's CEST imaging was by Forsén and Hoffman (Forsén and Hoffman 1963). They measured hydroxyl proton transfer rates between salicylaldehyde and water by placing a saturation pulse on resonance with solute protons and recording the solvent signal intensity to study chemical exchange. It is this experiment, since adapted for imaging that is called saturation transfer or magnetization transfer in some publications. The term CEST was coined by Balaban and co-workers in subsequent studies which demonstrated signal amplification through the water peak via exchangeable protons using a number of metabolites (Ward *et al.* 2000). In fact the first non-paramagnetic reporter gene used *in vivo* was a non-metallic lysine rich protein (LRP) reporter gene designed by Gilad *et al.,* (2007) based on this premise. Currently LRP has been tested in 9L rat glioma cells *in vitro* with no apparent toxicity or detriment to cell viability. And *in vivo* where six mice, each containing two xenografted mammalian brain tumours engineered to express the LRP displayed significant signal intensity difference when compared to a control.

1.3.1.1 Different types of CEST

Proteins and peptides are abundant in cells and changes in the concentration and properties of these could help in the detection and identification of underlying pathologies. Amide proton transfer has been used to identify tumours in both rat (Zhou *et al.* 2003) and human brain tumours due to a higher protein and peptide content in respect to normal brain tissue and/or increased proton exchange rates caused by increasing pH within the tumour (Jones *et al.* 2006)

Modifications of CEST include the addition of paramagnetic metals to shift the proton frequency of solute protons or water pools so that a more efficient transfer of saturated magnetization is achieved, this is known as paramagnetic CEST (PARACEST) (Zhang *et al.* 2003b) and used by several groups (Zhang *et al.* 2007) (Aime *et al.* 2005). This PARACEST effect results from a larger chemical shift difference between the exchangeable protons and bulk water resonances allowing the exploitation of larger exchange rates. Typically the chemical shift of CEST agents is in a range up to 8ppm from the bulk water peak, whereas PARACEST agents like Europium (III) can be irradiated at 50ppm downfield of bulk water and Terbium(III) complexes at -600ppm (Aime *et al.* 2005). The down side is that exogenous materials have to be employed and therefore do not fit into the remit of this project.

The ability to image endogenous polypeptides has taken CEST imaging down a variety of avenues with clinical applications. Endogenous CEST approaches have been used to detect urea in the kidney with the future potential of evaluating renal function (Dagher *et al.* 2000); glycogen in muscle (glycoCEST) which is important to help understand the pathophysiology of abnormal glycogen content in obesity, insulin resistance and type 2 diabetes (van Zijl *et al.* 2007), and glycosaminoglycans (gagCEST) in the knee to help aid diagnosis and monitoring of osteoarthritis (Ling *et al.* 2008).

1.3.1.2 Experimental Parameters of CEST Images

Chemical shifts are magnetic field dependent, and RF pulses used in CEST are decidedly specific which means shimming, the act of precisely modifying the magnetic field to reduce any field inhomogeneities within the sample, is imperative. With poor shimming the resonant frequency (chemical shift) of the CEST agent will

vary across the sample leading to incorrect targeting of the CEST RF pulse causing a variation in the CEST effect across the sample.

Temperature and pH are intrinsically linked to the rate of chemical exchange. Exchange rate increases with increasing temperature as described by Arrhenius' law, (which states that for many common chemical reactions at room temperature, the reaction rate doubles for every 10 degree Celsius increase in temperature) and is true for all CEST species. Indeed PARACEST agents have been used to devise non-invasive methods to measure temperature *in vivo* (Zhang *et al.* 2005) (Li *et al.* 2008).

CEST signal has been used as a measure of pH in a number of applications *in vitro* (Sun and Sorensen 2008) and *in vivo* using PARACEST agents (Sheth *et al.* 2011). This relationship is less straightforward than that with temperature and depends on the species being monitored and which area of the pH scale the change is occurring across. One must be careful not to confuse CEST signal of an exogenously administered CEST agent with a signal change due to an altered native tissue pH, such as the acidic microenvironment of malignant tumours (Gillies and Gatenby 2007).

CEST programs must adhere to stringent amplifier duty cycle limitations and specific absorption rate restrictions that prohibit use of lengthy saturation schemes when imaging humans *in vivo*. They are time consuming as a result of the multiple scans necessary to image just one slice let alone a whole organ. There is much interest in improving the CEST sequences to get better signal from the agents to more efficient scans and CEST is being utilised across a number of differing circumstances.

The asymmetric analysis to take account of the effect of the RF irradiation pulse on the water peak unrelated to the contrast agent does not account for severe B_0 or B_1 inhomogeneities. If the B_0 or B_1 field is not homogenous the scans are no longer symmetric and B_0 inhomogeneity dependent CEST artefacts are introduced. Correction algorithms have been written compensating for this in the three point CEST scan, at least for those caused by moderate fields (Sun *et al.* 2007).

1.3.2 Ferritin as a Transgene

A second potential transgene is one that increases the iron content of a cell. This would give contrast in the same manner as SPIOs, by increasing the R_2 (relaxation rate) of T_2 weighted images. Indeed, iron overload is often observed using MRI on patients with Beta thalassemia, the extent of signal change in T_2* weighted images is used as a means to estimate whole body iron (Zamani *et al.*) and iron deposition in the hepatic veins of patients with alcoholic cirrhosis is observed using T_1 gradient echo sequences, which have T_2* effects (Horowitz *et al.*).

1.3.2.1 Iron

Iron is essential for the proper functioning and survival of cells across all three domains of life, eukarya, prokarya (Andreini *et al.* 2009) and archaea (Potrykus *et al.* 2010). In living tissue it exists in a ferrous (Fe^{2+}) or ferric (Fe^{3+}) form and accepts and donates electrons dependent on its oxidation state. Indeed, evidence from organisms closely related to the last common ancestor suggest Fe(III) is likely to be the first electron acceptor and this metabolic change provided an energetic advantage over fermentative microorganisms (Vargas *et al.* 1998) Without iron cells loose the capacity for electron transport and energy metabolism (Swinkels *et al.* 2006). However, free iron causes damage via the Fenton reaction; in eukaryotes mitochondria are the main source of oxygen radicals capable of generating hydrogen peroxide (H_2O_2) which reacts with Fe^{2+} producing Fe^{3+}, a hydroxyl anion and a Fe-catalysed hydroxyl radical ($\bullet OH$) – one of the most reactive species in nature (Equation 1) (Curtin *et al.* 2002; Symons and Gutteridge 1998) causing damage to cellular membranes, proteins and DNA. In addition the ferric iron can be reduced by reductants to ferrous creating a vicious cycle of free radical production (Arredondo and Nunez 2005; Carter 1995). Cells have evolved complex methods to regulate the intracellular iron pool on both a cellular and systemic level and iron handling varies depending on cell type (Swinkels *et al.* 2006). Intracellular iron content can be increased by altering the expression of one or more, of the iron regulatory proteins in the cell. These proteins include ferritin (Ft), the primary intracellular iron storage protein and the transferrin receptors (Tfrc) that work on a cellular basis controlling iron homeostasis.

$$(1)\ Fe^{2+} + H_2O_2 \Longrightarrow \underset{oxidized}{Fe^{3+}} + OH\bullet + OH^-$$
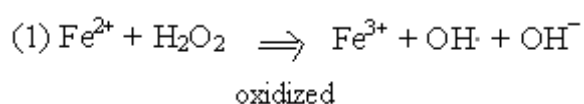
Equation 1: Demonstrates the free radical production resulting from iron's reaction with hydrogen peroxide

1.3.2.2 Ferritin

Ferritin converts ferrous to ferric iron, storing it safely inside a globular protein shell consisting of 24 subunits forming large highly stable complexes. Ft demits ferrous iron to a large cavity which can contain up to 4,500 Fe atoms in a ferric hydroxide core resembling the mineral ferrihydrite (Cowley *et al.* 2000). They are largely cytosolic with a minor portion present in serum in vertebrates (Arosio and Levi 2002). Ferritins have been characterised in a large number of organisms, reviewed in (Harrison and Arosio 1996) and there are numerous copies of the ferritin genes throughout the genome of the human, rat, and mouse. Most are intronless psuedogenes but the locus of the active gene has been identified (Harrison and Arosio 1996). Initial studies on horse spleen ferritin led workers to the assumption that all ferritins were composed of a single subunit type. This was challenged in subsequent studies on the human heart and liver which showed subunits from the two tissues differed in mobility during electrophoresis in denaturing gels leading to the coining of the subunits H (heart) or L (liver). Ultimately more ferritins from a variety of tissues were examined with similar mobilities to the H and L subunits, and when both types were found in the same cell the nomenclature changed to H (heavy) and L (light) based on their sizes, 21 kDa and 19 kDa respectively. The ferritin heavy (Fth) to ferritin light (Ftl) ratio is not fixed and subunits are interchangeable dependent on cell type, development transition or pathology. Tissue specific ferritin isoforms can be categorised as basic (Ftl rich) or acidic (Fth rich) isoferritins and certain forms of acidic isoferritins are implicated in functions distinct from iron homeostasis control and are mentioned later. Although the two subunits share approximately 50% sequence similarity and similar 3D structures (Harrison and Arosio 1996) they have different functions. The Fe (II) binding is initiated only in the Fth subunit at a specific site named the ferroxidase centre (Levi and Arosio, 2004), after which nucleation ensues in the cavity and further Fe(II) aggregate to form the iron core.

1.3.2.3 Post-transcriptional control of Fth and Ftl

Fth and Ftl are on different chromosomes and transcriptionally independent (McGill *et al.* 1987). The proteins are tightly regulated post-transcriptionally by iron availability through the iron responsive elements (IRE), and iron regulatory protein (IRP) system (Figure 1.4). The IRE forms a stem loop secondary structure originally

predicted by computer analysis on the 5' end of the Ft mRNA and the 3' end of the transferrin receptor (Tfrc) mRNA (Leibold and Munro 1988). IRP, of which there are two forms IRP1 and IRP2, bind to IREs in an iron dependent manner. IRP1 is generally more abundant than IRP2 and is a bifunctional protein; at times of high free iron content it binds with an iron complex and is unsuitable for IRE binding resulting in degradation of Tfrc and translation of Ft mRNA (Harrison and Arosio 1996). In this state it has a second function; it adopts an aconitase conformation and is involved in citrate metabolism catalysing the isomerization of citrate via cis-aconitate to iso-citrate. IRP2 on the other hand is down regulated by iron and displays no aconitase activity. At periods of low iron content the unbound form acts as a repressor, binding instead to the IRE inhibiting translation of Ft mRNA and lengthening the half-life of Tfrc mRNA (Harrison and Arosio 1996) (Figure 1.4). If either Ft or Tfrc are overexpressed, the other will increase accordingly. For example overexpression of Fth, leads to the distribution of iron toward a ferritin bound form which induces iron uptake into the cell via a concordant increase in Tfrc (Cozzi *et al.* 2000), which should generate increased contrast in T_2 and T_2^* images. The advantage of a reporter gene based on an iron regulatory protein is the ability to use endogenous iron sources rather than exogenous supplements.
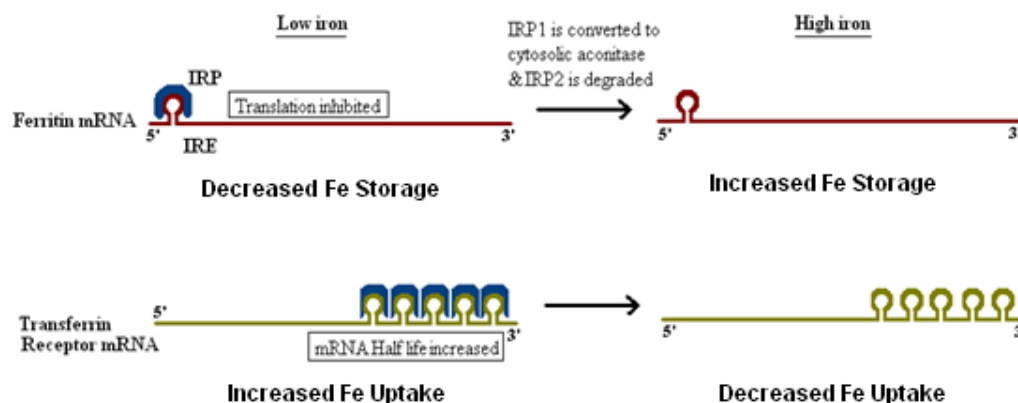

Figure 1.4: IRE/IRP regulation of ferritin: at low iron levels IRP 1 or 2 binds to the stem loop secondary structure IRE to inhibit ferritin mRNA translation and lengthen the half-life of Tfrc mRNA. At high iron concentrations the IRE remains unbound, Ft translation ensues and Tfrc is degraded. IRP1 becomes aconitase and assists in citrate metabolism.

1.3.2.4 Choosing the Ferritin subtype

Heavy subunit

The H chain harbours the ferroxidase centre crucial to cellular iron regulation and detoxification. Experiments disrupting the Fth gene producing Fth negative homozygotes suggests there is no functional redundancy between the two subunits as the embryos die between 3.5 and 9.5 days of development and L homopolymers are not able to efficiently maintain healthy iron homeostasis (Ferreira *et al.* 2000; Thompson *et al.* 2003). Fth heterozygotes are viable but show oxidative stress and apoptosis in the brain with apoptosis markers Bax and caspase-3 being detected in heterozygous mice but not in wild type (Thompson *et al.* 2003). The heterozygous mouse model displays a similar iron management protein profile to PD and AD. Mutational analysis of the C terminal region of the mouse Fth subunit have shown it plays a major role in protein stability and can diminish the capacity to incorporate iron (Ingrassia *et al.* 2006).

Light subunit

What is the requirement of the L chain and so, what is the disadvantage of too many H chains? Vertebrates have an additional L subunit which appeared when birds and mammals diverged from the last common ancestor during evolution 200 million years ago, this light chain predominates in iron storage tissues and during iron overload. It lacks the ferroxidase activity apparent in the H chain (Levi *et al.* 1994a), instead the centre is substituted with the formation of an intra chain salt bridge further stabilising the protein (Santambrogio *et al.* 1992). This subunit has acidic residues on the surface cavity facilitating iron nucleation and an increased turnover of the ferroxidase centre. Overexpressing the Ftl subunit on its own, due to its lack of the catalytic centre, is unlikely to alter iron metabolism and would remain an apoferritin (Arosio and Levi 2002). This is also confirmed when iron control is observed in hereditary hyperferritinemia cataract (HHC) syndrome. Mutations in the 5 base sequence of the CAGUG loop IRE sequence of Ftl cause HHC resulting in an excess of ferritin synthesis (Aguilar-Martinez *et al.* 1996; Girelli *et al.* 1995). Although as ferritin crystals build up and are deposited in the eyes lens there is no evidence of alterations in iron metabolism at the systemic and cellular level (Beaumont et al 1995). The importance of this latter example may be highlighted in the result mentioned earlier, that homopolymers aren't as efficient as heteropolymers (Levi *et*

al. 1992). Even so, adverse brain pathology hasn't been observed in HHC so localised Ftl overexpression, as in graft conditions, may not be an issue.

Mitochondrial Ferritin

The Levi group discovered another type of ferritin, mitochondrial ferritin (Mtf), encoded as an intronless gene on chromosome 5q23.1 (Levi *et al.* 2001). MtF is a novel H-type ferritin that has little or no tissue expression in all organs bar the testis. At high levels it can result in an iron deficient phenotype in the cytosol and decreased expression of ferritin (Drysdale *et al.* 2002). MtF is hypothesised to be important in mitochondrial protection where high metabolic activity occurs, ie the testis and more recently it was found to be present in neurons (Arosio and Levi 2002).

Acidic variables – other ferritins and dimers

There are a number of other ferritins including a superheavy mRNA and its peptide (43kDa) identified in erythroleukemia cells similar to Placental isoferritin (Shterman *et al.* 1989). Peptide mass fingerprint analysis suggested a H chain homodimer present in purified rat hepatocyte conditioned media, but this turned out to be Fth/L heterodimers by the presence of a 22 kDa band identified as a ferritin monomer, separated by SDS–PAGE (Bresgen *et al.* 2007). 64kDa trimers have also been found secreted from melanoma cells using Western blotting (Gray *et al.* 2001). Melanoma derived Fth and P43 placental isoferritin seem to contain a 43kDa Ft subunit which is believed to represent a Ft dimer. The immunosuppressive melanoma derived H chain ferritin has been recognised as a 21.5 kDa Fth (Gray *et al.* 2001). A novel Ft called PLIF (placental immunomodulatory ferritin) has been cloned from human placenta and is homologous to the Fth sequence apart from a novel 48 amino acid sequence on the c terminus (Moroz *et al.* 2002). It seems not to be controlled by iron availability as the mRNA does not include an IRE sequence but data suggests it is an embryonic immune factor and potentially adapted by certain cancer types to evade the immune system (Moroz *et al.* 2002). Antibodies cross react to both PLIF and P43 and share similar immunomodulatory properties and Moroz concluded P43 represents a PLIF dimer (Moroz *et al.* 2002).

As we can see there are a number of ferritin types but not all have the characteristics required to give MRI contrast. The Fth and Ftl have the strongest potential for MRI

contrast. Interestingly transfection of human Fth and Ftl chains in COS cells under strong promoters did not prove informative as the exogenous and endogenous ferritins did not co-assemble and so iron uptake and cellular metabolism seemed to remain unchanged (Cozzi *et al.* 2000). If Fth is up-regulated alone its ability to form heteroplymers with endogenous ferritin light may be hampered, and less efficient Fth polymers may result. Thus the importance of ensuring heteropolymer existence may be crucial to providing higher levels of MRI contrast than up-regulating either subunit alone.

1.3.2.5 Pathologies of abnormal iron homeostasis

Iron is the most abundant transition metal in the brain and a potential potent toxin to cells for the reasons mentioned earlier. At this stage it is prudent to ask whether increasing iron content by altering cellular iron modulation proteins will cause a detrimental effect in the brain. The answer is probably not, although there are many implications to over-expressing ferritin that are discussed below.

A wide range of symptoms can be displayed when normal iron homeostasis goes awry during iron deficiency, such as the irreversible alterations in myelination altering brain function of Sprague Dawley rats (Beard *et al.* 2003) and anaemia caused by redistribution of iron to macrophages during inflammation (Marx 2002). Or the exacerbating effect microbes have when competing for iron against a compromised host (Marx 2002).

In normal aging conditions ferritin is up-regulated in line with the increase in brain iron deposition, especially in the basal ganglia. Although it is still not certain whether these iron deposits are contributory, causative or just side effects, accumulating evidence implies abnormal iron metabolism (Halliwell 2001). It is when the protein becomes characteristically altered that problems ensue rather than up-regulation of normal elements of the storage system. For example; an adenine insertion into the Ftl polypeptide causes a rare movement disorder called neuroferritinopathy - it is thought apoferritins are formed that can contain little to no iron (Curtis *et al.* 2001). Also Heamochomatosis which leads to multiple organ dysfunction, is primarily caused by mutations in *HFE* gene, a gene thought to regulate the interaction between the Tfrc and transferrin (Tf) (Feder *et al.* 1996) but defects in other iron

regulatory genes hepcidin (*HAMP*), Tfrc 2*,* hemojuvelin *(HJV)*, and ferroportin have also been reported (Swinkels *et al.* 2006).

The role of Fth is not limited to iron sequestering in the Ft complex, there is strong evidence it plays an important role in chemokine receptor signalling and receptor mediated cell migration (Li *et al.* 2006). Cytokines are small, secreted proteins one class of which are the chemokines, specialising in attracting receptor bearing target cells with the ability to modify diverse brain properties. Much of our knowledge has so far come from the constitutively expressed chemokine CXCL12 and its major signalling receptor CXCR4 which mediates ERK1/2 activation and chemotaxis. CXCR4 was recently found to have Fth binding sites on the C and N terminus (Li *et al.* 2006). Fth displays an inhibitory role on CXCR4 and another receptor CXCR2 such that overexpression of wild type Fth attenuates CXCR4 signalling while activation is prolonged in Fth deficient cells (Li *et al.* 2006). The ramifications are greater for HIV positive opiate users. CXCR4 acts as a co-receptor for HIV envelop glycoprotein gp120 and is often co-expressed with μ opioid receptors. gp120 induces apoptosis in neuronal cells which is further exacerbated when opiates stimulate μ opioid receptors in the brain, causing an up-regulation of Fth that inhibits CXCR4 function in the brain. This reduces their neuroprotective qualities and exacerbates neuropathology (Sengupta *et al.* 2009). (For review (Abt and Meucci 2011)).

The roles outside iron storage regulation, particularly concerning Fth both mutated and normal forms, are widespread and, in addition to those mentioned above, include the following: Acidic isoferritins seem to play a role in mediating apoptosis (Bresgen *et al.* 2007); Fth is a physiological target and can be activated by NF-κβ to inhibit apoptosis induced by Tumour Necrosis Factor (TNF)α (Pham *et al.* 2004). Fth has immunosuppressive properties, inhibiting the response of lymphocytes, which melanomas take advantage of to evade destruction by immune cells (Gray *et al.* 2001). Several plaques identified from an immunoscreen from melanoma patient sera turned out to be Fth. It was hypothesised that mutations in the 3' end of the untranslated region involved in shortening the Fth half-life lead to a more stable Fth mRNA resulting in overexpression (Gray *et al.* 2001). Interestingly, where the ratio of Fth to Ftl is skewed in favour of the Ftl, there is an enhancement of lymphocyte activation (Gray *et al.* 2001).

Taken together, these findings reveal specific functions of Fth rich acidic isoferritins separate from their role regulating iron homeostasis, although many of the underlying mechanisms remain to be found. This highlights the importance of choosing the best cost:performance ratio when deciding which ferritin subunits give the best MRI contrast but also the incidental consequences this choice can bring about.

1.3.2.6 MRI properties of Ferritin

The MR properties of ferritin have been the focal point of extensive research since hypointensity was observed in the liver in T_2 weighted images and the importance of this effect was highlighted when applied to iron accumulation in the aging brain (Vymazal *et al.* 1992). Ferritin displays unique MR properties, instead of an expected quadratic dependence of the transverse relaxation rate on the strength of field, a linear dependence is observed (Gossuin *et al.* 2004; Vymazal *et al.* 1992). This is typically associated with <u>Superparamagnetism</u> (Gillis and Koenig 1987) (For MRI of SPIOs see section 1.4.2). Conventional theory asserts T_2 shortening is caused by dephasing of water protons as they diffuse through the field inhomogeneities of magnetic objects in this instance ferritin. And if B_0 is proportional to the perturbing magnetic object's field their contribution toward $1/T_2$ varies as the square of the field (Vymazal *et al.* 1992). But iron rich regions of the brain do not follow a quadratic dependence expected from paramagnetic iron, shown in primates under four different field strengths, but exhibit saturation at high field strengths usually explained by <u>antiferromagnetism</u> and Superparamagnetism (Bizzi *et al.* 1990). The source of this contrast was suggested to be a permanent magnetic moment within the Ft core, we now know ferritin has a superparamagnetic core and also displays superantiferromagnetism. The antiferromagnetic properties of ferritin display temperature dependence, the <u>Néel temperature</u> of a material is the temperature in which an antiferromagnetic agent becomes paramagnetic.

1.3.2.7 Ferritin as an MRI contrast agent

The first study to test ferritin overexpression as an MRI contrast agent in mouse ES cells used only the Fth subunit (Liu *et al.* 2009b). The contrast was generated through compensatory up-regulation of the Tfrc which leads to increased cellular iron in the Ft bound form. No toxicity was observed as determined by tumour growth over a 21 day period and mouse ES cell pluripotency seemed unaffected, as

demonstrated by neural differentiation and teratoma formation. However the contrast of Fth was at a comparable level of contrast with SPIOs only when more than 99% of the nanoparticles would have been lost from the cell through one mechanism or another. This demonstrated the advantage of SPIOs for short-term studies. hFth has been used as a MRI reporter gene to track dividing/differentiating stem cells in the beating heart of a rat, while simultaneously monitoring cardiac morpho-functional changes by using lentiviral vectors to introduce Fth into stem cells and intramyocardially injected after a myocardial infarction had been induced (Campan *et al.* 2011). Conversely it has been noted that in experiments where only the Fth chain is up-regulated, about half form homopolymers with only trace amounts of iron present, whereas those with as little as 1 or 2 Ftl chains contain the iron cores (Cozzi *et al.* 2000). Ferritin hybrids of both polymers are more efficient at incorporating iron than their homopolymer counterparts (Levi *et al.* 1994b) . Levi provided the first direct evidence in 1992 that Ftl:Fth heterodimers are more efficient in taking up iron than their homodimer counterparts, and the two subunits are complementary (Levi et al 1992). The Fth chain is the main regulator in ferritin production, it has a ferroxidase catalytic site involved in regulating iron availablility that, more importantly, may act to decrease availability of potentially toxic Fe(II). Upregulation of the Fth chain is coupled with an upregulation of the Tfrc and of IRP activity with reduced production of ROS (Epsztejn *et al.* 1999)**.**

In 2010 a paper providing proof of principle backing up the part of the initial rationale here was published. Human ferritin heavy and light subunits were joined via a flexible linker producing as a single transcript under the control of a CMV promoter (Iordanova *et al.* 2010). Cells were transduced with an adenovirus containing the transgene and cell pellets were imaged using an 11.7T Bruker microimaging system. The Ftl connected to Fth via a linker transgene induced a significantly higher R_2 relaxation rate in the cell pellets compared to either transgene expressed alone or the heavy followed by light transgene. While the first biologically active Fth/Ftl hybrid, developed by placing the Fth directly at the N terminus of the Ftl, had equivalent iron storage capacity to standard Ft (Lee *et al.* 2002). The Ftl followed by a flexible linker and the Fth has increased iron content, made possible by a larger protein cage estimated from TEM images and a slight hydrodynamic size difference measured by dynamic light scatter, which is likely the cause of increased MRI contrast (Iordanova *et al.* 2010). Using this adenovirus they also inoculated unilaterally into mouse cortex

and striatum and imaged 4 days post injection. While a T_2 weighted spin echo image suggests significant contrast compared to inoculation with a Lac Z control, this work is still being quantified (Iordanova *et al.* 2010a) but provides evidence for ferritin overexpression acting as a sensitive contrast agent. However, the current combination of the CMV promoter and adenovirus delivery system lends itself to fewer applications than a cell line with a stably expressed protein. Using this same replication deficient, type 5 adenovirus, the Fth Ftl chimera has since been used to visualise the migration of native primary neuronal progenitors from the SVZ to the mouse olfactory bulb (Iordanova and Ahrens 2011).

1.3.2.8 In Summary

Each new application of ferritin should be carefully evaluated because of iron's central role in multiple pathologies. Supporting the long term safety of ferritin overexpression, mice chronically overexpressing Fth in liver hepatocytes (liver-hfer mice) were studied over two years (Ziv *et al.* 2010). As expected, there was an increased R2 value (4.7T and 9.4T Bruker) and importantly no changes in liver, brain, heart, kidney and spleen phenotype were recorded (Ziv *et al.* 2010).

To summarise, overexpression of Ftl is unlikely to act as a good contrast due to its lack of ferroxidase centre and thus an inability to take up iron efficiently. In addition it is quickly broken down in a low iron environment and a high iron diet is necessary. Over-expression of Fth has shown contrast can be achieved but homopolymers may well be occurring which result in a less efficient storage system. Over-expressing both of these subunits could lead to improved MRI contrast, with few side effects other than some protection against oxidative stress (Cozzi *et al.* 2000; Epsztejn *et al.* 1999; Genove *et al.* 2005).

1.4 The transplantation paradigm: primary and stem cell transplantation in HD animal models

Cell replacement for neurodegenerative disorders is one therapy whose analysis in experimental models fails to provide comprehensive information, specifically on a temporal level *in vivo*. Huntington's disease (HD) is the primary model used here on which to focus both the necessity and establishment of an *in vivo* method to follow differentiated stem cells after transplantation. It is well established in the laboratory

and in addition is gaining acceptance as a good paradigm for transplantation in HD (Rosser *et al.* 2011b).

1.4.1 Cell transplantation

The view was once held that neuronal loss in the adult human brain is irreversible, because dying neurons cannot be replaced. This idea was re-evaluated after evidence confirmed neurogenesis in the dentate gyrus of the adult hippocampus (Eriksson *et al.* 1998) and subventricular zone (Doetsch *et al.* 1999). Even so the adult mammalian central nervous system (CNS) has weak capabilities for both endogenous cell replacement and the rewiring of specifically organized long distance connections, both essential for functional recovery (Rossi and Cattaneo 2002). Cell transplantation therapies for neurodegenerative diseases aim to overcome the inability of the CNS to replace lost components and/or may provide benefit to host cells in the form of trophic support. In addition this therapy needs to be competitive, offering advantages over any alternatives and in terms of circuit reconstruction can only yield benefits if the donor cells integrate fully into the brain circuitry.

1.4.2 Huntington's Disease as a Model

HD is one of a collection of neurodegenerative disorders associated with abnormal expansion of CAG trinucleotide repeats in specific genes. HD was eloquently described back in 1872 by George Huntington as a 'hereditary chorea' (Huntington 2003). Albeit a rare genetic disorder, the frequency of the mutation at 4-8 people per 100,000 in Europe, (Harper 1992), is thought to be an underestimate and it may well be twice as prevalent in the UK as previously believed (Spinney 2010). HD is caused by an autosomal dominant mutation and the pathophysiology causes severe motor, cognitive and psychiatric symptoms. There remains little hope for the individuals it affects and to date there are no disease modifying treatments available to those diagnosed with HD which consequently devastates not only their lives but also the people who care for them. Potential therapies include pharmaceutical based medications (antipsychotic medications and some that can partially ameliorate chorea, although none have yet addressed neuroprotection or repair of the brain), genetic based therapies (interfering RNAs that aim to down regulate, silence or block huntington gene expression using interfering RNAs of mutant gene expression) and cell based (reparative strategies to replace the lost neurons by cell transplantation (for review see (Handley *et al.* 2006). Here we concentrate on the development of

robust analysis techniques for cell transplantation therapies that have potential for HD symptom alleviation or postponement. Alongside PD it is an exemplar disease in which longitudinal analysis of grafts is highly sought after yet but not currently possible without many associated problems mentioned previously.

1.4.2.1 Pathology of HD and Regeneration

HD characteristically presents with enlargement of the ventricles resulting from a decrease in striatal volume and cortical degeneration (Figure 1.5). It is unknown whether cortical degeneration is secondary to the striatal degeneration but once HD related striatal deterioration begins it further exacerbates that of the cortex (Munoz *et al.* 2001). In the striatum the unstable polyglutamine expansion in the Huntingtin protein causes selective neuronal loss of GABAergic medium spiny neurons (MSN) (Beal and Martin 1986), specifically in the caudate and putamen (Ross and Margolis 2001). Interneurons are generally spared and moderate gliosis is associated with cell death (Selkoe *et al.* 1982).
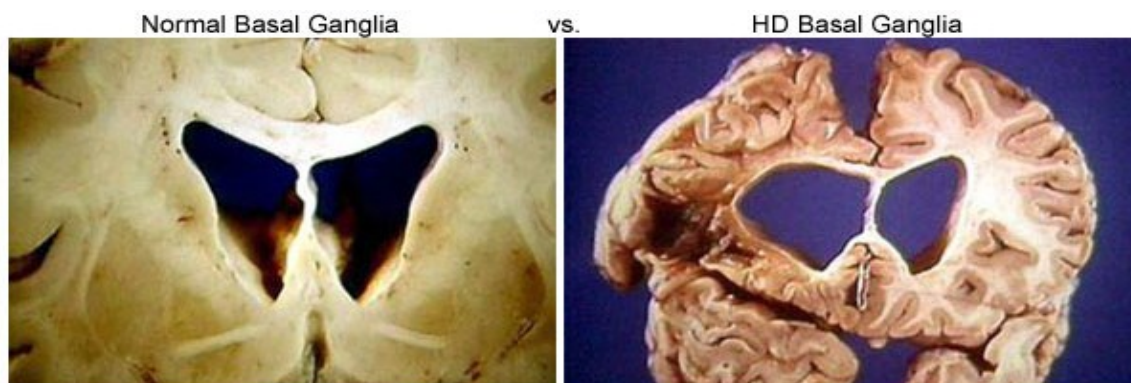
Figure 1.5: Photograph of a fixed normal and HD specimen. Note the atrophy of the caudate nucleus and putamen

The striatum is a highly organized structure that, along with the subthalamic nucleus, globus pallidus and substantia nigra, forms part of the basal ganglia (Gerfen 1992). The MSNs account for 90-95% of the striatal neuron population and named so after the secondary and tertiary dendrites branching from the 20-25µm diameter cell body, which are densely covered in spines (Kemp and Powell 1971).

1.4.3 The Basis of Transplantation studies in Neurodegenerative diseases

Cell transplantation therapies have developed over the last 4 decades, based on the premise that cells lost from the brain during manifestation of neurodegenerative disease can be replaced, thus restoring lost circuitry to provide functional benefit. Studies in the 1970's demonstrated survival and integration within the host nervous system of embryonic dopamine neurons into the rat anterior eye chamber (Olson and Seiger 1975). The first reports providing proof of graft-induced functional recovery were in animal models of PD and were assessed by behavioural and histochemical analyses (Perlow *et al.* 1979), opening up a new field from which open label trials followed. The large body of work done with PD studies provides a rationale, but specific and substantial studies with robust analysis following graft development are required. A Scandinavian trial by Lindvall and colleagues was the first to show really convincing data that foetal transplantation can result in marked clinical improvements in bradykinesia and rigidity in idiopathic patients, using PET to monitor Flourodopa uptake which was increased in the grafted hemispheres (Lindvall *et al.* 1990; Lindvall *et al.* 1994; Piccini *et al.* 2000; Wenning *et al.* 1997). In addition the grafts have been shown to survive for a number of years, while providing functional benefit with increased uptake of fluorodopa in the putamen, confirmed by tyrosine hydroxylase (TH) IHC that provided more information on the direction of the dopaminergic fibre growth (Kordower *et al.* 1995). Since the original trials began improvements in techniques have resulted in long lasting symptomatic improvement to the order of 30 – 50% in the Unified PD Rating Scale (UPDRS) (Dunnett *et al.* 2001). In response to the results of open labeled trials and due to the effect placebos can have in clinical trials, placebo-controlled double blind trials commenced. Two trials, Denver-Columbia (Freed *et al.*, 2001) and Tampa Mount Sinai (Olanow *et al.* 2003) demonstrated initial improvement after transplantation compared with control but benefits diminished over time and patients presented with severe graft induced dyskinesia's (GID) not reported previously (Freed *et al.* 2001; Hagell *et al.* 2002; Olanow *et al.* 2003). However, it should be noted that the regime used in these two trials was dis-similar to that of other trials, neither used robust immunosuppression techniques and the method of delivery had not been extensively tested as those in previous trials. Contrary to Lindvall's trial where improvements over their previous studies (Lindvall *et al.* 1987), resulted, in part, from a culmination of minor changes such as smaller cannula size and improved tissue handling (Lindvall *et al.* 1990)

Freed's study was based on less substantial foundations. Not only was it grossly underpowered but the frontal approach of stereotactic injection and culturing foetal cells for a month prior to grafting as nondissociated solid tissue strands were methods not thoroughly tested in animal models (Freed *et al.* 2001). Never the less the symptomatic relief in the first 4-6 months of the Freed and Olanow trials was in line with the improvement seen in the Lund trial (Wenning *et al.* 1997). These more recent trials still rely heavily on PET monitoring of Fluorodopa activity to give an idea on graft survival (Freed *et al.*, 2001)(Olanow *et al.* 2003). While it is unknown which type of PD would benefit most from transplantation, the Lund series demonstrates that when the conditions are right improvement is possible (Piccini *et al.* 2000; Wenning *et al.* 1997). Furthermore steps have been taken to address GID in Transeuro, an EU funded project that is developing a template from which future clinical trials in the cell transplantation field can work from.

The requirements and benefits from cell transplantation for PD and HD are subtly different. The Bachoud-Levi study provided a big impetus for taking transplantation forward for HD (Bachoud-Levi *et al.* 2000). In the initial study (Bachoud-Levi *et al.* 2000) (Freeman *et al.*, 2000), the grafted cells showed no signs of being vulnerable to the pathological process which they are trying to stabilise. Whether this is the case long-term however has been recently brought into the spotlight, at least for HD. Studies by two groups, have shown graft survival is attenuated long-term: Bachoud-Levi (2006) demonstrated clinical improvement in three out of five patients that plateaued after 2 years. Freeman, found a foetal striatal tissue graft can survive unaffected by the disease process after 18 months and used MRI to indicate the needle tracts were inserted near to their targeted sites at the caudate nucleus (Freeman *et al.*, 2000). In a more recent study, however, Freeman's group found that the grafted MSNs deteriorated more rapidly than host neurons and reportedly underwent disease-like neuronal degeneration seemingly caused by the host environment rather than a direct effect of the primary pathology, of protein aggregates (ubiquitin) or abnormal huntingtin proteins (Cicchetti *et al.* 2009). The latter study conveyed much more detailed information about the graft due to the methods of IHC and electron microscopy carried out after death of the patients. This was a follow up report of two patients who died almost 10 years post transplantation (Hauser *et al.* 2002). The authors compared these grafts with Freeman et al's graft at 18 months (Freeman *et al.* 2000) in terms of calbindin staining. The ratio of calbindin

staining of the graft to the immediate staining surrounding the host tissue is reported to be lower in the 10 year grafts than Freeman et al's, inferring relative calbindin loss in host and graft over time. It has been noted that the calbindin staining of the host tissue was much lower in the short term grafts and actually the intensity of the grafts from the two studies were little different (Rosser *et al.* 2011a). Furthermore in the same review by Rosser et al, they point out, contrary to Ciccetti's viewpoint, the lack of aggregates or HD-like degeneration of the grafted cells indicate the grafted cells were not affected by the disease process in the same way the surrounding host tissue was (Rosser *et al.* 2011a). Waiting until after death for detailed information on the graft survival in either the clinical trials or research using animals, misses vital temporal information. Better methods of monitoring are still not available for the latest trial – a large multicentre French speaking network trial that is underway in which a large number of patients have been transplanted and we are awaiting news on the state of the data at present. This is being coordinated by the team in Creteil – Bachoud-Levi and likely not to provide any more information than that given by PET and behavioural monitoring. The advantage of transplantation in HD is that patients are diagnosed from an early stage unlike PD where there is significant cell loss by the time of diagnosis. Thus, we can target transplants earlier before too much atrophy ensues. Just because only a temporary improvement has been achieved to date this is not necessarily the best that can be achieved. It seems there is a need for a greater number of cells per transplant and to decrease the immune response, both points an appropriate stem cell technology could address.

The progression of cell transplantation therapies towards the clinic must be founded on convincing and unequivocal preclinical data from the best animal models, using robust analysis methods that garner maximum information with precision. The risks and benefits of such therapies need to be properly assessed longitudinally through analysis in live models, for which there is not currently an ideal technique. To investigate original and robust ways to do this we first need to recognize what we want to know, discerning what can and what needs to be accomplished. The use of MRI is one technique with which we can achieve longitudinal analysis in live models. This has a wider potential than tracking grafted cell in neurodegenerative diseases, and may benefit many aspects of regenerative medicine and cancer biology.

1.4.4 The Graft

A cell suspension graft for transplantation into the adult rodent brain is typically made up of between 450,000 - 500,000 cells/µl, with 2 µl transplanted by stereotactic injection per hemisphere. The graft is measured empirically by density or volume. Density is an indirect measurement of fibre outgrowth; measuring how much reinervation there is compared to normal. Volume is a measure of the graft core, it is this reading that can currently be imaged using MRI reporters. Realistically MRI reporters can provide information down to a spatial resolution of 0.09 mm^3 and with graft cores in rodents reaching about 0.72 ± 0.1 mm^3 at 12 weeks following transplantation (Klein *et al.* 2007). We can expect several MRI voxels to fit comfortably within this region, providing good contrast if there is any to be seen. The variability in graft size is huge with volumes ranging from 19.24 to 962.32mm^3 in rodents when using ES cell derived neuroblasts as the donor source (Sophie Precious, unpublished observations). While attempts to address this variability have been made by refining the method of transplantation (Nikkhah *et al.* 1994) it still poses an issue in many laboratories. There are a few paths the grafted cells can follow. One of the undesirable paths is the development of teratomas if using embryonic stem (ES) cells or graft overgrowth if using primary foetal neural cells (Keene *et al.* 2009). The graft can also be lost altogether or the cells can exhibit various degrees of migration. Primary neural cells from both xenografts and allografts are capable of migrating from the site of injection (Hurelbrink *et al.* 2002; Hurelbrink and Barker 2005). In successful grafts, the cells persist, integrate and function, thus replacing the lost cells. They may have ameliorating knock-on effects outside the area of the grafted striatum; by replacing the MSN's in the striatum grafting can help preserve the target area for some cortical efferents, which may or may not have resulted in loss of the cortical cell body, thus providing support to the otherwise degenerating cortex (Munoz *et al.* 2001). MRI reporters monitor the graft *in vivo* and should abnormalities, such as graft overgrowth or loss of graft, occur neither time nor money is spent on an animal not fit for purpose.

Primary Foetal Tissue

The first studies using primary foetal tissue as a source of cells for neural transplantation have provided a proof of principle for transplantation therapy rather than a rationale for immediate long term treatment. Successful clinical trials so far

have been based on the transplantation of primary human foetal tissue, obtained from elective terminations of pregnancy. Tissue is transplanted into the host striatum from regions of the developing brain, for example, the ganglionic eminence (origin of striatal MSNs lost in HD), ventral mesencephalon (origin of dopaminergic cells lost in PD), and neocortex, (Kelly *et al.* 2011). Human foetal striatal cells contain neuronal precursors that can differentiate and mature into medium spiny neurons, as well as other cell types of the developing central nervous system (Li *et al.* 2008b). Some reports have shown grafted cells have the capacity to migrate to areas where the cells are needed in response to insult (Yang *et al.* 2009). Foetal tissue is associated with a number of constraints, including the number of foetuses required per patient, varying from 4-8 donors per patient (Keene *et al.* 2009; Kopyov *et al.* 1998) making it difficult to synchronize the attainment of foetuses at the required gestational age, patients and surgeons. An alternative and standardised source circumventing these issues comes in the form of stem cells. There are several sources from which potential stem cells can be derived and used for cell grafting.

Stem Cells

Stem cells are characterized by the ability of self-renewal (symmetric division) and potential to differentiate into a diverse collection of cell types (asymmetric division), replenishing both specialised cell types and maintaining a normal turnover. Stem cells can be derived from a variety of sources; for example the inner cell mass of blastocysts, foetal tissue and many adult tissues including the adult human brain (Eriksson *et al.* 1998). The benefit of stem cell use is not just about obtaining a standardized source, but allowing opportunities to manipulate the cells systematically prior to use. Once transplanted the proliferative capacity that can give rise to neuronal stem cell derived tumours can also be circumvented through direct modification prior to transplantation through expression of a suicide gene (Schuldiner *et al.* 2003).

Protocol development, such as using a chemically defined medium, to direct differentiation to the cell type of choice is of particular therapeutic significance (Bouhon *et al.* 2005). There are a number of options when it comes to choosing which stem cell source will be most appropriate for cell replacement therapies as outlined above. For the purpose of this thesis I focused my attention on ES cells.

Pluripotent cells

ES cells are derived from the inner cell mass of the embryo at the blastocyst stage (Evans and Kaufman 1981; Martin 1981). They have the potential to generate cells from any of the three primary germ layers; ectoderm, endoderm and mesoderm, and have the capacity for extensive expansion. Directed differentiation down many lineages have been demonstrated including neuronal (Bain *et al.* 1995), chondrocytic (Dexheimer *et al.* 2012) and cardiac (Liu *et al.* 2012). Human ES cells were derived from pre-implantation embryos and cultured for long periods of time, retaining stable developmental potential (Reubinoff *et al.* 2000; Thomson *et al.* 1998). The original cell lines were from blastocyst cultures and not clonally derived, therefore pluripotency was only demonstrated for a population of cells. Although efficiency of clonally deriving human ES cells is not as straight forward as their murine counterpart, pluripotency of a single human ES cell has been confirmed (Amit *et al.* 2000).

Mouse and human ES cells use different signalling pathways to retain their pluripotent state. Inhibition of lineage commitment in mice typically involves exogenous factors such as cytokine leukaemia inhibitory factor, LIF, and BMP4, while human ES cell pluripotency is typically maintained using activin, nodal and FGF. Interestingly mouse epiblast stem cells, EpiSC, have culture requirements and properties more similar to human ES cells than human ES cells have to mouse ES (Brons *et al.* 2007; Tesar *et al.* 2007; Vallier *et al.* 2009). It seems EpiSC and ES cells may share a common ground state (Silva and Smith 2008). Not all characteristics are verifiable in human ES cells, such as contribution to the germ line in chimeras, because of practical and ethical reasons. This combined with the relative ease with which mouse ES can be manipulated and the scope to generate transgenic mice makes mouse ES cells the cell type of choice for this work.

In this study we used mouse ES cells as a model system to develop MRI technologies. It is the differentiation of these cells down a neural lineage to replace cells lost during the disease process that we are interested in here. For this I predominately used the mouse ES cell line E14 (Hooper *et al.* 1987) that was derived from the inbred mouse strain 129/Ola in 1985. The mouse cell line E14 (Hooper *et al.*, 1987) has been used extensively worldwide in gene-targeting

programmes and also in vitro differentiation studies (Battersby *et al.* 2007; Bouhon *et al.* 2005).

Modifying ES cells

Of the numerous ES cell lines, many have adaptations increasing the range of their applications from identifying gene function to increased ease of cell sorting (Wernig *et al.* 2002). Random insertion techniques can result in various copy numbers, positional effects on the host genome and on transgene expression imposing spatial and temporal restrictions (Wilson *et al.* 1990). Some transgene studies use lentiviral vectors, these are considered one of the best options when requiring stable gene expression (Blomer *et al.* 1997). Once again the site of integration is unpredictable and not an ideal system for comparative studies. To comprehensively compare transgenes it is important to have the same experimental parameters where possible. Targeting the genes of interest (GOI) to a specific locus allows expression to be monitored reproducibly.

Promoters for tracking cell differentiation

Various gene expression patterns have been identified using Green Fluorescent Protein (GFP) as a reporter gene. GFP is a popular marker because it requires no substrate and is detectable in both fixed and live tissue by fluorescence microscopy (Chalfie *et al.* 1994). GFP has been valuable in the identification of various cell populations, such as the ubiquitous expression of tau-tagged GFP driven by the CAG promoter (Pratt *et al.* 2000), lineage specific expression (e.g. *Sox1*-GFP neural reporter in 46C cells, (Ying *et al.* 2003) and homologous recombination of GFP into the *Pitx3* locus to visualise dopaminergic neurons (Zhao *et al.* 2004)).

The strength of expression of these cell specific promoters must be taken into account. For instance, the glial fibrillary acidic protein (GFAP) promoter has tight cell-type specificity quantitatively, but it displays weak activity in cell lines and primary cultures (Smith-Arica *et al.* 2000). In the appropriate cell lines, the activity of the pCAGGs promoter is approximately 17 times stronger than the GFAP promoter and six times stronger than the neuronal specific enolase promoter (Smith-Arica *et al.*, 2000). Due to the importance of maximising contrast agent expression for robust contrast, promoters must be carefully considered before undertaking the arduous task of construction. While some promoters display ubiquitous activity, monitoring

cell differentiation *in vivo* relies on the contrast agent to be under a cell type specific promoter.

Choosing the appropriate promoter is one stage in improving transgene expression *in vivo*. Optimisation of the oft omitted elements, such as locus control regions and matrix attachment vectors, will enable expression more homologous to naturally occurring genes, in turn enabling stronger and increasingly stable gene expression (Papadakis *et al.* 2004).

1.4.4.1 Animal Models

Many of the main pathological and behavioural attributes of HD can be mimicked through use of a number of exogenous agents. Metabolic toxins, such as malonate and 3-nitropropionic acid who's primary target is the mitochondrion, result in selective striatal toxicity by inhibition of succinate dehydrogenase (Fernandez-Gomez *et al.* 2005) (Garcia *et al.* 2002; Huang *et al.* 2006). Its use has provided indications to the nature of HD pathophysiology; and excitotoxic amino acids such as kainic acid that has been superseded by quinolinic acid (QA) which is more reflective of HD pathophysiology. Excitotoxic amino acids such as kainic acid and quinolinic acid (QA) (the latter being more reflective of HD pathology) selectively kill the medium spiny GABAergic neurons and spare NADPH diaphorase neurons. Since the causative gene was identified, transgenic mice have been developed covering a range of CAG repeat lengths and exhibiting a progressive neurological phenotype (Mangiarini *et al.* 1996). More recently transgenic rhesus macaques have been created expressing exon 1 of the human *HTT* gene with 84 CAG repeats (Yang *et al.* 2008).

In the case of PD, the most common model used is the 6-OHDA lesion approach that ablates the ventral mesencephalic neurons of the substantia nigra.This mimics the nigrostriatal dopamine depletion found in PD with associated behavioural deficits (Heuer *et al.* 2012). These models provide the basis for pre-clinical trials and facilitate optimisation of protocols for transplantation therapies, such as optimum age of foetal donor tissue.

Provision of longitudinal evaluation of experimental animal models is an important stage in preclinical analysis for human cell transplantation in neurodegenerative diseases. The use of the immunosuppressant Cyclosporin A and its associated side

effects limit behavioural testing over long survival times (Murray *et al.* 1985). A neonatal desensitisation strategy has allowed long-term graft survival in the adult rat brain (Kelly *et al.* 2009a). The enduring survival of grafted animal models has been addressed and the available end point analysis, IHC, misses vital opportunities to study this model longitudinally, demonstrating the need for strategies to fully reap the benefits these experiments provide.

1.4.4.2 Graft Analysis

Following transplantation of cells in animal models, progression of graft development can only be determined with behavioural techniques and then post mortem analysis using IHC. IHC allows analysis at one time point and events up to that point can only be inferred. For animal studies this means a larger number of animals must be sacrificed to follow the graft over time (Pundt *et al.,* 1996). It is primarily histochemical techniques that have elucidated what we know about the structure of the brain and graft development so far. A variety of markers are used to elucidate cell types and distinguishing graft from host, such as markers specific for human nuclei when grafting human tissue into rodent models. Some useful markers are listed in table 1.1.

Stem cells raise their own unresolved concerns regarding grafting. Following transplantation of human stem cells into rodent brains, the absence of tumours at a given time point following transplantation do not exclude the possibility that they would have occurred subsequently (Lindvall, Kokaia and Martinez-Serrano 2004). It has been shown that implantation of ES cells into the species from which they were derived are more prone to formation of teratomas compared to xenotransplantation (Erdö *et al.,* 2003). This only acts to emphasize the importance of rigorous *in vivo* analysis to follow migratory stem cells while distinguishing between host and donor.

	Description
Donor cell markers	
HuNu	Human nuclei (detection of human cells grafted into rodent models)
GFP, lacZ	Reporter genes used to tag donor cells
Neural markers	
MAP2	Microtubule assembly – essential for neurogenesis
Doublecortin	Microtubule-associated protein-neuronal precursor cells and immature neurons
NeuN	Neuron-specific nuclear protein
β- tubulin	Neurons
TH (Tyrosine hydroxylase)	Dopaminergic cells (Typically for PD)
DARPP 32 (dopamine- and cyclic AMP-regulated phosphoprotein, 32kDa)	Mature medium spiny neurons
AChE (acetylcholinesterase)	Patch matrix structure of the striatum
CNS marker	
GFAP (Glial fibrillary acidic protein)	Astrocytes
Immune response marker	
Iba1	Macrophages and microglia
CD68	Macrophages
Ox42	Macrophages

Table 1.1: Typical Histochemical Markers

1.5 Aims

To determine the potential of transgenes based on expression of a CEST artificial gene and ferritin as MRI contrast agents, alongside the widely used SPIO contrast agents. To determine if Ftl/Fth works successfully as a MRI contrast agent transgene, and if it will provide better contrast and less toxicity to the cells than when only Fth is overexpressed which is often expressed alone in the literature. To try and increase the speed of the CEST scans so they are more applicable to *in vivo* tests without compromising the quality. Finally, to determine how the resulting MRI contrast from SPIOs can be interpreted compared to graft measurements using IHC.

2 General Methods

2.1 Plasmid Construction, Molecular Cloning

Plasmids

*Plasmid maps in Appendix 1. Plasmids marked with * were gifted by Jody Haigh (Nyabi et al. 2009).*

DV2*   Destination vector for ROSA26

LRP   200 lysine residue plasmid gifted from Assaf Gilad (Gilad *et al.* 2007)

pCAGGS-CreIRES-puro Cre recombinase plasmid for floxing out STOP codon

pEC   pCAGGs and IRES EGFP

pEC-FtI/Fth   pEC vector with the FtI/Fth transgenes

pENTR-2B   For entry of GOI into the Gateway system (Invitrogen)

pENTR-IRES-eGFP-Luc* pENTR vector containing marker

pENTR-pCAGGs*   pENTR vector containing promoter

pENTR-2B-FtI/Fth   pENTR vector containing Ft subunits

Targeting Vector FtI/Fth Combination of pENTR vectors and DV2

2.1.1   Production of Competent Cells

Modified from p1.82-1.84 (Sambrook *et al.* 1989)

A stab was taken from -80 °C stock of DH5α (Invitrogen, California, USA), transferred to 10mls Luria-Bertani (LB) media (Invitrgoen) and grown at 37°C in a rotary shaker, 220 rpm, for approximately three hours until OD_{600} = 0.35- 0.4.

In House Production of Chemically Competent Cells

Cultures were cooled for 10 minutes on ice to 0 °C then centrifuged at 4000 rpm for 10 minutes at 4 °C. Supernatant was removed and allowed to drain away by inverting the tube for one minute on a paper towel. The pellet was resuspended in 10

ml of ice cold 0.1M $CaCl_2$, incubated on ice for 30 minutes in a cold room at 4 °C, followed by centrifugation at 4000 rpm for 10 minutes at 4 °C. Supernatant was then decanted from the cell pellets and excess allowed to drain away. Each pellet was resuspended in 1.2 mls of ice cold 0.1 M $CaCl_2$ and left for 1-1.5 hours in a cold room at 4 °C. 800 µl of 50% Glycerol and 50% $CaCl_2$ was added, the sample was then divided into 100 µl aliquots using cold pipette tips and stored at -80 °C.

In House Production of Electro competent cells

Cells were aseptically transferred to ice cold 50 ml falcon tubes and cooled to 0 °C for 10 minutes. Cells were recovered at 4000 rpm for 10 minutes at 4 °C, the media decanted away and the pellet resuspended in ice-cold 10 mM $CaCl_2$ at half the volume of the original media used. Cells were centrifuged at 4000 rpm for 10 minutes, 4 °C. The same steps should be taken once again using 1/50 then 1/500 dilutions to resuspend the pellet in two more stages. For the final resuspension of the pellet a 10 % glycerol in $CaCl_2$ solution was used and cells subsequently stored at -80 °C.

2.1.2 Transformation of Competent *E. coli*

Heat Shock

For the transformation, 5 to 10ng of plasmid DNA was added to One shot DH5α or library efficiency DH5α chemically competent *E. coli* (Invitrogen or in house produced) and left on ice for half an hour. The cells were heat shocked at 42 °C for 45 seconds and replaced back on ice for two minutes. 0·9 ml of SOC media (Invitrogen) was added to the bacterial suspension and incubated at 37 °C, in a rotary shaker at 220rpm for one hour. Dilutions of the suspension were plated on LB agar with the appropriate antibiotic as well as plates of neat suspension, the remaining bacterial suspension was spun down for three minutes and streaked onto a separate plate in 150 µl solution. The plates were incubated overnight at 37 °C.

Electroporation

Immediately on defrosting electrocompetent cells, 5 to 10 ng of plasmid DNA was added with gentle dispersion of the DNA throughout the *E. coli* and 50 µl aliquoted into a 2.0 mm BioRad cuvette (BioRad, California). *E. coli* was electroporated in a BioRad machine at 2.5 kV and immediately transferred to 1 ml of SOC (Invitrogen)

media and incubated for one hour at 37 ℃, 220 rpm. Suspensions were streaked on LB agar plates with the appropriate antibiotic and incubated overnight at 37 ℃.

2.1.3 Plasmid Mini Prep

For all preparations of plasmid DNA either a colony from a master plate was picked or a stab taken from a glycerol stock, grown in 2 ml of LB media containing the appropriate antibiotic, overnight, at 37 ℃, in a rotary incubator at 220 rpm. The resulting culture was centrifuged for three minutes at 12,000rpm, to obtain a pellet. Minipreps were run using one of a number of techniques, typically alkaline lysis was used to screen a number of colonies and kits used when samples were to be sequenced. The samples of DNA were run on an agarose gel to check quality and quantity as well as a checking the concentration on a Nanodrop 2000 (Thermo Scientific, Massachusetts, USA) and stored at -20 ℃.

Several methods were tested and optimised for plasmid cloning, these include STETL p1.29, 1.34 (Sambrook *et al.*, 1989), but for routine plasmid preparations the Alkaline Lysis method and Qiagen (UK) kit were used.

Qiagen or Machery-Nagel

The bacterial suspension was centrifuged and either a Macherey-Nagel (Cat No. 744588, Germany) or Qiagen (Cat No. 27106, Germany) mini prep was performed on the resulting pellet according to manufacturer's instructions.

Alkaline Lysis Miniprep

Adapted from p1.25-1.28, B.22 (Sambrook *et al.*, 1989)

The pellet was resuspended in 100ul of autoclaved solution I (50mM glucose, 25mM Tris Cl (pH 8.0), 10mM EDTA (pH 8.0)) by vigorous vortexing, 200ul of freshly prepared solution II (0.2N NaOH, 1% SDS) was added and the tube inverted a number of times. This was left on ice for 3 minutes before 150ul ice cold solution III (5M potassium acetate, glacial acetic acid, water) was added and once again the tube inverted a number of times until the components were thoroughly mixed. This was spun for 5 minutes at 12,000 rpm and the supernatant decanted off into a phase lock gel tube (5Prime, Germany) with an equal volume of phenol chloroform and shaken by hand. This was spun for 5 minutes, at 12000 rpm and the aqueous phase

removed. An equal volume of isopropanol was added Twice the volume of 100% ethanol was added, votexed briefly and spun for 5 minutes, 12000 rpm leaving a pellet. This was repeated with 100µl 70% ethanol but without vortexing. Following this, as much liquid as possible was removed from the pellet and it was left for a few moments to dry. The pellet was redissolved in 50 µl of TE with RNase A (20ug/ml) (Sigma, USA).

2.1.4 Endotoxin Free Maxiprep

To produce large amounts of endotoxin free plasmid DNA an Endofree maxiprep kit (Cat No. 12362, Qiagen) was used according to the manufacturer's instructions. A colony was either picked from a master plate or a stab from a glycerol stock was taken and inoculated in 3 ml of LB media with appropriate antibiotic for 8 - 12 hours at 37 ºC, 220rpm. 100 µl of this suspension was then used to inoculate 100 ml of the same media overnight under the same conditions. The resulting bacterial suspension was harvested by centrifugation at 4 ºC, 6,000 x g for 15 minutes and the Qiagen kit method carried out according to manufacturer's instructions.

2.1.5 Glycerol Stocks

Stocks of the *E. coli* containing the plasmid of interest were made by adding 60% glycerol to 500 µl of the bacterial suspension from an overnight culture at a 1:1 ratio, and mixing well. Stocks were stored at -80 ºC.

2.1.6 Restriction Digests

Restriction digests were performed to check ligations and subcloning purposes. Enzymes were bought from a number of companies including NEB (New England, USA) and Fermentas (Germany). Incubation temperature and time was enzyme and DNA concentration dependent, varying between 15 minutes and 4 hours. In each case reactions were set up using manufacturer's buffers and conditions, a typical reaction was set up as shown below.

DNA	(0·2 -1µg for plasmid checks, 5 µg – 40 µg for cloning)
Restriction Buffer (10X)	1X
BSA (100X)	1X (dependent on enzyme)
Restriction Enzyme	1µl is usually sufficient, dependent on enzyme
Water	Make up to 25 µl for checks, 100-150 µl for cloning

Compete digestion was checked by gel electrophoresis. The restriction enzymes were inactivated through heating if necessary at 65 ºC for 20 minutes and the DNA purified by gel extraction or phenol/chloroform precipitation.

If downstream ligation reactions were required the vector was treated using calf intestinal alkaline phosphatase (CIP) (NEB). 0·5 units of CIP would be added directly into the reaction after a complete digestion had been confirmed and restriction enzyme inactivation. The sample was incubated for 20 minutes at 37 ºC followed by purification.

2.1.7 Agarose gel electrophoresis

DNA fragments to be analysed were run on 0.8 – 2 % (w/v) agarose gels, dependent on fragment size, containing 2·5 µl safeview (NBS biologicals, England, UK) for every 100ml of gel. Guanosine (1mM) (Sigma) was added to the agarose gel when carrying out a gel extraction downstream, to protect digested DNA aginst UV damage (Grundemann and Schomig 1996). The gel was placed in a tank containing 1x TAE buffer (40 mM Tris, 1µM EDTA pH 8·0. 0·1 % Acetic Acid) and run at a constant voltage of 100 V for half an hour upwards. Fragments were identified against a 100bp or 1kbp ladder that was run simultaneously. Bands were viewed using a wavelength of 254 nm, when bands need to be excised to limit DNA damage a wavelength of 365 nm was used.

Fragment Extraction from Agarose Gels

Digested vectors and/or inserts were visualised under UV light (365 nm) with a protective cover and excised from gels using either a sterile scalpel or gel extracting pipette tip. The fragment was purified using a QIAQuick Gel Extraction Kit from Qiagen in accordance with the manufacturer's instruction.

2.1.8 DNA Purification

Qiagen PCR Purification kit

DNA was purified using Qiagen's QIAquick purification kit (Cat No. 28104) based on the manufacturer's instructions.

Phenol Chloroform Purification of DNA

To purify the DNA one volume of phenol:chloroform:isoamyl alcohol 25:24:1 (Sigma) was added to the sample and briefly vortexed to mix, followed by centrifugation at 13,000 rpm for 5 minutes. Supernatant was moved into a new polypropylene eppendorf. The above steps were then repeated with chloroform only. 0·1 volumes of sodium acetate, 3M, pH 5·0, 1µl of glycogen and 2·5 volumes of 100 % ethanol are then added before precipitating at either -80 ºC for one hour, -20 ºC overnight or 15 minutes on dry ice. The sample was then spun down for 10 minutes at max speed. Supernatant was removed, 100 µl of 70 % ethanol was added and centrifuged at maximum speed for 10 minutes. Supernatant was aspirated off and the pellet left to dry for up to 10 minutes and subsequently dissolved in 30 – 100 µl 0·5× TE or water.

2.1.9 Ligation

Inserts were ligated into plasmids as part of various subcloning steps. Vector and insert concentrations for the ligation reactions were determined using the following formula, with vector concentration at 100ng:

Vector concentration (µg)/vector size (bp) = insert concentration (µg)/insert size (bp)

The DNA vector to insert ratios typically used were 1:3, 1:5, 1:8. DNA was combined with T4 DNA ligase and ligation buffer containing dNTPs in the smallest possible volume without the enzyme exceeding 10 % and left at room temperature overnight.

2.1.10 TOPO

The TOPO reaction was carried out as follows using Zero-Blunt-TOPO cloning kit (Cat No. K2800, Invitrogen), 2µl of the fresh PCR reaction was added to 0.5µl of the salt solution and 0.5µl to the pCR®II-Blunt-TOPO® and incubated at room temperature for 5 minutes before being placed on ice. The whole 3µl reaction was transformed using the relevant competent cell type and grown using the required antibiotic resistance (see *E.coli* transformation section).

2.1.11 Gateway

LR Clonase reactions: LR reactions were performed using Gateway® Clonase Enzyme mix (Invitrogen) following manufacturer's instructions with brief previous modifications based on Nyambi *et al*'s work (Nyabi *et al.* 2009). For the multisite LR

reactions 100ng of each of the three pEntry vectors containing eGFP luciferase, pCAGGs or the GOI were incubated for 8 hours at room temperature with LR Clonase II mix. The pROSA26 destination vector, DV2, was then added with additional Clonase II mix over night at room temperature. Protinase K incubated for 10 minutes at 37°C to stop the reaction.

2.1.12 RNA extraction

ES cells were either harvested as described above and mixed with RLT buffer (from Qiagen RNAeasy kit) and 1 µl β- Mercaptoethanol per 100 µl buffer RLT to denature ribonucleases during cell lysis or RLT buffer was added directly to the plate after media had been aspirated off and adhesive cells were scrapped off. Qiashredder (Cat No. 79654, Qiagen) and RNeasy kits (Cat No. 74104, Qiagen) were used to extract RNA from the cells and the concentration of RNA was determined on the NanoDrop. DNase treatment is performed simultaneously as recommended by the manufacturer's protocol when carrying out the QIAshredder kit using RNase-free DNase (Cat No. 79254, Qiagen). RNA was stored at -80°C.

2.1.13 First Strand Synthesis

To make the cDNA 1 µg in 10 µl of DNAse treated RNA, as measured on the NanoDrop, was added to the following mixture:

1µl	1/12 dilution of random primers (3 µg/µl) (Invitrogen)
1 µl	10mM dNTP mix
X µl	water to total 12 µl

This was heated to 65 ºC for 5 minutes, then chilled on ice after a quick spin before the following components were added:

4 µl	5 x first strand buffer
2 µl	0.1M DTT
1 µl	RNAse Out Rnase Inhibitor (Invitrogen)

This was incubated at 25 ºC for 2 minutes before 1 µl of Superscript II RNAse (Invitrogen) was added, then incubated at 25 ºC for 10 minutes, 42 ºC 50 minutes and finishing with 70ºC for 15 minutes. PCR amplification reactions were then carried out on the cDNA.

2.1.14 PCR amplification

PCR was used for cloning, plasmid analysis and RT PCR. The different primers used are shown in table 2.1. Primers were designed using NCBI's primer BLAST and sigma genosys primer calculator (http://www.sigma-genosys.com/calc/DNACalc.asp) and checked for specificity when necessary using NCBI BLAST.

Primers optimisation included modifying the $MgCl_2$ concentration, temperature gradient and addition of DMSO.

To amplify inserts from plasmids, forward and reverse primers flanking the region of interest were ordered (Eurofins MWG Operon, Germany) with various additions to the original DNA when required. The reaction (see typical reaction below) underwent an initial denaturation of 95 ºC for 5 minutes, and typically 35 cycles of denaturing, annealing and elongation in a thermal cycler (Techne, TC 512). Each step had a specific temperature depending on DNA and polymerase used. Followed by a final extension for 5 minutes and stored at 4 ºC.

A Typical Reaction:

DNA	0·1-5ng/µl
Primers (10µM)	1:1 ratio
Polymerase	0·5 µl
dNTPs (10mM)	0·5µl
Buffer (10x)	2·5µl
$MgCl_2$	1-4mM
Water	x µl up to total volume of 25 µl

Sequence checks for PCR products

Once a clonal population had been established with the appropriate PCR fragment, the correct amplification of that fragment was confirmed through sequencing. Miniprepped samples were sent to in house Sequencing Core at Cardiff University. Data was received as text files and electropherogram and compared with original text sequences using NCBI's Nucleotide BLAST to align two sequences. Sequences were stored in a database for use in Vector NTI.

Primers	Sequence 5'-3'	Notes
Ferritin modification primers		
Ftl kozak (F)	ATA GAA TTC GCC GCC ACC ATG AGC TCC CAG ATT CGT CAG	Adds Kozak sequence to Ftl
Ftl 2A (R)	ATA GGA TCC TGG GCC AGG ATT CTC CTC GAC GTC ACC GCA TGT TAG CAG ACT TCC TCT GCC CTC TCC ACT GCC GTC GTG CTT GAG AGT GAG	Adds BamHI and 2A and removes stop from 3' end of Ftl
Fth EcoRI (R)	CAT GAA TTC TTA GCT TTC ATT ATC ACT	Add EcoRI to 3' end of Fth
Fth BglII (F)	ATA AGA TCT ATG ACG ACC GCG TCC ACC	Add BglII to 5' end of Fth
Confirmation of Expression clone recombination and Position in Genome		
PCAGGS R1	CCC CCT GAA CCT GAA ACA TA	
Ft L1	GTA GGA GGC CTG CAG GTA CA	
Luc R3	AGC CAG ATT TTT CCT CCT CTC	
ROSA R3	ACT CCA CTG CAG CTC CCT TA	
G1for	TAG GTA GGG GAT CGG GAC TCT	
R26 3' RC	GCG GGA GAA ATG GAT ATG AA	
Luc L3 RC	GAG AGG AGG AAA AAT CTG GCT	
GAPDH F	ACC ACA GTC CAT GCC ATC AC	
GAPDH R	TCC ACC ACC CTG TTG CTG TA	
Southern probe primers		
R26 5' probe F	GGA ACA ATT GGC AAA AGG AA	
R26 5' probe R	CTA CTC TGG TCT CCC CTT TTT G	
R26 3' probe F	GGC ACT GTT CAT TTG TGG TG	
R26 3' probe R	TGG AGG CTA GAA GCT GGT GT	
Sequencing Primers		
M13 Reverse	CAG GAA ACA GCT ATG AC	
M13 (-20) forward	GTA AAA CGA CGG CCA G	
Expression check		
LacZ F 70	CGG TGA TGG TGC TGC GTT GGA	
LacZ R 71	ACC ACC GCA CGA TAG AGA TTC	
FTHF1		
FTHR1	GCT TTC ATT ATC ACT GTC TCC C	
FTHCheck F	TAC GCC TCC TAC GTT TAC C	
FTHCheck R	GCT TTC ATT ATC ACT GTC TCC C	
LRP sense	GAA AGG ATC TAT GAA GAA GA	
LRP antisense	CGG CCA GTA ACG TTA GGG GG	

Table 2.1: Primers used in this report

2.1.15 Southern Protocol

Southern protocols were either carried out according to manufacturer's instructions or adapted from p 9.31-9.57 of (Sambrook *et al.* 1989)

DNA isolation from ES cell clones in 96-well plates

This procedure allows cell lysis, DNA precipitation and the restriction digestion in the original 96-well plate where ES cells were grown (Ramírez-Solis *et al.* 1992). Two replica plates were used for DNA isolation, one is processed for Southern blot analysis, leaving the second plate as a back up stored at -20 °C. Cells were lysed and genomic DNA isolated when the majority of clones were confluent. The orange colour of the media within 24 hours after its change indicates the correct high density of cells.

Media was aspirated from each well and washed twice with PBS. 50 µl lysis buffer (10 mM Tris-HCl, pH 7.5; 10 mM EDTA; 10 mM NaCl; 0.5% sarcosyl; 1 mg/ml Proteinase K added directly before use.) was added to each well. Plates were incubated overnight at 55 °C in a humid atmosphere achieved through wrapping the plates in parafilm and placing in a container with wet paper towels. The next day, 100 µl of cold NaCl/ethanol mixture (150 µl of 5 M NaCl per 10 ml of cold 100% ethanol, prepared fresh) was added to each well. The plate was left undisturbed at room temperature for at least 60 minutes until the precipitated DNA attached to the dish, which showed white against a dark background. Liquid was drained by gently inverting the plate on a paper towel. Wells were rinsed with 150-200 µl 70% ethanol, inverting the plate each time. DNA can be stored in 70% ethanol at –20 °C. Plates were inverted after the final wash and allowed to air dry for 10-15 minutes before being resuspended in TE or water.

Extracting genomic DNA From 10cm plates

ES cells were cultured to 90% confluency on a 10cm petri dish (Nunc), the media was aspirated off cells were washed once with PBS. The cells were removed by adding 2.5mls trypsin (Invitrogen) and incubating for 2 minutes at 37ºC, the cells were spun down, the trypsin aspirated off then washed for with PBS. Four millilitres of lysis buffer (100mM Tris-HCL (pH 8.5), 5mM EDTA, 0.2% SDS, 200mM NaCl, 100µg/ml Protinase K) was added and cells transferred to a 15 ml eppendorf that was incubated overnight at 55ºC. The sample was agitated at room temperature for

15 minutes then one volume of Tris buffered phenol was added and incubated for 30 mins at room temperature, gently agitated. Following centrifugation at 13000rpm for 5 mins the aqueous phase was removed and added to an equal volume of phenol/chloroform (Sigma), this was incubated for 30 mins, centrifuged at 13000rpm for 5 mins and the aqueous phase removed and added to an equal volume of chloroform. It was gently agitated and spun for 5 mins, once the aqueous phase was removed the DNA was precipitated by adding one volume isopropanol and 1/10 volume sodium acetate and rocked at room temperature until DNA precipitate was visible. This was spooled out and washed twice with 70% ethanol and the pellet collected by centrifuging and aspirating off all ethanol. Any residual ethanol was air dried and the pellet dissolved in an appropriate volume of TE or water and left at room temperature overnight to dissolve. The DNA was measured either by running a sample on a gel or shearing a sample with vigorous pipeting and measuring on a Nanodrop 2000. Samples were stored at 4 ºC.

Transfer of DNA to solid supports

After cutting typically 10-20µg DNA with appropriate restriction enzymes (see section 2.1.6), the sample was run on a 0.7% agarose gel at 15V, o/n, alongside a 1kb DNA ladder. The gel and ruler was imaged by UV using a Gel Doc 2000 (BioRad). The DNA was depurinated in 0.25M HCl for 15 minutes, then denatured in 0.4M NaOH for 30 mins. The capillary transfer method was used to transfer the DNA fragments from the agarose gel to the Hybond N+ nylon membrane (GE Healthcare) using 0.4M NaOH over night. Capillary action was maintained by stacking dry paper towels upon 5 pieces of Whatmann paper on top of the membrane.

The membrane was neutralized with 0.5M Tris HCl, pH 7.7 for 30 mins with gentle agitation. The membrane was air dried and the DNA crosslinked to the membrane using UV (254nm at 0.120 joules/cm^2) crosslinker (Kill Bond, UVI-tec).

Southern's were performed using the Phototope kit (NEB) and following the manufacturer's instructions or using ^{32}P. The probes were PCR amplified from genomic DNA and purified using a PCR purification kit (Qiagen).

The amount of probe necessary was determined through the following equation:
(membrane area (cm²)) x (hybridization solution (ml/cm²)) x (template concentration (ng)) = Probe (ng)

Probe Labelling using Biotin

Following NEBlot Phototope Kit (Cat No. 7550, NEB) 100ng of template DNA was diluted in 34µl of nuclease free water and denatured for 5 mins at 100ºC then transferred to ice for 5 mins before briefly centrifuging. Klenow fragments, dNTPs with biotin dATP and labelling mix containing biotinylated random octamers was added to the template DNA and incubated at 37ºC for one hour. The reaction was terminated with 0.2M EDTA pH 8.0. The synthesized probes were separated from unincorporated nucleotides adding 1/10 volume NaAc and one volume Isopropanol mixing and spinning for 5 minutes (see ethanol precipitation in General Methods 2.1)

Determining level of Probe Biotinylation

Serial dilutions of the probe in 0.1 N NaOH were made ranging from 10^{-1} to 10^{-7} and 1µl was dropped onto Hybond membrane. Alongside these the biotinylated control DNA and Biotinylated 2-Log ladder were diluted to 10^{-7} and spotted alongside. After they had completely dried the Phototope Star detection kit (NEB) was used to detect the dilution sets.

Southern Protocol

20x SSC was prepared by dissolving175.3g NaCl and 88.2g Na citrate into 800ml H2O then adjusting to pH 7.0 with 1M HCl the volume was made up to 1 litre with H2O and sterilized through autoclaving.. The membrane containing the target DNA was immersed in a tray of 6x SSC for 2 minutes then slipped into a heat sealable bag with 0.2 mls of prehybridization solution (5x Denhardt's reagent (Sigma), 0.5% SDS, 100µg/ml denatured, fragmented fish sperm (Roche, Switzerland), 6 x SSC) for each square cm of membrane. Once as much air as possible was removed from the bag it was heat sealed shut and incubated for 2 hours at 68ºC. The bag was opened at the corner and 20ng/ml of probe was added and the bag resealed and incubated over night at 65 ºC with moderate shaking. The next day the membrane was washed starting with 2x SSC, 0.5% SDS room temperature, 5 mins, then 2x SSC and 0.1% SDS for 15 mins. Followed by a 0.1x SSC and 0.5% SDS wash at 37 ºC for one hour then change the membrane to a fresh batch of the solution at wash for a further hour at 68 ºC. The final wash was briefly in 0.1x SSC with no SDS before moving on to phototope detection.

Phototope Detection

For detection of biotinylated DNA on Southern Blots and Dot blots Detection Solutions (DS) A (1x) (5% SDS, 125mM NaCl, 25mM sodium phosphate, pH 7.2), B (1/10 dilution of solution A) and C (1x) (10mM Tris-HCL, 10mM NaCl, 1mM MgCl$_2$, pH9.2) were first prepared. All washes and incubations below are done at rt for 5 mins with moderate shaking unless otherwise stated. The membrane was placed in a hybridization bag with 0.1ml of DS A per cm^2 to wash. The wash was replaced by 0.05 ml per cm^2 of a 1/1000 dilution of streptavidin stock in DS A and incubated in abovementioned conditions. The membrane was then washed twice with 0.5ml per cm^2 of DS B. The biotinylated alkaline phosphatase was diluted 1/1000 with DS A and added at 0.05 mls per cm^2 and incubated with the membrane. The solution was washed in 0.5mls per cm^2 DS A then twice with 0.5mls per cm^2 of 1x DS C. To detect the DNA the CDP-Star reagent was diluted at 1:100 in 1x CDP-Star dilution buffer, reflecting applications recommended for maximum sensitivity. The solution was added at a volume of 0.025 mls per cm^2 of membrane to the hybridization bag and incubated as normal. Chemiluninescent film (Roche) was used to detect the biotinylated probe at an exposure time of one minute at 30ºC.

Probe Labelling Using ^{32}P

An NEBlot kit (Cat No. N1500, NEB) was used to label the probes with α ^{32}P dCTPs. Briefly, the template DNA was denatured at 100°C for five minute and moved to ice for five minutes before a short centrifugation. The template was incubated at 37°C for one hour with buffer containing octadeoxyribonucleotides, dNTPs, α ^{32}P dCTP (50µCi) and DNA polymerase I – Klenow fragment. The reaction was terminated by addition of 0.2M EDTA pH8.0. To remove the unincorporated nucleotides a filter was prepared with glass wool and Sephadex and centrifuged for one minute at 1000rpm. The probe was denatured as above and transferred onto the sephadex and centrifuged for one minute at 1000rpm, followed by an addition of TE buffer to wash through any remaining probe. The flow through was collected and added to the hybridisation buffer.

Prehybridisation of the membrane was carried out using Church Buffer with salmon sperm (100µg/ml) for one hour at 65°C. The probe was added to the buffer and incubated overnight at 65°C.

The membrane was washed with 2x SSC, 0.5% SDS room temperature for 5 minutes. Radioactivity was checked with a Geiger counter before determining whether to continue with a second wash using 0.1x SSC, 0.1% SDS for 30 minutes. Further washes were based on Geiger counter readings.

Super RX Fuji Medical X ray film (FujiFilm) was exposed to the membrane over various time intervals and the membrane developed.

Stripping Southern Membranes

The membrane was rinsed in water and incubated at 0.4 N NaOH, 0.1% SDS at 80ºC for 30 mins. It was then rinsed for a further 30 mins at 25 ºC in 0.2 M Tris-HCl, 0.1 x SSC. The membrane was either stored in 1x SSC at 4ºC, 20ºC or directly reprobed.

2.1.16 Western Blot

Western protocols were adapted from 18.60-18.75 of (Sambrook *et al.* 1989)

Protein Extraction from Cells in Monolayer

Confluent 6 cm dishes were washed with cold PBS and placed on ice. 500µl of ice cold lysis buffer (RIPA buffer (Sigma), 1x complete mini solution (Roche, Switzerland)) was added and cells scraped with a rubber policeman (Corning Incorporated, Corning, USA). Cells were incubated for 30 minutes at 4 ºC with intermittent agitation after which they were centrifuged for 20 minutes at 4 ºC at 12,500 rpm. The supernatant was transferred to a fresh tube and the pellet discarded, samples were stored as aliquots at -80 ºC.

Protein Extraction from Liver Tissue

Human foetal liver was collected from an elected abortion, crown-rump length 33mm washed in PBS and added to RIPA buffer and 1x complete mini protease inhibitor cocktail (Roche). The liver was then homogenised using lysing matrix tubes (MPBio, California, USA) and a Precellys 24 lysis and homogeniser (Bertin Technologies,). The homogenised solution was incubated at 4°C for 30 minutes and centrifuged at 4°C for 20 minutes, at 13, 000rpm. The supernatant was aliquoted into fresh tubes and stored at -80°C.

Protein Assay

A standard was prepared using a dilution series of bovine serum albumin (BSA) ranging from 2mg/ml to 25µg/ml, and 25µl of each standard were triplicate plated in a 96 well plate alongside 25µl of the unknown samples. The bicinchoninic acid (BCA) working reagent from the Pierce BCA Protein Assay kit (Cat No. 23227, Thermo Scientific) was prepared as recommend by the manufacturer and 200µl was added to each sample and mixed thoroughly on a plate shaker for 30 seconds. The plate was incubated at 37°C for 30 minutes and then allowed to cool to room temperature. The absorbance was read using a Bio-Tek plate reader (Epson, California, UK) at an absorbance of 590nm.

Western Blot

A polyacrylamide resolving gel was prepared and left to set with distilled water layered on the surface. The water was removed and replaced with a stacking gel and left to set with the appropriate comb size. Lamaelli's loading buffer (Sigma, UK) was added to the protein at a 1:1 ratio and incubated at 95°C for five minutes to denature the protein samples. Samples were loaded into the gel wells alongside a full range rainbow ladder (GE Healthcare, UK) and run at 80V through the stacking gel and 120V through the resolving gel for two hours. The Hybond ECL membrane (GE Healthcare, UK) was soaked in distilled water briefly and then in transfer buffer for 10 minutes. The gel, sponges and four pieces of filter paper were soaked in transfer buffer before being layered with the filter paper sandwiching the gel and membrane. The transfer took place overnight in a cold room at 25V, with a magnetic spinner in the tank. The following day the membrane was washed in TBS once, then washed once with wash buffer, stained briefly with Ponceau S (0.1% Ponceau S in 5% acetic acid) and washed four to five times in wash buffer on a shaker to remove the stain. Antibody blocking solution was added and incubated for one hour, shaking. The solution was then changed to new blocking buffer including the antibody at the appropriate concentration and left for two hours. The membrane was then washed six times for five minutes each with Wash buffer. The appropriate secondary horseradish peroxidase linked whole antibody, at a dilution of 1/10000 in blocking solution, was incubated with the membrane for one hour. The membrane was washed with Wash buffer six times. The membrane was placed in a developing cassette and 0.5mls of SuperSignal West Dura Stable peroxide buffer (Thermo

Scientific, Massachusetts, USA) mixed in a 1:1 ratio with SuperSignal West Dura Liminol/Enhancer solution placed on the membrane for five minutes. The solution was poured off and Chemiluminescent film (Roche) was placed over the membrane and exposed for various time intervals.

2.2 *In Vitro* Methods

2.2.1 Culture and Maintenance of Mouse ES Cells

The ES cell line E14 was used in this study (Hooper et al 1987). It was derived from the inbred mouse strain 129/Ola in 1985 by Dr. Martin Hooper in Edinburgh, Scotland, and obtained in 1990 at passage 11. The mouse cell line E14 (Hooper *et al.,* 1987) has been used extensively in this lab (Bouhon *et al.,* 2005; Battersby *et al.,* 2007) and due the ease with which it can be transformed (Tsuda *et al.,* 1997) will be used in this study. Two other cell lines derived from E14 were used because their modifications that could benefit downstream analysis. The Tau-GFP cell line carries a tau-tagged GFP protein that is ubiquitously and constitutively expressed (Pratt *et al.* 2000), and the 46C cell line was created by a GFP knock in to the open reading frame of the *Sox1* gene (Ying *et al.* 2003) All three cell lines were gifted historically to Nicholas Allen.

Mouse ES cells were maintained in ES cell culture medium, which consisted of Knock Out DMEM (Gibco, Invitrogen), supplemented with 15% knockout serum replacement (KSR) (Gibco, Invitrogen), 1% Penicillin / Streptomycin (Invitrogen), non-essential amino acids (1mM) (Invitrogen), L-glutamine (2mM) (Invitrogen), β-mercaptoethanol (0.1mM) (Sigma) and 1000U/ml leukaemia inhibitory factor (LIF) (Chemicon, California, USA) or the appropriate volume of LIF produced in house (See Appendix 2).

ES cells were maintained on 10 cm, 6 cm, 6 well, 24 well or 96 well plates (Nunc, Thermo Scientific), depending on application coated with 0.1% gelatin (Stem cell Technologies, France). Medium was changed daily and cultures were passaged every 2-3 days depending on the degree of confluence. When passaging, culture medium was aspirated off and cells were washed with phosphate buffered saline (PBS) pH 7·4 (PAA labs, Austria), 0.1% Trypsin/EDTA (Invitrogen) was applied to lift off adhesive cells and left at 37 ºC for 2-3 minutes. The enzymatic process was inhibited by addition of ES cell culture medium. Cells were harvested by

centrifugation for three minutes at 1000 rpm and resuspended in the appropriate volume of ES cell culture medium. The cells were counted using a haemocytometer and replated at 1.8 x 10^6 cells per 10 cm plate.

2.2.2 Differentiation using chemically defined media

When cells were approximately at 60% confluency, the plate was split using Accutase (PAA) for 15 mins at 37 °C, cells were then washed in PBS and 5x10^5 cells were plated onto a 10cm dish in Neural differentiation media (ADF) (Gibco). ADF consisted of Advanced DMEM F12 (Gibco) supplemented with Lipid concentrate (1x) (Gibco), Transferrin (7.4µg/ml) (Sigma), Insulin (10mg/ml) (Calbiochem), β-mercaptoethanol (0.1mM) (Sigma), Pen/Strep (1x) and Glutamine (1x). Cells were grown as sphere cultures and media was changed every second day by harvesting the cells through centrifugation at 500rpm for three mins and resuspending in new ADF. From day four FGF2 (20ng/ml) (Peprotech) was added to the media. Cells were plated on poly-L-ornithine (PAA, Stem Cell Technologies) dependent on end point; 2.5 x 10^4 cells in 50µl were plated per well on a 24 well plate when cells were to be fixed, and 5 x 10^5 plated on a 10cm when they were to be transplanted. For transplantation cells were grown to day 16. When growing for over 16 days cells were plated on laminin (Sigma) treated plastics, by adding 80µl of 0.1 mg/ml laminin diluted in PBS with Ca^{2+} and Mg^{2+}, to each cover slip and left for two hour at 37°C. Immediately prior to plating down, the laminin was aspirated off but not allowed to dry.

2.2.3 Poly-L-Ornithine coating

80µl of PLO was added to glass coverslips in 24 well plates, put in fridge and left o/n. The next day the PLO was removed and washed once with PBS. They were left to dry for 10 mins before use. Alternatively the PLO can be incubated on the coverslips at 37°C for one hour, washed with PBS and dried before use.

2.2.4 Preparation of Frozen Stocks

The above steps for cell passaging were followed but resuspension of the pellet after centrifugation was in 10 % DMSO (Sigma) solution in ES cell culture media and stored in cryovials (Nunc). One 10 cm confluent plate was split into 4 cryovials at 1 ml per vial and then slowly cooled using a cryochamber (Nalgene) at -80 °C.

2.2.5 Thawing of Frozen Stocks

Cryovials were immediately placed in a 37 ºC water bath until thawed. Immediately on thawing cells were taken up and washed in 10 ml of ES cell culture media and centrifuged at 1,000rpm for 3 mins. Media was aspirated off and cells were plated on a 10 cm plate. For MEFs one cryovial was split onto four 6cm plates, giving approximately 2.5×10^5 cells per plate.

2.2.6 Cre Adenoviral Transduction

Cells plated in 24 well plates were washed with serum free DMEM and 1ml of serum-free media was added to each well. A multiplicity of infection (MOI) of 500 provides highly efficient gene transduction into primary MEFs with little to no effect on cell viability. We used an MOI range of 5, 100, 300, 500, 1000 and 3000, calculated using:

Desired MOI x number of cells plated = *x* viruses needed

Volume of virus stock needed (µl) = $\dfrac{(x \text{ viruses needed } \times 1000)}{(\text{Concentration of virus stock})}$

The virus was added to each well and the plate gently rocked to disperse the virus and the cells incubated over night at 37°C. The following day the media containing virus was removed and the cells washed with PBS and normal media added to each well.

2.2.7 Transfection

All transfections were carried out in accordance with the manufacturer's instruction.

Electroporation (BioRad electroporator and cuvettes)

$5\text{-}10 \times 10^6$ cells were resuspended in PBS with 25µg of circular or linearised DNA and electroporated at 800 V and 3mF using a BioRad Gene Pulser. Cells were plated onto six 10cm plates which were either coated with gelatine or had been previously been covered in MEFs.

Lipofection (Invitrogen reagents)

Cells were plated in normal ES cell culture media minus the antibiotics 24 hours prior to lipofecting. On the day of transfection 2-5 µg of plasmid DNA was added to

Optimem medium (Invitrogen) to give a final volume of 50 µl, and the appropriate amount of lipofectamine was diluted in Optimem giving 50 µl total volume and incubated for five mins at room temperature. The two solutions were gently mixed together and incubated for 20 minutes. Cells were incubated with accutase into a single cell suspension, washed in PBS and counted. 5µg DNA and 4 µl Lipofectamine 2000 were added to two mls of Optimem media and $2x10^6$ cells that were previously harvested by centrifugation were resuspended in the medium. Cells were plated on gelatine for six hours after which point the media was substituted back to normal ES cell culture media.

Nucleofection (Lonza AMAXA kits and nucleofector)

Cells were incubated with accutase into a single cell suspension, washed with PBS and counted, $2x10^6$ cells were then centrifuged at 1000rpm for 3mins, to form a pellet. These cells were resuspended in 100 µl of Nucleofection solution which had been prepared previously by adding 78 µl Nucleofector solution to 22 µl supplement with 5-10 µg of plasmid DNA. The solution containing the cells was transferred into an amaxa certified cuvette and placed into the cuvette holder of the amaxa nucleofector II, cells were nucleofected under programme A-024. Immediately 500 µl of warm media was added to the cuvette and using the plastic pipettes provided, cells were transferred to two 10cm gelatine coated plates with 10mls of ES cell culture media and incubated under standard culture conditions.

Following Transfection

Forty eight hours after transfection the selection agent was added to the media. Selection was carried out for 7 days and the ES cell clones picked onto 96 well plates, plated with MEFs or gelatin coated plates. The initial 96 well master plate was split in the subsequent 7 days onto four 96 well plates. PCR analysis was performed on one of the plates the following day. Two of the 96 well plates were frozen as backups at confluence and the remaining plate was used to expand PCR positive clones onto two 24 well plates: one was grown to confluence and genomic DNA prepared for Southern analysis; the other was expanded onto 6 well plates where positive clones were frozen in liquid nitrogen.

2.2.8 X gal stain

Cells were washed with 1x DPBS and fixed using 2% formaldehyde for 5 minutes. Cells were washed three times each for three minutes with 1x DPBS. X-Gal *(5-bromo-4-chloro-3-indolyl-beta-D-galactopyranoside)* (Melford laboratories, England, UK) was reconstituted in Dimethylformamide at 50mg/ml and 5µl of X gal was used to every 1 ml of ferro/ferri-cyanide solution (1.050g Ferrocyanide, 0.825g Ferricyanide, 0.2g $MgCl_2$, 495 ml PBS and stored in the dark at 4°C) and incubated overnight at 37ºC. Cells were then visualized in bright field to observe blue precipitate and thus confirm lacZ gene expression**.**

2.2.9 Prussian Blue Stain

Cells were fixed in 4% Formalin for 20 minutes at room temperature and washed three times with PBS 1x. The slides were incubated for 20 minutes in freshly made 2% HCL, 2% Potassium Ferrocyanide solution. Sections were washed in running water before dehydrating through graded alcohols to Xylene for one minute per solution and mounted using DPX resin.

2.2.10 Primary Tissue

Dissection

Mouse embryos were collected in Hank's Balanced Salt Solution (HBSS) (Gibco) at embryonic day 14. The brains were removed and the substantia nigra was dissected from the ventral mesencephalon, shown in Figure 2.1. The dissection was performed in a laminar flow hood using a dissecting microscope.
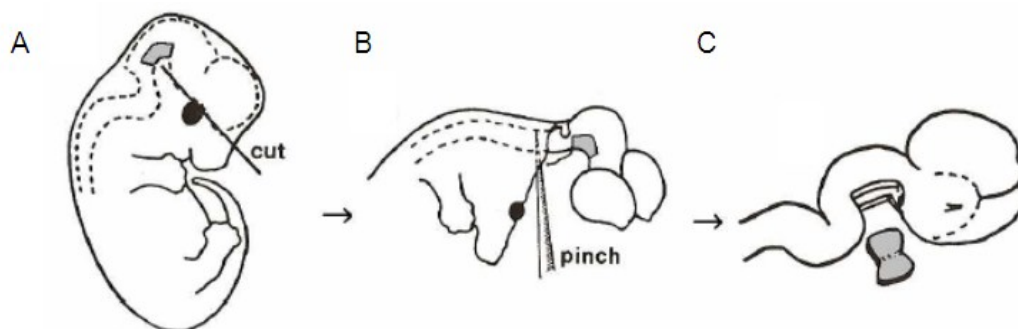
Figure 2.1: After the foetus was removed the spinal cord is severed and the brain removed (A and B). From the ventrolateral perspective the substantia nigra (grey) was dissected from the ventral mesencephalon by three cuts using iridectomy scissors (C). The cuts are toward the dorsal surface of the tectum, the thalamus and the third horizontally between them to remove the substantia nigra (Adapted from Dunnett and Bjöklund, 1992).

The dissected tissue was washed in HBSS and incubated at 37°C for 20 minutes in 0.1% trypsin, 0.5% DNase in HBSS to achieve a close to single cell suspension. Trypsin inhibitor (Sigma) and DNase were added for a further 5 minutes at 37°C. Trypsin was removed through washing in DMEM/F12 (Gibco) and centrifuged at 1000rpm for 3 minutes. The cells were resuspended in 200µl fresh DMEM/F-12 and triturated with a 200µl pipette to reach a single cell suspension. Cell counts were performed using a haemocytometer on 10µl of the cell suspension that was diluted with 0.4% trypan blue (Sigma) as detailed below.

2.2.11 Cell counts

10µl of the cell solution was added to the haemocytometer and glass cover slip, cells in the central square were counted and total cell counts were worked out using the following equation

Cells counted/Squares counted x Dilution factor x 10 = Cells/µl

If using Trypan Blue (Sigma) 8µl of cell suspension was incubated for 1.5 minutes in a one one to one ratio with Trypan Blue before counting on a heamocytometer.

Counting cells on coverslips: When doing cell counts for IHC four coverslips were counted per sample and from each coverslip four fields of view were counted and an average was taken.

2.3 *In Vivo* Methods

All animal experiments were performed in compliance with local ethical guidelines and approved animal care according to the UK Animals (Scientific Procedures) Act 1986 and its subsequent amendments. The following work was carried out under Project Licence 30/2498 and my Personal Licence 30/8441 except in the case of the teratomas, performed by Susie Hunter (Project Licence PPL30/2670); Grafting of the expanded WGE performed by Rike Zeitlow (Project Licence 30/2498); and the 6-OHDA lesions and subsequent grafting performed by Ludivine Breger (Project Licence 30/2498). Coordinates for grafting were taken using the rat brain atlas (Paxinos and Watson 1986) and the mouse brain atlas (Paxinos and Franklin, 1997).

2.3.1 Animal Husbandry

Adult 129sv (bred in house, initially from *Harlan*, UK) mice bred in house and Sprague-Dawley rats (*Harlan*) were used. Animals were housed in cages of up to four per cage in natural light-dark cycles and with access to food and water *ad libitum*.

Surgery was performed under gaseous isoflurane anaesthesia, induced in an induction chamber with isoflurane and oxygen and maintained by passive inhalation of isoflurane (1-2 l/min) (IVAX, UK) and a mixture of oxygen (0.8 l/min) and nitrous oxide (0.4 l/min). Animals received analgesia by sub cutaneous injection of Metacam (0.5μl mouse, 30μl rats) (Boehringer Ingelheim, Germany) whilst under anaesthesia, and received saline glucose (0.5ml mouse, 5ml rats). Animals were recovered in a heated recovery cage.

Cyclosporin A (Sandimmun, 10mg/kg) (Novartis, Hampshire, UK) was administered on daily basis via intraperitoneal injections when experiments involved xeno-transplantation. Injections commenced the day prior to transplantation for the duration.

2.3.2 QA Lesion

Rats

To Quinolinic Acid (QA) lesion rats 0.75μl of 45nmol QA solution was infused at for 1.5 minutes each at two sites using a Hamilton syringe attached to a pump and

cannula. Stereotaxic coordinates from bregma were +0.4/+1.4 mm anterior-posterior (AP), -3.2/-2.4 mm medial-lateral (ML) and the dorsal-ventral (DV) below dura were -5.0 mm and -4.0 mm. The needle was left at the lesion site for an additional 3 minutes following the QA infusion. The needle was removed, the incision was sutured and the animals were administered a subcutaneous injection of 5ml saline glucose into the scruff and an intramuscular injection of 0.15ml diazepam into the upper leg.

Mice

The QA lesions in mice were performed in the same manner as in rats but with the following alterations. 0.5µl QA was infused at one site for 4 minutes at the stereotaxic coordinates from bregma +0.9mm AP, -1.8mm ML and -2.7mm below dura. Following lesioning the needle was left at the site for 4 minutes before withdrawal. Mice received a subcutaneous injection of 0.5ml saline glucose into the scruff and 0.03ml diazepam intramuscular injection.

2.3.3 6-Hydroxydopamine

Rats received an injection of 3 µl 6-OHDA (hydrobromide salt) (Sigma) over 3 minutes using a 30-guage cannula connected to a 10µl Hamilton syringe via fine polyethylene tubing, the syringe was positioned in a Microdrive pump set to deliver at 1µl/min. Two minutes of diffusion time was allowed to elapse before gentle retraction of the cannula following the injection.

2.3.4 Grafting in QA Lesioned animals

A cell suspension of 2µl total volume was grafted into an adult rat brain (5 x 10^5 cells) or adult mouse brain (2.5 x 10^5) at a rate of 1 µl/minute with 1 minute at two heights, using a Hamilton syringe. Grafts were either contralateral or ipsilateral to the lesion at, unless otherwise stated, stereotaxic coordinates +0.6 mm AP and +/-2.8 mm ML from bregma, at two heights -5.0 mm and -4.5 mm below dura for rats and +0.9 mm AP and -1.8 mm ML from bregma, at two heights -2.7 mm and -2.4 mm DV for mice. The needle was left at the graft site for a further two minutes prior to withdrawal. The incision was sutured and the animals recovered.

2.3.5 Perfusion

Animals were terminally anaesthetised through injection of Euthatal (0.5ml intraperitoneal) (Merial, France) the chest was opened by thoracotomy and the descending aorta clamped. A needle attached to a motorised pump was inserted into the heart through the ventricle and a small incision made in the right atrium. Animals were transcardially perfused with prewash (pH 7.3) for two mins until the blood ran clear, then with 1.5% PFA for four mins. Brains were removed and post fixed in 1.5% PFA overnight and transferred to 25% sucrose in prewash.

2.3.6 Immunohistochemistry

Brains were sectioned coronally at 40 µm thickness using a freezing stage microtome and stored in Tris buffered saline (TBS) pH7.4 with 0.2% sodium azide in 24 well plates at 4°C. A 1 in12 section series was taken for each immuno. Sections were washed in TBS and quenched for five mins in 10% hydrogen peroxide and 10% methanol. Sections were washed in TBS for 10 mins three times and then blocked in 3% normal serum in 0.2% triton X-100 in TBS (TXTBS) for one hour. Sections were transferred without washing to the appropriate concentration of primary antibody (see Table 2.2) in TXTBS with 1% normal serum and incubated o/n at room temperature. The following day sections were washed three times in TBS for 10mins a wash before incubating in secondary antibody in TBS with 1% normal serum for at least three hours. The sections were washed again in TBS three times for 10 minutes and streptavidin ABC (A and B at 1:200 dilutions in TBS with 1% serum prepared 30 mins before use) was added for a minimum of two hours. The sections were washed in TBS three times for 10 mins and then in 0.05M tris non saline (TNS) pH 7.4 and left overnight. Positive staining was visualised using either diaminobenzidine (DAB) at 0.5mg/ml in TNS with 12µl hydrogen peroxide (brown colour) or vector SG (Dako, Glostrup, Denmark) made up in TNS (grey colour). Following the colour change the sectoos were washed twice more in TNS and mounted on gelatine coated glass microscope slides and dried at room temperature. The mounted coverslips were dehydrated in ascending levels of alcohol, cleared in Xylene and mounted using DPX. Negative controls were performed in parallel without the primary antibody.

Antibody	Brand	Raised in	Concentration
Primary (Anti-)			
2A Peptide	ABS31 (Millipore)	Rabbit	1/1000 (WB)
β-Actin	8H10D10 (Cell Signalling)	Mouse	1/10000 (WB)
β-tubulin	T2200 (Sigma)	Rabbit	1/5000
Doublecortin	AB18723 (Abcam)	Rabbit	1/500
Ft Heavy Chain	AB75972 (Abcam)	Rabbit	1/1000 (WB)
Fth Chain	Ab65080 (Abcam)	Rabbit	1/500 (WB)
Ftl Chain (D-9)	Sc-74513 (Santa Cruz)	Mouse	1/500 (WB)
GFAP	Z0334 (DAKO)	Rabbit	1/2000
GFP	AB16901 (Millipore)	Chicken	1/4000
Nestin	Hybridoma Rat 401	Mouse	1/1000
Neu N	MAP 377 (Millipore)	Mouse	1/4000
TH	MAB 318 (Millipore)	Mouse	1/2000
Secondary (Anti-)			
Chicken IgG Biotin	BA9010 (Vector)	Horse	
Mouse IgG Biotin	BA2001 (Vector)	Rabbit	
Rat IgG Biotin	BA2020 (Vector)	Goat	1/200
Rabbit 594	A11037 (Invitrogen)	Goat	
Rabbit 488	A11034 (Invitrogen)	Goat	
HRP linked whole antibody			
Mouse IgG	NA931 (GE Healthcare)	Sheep	
Rabbit IgG	NA934 (GE Healthcare)	Donkey	1/10000

Table 2.2: Antibody List. Key: WB: Western Blot,

2.3.7 Cresyl Violet Staining

Brain sections were mounted onto glass microscope slides, previously double-subbed with 1% gelatin, and allowed to dry. Sections were subjected to 10 minutes in increasing levels of alcohol from 70%, to 95% and then 100%, followed by Chloroform/Ethanol (1:1) for 20 minutes and then decreasing alcohols for 10 minutes from 100% to 95% to 70% and then distilled water, before incubation in the cresyl violet (CV) stain for 10 minutes. Stained sections were rinsed in water, dehydrated in 70% and 95% alcohol, if necessary sections were then decolourised in 2.5% acetic

acid in 95% alcohol for 2-5 minutes, until the desired colour was achieved. Followed by a further dehydration in 95% and 100% alcohol and then cleared in xylene before coverslips were mounted using DPX mountant.

2.4 Imaging

2.4.1 Transmission Electron Microscopy for Morphological Study

Transmission Electron Microscopy (TEM) was carried out on cells that were accutased into a single cell suspension, pelleted at 500rpm for 5 minutes and washed in PBS. Pellets were fixed in 2.5% Glutaraldehyde diluted in 0.1M PBS, pH 7.4, for 1 hour at room temperature. Cells were washed twice in PBS for 5 minutes each. Cells were transferred to 1% osmium tetroxide in distilled water for one hour at room temperature for post fixation. They were washed twice with PBS before dehydration in descending concentrations of EtOH from 50% through 70%, 80%, 90% and three lots of 100% for 10 minutes at room temperature. They were then infiltrated with propylene oxide for 10 minutes at room temperature. To view the morphology in osmium treated samples, samples were resin infiltrated with Araldite CY212 (5g CY212, 5g DDSA, 0.15g BDMA) and propylene oxide (1:1 v/v) on a rotator at room temperature and left to evaporate off overnight. The following day the old araldite was removed and freshly made up, neat Araldite, with no propylene oxide was put on the pellets in polystyrene tubes. The samples were left over night at 60°C. Ultrathin sections (90-100nm) (Gold colour) were cut by reducing the size of the slices in a step wise fashion from 590nm (Green colour) were cut with a diamond knife on an ultracut-microtome (Reichert-Jung, Leica, UK). The sections were collected on a copper grid and counterstained with Reynold's lead citrate and 2% urinyl acetate for 10 minutes and examined under a Philips transmission electron microscope (Philips EM 208, Netherlands).

2.4.2 Magnetic Resonance Imaging

Magnetic resonance imaging (MRI) scans were carried out at Cardiff University's in house Experimental MRI Centre (EMRIC) using a high-field 9·4 Tesla (400MHz) small bore (20 cm) Bruker Biospec 94/20 MRI/MRS spectrometer equipped with S116 high performance gradient insert and avance II electronics. Scans were acquired using a 72mm id transmit/receive quadrature polarised birdcage rf coil or a 72mm ID linearly polarised birdcage volume coil (Bruker, Ettlingen, Germany)

coupled to a rat head 2 element quadrature combined surface coil (Bruker, Ettlingen, Germany). We used Paravision 5.0 and 5.1.

Animals were anaesthetised with 5% isoflurane in a 40% O_2/Air mixture at 1.2 L/min and transferred to a specialist MRI bed model # T10532 (Bruker, Ettlingen, Germany) with integrated circulating heated water and anaesthetic nose cone. Isoflurane was reduced to ~1.5-2% for maintenance of anaesthesia during scanning. The body temperature, breathing rate and heart rate were monitored throughout using the Model 1025 Monitoring and Gating System (SAI inc, Stony Brook, New York). Body temperature was maintained during recovery in a warm air V1200 recovery chamber (Peco Services Ltd) Set at 27 ^{o}C.

2.4.3 Quantification and photomicroscopy of grafts

Grafts were observed using a Leitz DRMB light microscope. Digitised images were captured with a Hamamatsu C4752 video camera and NIH 1.55.1 image analysis software. Cells expressing markers of interest were used to calculate graft volume using a Leitz light microscope and Olympus CASTgrid stereology software. Graft volume was calculated using the below formula where V = Graft volume area (mm^3), a = area (mm^2), M = section thickness (0.04mm) and f = frequency of sampled sections (1:12):

$$V = \frac{\underline{\Sigma a.M}}{F}$$

Images were taken using Leica DMRBE microscope, Leica DFC 420 C camera and Leica application suite V3 analysis software. Images were processed using Adobe Photoshop.

2.4.4 Statistics

Excell and SPSS software were used to analyse results. Data are expressed as mean±sem unless otherwise stated and analysed using one way analysis of variance (ANOVA) or Students T Test for normally distributed data. Grubbs test to detect outliers in FACs analysis.

The number of asterisks denote the level of significant difference on graphs, one, two or three asterisks are equivalent to $p < 0.05$, $p < 0.01$ and $p < 0.001$ level of significance, respectively.

3 Characterisation of SPIO labelled cells *in vitro* and *in vivo*

3.1 Aim

If wanting to track cells *in vivo* using MRI SPIOs are the method most often employed. They have been tested in a few different scenarios but results vary from case to case in respect to the effect on cells and the ability to accurately depict the graft. Here we wanted to test the applicability of SPIO labelling to striatal grafts of neurally differentiated mouse ES cells and other cell types important to the progression of cell transplantation in neurodegenerative disorders, namely primary tissue and expanded primary tissue.

3.2 Introduction

SPIOs are used as negative contrast agents (i.e. they produce a loss of signal) to label cells prior to transplantation for *in vivo* monitoring in longitudinal studies, rather than waiting for post mortem analysis. Stem cells, among other cell types, have been successfully labelled with FDA approved SPIOs and protamine sulphate to monitor migration and distribution of cells *in vivo* using MRI in many applications (Anderson *et al.* 2004; Arbab *et al.* 2004a; Frank *et al.* 2004; Liu *et al.* 2008; Ramaswamy *et al.* 2012; van Buul *et al.* 2009). While they provide very sensitive MRI contrast, they are associated with a number of detrimental effects in the cells, and the MRI signal can be difficult to interpret as discussed below. Cytoskeleton formation is hindered on SPIO labelling (Soenen *et al.* 2010a), with connotations both for differentiation of ES cells and reduced migration as a result of decreased motility in SPIO labelled neural stem cells (Cromer Berman *et al.* 2012). Apoptosis, necrosis, mitosis, migration and re-uptake of SPIOs by surrounding cells all confound the resulting MRI signal in ways not apparent until post mortem histology, making graft interpretation challenging (Pawelczyk *et al.* 2008; Terrovitis *et al.* 2008).

To date, various cell types have been labelled with SPIOs. SPIO labelled MSCs exhibit no apparent adverse effects (Ramaswamy *et al.* 2012; Sun *et al.* 2012), whilst less positive results were seen with neural stem cells (Cromer Berman *et al.* 2012),

skeletal derived stem cells (Pawelczyk *et al.* 2008), and cardiac derived stem cells (Terrovitis *et al.* 2008). ES cells likely take up SPIOs through receptor independent endocytosis (Bulte *et al.* 2001) and nanoparticles have been shown in mouse ES cell cytoplasm by transmission electron microscopy (TEM) (Jendelova *et al.* 2004). Labelling mouse ES cells with carboxydextran coated SPIOs has been shown not to affect self-renewal or differentiation down a neural lineage, but does perturb the cavitation of embryoid bodies (Krejci *et al.* 2008).

While the effects of SPIO labelling have been assessed in mouse ES cells, the wide range of results suggest the necessity for trialling each new application. While self-renewal of mouse ES cells has been shown to be unperturbed following SPIO labelling, the effects on differentiation towards a neural lineage using the chemically defined induction protocol used here has not previously been tested.

Very little has been done to monitor SPIO labelled primary tissue – the gold standard. This is important, as when analysing ES cells it is necessary to compare to this "standard". If it isn't known how they are affected in the gold standard then they can't be used in the main methods of transplantation or in comparison studies of ES cell versus primary tissue.

In this chapter, cells were labelled with SPIOs and protamine sulphate for detection following neural transplantation into whole animal disease models. Three different cell types were used; i) mouse ES cells (E14 and their derivatives: Tau-GFP and 46C), ii) primary neural cells taken from embryonic day 14 (*E14*) VM (The rationale is explained in the methods) and iii) expanded foetal neural precursors (FNP). Mouse ES cells and expanded FNPs were labelled for transplantation into the QA-lesioned striatal model of HD, and primary rat VM cells were labelled prior to transplantation into the striatum of 6-OHDA lesioned rats modelling PD. Graft assessment was carried out using MRI at different time points post-transplantation, followed by subsequent post mortem IHC. There are some discrepancies in measuring graft volume that could be related to the methodology and what the operator regards as real signal. This variation is considered here.

3.3 Methods

For further details on techniques see General Methods chapter 2.

A number of cell types were labelled with SPIOs and protamine sulphate to determine if the MRI signal from the grafted SPIO labelled cells would be a good representation of the graft *in vivo* when compared to IHC and the difficulties associated with analysis and methods of measurement using this approach is discussed.

SPIO labelling of neurally differentiated mouse ES cells

The neurally differentiated mouse ES cells were labelled with dextran coated SPIOs (Endorem, Guerbet, France) and protamine sulphate to determine if this combination led to intracellular SPIO labelling. E14, Tau-GFP and 46C (Ying et al, 2003) mouse ES cells were cultured under chemically defined conditions using ADF medium to promote neural induction (see General Methods, Chapter 2). On day 15 of ADF treatment Endorem was mixed with protamine sulphate (Wockhardt, England, UK) and incubated at 37ºC for one hour. Cells were harvested, media was aspirated off and half a volume of media was added to the plate containing Endorem at a concentration of 100µg/ml and protamine sulphate at a concentration of 3µg/ml, 6µg/ml or 9µg/ml. The cells were incubated for 4 hours before the rest of the media was added and the cells incubated overnight in a final concentration of 50µg/ml Endorem and 1.5, 3.0 or 4.5 µg/ml of protamine sulphate. After 24 hours the cells were washed twice for five minutes in PBS with Ca^{2+} and Mg^{2+} and three times for five minutes in PBS with Ca^{2+} and Mg^{2+}, supplemented with heparin (10U/ml) (Sigma). The cells were washed twice more with PBS containing Ca^{2+} and Mg^{2+}. Cells were either fixed or harvested using accutase treatment.

Grafting

For details of grafting neurally differentiated mouse ES cells see General Methods Chapter 2.

Grafting of SPIO Labelled Expanded WGE: To achieve larger graft volumes and test if Perls' staining can label the whole graft, *E14* Lister Hooded WGE, expanded for 9 and 12 days, was transplanted bilaterally into SD rats. Rats were unilaterally

QA lesioned. Coordinates for grafting were AP: +0.4, ML: -3.3, DV: -5.2/-4.2. Either 5 x 10^6 cells in 2μl were grafted without prior treatment or labelled with SPIO's overnight as detailed earlier.

SPIO treatment and grafting of Primary Tissue: To test whether VM tissue can be SPIO labelled, and the subsequent grafts visualised using MRI, in a way that is indicative of both the IHC and Perls' analysis, rat VM was SPIO labelled and grafted. *E14* VM was dissected from 12 embryos and plated as a monolayer on PLK coated plates, cells were labelled with SPIOs overnight as detailed earlier and washed the following day with PBS with Ca^{2+} and Mg^{2+} 5 x 5 minutes per wash, in two of these washes the PBS was supplemented with heparin to aid in SPIO removal. Cells were then incubated at 37°C in trypsin for 20 minutes and DNAse for 5 minutes. Cells were counted using Trypan Blue and the equivalent of 1.5 VMs were grafted in a 2μl volume into the 6-OHDA lesioned hemispheres of rats. Coordinates AP:+0.5, ML:-2.5, DV:-5/-4.

Analysis of SPIO Labelled Mouse ES Cells *in vivo* and *in vitro*

To assess the effect of SPIOs both *in vitro* and *in vivo* ICC, IHC and Perls' staining were carried as outlined below and further details of the methods can be found in General Methods, Chapter 2. Mouse ES cells were differentiated using chemically defined media down a neural lineage and SPIO labelled overnight.

ICC was carried out on mouse ES cells that were grown in culture to see if there was any difference in neural or glial markers following SPIO labelling, compared to non-labelled controls. Cells were labelled with Doublecortin and GFAP (1/2000) antibodies.

Grafts were assessed using CV stains (detailed in General Methods, Chapter 2), and IHC using antibodies for GFP when tau-GFP mouse cells were grafted. When performing histology on a SPIO labelled VM graft in a 6-OHDA lesioned animal the TH stain was used as an indirect measure of grafted cells.

Perls' staining was carried out on mouse ES cells grown in monolayer to see if the SPIOs were being taken up and not washed off following SPIO labelling. Perls' staining was also carried out on grafted brain sections as a means to monitor SPIO labelled grafted cells and correlate it with MRI and IHC.

Photomicroscopy and graft analysis

The graft volumes were measured in a number of ways to see if the SPIO signal using MRI was reflective of the IHC. The grafts were measured by stereology based on CV, Perls' staining, GFP and TH. The different measurements were compared to see how similar the MRI measurements based on SPIO labelled grafts were to more standard IHC techniques. The effects of operator discretion when measuring MRI and Perls' staining volumes were also taken into account. These were carried out as detailed in General Methods, chapter 2

3.4 RESULTS

3.4.1 *in vitro* analysis of SPIO labelled neurally differentiated mouse ES cells

Confirmation of SPIO labelling

It was necessary to confirm that the neurally differentiated mouse ES cells were successfully labelled, and that the SPIOs were intracellular, not just remaining on the outer surface. Mouse ES cells differentiated for 16 days were successfully labelled with SPIOs using protamine sulphate as demonstrated by Perls' staining (Figure 3.1). There were a lot of extracellular SPIOs that could not be removed following stringent washing techniques, evident after the Perls' stain. Intracellular SPIOs were confirmed using TEM (Figure 3.2). Cell counting based on Perls' analysis was confounded by the additional extracellular SPIOs. Sometimes large areas covering cells were completely obscured by the intensity of the Prussian blue, while other areas had no labelling visible (Figure 3.1.A). Of the protamine sulphate concentrations tested, 6µg/ml was found the best due to the increased ease with which the extracellular SPIOs could be washed off, compared to 3 µg/ml concentrations and the more even distribution of SPIOs compared to the 9 µg/ml.
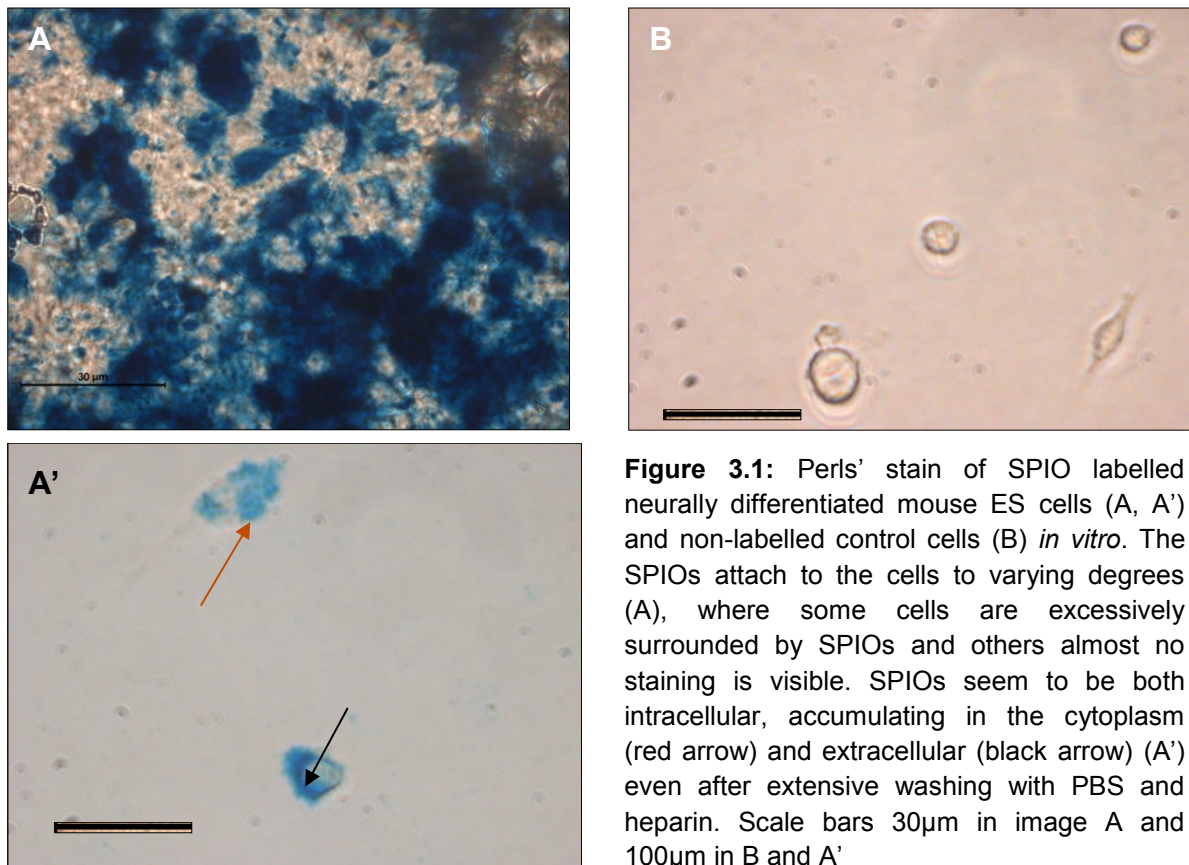
Figure 3.1: Perls' stain of SPIO labelled neurally differentiated mouse ES cells (A, A') and non-labelled control cells (B) *in vitro*. The SPIOs attach to the cells to varying degrees (A), where some cells are excessively surrounded by SPIOs and others almost no staining is visible. SPIOs seem to be both intracellular, accumulating in the cytoplasm (red arrow) and extracellular (black arrow) (A') even after extensive washing with PBS and heparin. Scale bars 30µm in image A and 100µm in B and A'
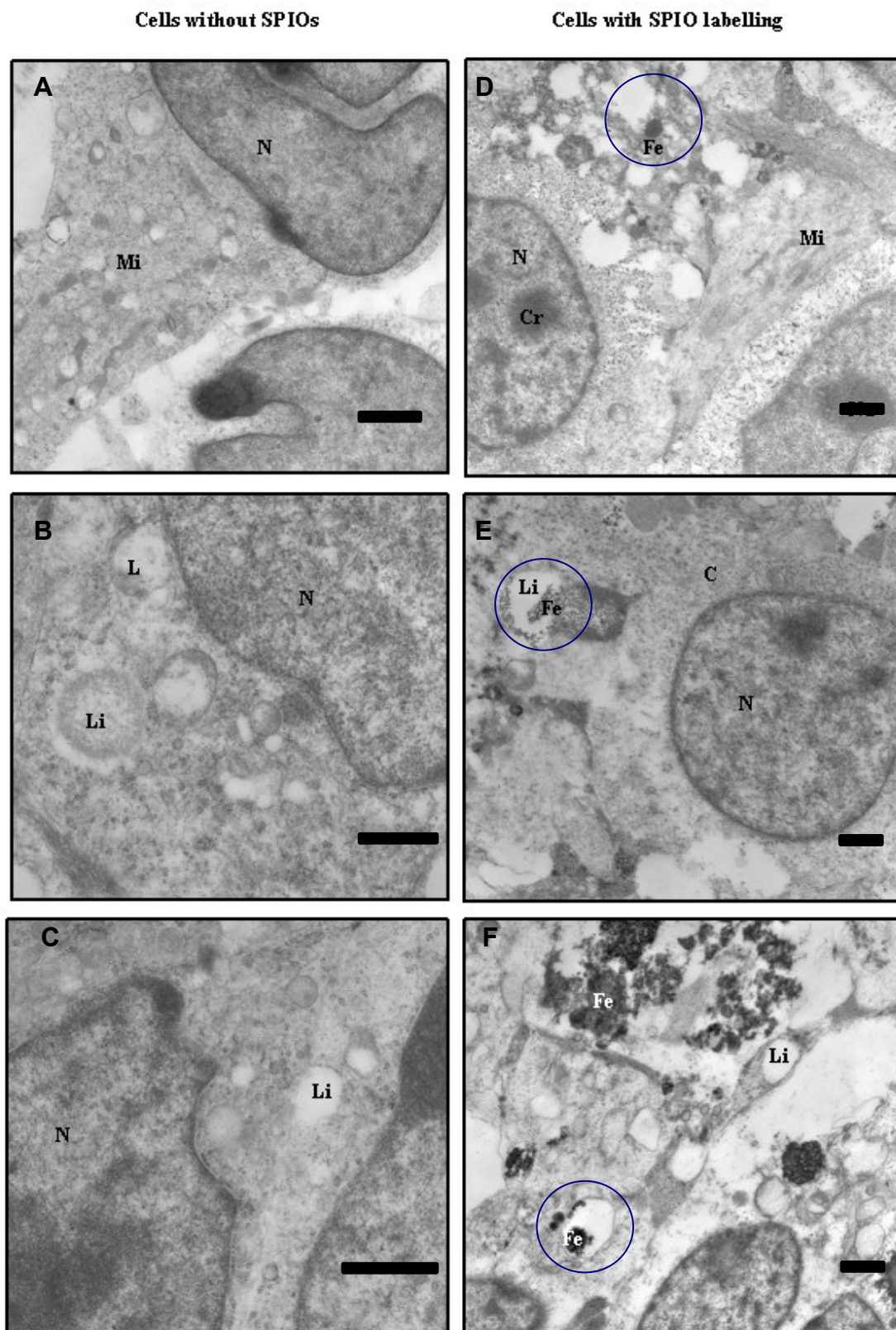
Figure 3.2: TEM analysis was carried out on non-labelled control cells differentiated for 16 days (A-C) and those that were SPIO labelled (D-F), demonstrating SPIOs are successfully taken up by cell lysosomes (circle in images D, E and F) and not just extracellular. Cr: Chromatin. , C: Cytoplasm, Fe: Iron, L: Lipid, Li: Lysosome, Mi: Mitochondria, N: Nucleus, Nu: Nucleolus. Scale bar 1μm

Effects of SPIO labelling on neural differentiation

SPIOs are known to affect cytoskeleton formation (Soenen *et al.* 2010a) and so have the potential to affect differentiation. Mouse ES cells differentiated down a neural lineage were labelled with SPIOs and cultured for a further 5 days before analysis. We wanted to determine if neural induction of ES cells was altered following labelling with SPIOs and protamine sulphate. The 46C mouse ES cell line used in this study has GFP tagged to Sox1, enabling analysis of Sox1 expression using the fluorescent GFP reporter. Although protamine sulphate is not known to affect stem cell differentiation this opportunity was taken to see if there was any change in Sox1 expression using different concentrations of protamine sulphate with SPIOs. There was no significant difference in Sox1 expression of 46C cells between the unlabelled control and cells labelled with SPIOs using different concentrations of protamine sulphate after differentiation for 20 days and labelling with SPIOs on day 15 ($F_{3,12}$ = 2.927; p = 0.077) (Figure 3.3, Graph 3.1).

Percentages of glial and neural cell types were determined for unlabelled cells compared to those treated with SPIO's and protamine sulphate. There was significantly more β-tubulin positive cells in the control sample than compared to those that were SPIO labelled (t_6 =-2.629; p = 0.039) (Graph 3.2). No significant difference was found between the numbers of GFAP positive cells compared to non-labelled cells (t_6 =0.640; p = 0.546).

Sox1 expression in SPIO labelled cells with varying concentrations of Protamine Sulphate vs control
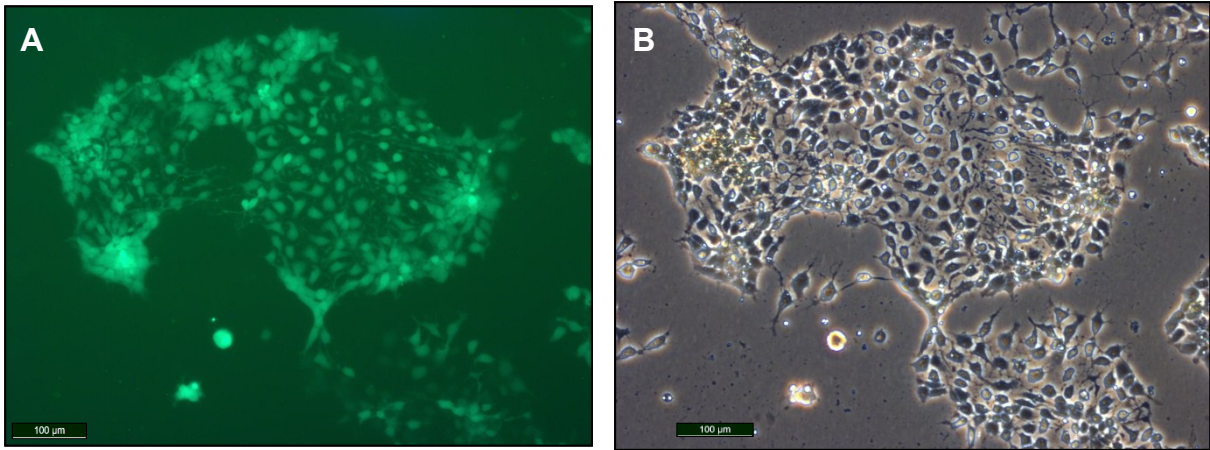
Figure 3.3: Following addition of SPIOs with varying concentrations of protamine sulphate the level of Sox1 expression was measured using the 46C cell line that expresses GFP when Sox1 is turned on using fluorescence (A) and bright field (B). Scale bar 100µm
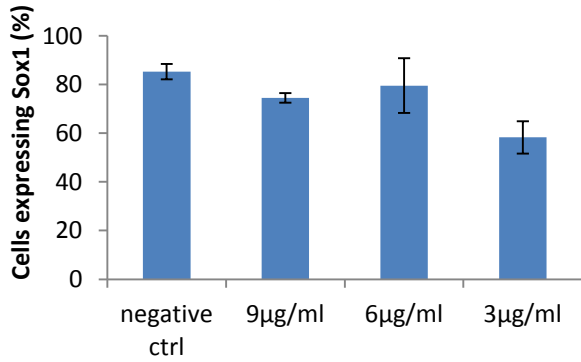
Graph 3.1: Cells were labelled with SPIOs using various concentrations of protamine sulphate and compared to untreated controls. No significant difference in Sox1 expression was observed ($F_{3,12}$ = 2.927; p = 0.077).
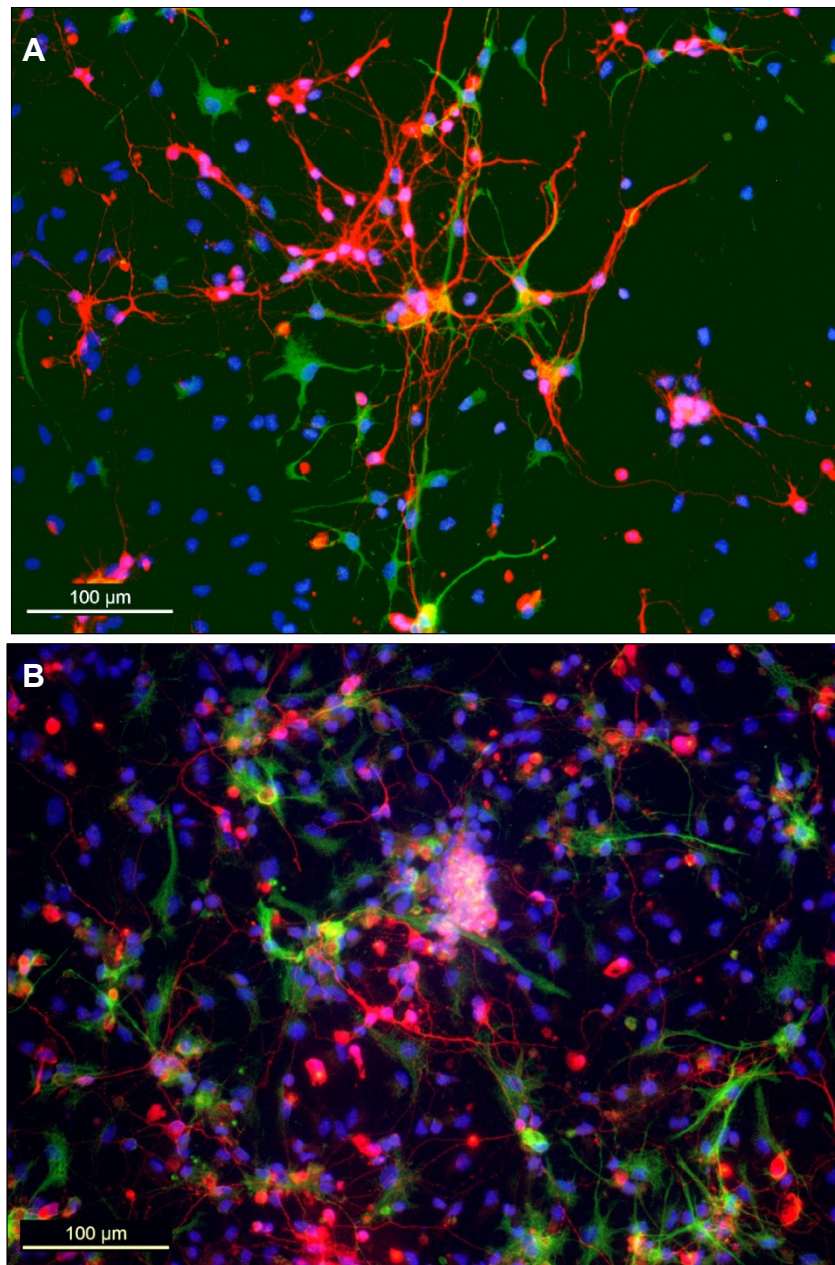
Figure 3.4: Mouse ES cells were differentiated to day 20 to monitor cells after SPIO labelling. Control cells (A) and cells labelled with SPIOs on day 15 (B) were labelled with β tubulin (red), GFAP (green), Hoescht (blue). Scale bar 100μm

Graph 3.2: The percentage of cells expressing glial (GFAP) or neural (β tubulin) markers in SPIO labelled and non-labelled cells were compared. There was no significant difference between the number of GFAP positive cells in the two populations (T_6 =0.640; p = 0.546). There were significantly more β-Tubulin positive cells in the control group compared to those treated with SPIOs (T_6 =-2.629; p = 0.039).

GFAP and β tubulin expression in SPIO labelled cells & controls

24hours

1 week

2 weeks (slice a)

2 Weeks (slice a + 1)
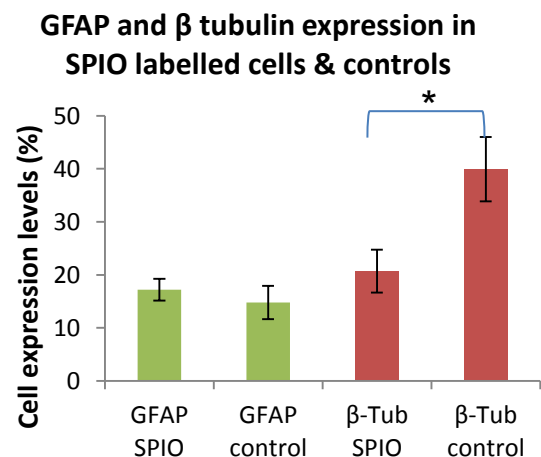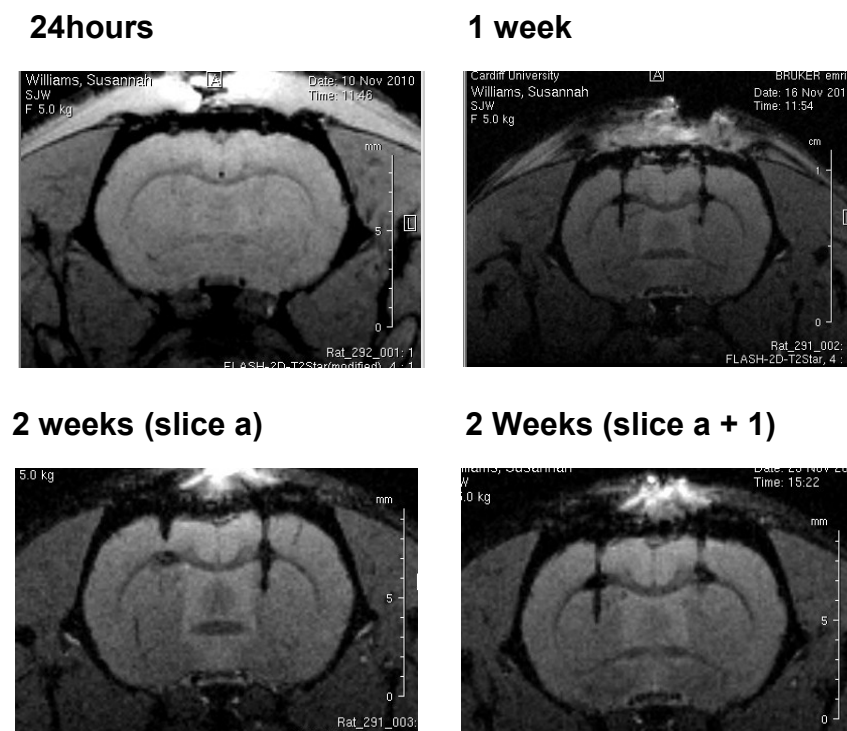
Figure 3.5: Rat with bilateral sham grafts to determine if the needle track's MRI signal can be removed or reduced by using a glass instead of metal cannula. The metal cannula was stereotactically inserted on the left hand side and glass on the right. MRI images were taken 24 hours, 1 week and 2 weeks following injection.

The needle track's MRI signal

The needle track, caused by the needle used to deliver cells to the brain, causes a signal drop out in the MRI image, and obscures the central area of the graft signal from a contrast agent. One of the possible causes is iron from the needle being deposited in the brain during injection and giving the signal drop out. To try and reduce the MRI signal arising from the needle track a thinner glass cannula was compared to the standard metal cannula. Two animals underwent bilateral sham grafts using 2µl of PBS, one hemisphere was grafted using a metal cannula and the other a glass cannula, the animals were imaged at three time points, 24 hours, one week and six weeks. MRI parameters were FLASH 2D T2*, TR 400.0ms, TE 8.5ms, Flip Angle 35° degrees. There was not a large enough difference between the MRI signals from the two cannula to make one more useful than the other (Figure 3.5), refuting the idea that the tracts are caused by the iron being deposited in the brain by the metal cannula.

3.4.2 Grafting of SPIO labelled neurally differentiated tau-GFP mouse ES cells into QA lesioned 129 mice

This experiment is to characterise how representable the MRI signal of live presence of SPIO labelled cells. SPIO labelled cells were grafted into QA lesioned mice to see if the MRI signal was comparable to gold standard IHC techniques and whether the Perls' stain accurately represented SPIO labelled cells *in vivo.* The Tau-GFP cell line was used because it expresses tau tagged GFP ubiquitously (Pratt *et al.* 2000) and IHC with the anti-GFP antibody would distinguish the graft from the host.

QA lesioned mice were grafted with SPIO labelled (Figure 3.6) or non-labelled tau-GFP mouse ES cells that had been differentiated down a neural lineage for 16 days (Figure 3.7). There was obvious signal drop out in the grafted region indicative of SPIO labelling in MRI images when cells were labelled with SPIOs prior to grafting. The non-labelled grafts were either not visible using MRI or there was a slight loss of signal, but any signal far weaker than that given when using SPIOs. CV staining showed disorganization of cells in the striatum indicative of grafted cells and surviving graft tissue was confirmed by IHC using an antibody against GFP staining of the Tau-GFP cell line. Perls' staining was used to pick up SPIO labelled cells, turning blue in the presence of iron. Perls' staining was evident in both labelled and non-labelled grafts (Figure 3.6.C Figure 3.7.D Figure 3.8.1-7c). To assess the 'non-specificity' of the Perls' stain, a section from an unrelated transplant experiment grafting non labelled rat WGE into a Black 6 rat was analysed. Perls' staining was observed throughout the graft region in a similar distribution whether cells were SPIO labelled or not. The intensity wasn't quantified and may have been less intense in the non SPIO labelled cases (Figure 3.9).

Graft volume was estimated from the MRI images, Perls' stain and GFP. There was variability in graft sizes and positions shown in the GFP IHC (Figure 3.8.1-7a) which was reflected in both the MRI (Figure 3.8.1-7b) and Perls' (Figure 3.8.1-7c). The grafts were generally quite small, all being under 3mm^3. Also differences in graft volume measurements within an individual animal, depending on whether the graft was measured from MRI, IHC or Perls' stain, are discussed further below.
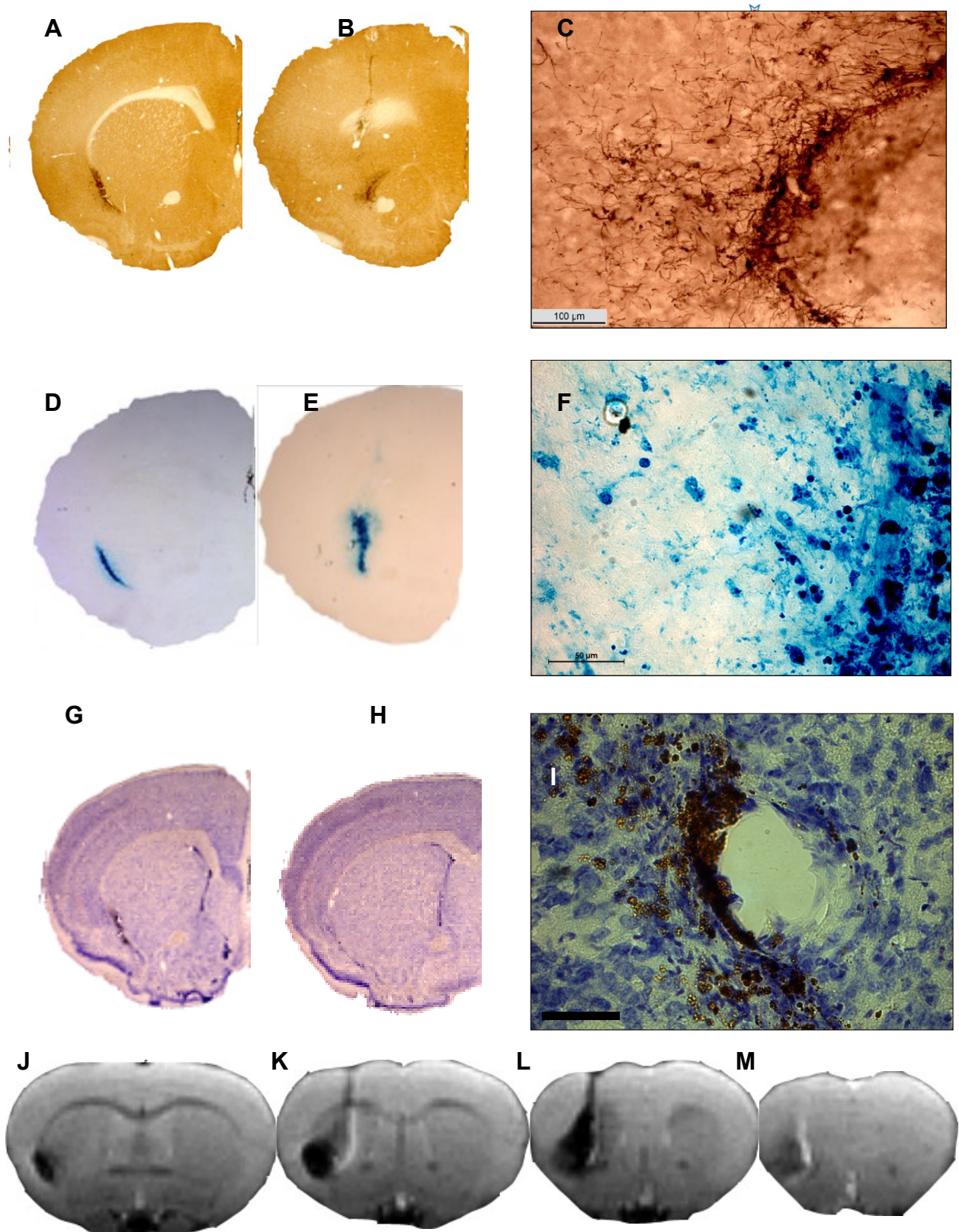
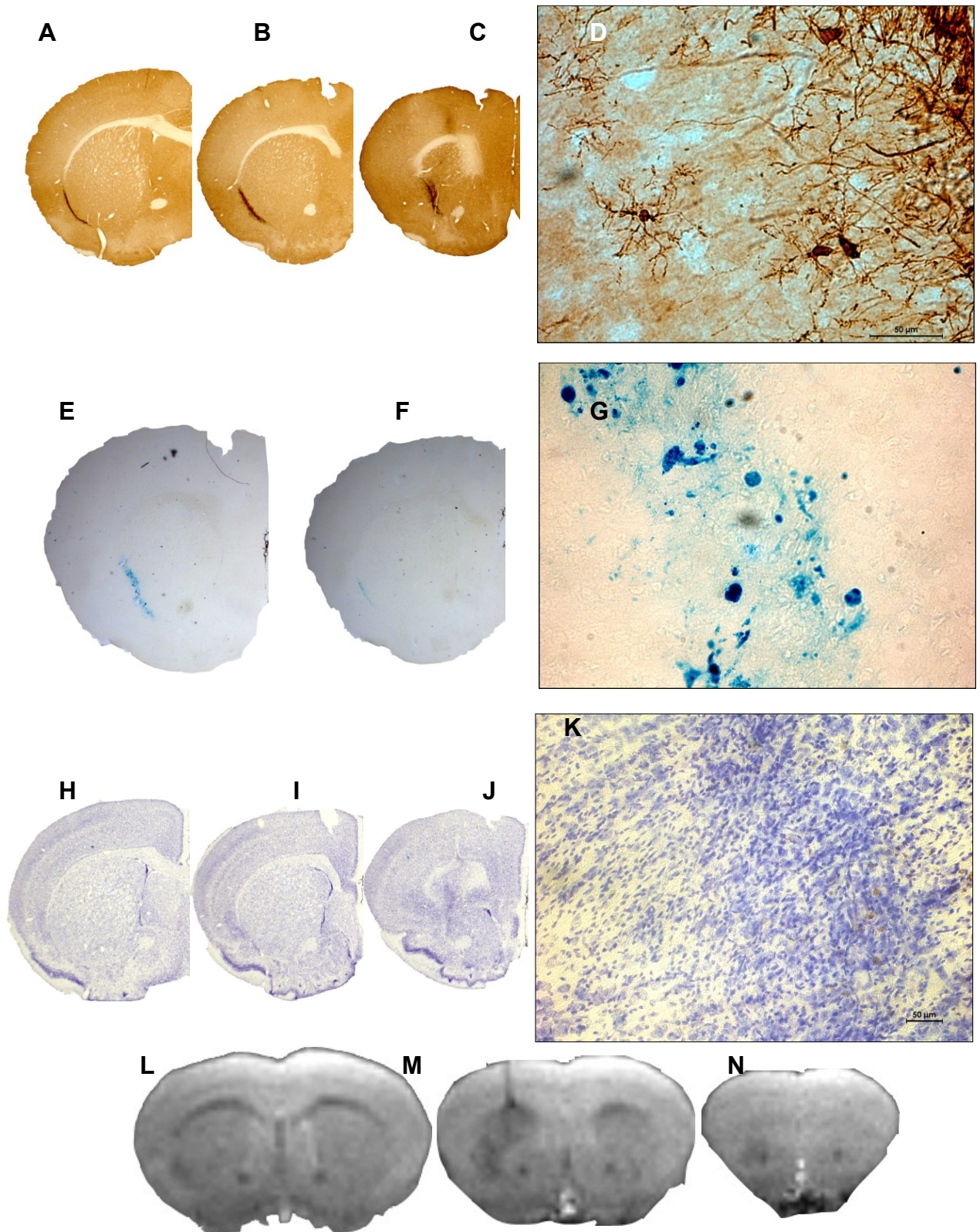**Figure 3.6**: SPIO labelled GFP expressing mouse ES cells differentiated down a neural lineage and grafted into the mouse QA lesioned striatum. Corresponding sections (1/12) all from a single specimen show low power images to view graft positioning GFP IHC (A,B), Perls' stain (D,E), CV (G,H) and MRI images at 6 weeks post graft (J-M). High magnification images show graft survival of GFP positive cells (C), Perls' staining (F) and disorganization of the grafted cells (I). Scale bar in C 100μm, and in F and I 50μm. (1.6x, 20x, 40x)

Figure 3.7: Control GFP expressing mouse stem cells differentiated down a neural lineage and grafted into mouse QA lesioned striatum. Corresponding sections (1/12) all from a single specimen show low power images to view graft positioning GFP IHC (A, B, C), Perls' stain (E, F), CV (H, I, J) and MRI images at 6 weeks post graft (L, M, N). High magnification images show graft survival of GFP positive cells (D), Perls' staining (G) and disorganization of the grafted cells (K). Scale bar in D 100µm, and in G and K 50µm. (1.6x, 20x, 40x)
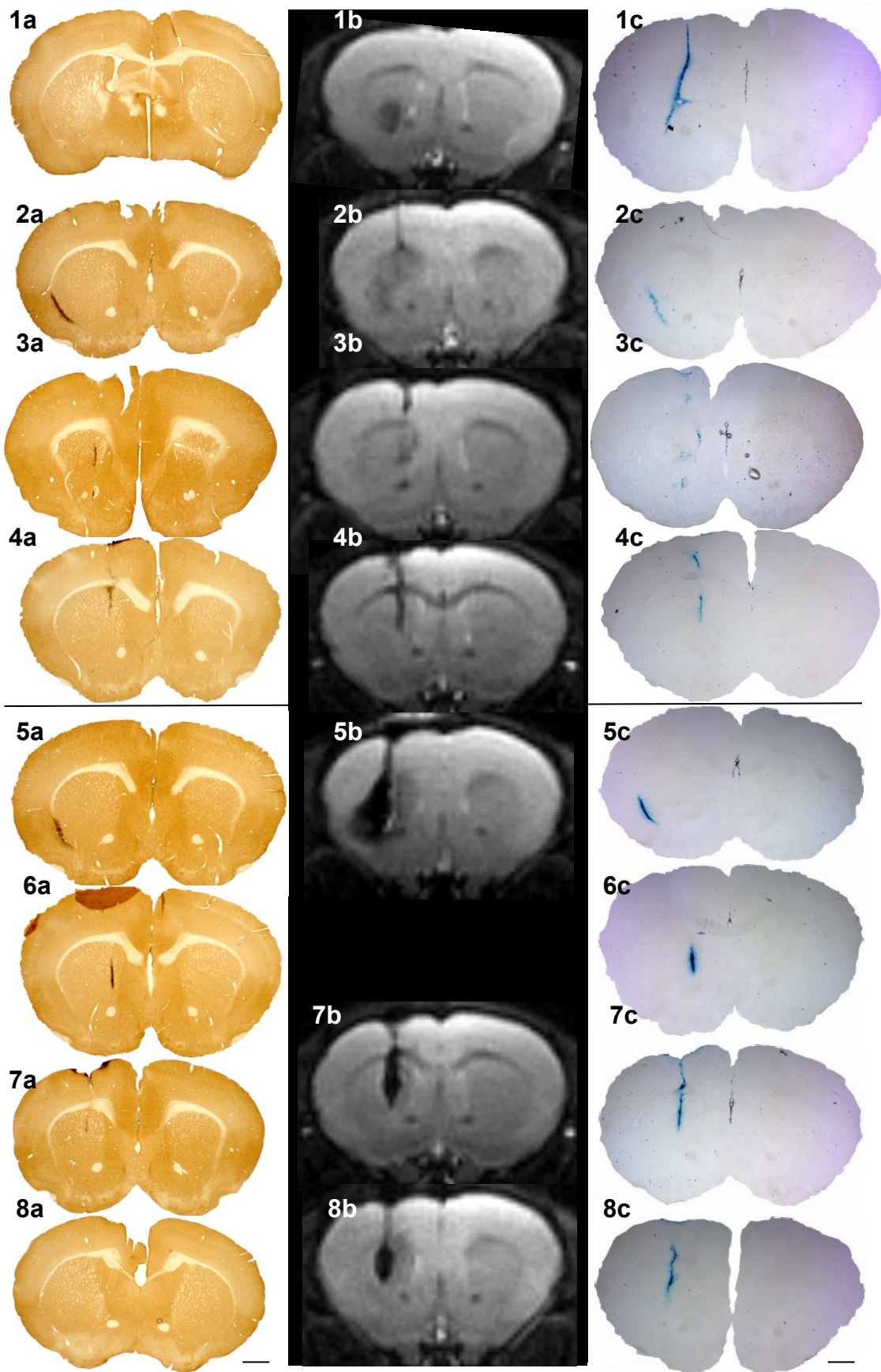
Figure 3.8: Overview demonstrating the variability of the graft sizes in the eight mice that were grafted into a QA lesioned striatum with neurally differentiated mouse ES cells. Images 1-4 are of grafts not labelled with SPIOs and images 5-8 are cells which were SPIO labelled. GFP IHC (A), MRI images 6 weeks post lesion (B) and Perls' stain (C). Scale bar 1000µm
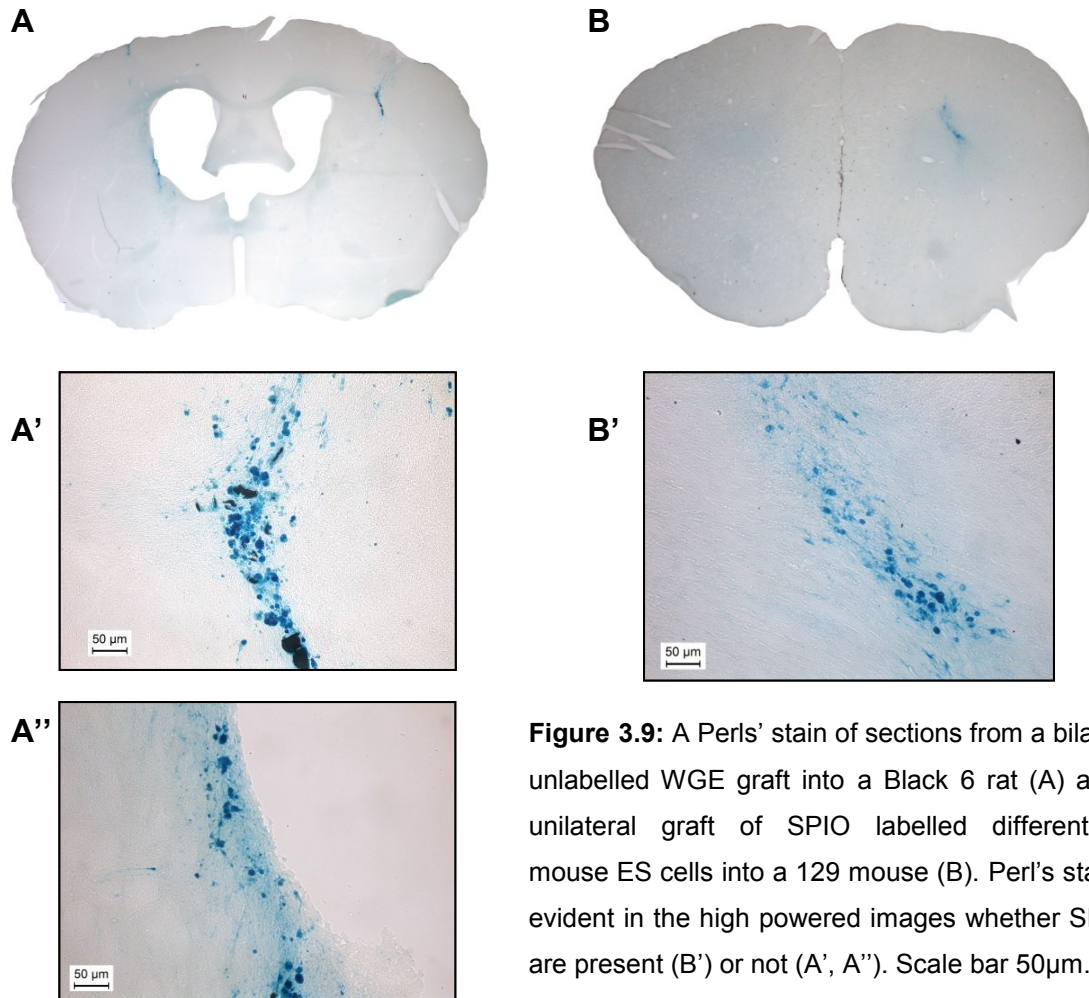
Figure 3.9: A Perls' stain of sections from a bilateral unlabelled WGE graft into a Black 6 rat (A) and a unilateral graft of SPIO labelled differentiated mouse ES cells into a 129 mouse (B). Perl's stain is evident in the high powered images whether SPIOs are present (B') or not (A', A''). Scale bar 50µm.

3.4.3 Comparing graft measuring techniques

To determine if the MRI signal from SPIOs gave an accurate representation of the graft volume it was compared against both the Perls' stain and IHC using GFP to pick up the grafted cells. There was no significant difference between the methods of measuring graft volume of the mice labelled with Tau-GFP cells, whether it was based on MRI, Perls' or GFP, when cells were SPIO labelled ($F_{2,9}$ = 0.092; p =0.913) (Graph 3.3). While there was no significant difference between control non-labelled grafts when measuring by the different methods ($F_{2,9}$ = 0.212; p = 0.813), the Perls' and MRI volumes are consistently smaller, suggesting that with a larger number of animals or less variability in graft sizes this may become significant. The grafted animals were scanned twice over a six week period and there was no significant change in graft volumes of non-labelled cells seen over this time (t_3 = 0.735; p = 0.516) (Graph 3.4). The SPIO labelled graft was significantly smaller in volume in the second scan (t_2 = -4.623; p = 0.044). The graft volumes measured with MRI here are inclusive of any areas of signal dropout ('comprehensive' method of measurement).

Comparison of Graft Volume measurement methods
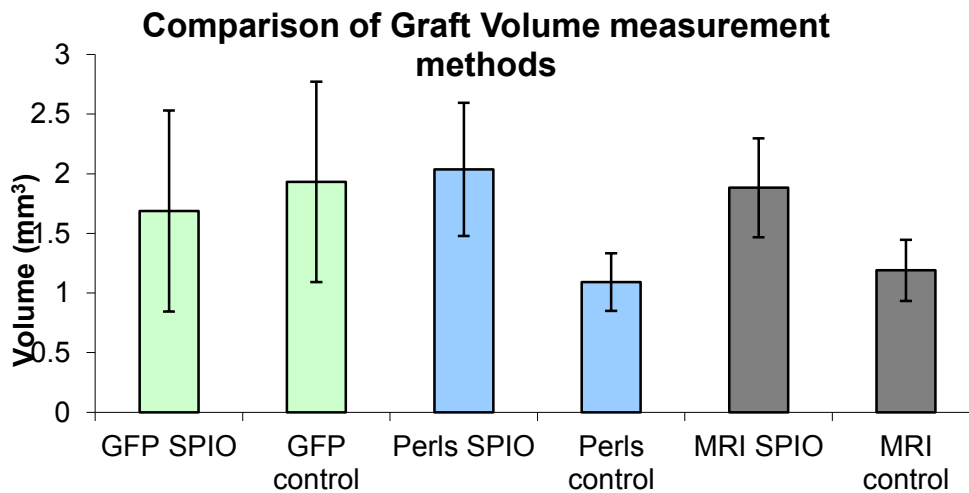
Graph 3.3: Graft volumes taken of cells that were either SPIO labelled or not and grafted in QA lesioned mice using GFP IHC, Perls' staining and MRI volumes. There was no significant difference between the three methods of measuring either when cells were labelled with SPIOs ($F_{2,9}$ = 0.092; p =0.913) or in the negative control grafts ($F_{2,9}$ = 0.212; p = 0.813). N= 4 apart from 'MRI SPIO' where N=3.

MRI Graft Volumes change over a 6 week period
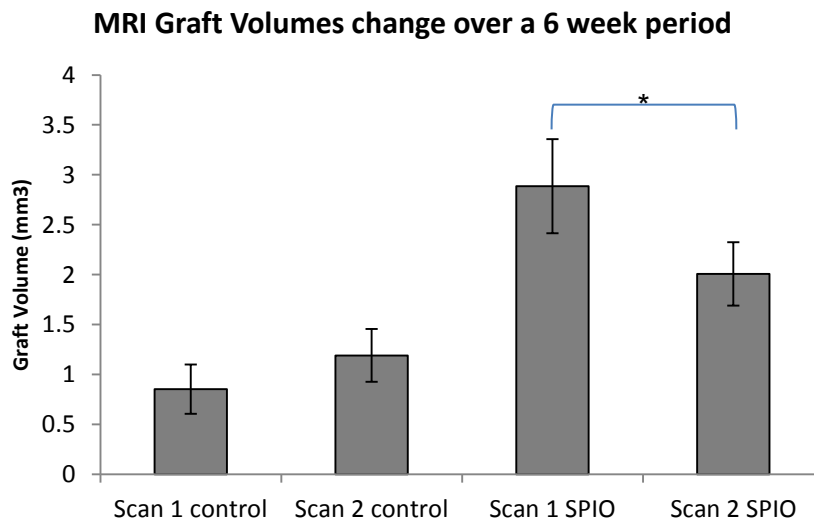
Graph 3.4: The animals were MRI scanned twice, once 24 hours after grafting and a second time 6 weeks later. There was so significant change in graft volume over the six week period when grafts had no labelling (t_3 = 0.735; p = 0.516). The SPIO labelled grafted were significantly smaller in the second scan (t_2 = -4.623; p = 0.044)

3.4.4 Analysing the Different Graft Volume Measuring Techniques

When measuring the volumes using MRI there is complete signal drop out from in SPIO labelled grafts at the centre, the border of the graft is not always definite and lighter shades of grey are observed at the periphery. There could be a number of factors attributing to the lighter contrast and to see if measuring only complete signal drop out was more indicative of graft volume both conservative and comprehensive measurements were made to see if there is a significant difference. The Perls' stain also has a lighter blue periphery that fades into background and under the same rationale both conservative and comprehensive measurements were made of this.

Comprehensive measures include all signal dropout and varying shades of grey different from the expected normal brain signal. While more conservative measures only the complete signal drop out. The conservative method shows a significantly smaller graft volume when cells are unlabelled compared to the comprehensive method (t_6 = 3.893; p = 0.008) and it seems the signal from lighter grey hemosiderin is being excluded from the result (Graph 3.5). There is no significant difference between the comprehensive and conservative cut offs when measuring SPIO labelled grafts (t_4 = 2.677; p = 0.055). While there is no significant difference between the MRI volumes of SPIO labelled compared to non-labelled grafts using the comprehensive volumes (t_5 = 1.992; p = 0.103), using the conservative practices the control grafts are significantly smaller in volume than SPIO labelled grafts (t_5 = 4.292; p = 0.008)

When recording the volume using Perls' under either conservative or comprehensive conditions there was no significant difference between the two measurement types either for SPIO labelled (t_6 = 1.811; p = 0.120) or non-labelled grafts (t_6 =1.415; p = 0.207), although there is a trend for smaller volume measure (Graph 3.6). There is not a significant difference in size between SPIO labelled and non-labelled grafts when measured conservatively (t_6 = -2.750; p = 0.796) or comprehensively (t_6 = -1.554; p = 0.171).

**Conservative vs Comprehensive Measuring
Strategies for Analysis of MRI Graft Volume**
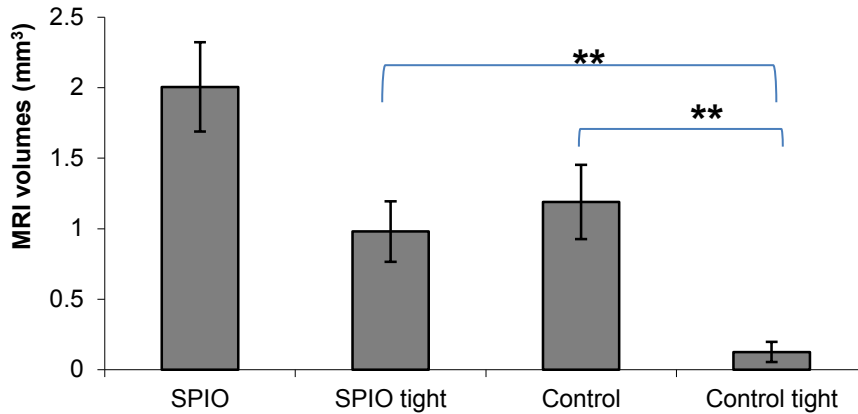
Graph 3.5: MRI: Comparison of graph measurements using MRI (A) based if the measurements were 'tight' to only the darkest areas of signal drop out or if they were more encompassing of the shades of grey around the periphery. There was a significant difference between the controls (t_6 = 3.893; p = 0.008) but not between the SPIO labelled graft volumes results between the two types of measurements (t_4 = 2.677; p =0.055). N=4 for 'control' and N=3 for 'SPIO'

**Conservative vs Comprehensive Measuring
Strategies for Analysis of Graft Volume given
by Perls Staining**
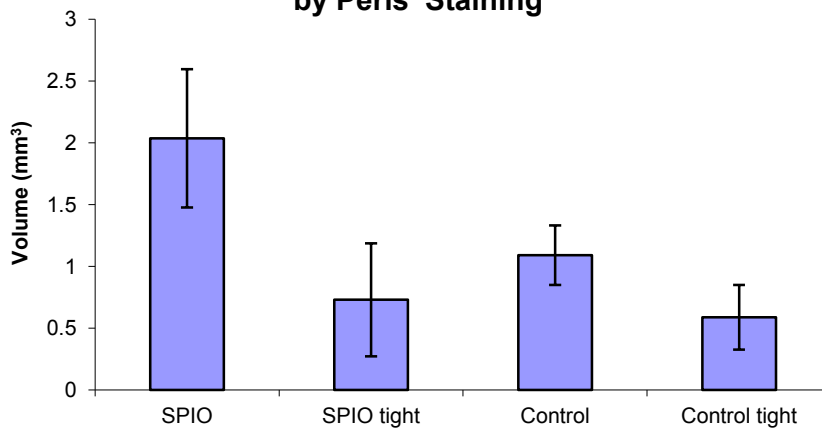
Graph 3.6: Comparison of graph measurements using Perls, based on if the measurements were 'tight' to only the darkest areas of Perls' stain or if they were more encompassing of the lighter shades of blue around the periphery. There was no significant difference between the Perls' stain inclusion methods between SPIO labelled grafts (t_6 = 1.811; p = 0.120) or unlabelled graft measurements (t_6 =1.415; p = 0.207). N=4

3.4.5 SPIO labelling of primary tissue and subsequent grafting

Primary tissue: There are two reasons for labelling primary cells i) They are the gold standard for comparison with stem cell transplants and therefore it is important to characterise their signal. SPIO labelled primary tissue such as VM has not been looked at in the literature to date and one can't assume SPIOs will have the same effect in primary cells as in ES cells, which are generally more robust. ii) Primary grafts tend to show less migration from the core of the graft and tend to produce more cohesive well demarcated graft masses. This may make it easier to compare the signal between the different imaging methods, e.g. Perls' stain, histology and MRI, in part because if the conservative method of measuring volumes is used it is unlikely graft will be excluded at the periphery.

Expanded WGE: An additional group considered for clinical applications are FNPs derived from primary tissue. They were included as they tend to be more proliferative, so could form an even larger graft than primary but less migratory than ES cells. Under the premise the larger volumes would extend outside the area of the needle track and provide more information on whether 'hemosiderin' induced Perls' stain could be distinguished from SPIO labelled cells, 9 and 12 day expanded WGE were labelled with SPIOs and protamine sulphate overnight.

in vitro SPIO labelling of expanded WGE and VM: 9 and 12 day expanded WGE and VM were successfully labelled with SPIOs using protamine sulphate as shown by Perls' stain in a similar manner to the neurally differentiated mouse ES cells (Figure 3.10).
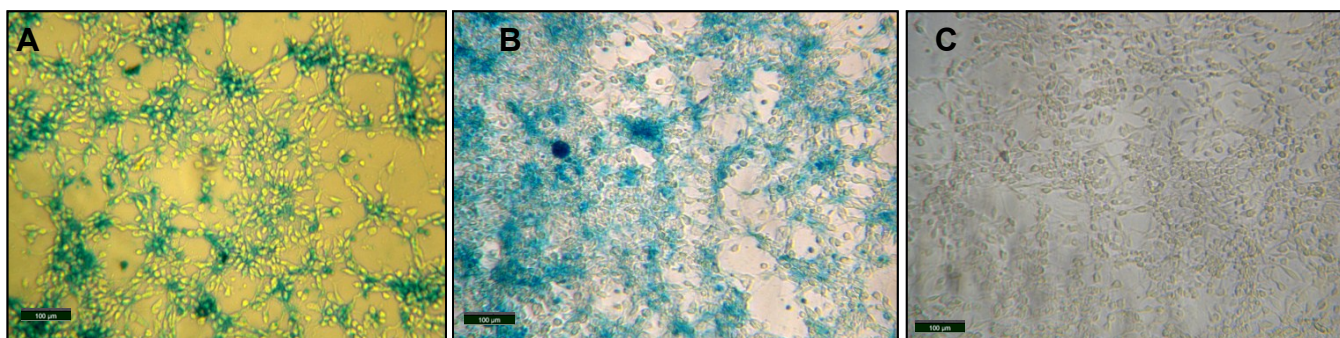
Figure 3.10: Rat VM and WGE were plated on PLK coated plates and SPIO labelled overnight. Perls' staining was carried out to confirm SPIO labelling in VM (A) and WGE (B), while non SPIO labelled cells showed no positive stain for Perls' (C). Scale bar 100µm

Transplanting SPIO labelled expanded WGE: To try and achieve larger grafts 9 and 12 day expanded E14 WGE were SPIO labelled and grafted bilaterally in a rat with a QA lesion in one hemisphere and no lesion the other side. The grafts were small and did not extend far from the needle track as shown by Perls' and CV staining (Figure 3.11 A, B, D and E). SPIO labelled cells gave obvious MRI signal contrast compared to control (Figure 3.11 C and F).
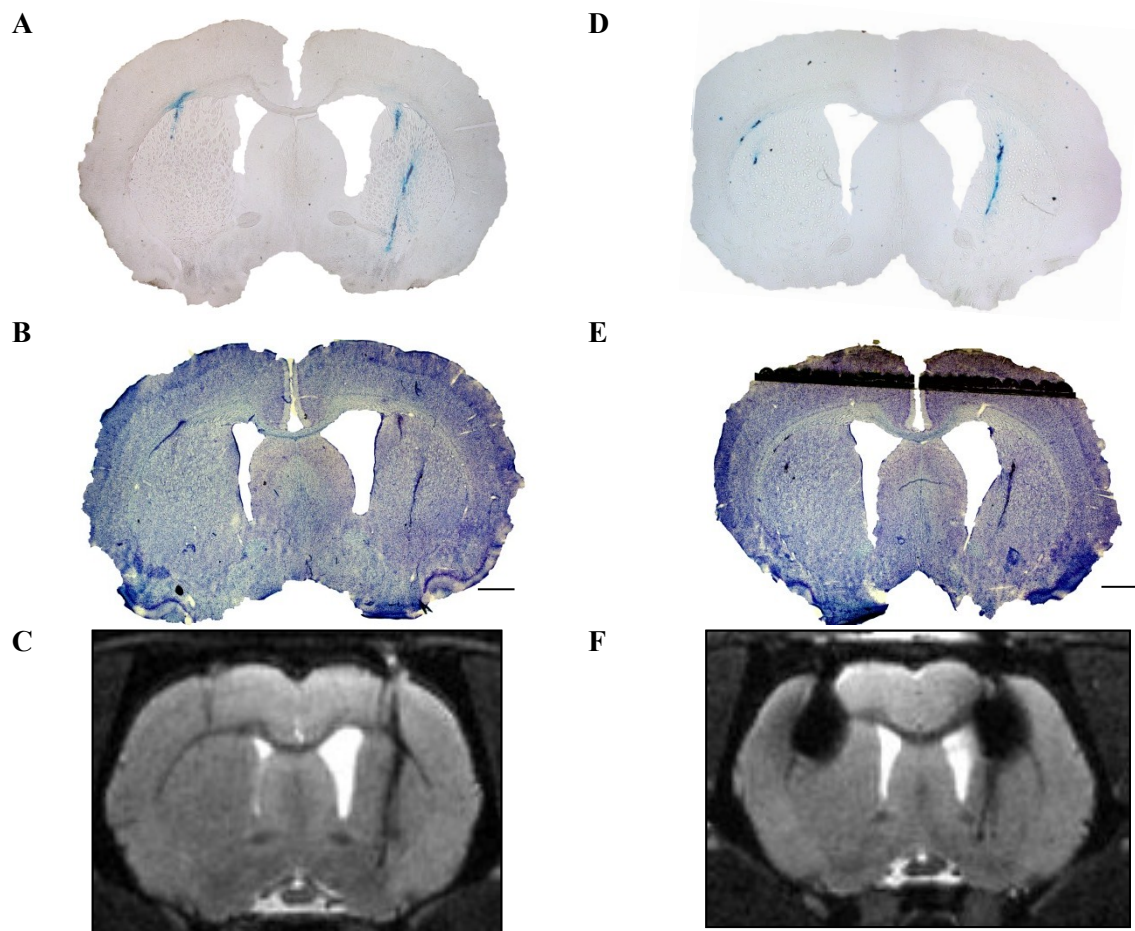
Figure 3.11: Four rats were bilaterally grafted with 9 and 12 day expanded E14 WGE to achieve larger graft sizes on which to test the Perls' stain. Two animals had grafts that were SPIO labelled (one animal shown here D-F) and two animals had grafts that were unlabelled (one animal shown here A-C). Histology sections 1/12 were stained with Perls' (A and D), CV (B and E). MRI was done within 24 hours prior to sacrifice (C and F).

SPIO labelling and grafting rat VM

Following dissection of rat VM the cells were successfully labelled with SPIOs overnight as determined by Perls' stain (Figure 3.12.A). Large grafts were seen using MRI and verified by CV and TH staining (Figure 3.12 A-C). There was no significant difference between the MRI, CV and Perls' graft measurements at 6 weeks post grafting ($F_{2,12}$ = 1.324; p = 0.302) (Graph 3.7). Grafts survived as evidenced by positive TH staining in the 6-OHDA lesioned area (Figure 3.12 C') and were functional (as demonstrated by behavioural testing not shown here).
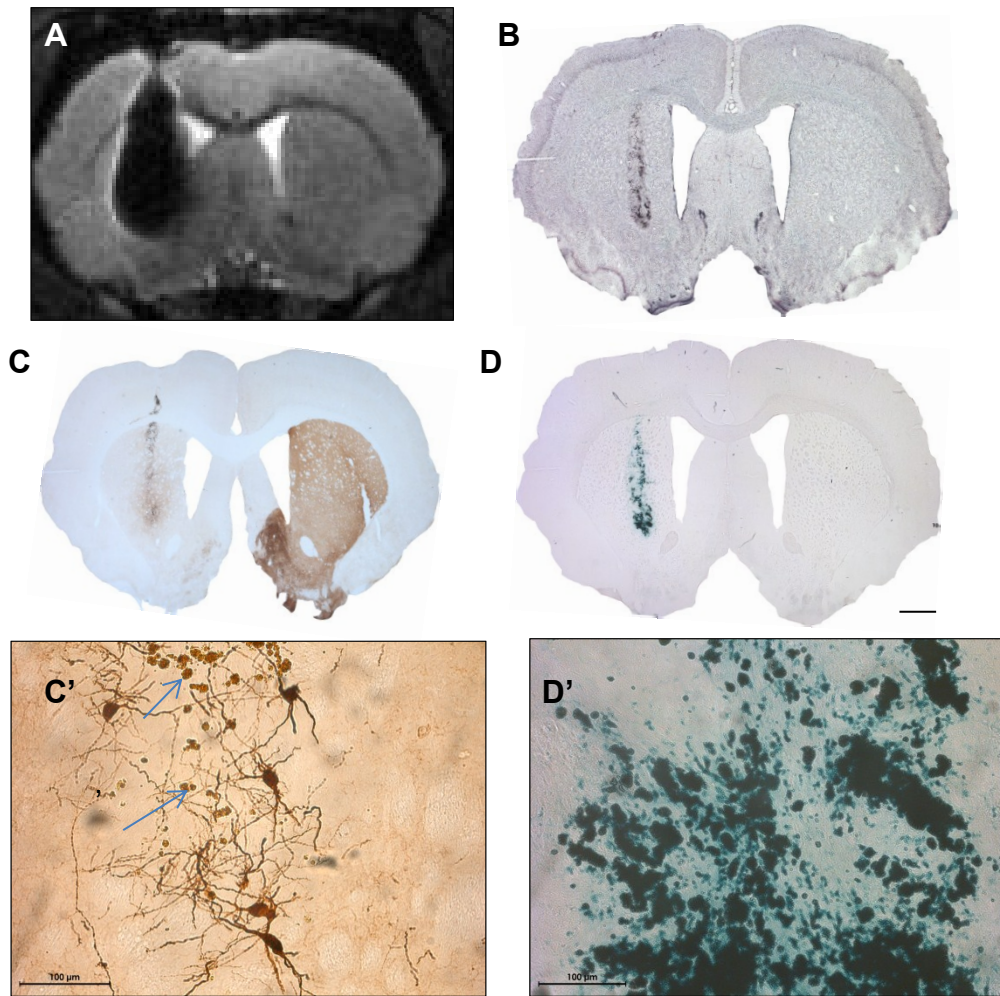
Figure 3.12: Images all from the same 6-OHDA lesioned rat with VM graft that was dissected 24 hours prior to grafting and labelled with SPIOs overnight. MRI RARE image taken at 6 weeks post grafting (A) , Low power (1.6x) 1/12 sections, give graft positioning using CV staining (B), TH labelled sections (C) and high power demonstrates surviving cells in the graft (C') and the arrow points to what looks like either hemosiderin or free aggregated SPIO particles, (D) shows the Perls' stain in a corresponding position to the graft and (D') shows a heavy, patchy Perl's staining over the entire grafted area. Scale bar 1000µm for the low power and 100µm for the high power images.

Graph 3.7: The volumes were calculated by MRI, Perls' stain and CV staining using stereology. At six weeks post grafting there was no significant difference between the grating measurements (F $_{2,12}$ = 1.324; p = 0.302).

Comparison of SPIO labelled VM graft volumes in 6OHDA lesioned rats
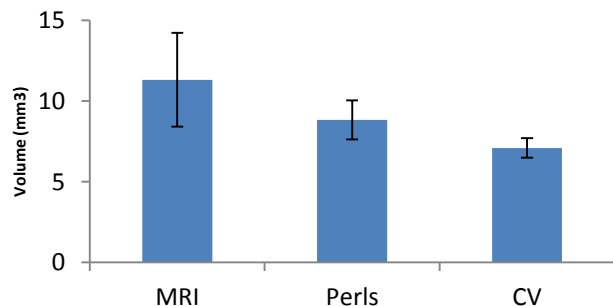
3.5 Discussion

The effects of SPIOs on mouse ES cells

SPIOs have been shown to affect differentiation as discussed in the introduction, therefore it was important to characterise differentiation in this experiment using the specific cell lines employed. The 46C cell line, used to test SPIO labelling, has a GFP knock in reporter into the open reading frame of the sox1 gene (Ying *et al.* 2003), an early marker of neuroectoderm (Wood and Episkopou 1999) and provides a convenient window to look at cells that go on to form the ventral striatum (Ekonomou *et al.* 2005). Although protamine sulphate has not been linked to any detrimental effect on differentiation previously, because it affects the uptake of SPIOs which are known to affect differentiation if not taken up properly, Sox1 expression was observed using the different concentrations. There was no significant effect on Sox1 expression after being labelled for 5 days with SPIOs and varying concentrations of protamine sulphate compared to the negative control. Glial marker GFAP and neuronal marker β-tubulin were assessed after differentiating the cells for 20 days, having had SPIO labelling cells at day 15. Differentiation down a glial lineage was unaffected, whether or not cells were labelled with SPIOS. β-Tubulin is a major constituent of microtubules, a component of the cytoskeleton, and cytoskeletal formation and microtubule architecture has been shown to be affected by the presence of SPIOs (Soenen *et al.* 2010a). In SPIO labelled cells there was a significant decrease in β-Tubulin compared to control. However, one should not be hasty in assigning the decrease to intracellular SPIO without further experimentation and a larger arsenal of antibodies. As we have seen in the literature, previous studies showing a detrimental effect on differentiation down a chondrocytic lineage (Kostura *et al.* 2004) was later deemed to be a result of extracellular SPIOs (Arbab, 2004b), with the intracellular being innocuous - at least in that respect.

Effects of Metal vs glass cannula on needle tract signal

The needle tract can produce an MRI artefact that can make the proper analyses of results and measurement of graft volumes difficult. To try and remove this artefact, a thinner glass cannula was compared to the usual metal cannula when performing a sham graft using saline solution. This would determine that the signal was not coming from the iron particles from the cannula being left in the brain, causing a

signal drop out. MRI visible tracks were seen in both hemispheres regardless of cannula used, and while the signal was not necessarily visible during the first 24 hours following grafting, it developed in the days following injection. This suggests the signal is the result of bleeding and the remaining hemosiderin in the area following surgery. The thinner diameter of the glass cannula did not decrease signal drop out and a change of needle was not warranted based on these results. Instead, awareness to stop bleeding around the bore hole in the skull, particularly relevant for surgery in rats, where more bleeding occurs, could help reduce the needle track signal. The scan type can also inadvertently enhance the needle track. For instance when observing signal from an overexpressed Ferritin transgene a programme more sensitive to change in T2, which overestimates the needle track MRI signal, is necessary (See chapter 3).

The problems of Perls' staining

In vitro: Perls' staining is commonly used to confirm SPIO labelling of cells *in vitro* (Arbab *et al.* 2005; Cohen *et al.* 2010; Frank *et al.* 2003; Magnitsky *et al.* 2008). When comparing the different concentrations of protamine sulphate as a TA for SPIOs there was no substantial difference observed. The *in vitro* Perls' stain showed heterogeneously labelled populations of cells varying from areas with little to no Perls' labelling, to heavily labelled cells in areas where the SPIOs could not be completely removed from the cell surface even after repeated and prolonged washing with heparin supplemented PBS. It was not possible to properly count Perls' labelled cells because often the staining would be so dense it was impossible to see how many cells were being stained. The protamine sulphate concentration was thus determined by its ease of use. Using the lower concentration (3 µg/ml) the SPIO's were harder to wash off the cells extracellularly, and in the higher concentration (9 µg/ml) the Perls' labelling indicated the SPIOs seem to attach more sporadically in clumps to the cells. The Perls' stain indicated internalised SPIOs but not with 100% certainty so samples were observed using EM confirming SPIOs were within the lysosomes of the cells.

Perls' staining in vivo: A common method of iron detection *in vivo* is Perls' Prussian Blue reaction for ferric iron and has often been used *in vivo* situations (Cohen *et al.* 2010; Magnitsky *et al.* 2008; Sadan *et al.* 2008). Although some studies went as far as Pearl staining sections in different conditions, e.g. QA lesion

and SPIOs, SPIO labelled cells, QA and SPIO labelled cells (Sadan *et al.* 2008), they often do not carry out Perls' staining on sections when no SPIOs are present. Had they done this it would have become apparent that ferric ferrocyanide, the insoluble blue compound produced in a Perls' reaction, is present in brain sections that have undergone surgery, whether SPIOs were used or not. A positive blue pigment appears in sections that have previously had surgery in the absence of SPIOs, be it sham or graft, metal or glass cannula used. The main hypothesis is that during surgery when blood vessels are broken the blood released remains as hemosiderin, in part due to the compromised immune reaction of the brain. The ferric iron in the hemosiderin reacts with Perls' reagent giving the positive response that is almost indistinguishable from cells labelled with SPIOs. This effect is already well known, the presence of hemosiderin after cerebral microbleeds can be identified using MRI and histology sections turn blue when reacted with Perls' reagent (Fisher *et al.*). MRI is commonly the method of choice when screening for acute strokes (Chalela *et al.* 2007). Quantifying the intensity of the Perls' may help distinguish labelled cells from hemosiderin.

Perls' staining *in vivo* seems to be useful when looking at the migration of cells away from the area of deposition in the brain. For instance when SPIO labelled human neural stem cells are transplanted in to the immature rat brain and migrate from the sub ventricular zone to the olfactory glomerulus or migrate to the area of injury in an adult cortical stroke model (Guzman *et al.* 2007). In a study by Sadan et al that reported a smaller Perl' s count in a grafted region that only received cells, compared to a grafts of SPIO labelled cells into a QA lesioned striatum, one could postulate that the smaller Perl's count was due to less needle track damage causing bleeding in the brain because this cohort lacked the QA lesion (Sadan *et al.* 2008).

Graft change over time

The grafted animals scanned twice over a 6 week period may not have shown any significant difference in graft volume over this time, but the decrease in volume seen in the SPIO labelled cells, compared to the smaller change in graft volume observed in the non-labelled cohort, maybe indicative of SPIO's being engulfed by macrophages and removed in the former, compared to the hemosiderin causing signal in the latter than is known to remain in the brain for months (Graph 4.5).

GFP vs Perls' vs MRI

The MRI doesn't indicate density of the cell population and gives the impression of a large graft when in fact the area can be quite sparsely populated. The difference in graft volume between the different methods of measuring, GFP, Perls, and MRI, were surprisingly similar considering the blooming effect of the SPIOs during MRI. While there was no significant difference this could be attributed to the high variability from the graft sizes and the small size of the grafts. The needle tract mark contributes a lot to both the Perls' and MRI signal giving a volume of up to 1.34mm^3 for Perls' and 1.96 mm^3 for MRI, the sometimes complete overlap between the needle track and graft in these types of experiments presents rather a large problem. The best approach, other than restricting the MRI use to areas where hemosiderin in the tissue isn't a problem, may be to use only heavily labelled cells and a trained eye, because it is possible to distinguish the intensity of heavily SPIO labelled cells against needle track due to the SPIO's blooming effect expanding out of the needle track region. While studies are purporting that it is possible to distinguish single SPIO labelled cells (Shapiro *et al.* 2006) in the grafting model used here this would be difficult during the analysis to determine whether it is real signal or not. Alternatively using SPIOs in experiments where larger grafts are typically formed as a matter of course, like in the SPIO labelled VM grafts used here seems more useful than using SPIOs in mouse grafts which are generally smaller and don't expand far from the needle track region. So far we have seen that labelling VM with SPIOs doesn't hamper the establishment of large, surviving, functional grafts and looking at graft rejection in this model would be useful to monitor the efficacy of SPIOs.

Another aspect not properly represented in the literature is what happens if the graft completely fails in the striatum and whether the SPIO signal can be reflective of this, and how long it will take the SPIOs to be removed from the system. Following on from the work here using primary VM in the 6-OHDA lesioned animals, the graft could be later rejected by sub cutaneous injection of the original donor tissue. Alternatively, withdrawing immunosuppression from xenograft models also presents the opportunity to follow graft rejection and its portrayal through MRI imaging of SPIOs.

In an effort to increase graft size to see if the Perls' stain, while unhelpful for small grafts remaining in the needle track area, can be useful for larger grafts that go

beyond the area of the needle tract, *E14* Lister Hooded WGE expanded for 9 and 12 days with and without SPIOs were grafted into QA lesioned CD rats. Unfortunately these grafts didn't grow as expected and the Perls' was equally dark and in the same positions as the needle tract in all cases.

MRI volume conservative vs comprehensive

It is not possible to merely work out the contribution of the needle tract and minus the size of the signal from the MRI volume of the SPIO associated grafts due to overlap of the graft and injection site. If being more selective when measuring MRI volume and only attributing the darkest areas to SPIO contrast, it is possible to decrease the control graft volume to almost zero and a significantly different read out from true SPIO signal. Unfortunately it is likely cells with low levels of SPIO labelling that migrate to the outside perimeter of the grafted area, would be considered SPIO negative and the graft underestimated using this restriction. In addition when we compared the 'tight' MRI volume to the GFP volume we see a large underestimation of graft size using MRI and it seems that measuring all potential SPIO signal is important but regard the result with caution.

 In the non-labelled controls it does seem that the Perls' and MRI are more similar to each other and not necessarily indicative of the larger volume calculated using the GFP. Perl's and MRI correlate more closely and it seems Perls' provides a general measurement of MRI signal not necessarily linked to labelled cells.

In conclusion SPIO signal does provide a measure of graft volume *in vivo* and can label migratory cells over small distances. The SPIOs are difficult to wash from cell surfaces and may be the cause of differences seen in differentiation markers compared to controls here, as has been the case when chondrogenesis was blocked by extracellular but not intracellular SPIOs (Arbab *et al.* 2004b; Bulte *et al.* 2004; Kostura *et al.* 2004) and should be investigated further. SPIOs can successfully label both ES cell, expanded WGE and VM and following grafting similar volumes are given from the MRI scanning as from the IHC. Longer term studies can now be taken forward, including graft rejection studies and further characterisation. It is likely SPIOs will continue to be used as a marker of cell location but only until a better alternative is developed.

4 Ferritin as an MRI Contrast Agent

4.1 Aim

To construct and test an MRI contrast agent transgene based upon conditional expression of Ftl and Fth subunits separated by a 2A self-cleaving peptide, in both *in vitro* and *in vivo* environments. Expressing both Ft subunits transgenes may improve signal and have less detrimental effects on the cell than exspressing either alone.

4.2 Introduction

A change in a tissue's iron content gives a change in MRI signal without the constraints of using additional substrates. Ferritin bound iron seems to be the primary determinant of MRI signal contrast in gray matter (Vymazal *et al.* 1996) and MRI has been used to detect the change in endogenous iron content *in vivo* in the age related increase in the human brain (Bartzokis *et al.* 1997) and the increase above and beyond the normal level of iron in neurodegenerative disease states like PD (Bartzokis *et al.* 1999), Alzheimer's and HD (Bartzokis and Tishler 2000). Iron homeostasis is regulated by a number of transport and storage proteins (Bothwell 1995) but it is the Fts in particular that seem to be well suited for use as MRI contrast agents. Fth is associated with the rapid uptake and reutilization of iron while Ft L is involved with long term iron storage. Distribution of different sub units in the brain reflect this, for example Fth is more prevalent than Ftl in neurons in the cerebral cortex that require a reusable supply of iron, while microglia, which are mostly scavengers contain more Ftl and oligodentrycytes express both heavy and light (Connor *et al.* 2001) (Zecca *et al.* 2004)).The impact on the disease a treatment is trying to 'cure' by over-expressing Ft genes in cells must be seriously considered, taking into account the detrimental effect that iron can have in the brain, for example a mutation in Ftl leads to a dysfunctional protein causing a dominantly inherited basal ganglia disease (Curtis *et al.* 2001). Iron deficiency and overload causes a range of detrimental pathological effects (Andrews 1999) and while a decrease in Fth is detrimental (Ill *et al.* 2006) an increase can provide protective qualities (Pham *et al.* 2004), even protecting against MPTP induced parkinsonism in mice (Kaur *et al.* 2003). This effect may only have a temporal specificity, since as the mice age chronic overexpression of Fth results in an increased susceptibility to PD which

seem to be a result of increased iron availability (Kaur *et al.* 2009; Kaur *et al.* 2007). There are on-going studies to illuminate the exact mechanisms of iron involvement in the brain and, as with overexpression of any protein, it will be important to determine the effect of Ft on a case by case basis. There is substantial sequence similarity between mouse and human Fth and Ftl genes (Beaumont *et al.* 1989; Torti *et al.* 1988) but they are not completely functionally equivalent. hFth has a higher binding capacity for iron than mouse isoforms and therefore has a superior chelating ability (Rucker *et al.* 1996).

The Ft core displays antiferromagnetic and superparamagnetic properties (Haacke *et al.* 2005). At high iron loading the Ft <u>relaxivity</u> is constant per iron molecule but the relaxivity increases at low iron loading so when one expresses Ft, independently of iron content, high relaxivity can still be achieved (Gottesfeld and Neeman 1996). Of the iron storage proteins only ferritin has a field dependent increase in R_2 that could provide quantitative information on ferritin content. (Bartzokis *et al.* 1993). Meaning that with access to two different field strengths, iron concentration can be calculated because of the associated change in R2 of the Ft-bound iron.

Two pioneering studies in 2005 reported that as cells sequester iron from the organism, due to metalloprotein over-expression, they become superparamagnetic and suitable for MRI studies (Cohen *et al.* 2005; Genove *et al.* 2005). These cells give contrast *in vivo* with no other exogenous metal supplementation required, simplifying delivery, and *in vitro* with or without iron enriched media (Genove *et al.*, 2005). Ft and Tfrc production are tightly regulated in response to the labile iron pool, Ft over-expression will decrease the labile iron pool, leading to Tfrc upregulation to bring in more iron to the cell, thus a higher iron content (Welch, 1992). Different approaches have been taken to achieve MRI contrast; Genove *et al.*, used a replication defective adenovirus to transfect human Fth and Ftl chain transgenes into the mouse brain, eliciting MRI contrast (Genove *et al.*, 2005). Cohen *et al.,* overexpressed the murine Fth subunit in a Tet-inducible system in C6 rat glioma cells, resulting in T_1 and T_2 relaxation time shortening (Cohen *et al.* 2005). Soon after these initial studies both the Tfrc and Fth gene were stably over-expressed using random integration in the immortalized mouse cerebellar progenitor cell line, C17, and imaged in 1.5 and 7T MR scanners (Deans *et al.*, 2006). MR contrast was significantly different from control *in vivo* when cells were supplemented with human

holo-transferrin and iron citrate, however, MRI failed to detect transgenic cells *in vivo* when they were transplanted without supplementation (Deans *et al.* 2006). Although no detrimental effects were found with over-expression of Fth and Tfrc, using a supplement loses one of the benefits of using Ft transgenes for MRI. The Tfrc reporter system may cause cell toxicity; an anticancer drug, doxorubicin, that induces Tfrc expression, causes Tfrc dependent iron uptake responsible for the apoptosis associated with use of doxorubicin (Kotamraju *et al.* 2002) and via the Fenton reaction increases in Tfrc could elevate free radical formation due to the increase in free iron. In a second study using mouse ES cells, expression of human Fth was established using a lentiviral vector and monitored *in vivo* addressing questions of viability, pluripotency and functionality with positive results on a 4.7T scanner, importantly without supplementation (Liu *et al.* 2009b). The effect on growth rate of overexpressing Fth varies depending on cell type. In C6 glioma cells (Cohen *et al.* 2005) and mouse erythroleukemia cells (Picard *et al.* 1996) growth rate is not affected. In contrast, in HeLa cells growth rate decreases as Fth content increases following stable integration (Cozzi *et al.* 2000).Furthermore transgenic mouse ES cells expressing human Fth chains have been established showing no toxicity effects or influences on stem cell pluripotency (Lui et al, 2009 unpublished). The sequences used in these experiments exclude the regulatory iron response elements allowing constitutive expression. Since it was first suggested that Fth could act as an MRI contrast agent various adaptations have been suggested to improve signal, modifications to cause Ft aggregation by binding it to cytoskeletal elements will likely improve transverse relaxation, as hypothesised by computer simulations and cross linking Ft at short distances to actin and polymerizing *in vitro* (Bennett *et al.* 2008).

In this chapter, I aimed to develop a mouse ES cell model for the conditional expression of Ft transgenes. The majority of studies manipulating the iron regulatory system for MRI contrast over-express the Fth gene (Campan *et al.* 2011; Cohen *et al.* 2005). However, based on observations that transgenic Ft subunits don't combine with endogenous Ft (Cozzi *et al.* 2000) and only form homopolymers which remain as apoferritins (Arosio and Levi 2002; Curtis *et al.* 2001), a transgene co-expressing both Fth and Ftl has potential to give better contrast. Especially considering that it is the Ftl that is involved in the long term storage of iron (Boyd *et al.* 1985). Further the increased resistance of Ftl to denaturation (Santambrogio *et al.* 1992) may provide additional protective effects. Studies done to date have overexpressed Fth either

transiently or stably, and all result from random transgene insertion after use of adenoviruses, lentiviruses (Shan 2004) and pronuclear injection of plasmids. In order to achieve conditional transgene expression, and enable the comparison of different transgenes for MRI contrast without the confounding effects of transgene position-effects and variable copy number (Wilson *et al.* 1990) I decided to use the approach of targeted transgene integration at the ROSA26, a well validated safe harbour locus (Nyabi *et al.* 2009). To generate transgene vectors we also aimed to take advantage of a recently developed Gateway cloning strategy for the rapid generation of ROSA26 locus gene targeting vectors (Nyabi *et al.* 2009), using a Fth and Ftl devoid of IREs and separated by a self-cleaving 2A sequence. The 2A sequence allows both subunits to be expressed at equimolar concentrations (Trichas *et al.* 2008). The CAG promoter was chosen because it is a strong promoter and found to work well in ES cells as mentioned previously.

The ROSA26 locus encodes three transcript of unknown function only one is coding and disruption of two out of three of these transcripts do not perturb growth or viability in homozygous mice (Zambrowicz *et al.* 1997). ROSA26 provides good control of transgene expression with a high targeting efficiency and ubiquitous moderate expression (Friedrich and Soriano 1991; Sorgi *et al.* 1997)Soriano 1999. This locus has been taken advantage of using Multisite Gateway® technology (Invitrogen) based on recombination studies done by Hartley et al (Hartley *et al.* 2000). It enables multiple genes to be inserted simultaneously and in a specific order, permitting strong promoters such as pCAGGs to be targeted alongside the gene of interest (GOI) further increasing expression levels. The use of this *in vitro* recombinase based system has improved the ease of vector production compared to older techniques that required complex vector construction. Nyabi and colleagues generated Cre/loxP conditional ROSA26-targeted ES cells using Gateway® cloning to build target vectors (Nyabi *et al.,* 2009). The components they used include pCAGGs followed by a loxP-flanked β-galactosidase neomycin fusion gene (β-geo) and three polyadenylation signals (3xpA), preventing transcriptional read through, the GOI and an IRES eGFP with or without a luciferase reporter. The construct confers neomycin resistance and conditional expression allows the cells to grow unperturbed until the specific GOI is required; following transfection of plasmid DNA encoding Cre, subsequent Cre recombinase-mediated excision of the floxed PGK-neo-3xpA (STOP) cassette ensues bringing the GOI-IRES-eGFP under the control of

pCAGGs. Gateway® cloning requires the GOI to be inserted into an entry clone by one of four possible techniques, the one utilised here uses standard restriction enzymes and ligases. Once the entry clone is complete the Gateway® system uses the LR reaction to make the expression vector or the BP reaction to make new entry clones. The LR reaction takes advantage of the bacteriophage lambda recombination proteins, Integrase and Excisionase and the *E.coli* encoded protein Integration Host Factor. These L, R, B and P's are abbreviations of restriction sites attX, where X would be the L, R, B or P. Entry clones have L's that when cut have sticky ends that match with a destination vector containing attR sites, hence the name LR reaction (Figure 4.1). The high efficiency is due to the ccdB gene that prevents phage growth in the medium, as well as the two antibiotics. This reaction is totally reversible and more entry clones can be generated using the BP reaction from the expression clone.
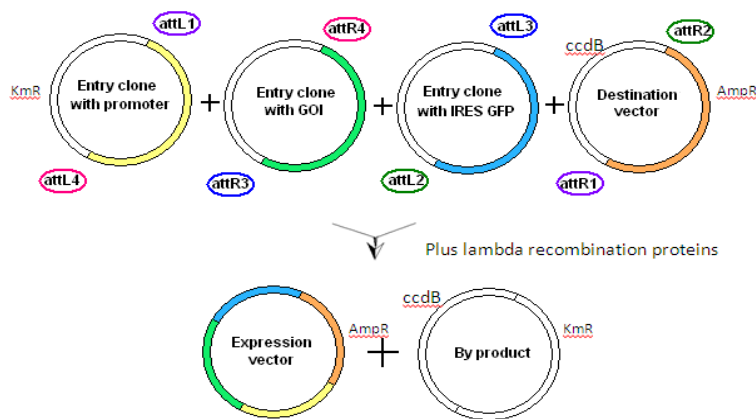
Figure 4.1: The LR reaction shows how three entry vectors can recombine with a destination vector by virtue of their attL and attR sites and exposure to particular enzymes, integrase and excisionase. The result is an expression clone and a by-product consisting KmR and a ccdB gene.

Iron Supplementation of the Media

Iron supplementation of the media when overexpressing Ft can improve signal, as demonstrated when monitoring solid tumours in mouse models (Feng *et al.* 2012) and in *in vitro* MRI measurements (Deans *et al.* 2006; Genove *et al.* 2005). There are a number of methods to supplement media with iron. Transferrin, a component of Gibco's knockout serum replacement media, is commonly used in cell culture to provide iron to cells in a physiologically safe and effective form. Transferrin is therefore present in the chemically defined ES cell media with 15% KSR containing 157.6µg transferrin per 10 mls. This should provide enough iron to give contrast in MRI based on previous work (Cohen *et al.* 2005). Samples with further iron supplementation using Ferric Ammonium Citrate were set up, although supplementation should not be a necessity for MRI contrast *in vivo* (Liu *et al.* 2009b). Iron uptake increases linearly with increasing concentrations of transferrin in culture of mouse hepatocytes (Cole and Glass 1983) and it is necessary to confirm change in MRI contrast is a result of the transgene not the supplement alone.

4.3 Experimental Design

For further details of the techniques performed here see general methods Chapter 2. All primer sequences can be found in Table 2.1

This section involves two methods of expressing the Fth and Ftl transgenes under the control of a pCAGGS promoter. One details the construction of a targeting vector to target the ROSA26 locus, the other vector was constructed to be expressed following random integration into the genome.

Targeting the ROSA26 locus

pENTRY plasmid construction

Fth and Ftl cDNA were received as a gift from Eric Ahrens, University of Pittsburgh School of Medicine (Genove *et al.* 2005). pEntry clones were generated through PCR amplification of the Ft cDNA with the addition, at the 5' end, of a kozak sequence, EcoRI site, and at the 3' end the STOP codon was removed and a 2A self-cleaving peptide sequence and a BamHI site were added to the Ftl (Primers: 'Ftl kozak' and 'Ftl 2A'). To the Fth cDNA a BglII site was added to the 5' end and an EcoRI site to the 3' (Primers: 'Fth EcoRI' and 'Fth BglII'). The two products were independently inserted into a pCR-Blunt-II-TOPO using a Zero Blunt TOPO kit (Invitrogen). Using Zero Blunt II TOPO PCR cloning kit, version K, (Invitrogen) 4µl of fresh PCR product, 1 µl of salt solution and 1µl pCR-Blunt-II-TOPO vector were incubated at room temperature for 5-10 minutes while Top10 (Invitrogen) competent cells were thawed on ice. The TOPO mix was added to the Top10 cells, left on ice for 5 – 10 minutes and a heat shock transformation was carried out at 42°C for 30 seconds. The vial was placed on ice for 2-3 minutes before addition of 250 µl SOC media followed by a one hour incubation at 37ºC and 200 rpm. 50 µl transformed cells were then spread onto an LB agar plate with 50µg/ml kanamycin, and incubated overnight at 37°C. Sequences were confirmed by sequencing at Cardiff University in house sequencing core using 'M13 reverse' and 'M13 (-20) forward' primers (Table 2.1). The Fth insert was digested from the TOPO vector using BamHI and NotI, and phenol/chloroform purified. The product was ligated into pENTR2B Dual Selection vector that had been cut with the same restriction enzymes and CIP treated. The insert was checked by restriction digest using AlwnI and SacI. The Ftl was digested from the TOPO vector using BamHI, purified and ligated into the

pENTR2B-Fth that was linearized with BglII, CIP treated and purified. The resulting colonies were picked and orientation was confirmed by restriction digest using SacI.

Targeting Vector Construction

The destination vectors for targeting the ROSA26 locus and pEntry vectors: destination vectors pROSA26-DV1 (LMBP 6350), pROSA26-DV3 (LMBP 6352) and pROSA26-DV2 (LMBP 6351) and pEntry vectors *att*L4-pCAGGs-*lox*P-βgeo-3xpA-*lox*P-*att*R1 vector (LMBP 6354), *att*R2-IRES-eGFP-*att*L3 vector (LMBP 6353) and pEntry *att*R2-IRES-EGFP-Luciferase-pA-R3 (6440), were generated and gifted to us by Jody Haigh, Ghent University (Nyabi *et al.* 2009). pEntry *att*R2-IRES-EGFP-Luciferase-pA-R3 was used instead of the attR2-IRES-eGFP-attL3 as it has a better reporter with an optimised polyadenylation sequence and expression of both eGFP and luciferase reporters. LR reactions were performed using Gateway® Clonase Enzyme mix (Invitrogen) following the manufacturer's instructions with minor modifications described previously (Nyabi *et al.* 2009) (Figure 4.2). For the multisite LR reactions 100ng of each of the three pEntry vectors containing eGFP luciferase, pCAGGs or the GOI were incubated for 8 hours at room temperature with LR Clonase II mix. The pROSA26 destination vector, DV2, was then added with additional Clonase II mix over night at room temperature. Proteinase K added for 10 minutes at 37°C to stop the reaction. The LR reaction was transformed into DH5α competent cells (Invitrogen) propagated at 28°C in 300μl of SOC media for 90 minutes with gentle agitation and plated on LB-AMP agar plates for culture at 28°C overnight. To avoid recombination all subsequent bacterial expansions of the targeting vector took place at 28℃. Colonies were picked and verified by restriction digestion using SalI (NEB) and PCR (Primers: 'Ft L1' with 'PCAGGS R1' and primer pair 'Luc R3' with 'ROSA R3') over the recombined att sites.
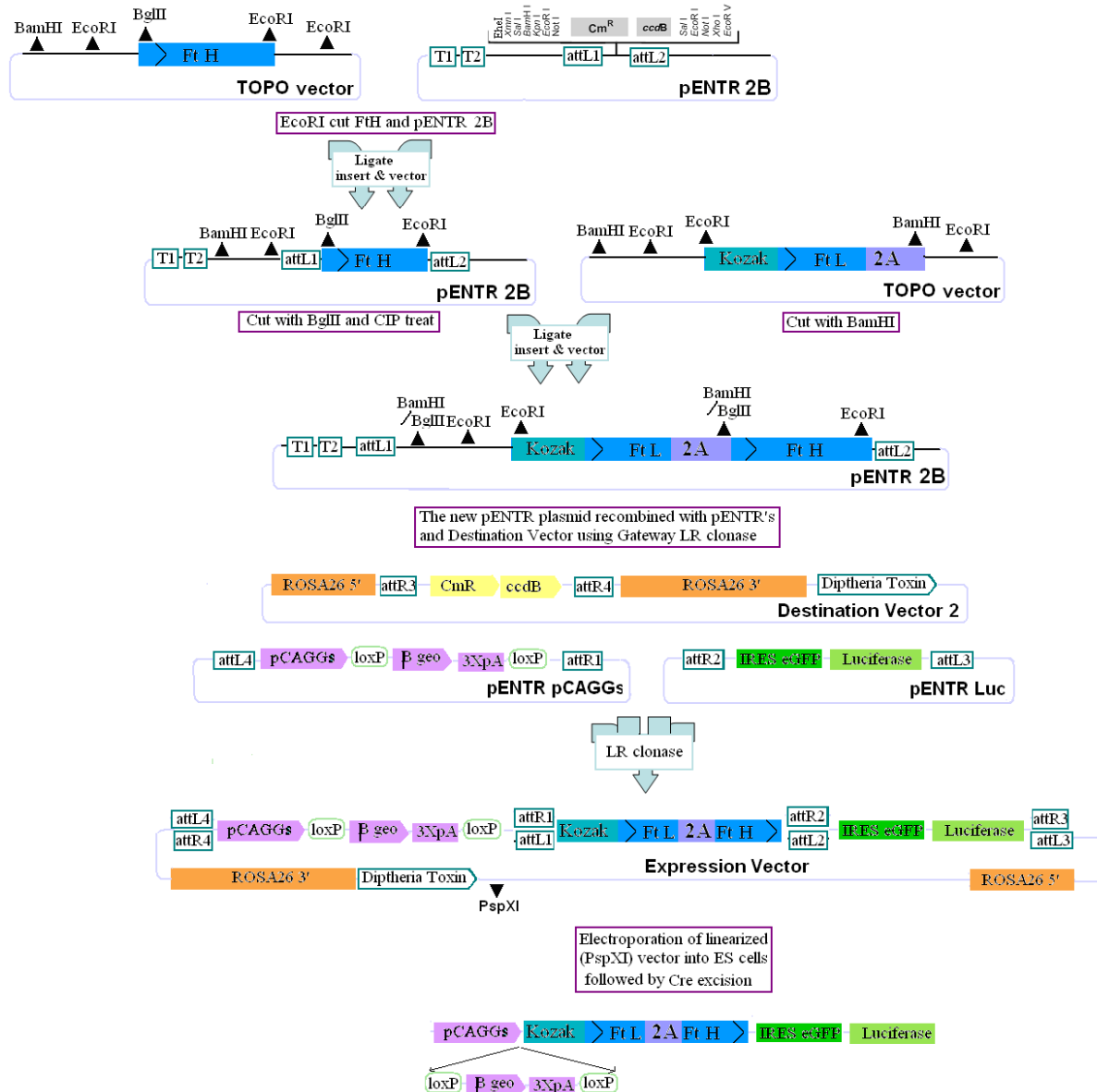
Figure 4.2. : Gateway strategy from pENTR construction to electroporation into ES cells and Cre excision.

Random Integration Vector Construction

The pEC vector contains a PCAGGS promoter, multicloning site and an IRES GFP, pEC was constructed in house by Emma Cope by replacing the CMV promoter in pIRES2-eGFP with the CAG promoter from pCAGGIG. To insert the Ftl/Fth under the control of the PCAGGS promoter both were cut with EcoRI and the pEC vector CIP treated. The Ftl/Fth was removed from the pENTR plasmid by gel extraction using EcoRI (GeneClean II kit, Cat 1001-400) ligated into the linearized pEC vector overnight and transformed into DH5α (Invitrogen). The orientation was checked in resulting colonies by restriction digest using HindIII (NEB) (correct profile: 991 and

6577 bp) (Figure 4.3). The correct plasmid was expanded and purified using Endofree Maxiprep (Qiagen).
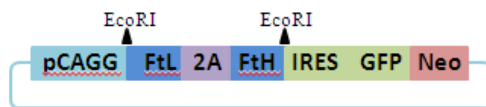
Figure 4.3: The Ft2A sequence was inserted into a pEC vector following a pCAGGs promoter and preceding an IRES GFP and containing a neomycin resistance gene.

Nucleofection of mouse ES cells

To achieve stable cell lines expressing Fth and Ftl the Gateway vector and random integration vector (pEC-Ftl/Fth) were transfected into mouse ES cells. pEC-Ftl/Fth was nucleofected using either 10µg of circular or linearized vector (cut with SpeI). The cells were incubated with accutase to achieve a single cell suspension, washed with PBS and counted, $2x10^6$ cells were then centrifuged at 1000rpm for 3mins, to form a pellet. These cells were resuspended in 100 µl of Nucleofection solution which had been prepared previously by adding 78 µl Nucleofector solution to 22 µl supplement with 10 µg of either expression vector or the control DNA. The solution containing the cells was transferred into an amaxa certified cuvette and placed into the Amaxa Nucleofector II, cells were nucleofected under programme A-024. Immediately 500 µl of warm ES media was added to the cuvette and using the plastic pipettes provided, cells were transferred to two 10cm gelatine coated plates with 10mls of ES cell culture media and incubated under standard culture conditions. 24 hours following transfection G418 (300µg/ml) was added to the media to select for neomycin resistant cells and selection carried out for a minimum of 7 days, after which point surviving colonies were picked into 96 well plates and expanded.

Targeting Vector Clone Analysis:

X-Gal treatment on 96 well plates

Following transfection with the Gateway targeting vector, colonies were picked into 96 well plates, fixed and treated with X-Gal, as detailed in the General Methods section, Chapter 2, to confirm β-galactosidase expression and so successful transfection.

Confirmation of ROSA26 gene targeting

Southern Blot: To confirm targeting to the ROSA26 locus Southern blots were performed (See General Methods, chapter 2) on 30 β-galactosidase positive colonies and negative control gDNA from E14 cells. PCR probes were created from amplification of mouse ES cell gDNA using primer pairs "R26 5' probe F" with "R26 5' probe R" and "R26 3' probe F" with "R26 3' probe R" and amplified with high fidelity platinum polymerase following the manufacturer's instructions (Figure 4.4). The cycling conditions were as follows for both primer pairs: denaturing, annealing, elongation temperatures were at 94, 56 and 58°C respectively.
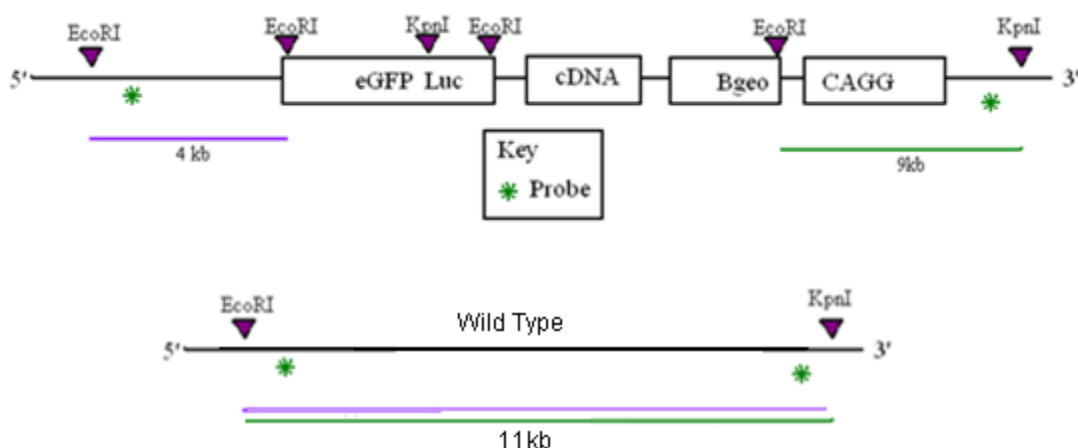
Probe	Enzymes	Targeted Size (kb)	WT Size (kb)
5'	EcoRI/ KpnI	4	11
3'		9	11

Figure 4.4: Position of vector in gDNA following correct targeting to the ROSA26 locus demonstrating EcoRI and KpnI cut sites and expected probe sizes. Wild type locus with probe annealing below and table depicts the expected sizes.

Confirmation of Targeting by PCR: To determine if the targeting vector had correctly targeted the ROSA26 locus PCRs were carried out with primers that spanned the area of recombination at the 5' homology arm. Three polymerases were tried; GoTaq polymerase (Promega, Wisconsin, USA), Expand polymerase (Roche) or Megamix (Cambio, UK). Primer pairs external "G1for" with "ROSA 3' RC" to pick up the wild type locus and 'G1for' with 'Luc L3 RC" to pick up the correctly targeted

locus (Figure 4.5) were used with an expected band product size of 1.4kbp. Primers were tested over a range of $MgCl_2$ concentrations from 1.5-5mM, and a range of temperatures at 55 - 65°C. Titrations of gDNA concentrations were used at 5µl, 1µl, 1/10 and 1/5 dilutions. Touch down PCR was carried out with denaturing, annealing and elongation for 94°C, 64°C and 72°C respectively with the annealing temperature decreasing in each cycle in 1°C increments until it reached 52°C after which point the annealing temperature was maintained for a further 25 cycles. PCR was also carried out with primers for GAPDH, Neomycin and LacZ genes using GoTaq flexi (Promega).

Ft Expression Confirmation by PCR: A nested PCR was carried out to try and find any low concentration of human Ft present, in cDNA samples from LacZ positive clones. Human foetal brain cDNA as the positive control and mouse ES cell cDNA for the negative, using primers 'FTHCheck F' and 'FTHCheck R' for the first round and primers 'FTHF1' and 'FTHR1' (programme: 35 cycles, 95°C, 58°C, 72°C).
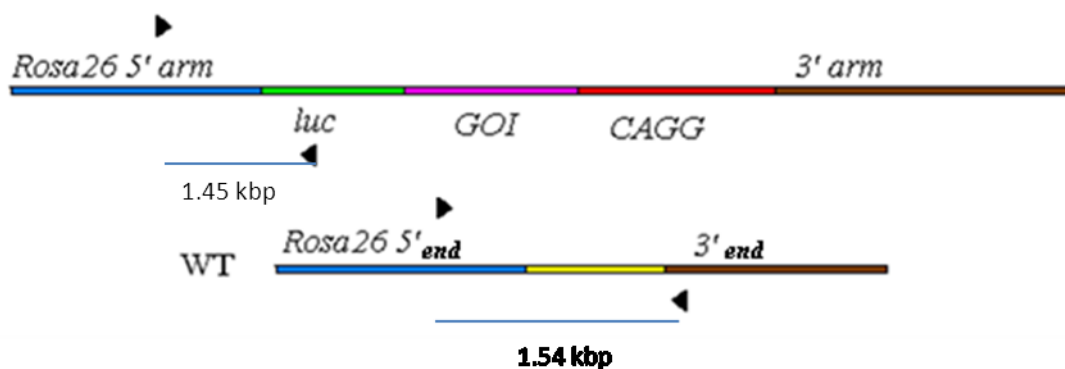
Figure 4.5: Primer positions denoted by black arrows to demonstrate recombination of the Gateway targeting vector Primers pair: forward external for both images is "G1for" and the reverse on the top strand is "Luc L3 RC" and for the bottom is "ROSA 3' RC"

B-Geo Excision

To flox out the β-geo in two β-galactosidase positive clones (Blue A and Blue B) Adenoviral Cre, AD5-CMV-Cre, and electroporation using a Cre recombinase containing plasmid (pCAGGS-CreIRES-puro) were used. 30µg of Cre plasmid was lipofected and electroporated at 240V, 500µF into BlueA and BlueB. The Cre plasmid had a puromycin resistance gene and to reduce the background of non-transfected cells they were treated with puromycin (1µg/ml) for 7 days. After which

point colonies were picked into 96 well plates, subsequently grown and triplicate plated, with one 96 well plate being frozen at -80°C, another was lysed for protein extraction and the third was fixed and stained with X-gal. Fluorescence microscopy for GFP expression and a luciferase assay was also carried out to try and determine successful floxing. B-galactosidase negative colonies were expanded; stocks were frozen at -80°C and in liquid nitrogen.

Western Blot: To determine if the Ftl/Fth transgenes were being expressed in the mouse ES cell clones, protein was collected and tested for the two Ft subunits and the 2A self-cleaving peptide. Western blotting was carried out as described in the General methods, chapter 2, with a 12% polyacrylamide resolving gel. Human ES cell and human foetal liver protein was used as positive controls and mouse ES cell protein as a negative control. A range of antibodies was used; anti-ferritin heavy chain antibody (Abcam, ab75972) that does not cross react with mouse or rat and used at a range of concentrations: 1:500, 1/1000 and 1/2000. Also an anti-ferritin heavy chain rabbit polyclonal antibody (Abcam, ab65080) at 1/500, anti-Ferritin Light chain (D-9) mouse monoclonal antibody (Santa Cruz, sc-74513) at 1/250 and an anti-2A peptide rabbit polyclonal antibody (Millipore, ABS31) at 1/1000 were used. Anti-β-actin antibody (Cell Signaling, 8H10D10), at 1/10,000, was used as a measure of protein concentration across the samples. The milk (Marvel) concentration for the anti-Ferritin Light primary antibody stage was 1%, all other stages and antibodies used 5% milk throughout. The appropriate secondary antibody was used at 1:10,000.

Analysing the Effects of Ftl/Fth Overexpression

Expressing human Ft to act as a contrast agent in mouse ES cells may perturb the cell's normal growth, and so viability, apoptosis and proliferation rates were determined and compared to controls.

Flow cytometric analysis of DNA content using propidium iodide to measure cell proliferation: Cell proliferation was measured using propidium iodide staining to determine the DNA content of cells. A single cell suspension was generated following incubation with accutase (PAA Laboratories) at 37°C for 5 minutes and resuspended in 1ml PBS, centrifuged at 1,000 rpm for 3 minutes and fixed in 1ml of cold 70% Ethanol. They were then incubated for one hour and could be left up to one

week at 4°C. Cells were centrifuged at 1,000rpm for five minutes and washed in PBS, pelleted at 1,000 rpm for three minutes and resuspended in PBS containing 40µg/ml propidium iodide and 100µg/ml RNAse A, then incubated at 37°C for 30 minutes. Samples were stored in the dark until flow cytometric analysis usign channel 585_42 PE-A and carried out in triplicate. During flow cytometry 30,000 events were recorded on a BD FACS Canto analyser. Scanning took place in the CITER Stem Cell Suite and Flow Cytometry Unit, School of Biosciences using a BD FACS Canto analyser and FACS Aria cell sorter.

Results were analysed based on cell cycle algorithms using the FlowJo Software. Primary gating was applied via forward scatter and side scatter to eliminate debris and doublets, cell cycle analysis was applied to the histogram according to the Watson pragmatic model which separates out the G1 and G2 stages of the cell cycle.

Wst1 assay as a measure of metabolic activity: Metabolic activity was measured by the reduction of tetrazolium salt to a formazan dye. 10µl of Wst1 reagent (Roche) was added to each sample in triplicate in a 96 well plate format and incubated for 2 hours at 37°C. The absorbance was read on BMG Fluostar and the absorbance taken at 450 nm and 590 nm.

Caspase assay as a measure of apoptosis: Caspasae 3 and 7 activity were measured to determine apoptosis levels. Caspase-Glo 3/7 assay reagent (Promega) was added in a 1:1 ratio to cells in triplicate in a 96 well format. Cells were incubated at 37°C for one hour and luminescence read on an Ascent ThermoSkan plate reader (Thermo Scientific). Background luminescence was subtracted using readings from a blank consisting of media with caspase reagent only and were normalized to cell number.

Transplantation of mouse ES cells Transfected with Ftl/Fth containing constructs

To image Ftl/Fth expressing cells *in vivo* Mouse ES cells were differentiated to neural progenitors to day 16 using chemically defined media, as detailed in chapter 2 and 5 x10^5 cells were grafted into QA lesioned Sprague Dawley rats. Stereotaxic co-ordinates AP: 0.6, ML: 3.1, DV: -5/-4 with 1µl of cell suspension per depth. Animals were immunosuppressed with cyclosporine (Sandimmun, Novartis) 10mg/kg, daily, commencing one day prior to transplantation and maintained until sacrifice.

MRI to pick up Expression of Ft subunits

The expression of Ft subunits should provide MRI signal that can be used to distinguish grafted cells from host. Following transfection of the Ftl/Fth into mouse ES cells the cells were prepared to be imaged as cell pellets *in vitro* and after transplantation into a rodent model as grafts into the brain and as teratomas.

MRI for Targeting Vector: *Cell pellets:* MRI was performed using Multi slice multi echo (MSME) axial TR 3,500ms and a range of TE from 11ms to 220ms in steps of 11ms. FLASH 2D T2* with TR/TE parameters of 800/ 8.5ms, 800/4.5ms and 1200/15ms.

Animals: MRI was performed 24 hours following surgery and again 6 weeks later. Animals were scanned using FLASH 2D T_2*, TR/TE = 1,200/15ms, SI 0.30/0.30mm.

MRI for Random Integration: Cells prepared for MRI were cultured as normal with either standard media or with media supplemented with iron. Cells were exposed for 48 hours to either Transferrin (Sigma) at 1mg/ml or 0.5mg/ml or Ferric ammonium citrate (Sigma) at 200μM. Cells were fixed with 4% PFA and pelleted into a modified 96 well plate for the MRI.

The pellets were scanned using FLASH 2D with varying TR/TE of 800/8.5, 800/4.5 and 1200/15. A multi-slice-multi-echo scan was performed with a TR of 10,000 ms and TE 20-320 in of 20ms steps, and a spin echo TE 11ms

Immunocytochemistry

Fluorescent immunocytochemistry was performed as detailed in Chapter 2 on cell cultures fixed with 2% PFA for 15 minutes. Primary antibodies used were Doublecortin (1/) (Abcam) and GFAP (1/2000) (Dako) and secondary Anti-rabbit 488 and Anti-rabbit-594 respectively both 1/200.

Immunohistochemistry

Animals were transcardially perfused and brains taken at six weeks post transplantation for histological analysis. They were sectioned coronally on the freezing stage microtome at 40μm. 1:12 series was taken for Nissl staining using CV, and IHC with anti-Neu N (1/4000), anti-Ferritin (1/1000), anti-GFAP (1/2000). The immunohistochemical staining protocol was the same for each antibody, as described in Chapter 2.

4.4 Results

The MRI properties of mouse ES cells expressing human Ft subunits were assessed by constructing two vectors one based on targeting the ROSA26 locus and the other for random integration. After transfection into mouse ES cells the effects of Ft were tested in a biological and an imaging sense.

4.4.1.1 Generation and targeted Integration of the Ftl/Fth transgene

Generation of the Ftl/Fth-ROSA26 targeting vector involved a multistep cloning process outlined above. Correct cloning of Fth and Ftl inserts proved difficult and troubleshooting stretegies were used to achieve success. These are recorded below.

Ferritin Strategy #1

Following ligation of the Ftl insert into the TOPO vector containing Fth, 35 colonies were checked using miniprep methods and orientation determined by restriction digest. All colonies contained the Ftl insert in the wrong orientation.

Ferritin Strategy #2

In order to correct this, an attempt to force the insert into the vector in the correct orientation using BglII and SpeI was performed. This resulted in four colonies. Similar checks were carried to determine the insert orientation using EcoRI but none contained the Ftl insert.

DH5α library efficiency cells were used initially and when no inserts were in the correct orientation Stbl3 cells were tried in case they were able to handle the insert. Neither *E.coli* strain resulted in insertion of Ftl in the correct orientation.

Ferritin Strategy #3

Certain entry vectors have an rrnb transcription termination sequence preventing basal expression of the GOI in *E.coli.* As entry into the pENTR vector was necessary to access the Gateway system a new strategy was formulated. This strategy assumed *E.coli* cannot express both ferritin chains and survive and the presence of an rrnb sequence would allow both genes to be inserted in the correct orientation and allow propagation using *E.coli* DH5α. Fth was ligated into pENTR 2B Dueal Selection vector after restriction digestion of both independently using BamHI and

NotI and CIP treatment of pENTR2B. The Fth insert orientation was confirmed by a double digestion using AlwNI and SacI (correct profile: 1852 and 1016 bp). The plasmid was then linearized using BglII and ligated with FtI that had been digested from the TOPO vector using BamHI resulting in 68 colonies. The orientation was confirmed by miniprepping followed by restriction digestion using PvuII (correct profile: 2506 and 1066bp) and SacI (correct profile: 2895 and 677bp) (Figure 4.6 (A and B). This method resulted in the correct FtI/Fth pENTR plasmid.

Generation of the targeting vector

The conditional ROSA26 DV2 was recombined with pENTR vectors containing an IRES-eGFP-Luciferase, one containing the pCAGGs, and a third containing the pENTR FtI/Fth. This was confirmed by PCR across the att1 (primers: 'pCAGGS R1' and 'FtI1') and att3 (primers: 'Luc R3' and 'ROSA R3') recombination sites and restriction digestion using XhoI (correct profile: 12695, 4243, 3752 and 1330 bp) and SalI (correct profile: 9432, 5055, 4368, 1804 and 1361) that gave the correct restriction profile in six out of 12 colonies (Figure 4.6 (C-F)).
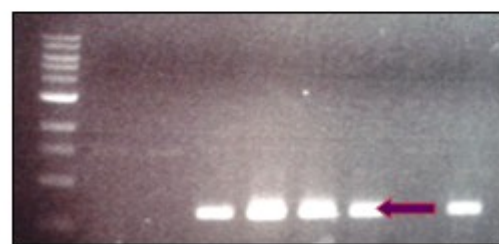
pENTR2B with FtLH

A) PvuI

B) SacI

Expression Vector

C) XhoI

D) SalI
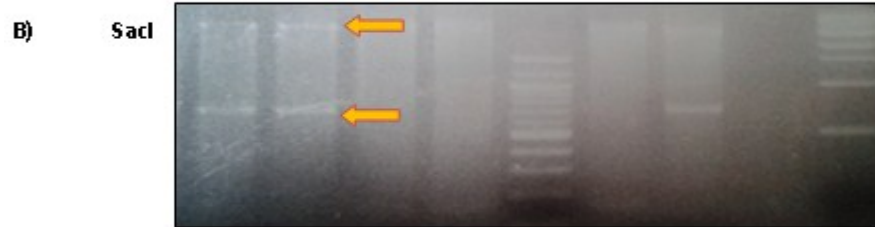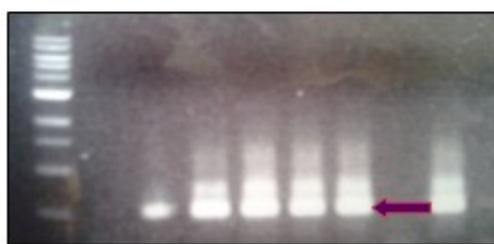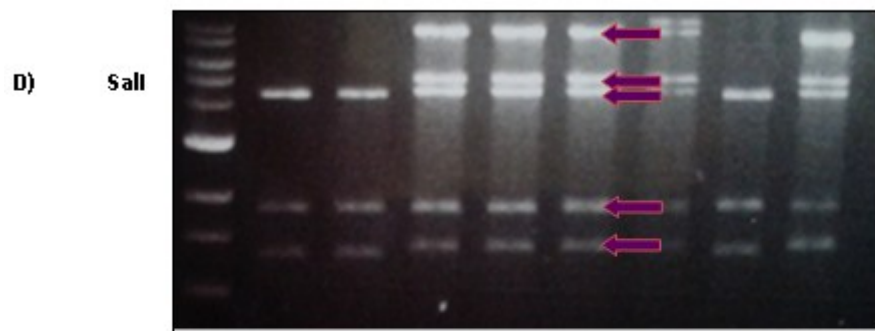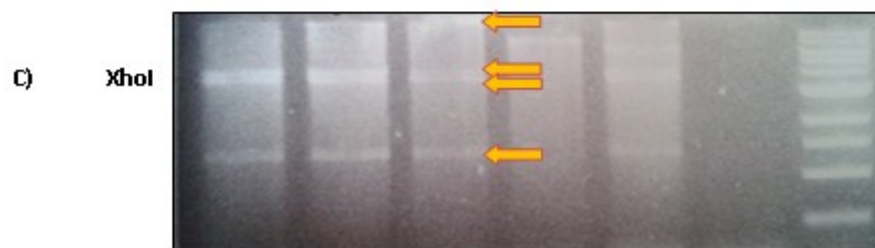
E) PCR #1

F) PCR #3

Figure 4.6: The correct orientation of Ftl and Fth in pENTR2B was confirmed by restriction digestion using PvuI (2506; 1066 bp) (A) and SacI (2895; 677 bp) (B). Following the LR clonase reaction correctly recombined vectors were confirmed by restriction digest using XhoI (12,695; 4,243; 3,752; 1,330 bp) (C) and SalI (9,432; 5,055; 4,368; 1,804; 1,361 bp) and PCR with primers over the att1 site (554 bp) (E) and att3 site (503 bp) (F). 1kb ladder (NEB) in all pictures, 100bp ladder (NEB) also in picture (B).

In vitro assessment of mouse ES cells transfected with the Ftl/Fth targeting vector

Cells underwent G418 selection for 10 days following transfection with the targeting vector. Colonies were picked into 96 well plates and treated with Xgal revealing all colonies that stained blue (LacZ positive) (Figure 4.7A). Since ROSA26 provides ubiquitous expression replicates from colonies where every cell was dark blue were picked and taken forward at this stage.
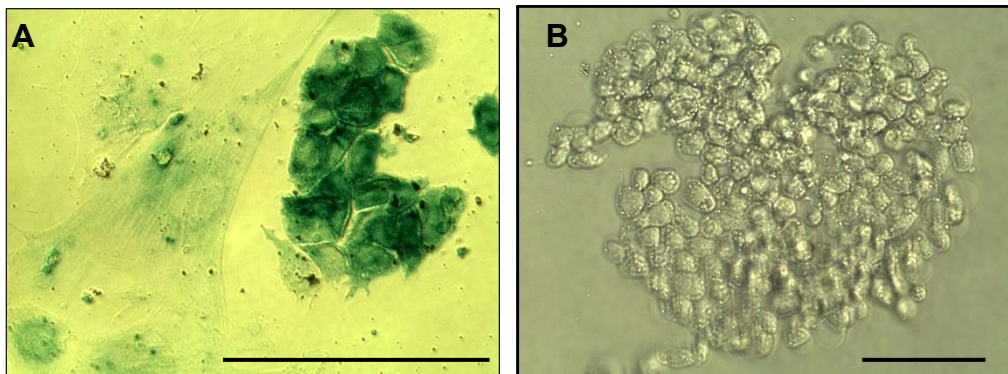

Figure 4.7: Transfection of mouse ES cells with the Expression clone resulted in blue staining (LacZ positive cells) (A). Following transfection of LacZ positive colonies with a Cre plasmid the Stop codon and β-geo was floxed out and white colonies (Lac Z negative) were selected (B) Scale bar 50 µm

To determine if the targeting vector recombined within the ROSA26 locus PCR and Southern blots were carried out:

PCR: The primers spanning the recombination sites of the targeting vector to the gDNA at the ROSA26 locus showed no positives using GoTaq Flexi. Expand polymerase (Roche) gave a series of non-specific bands. Altering DNA concentration, $MgCl_2$ concentration and Touchdown PCR equally did not give any bands of the correct size for wild type or the targeted locus. PCR using Megamix elucidated no bands. GAPDH and Neomycin primers gave positive results in all samples checked except the negative controls for Neomycin primers, and at all the DNA concentrations tested. PCR for LacZ showed no positive results.

Southern Blot: Southern blots at the three prime and five prime end did not elucidate any positive or negative clones using chemiluminescent or radioactive methods.

Turning on Ftl/Fth expression through excising β-geo

In the interests of time while targeting of the gene was assessed by Southern blot and PCR and because of the ubiquitous nature of LacZ expression in certain cloens, two were taken (Blue A and Blue B) to flox out the Stop β-geo. To flox out the STOP codon allowing the Ftl/Fth gene to be expressed a Cre plasmid and an adenoviral Cre were used. GFP and luciferase expression should be apparent following successful floxing but fluorescence microscopy detected no GFP.

Colonies transfected with the Cre plasmid and cultured under puromycin selection were picked and treated with X gal. The majority, 8 out of 10 colonies, were white, indicating loss of the lacZ gene and these were taken forward (Figure 4.3B).

One white colony from each parent (Blue A and Blue B) was then taken forward for further tests, and named White A and White B respectively.

Following tests were carried out on Blue A and B and White A and B

Characteristic	'Blue' cells should be:	'White' cells should be:
LacZ	Positive	Negative
Neomycin	Resistant	Susceptible
Ferritin	Not expressed	Expressed
GFP	Not expressed	Expressed
Luciferase	Not expressed	Expressed

Western Blot: To determine if the human Fth was being expressed western analysis was performed and showed Fth protein in human foetal liver and HeLa cells but no Fth protein was detected in both Blue and White colonies (Figure 4.8). Antibodies for β-Actin showed strong signal in all samples after 5 second exposure to the chemiluminescent film.
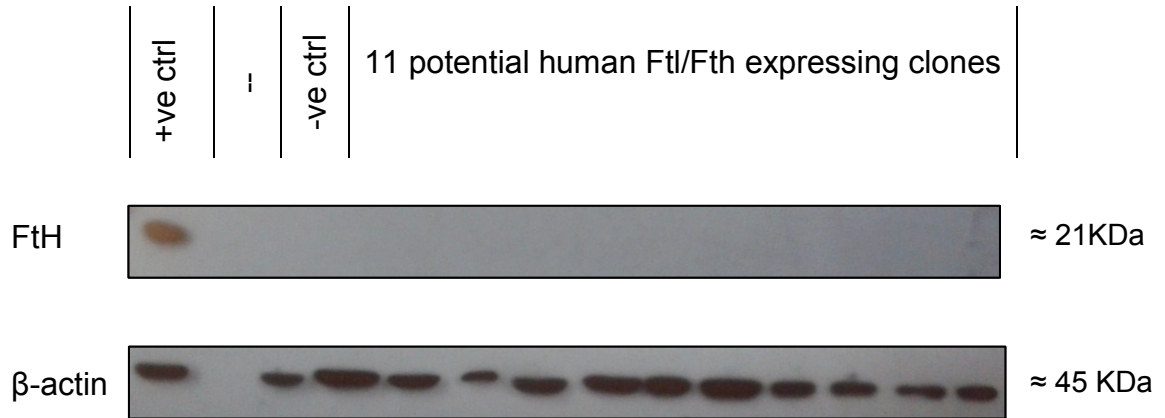
Figure 4.8: E14 cells were transfected with the Gateway targeting vector, Lac Z positive cells were then transfected with the Cre plasmid. Resulting white colonies were analysed for FtH content. The β-actin demonstrates relative protein levels in each lane. Human foetal liver protein was used as a positive control and the Blue pre floxed clone as the negative control.
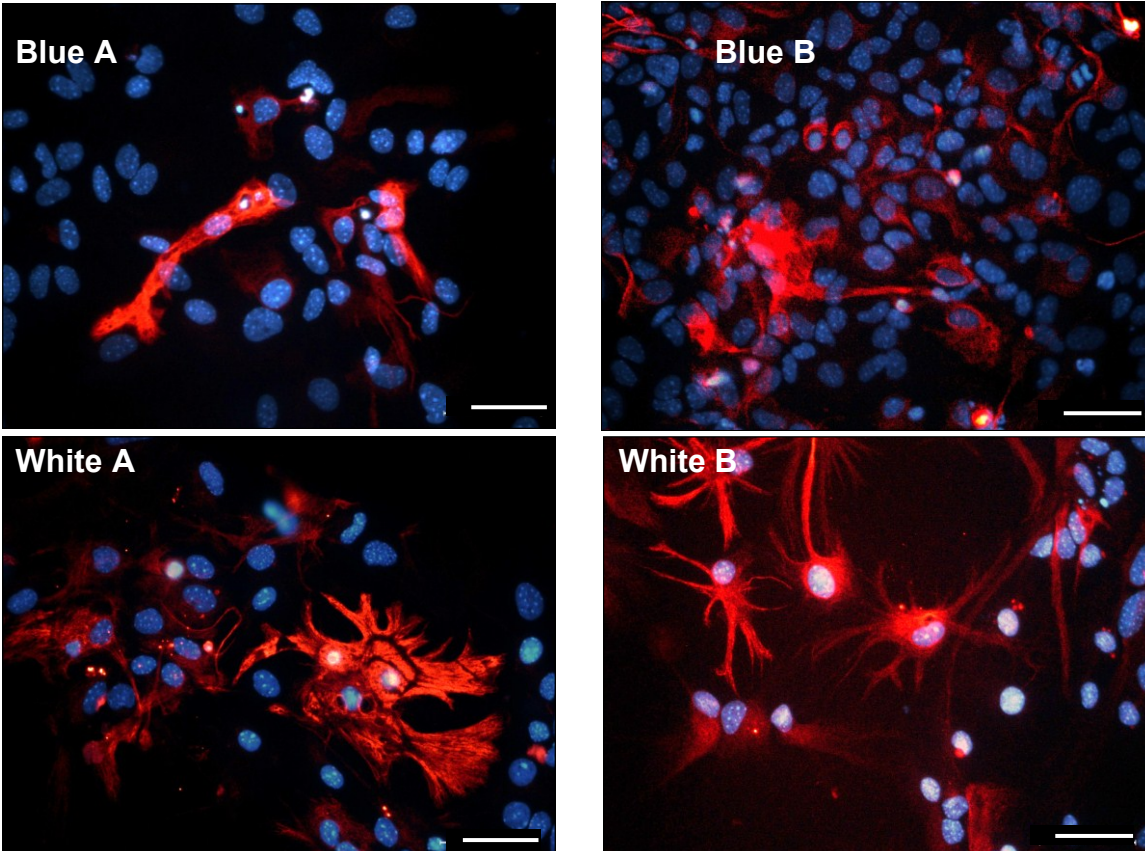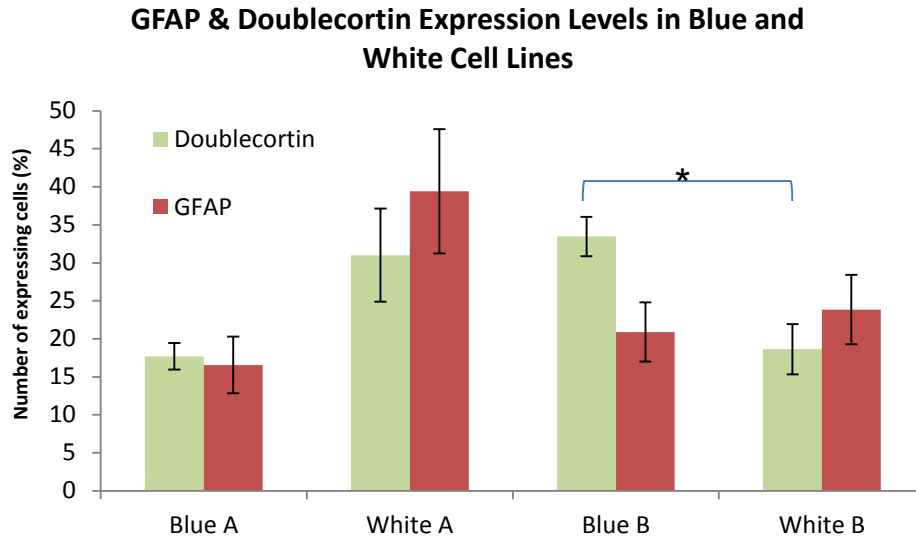
Doublecortin
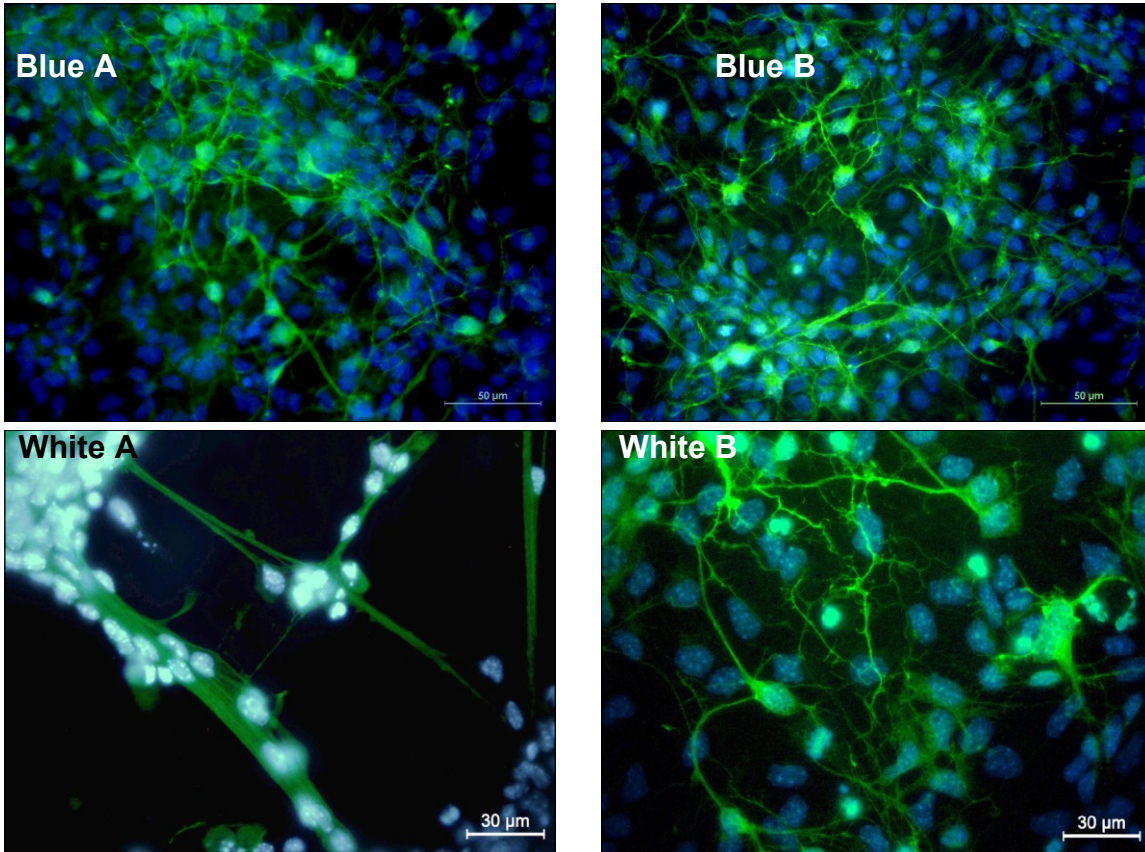
GFAP

Figure 4.9: Two cell lines, Blue A and Blue B, were transfected with a Cre plasmid to remove the Stop codon and turn on Ftl/Fth transgene expression. These and their 'daughter' floxed cell lines, White A and White B, were differentiated down a neural lineage and expression levels of Doublecortin and GFAP were compared. Scale bar 50µm (Doublecortin Blue A and Blue B) and 30µm (for the rest)

Nested PCR*:* After PCR did not pick up any Ft expression in the transfected clones nested PCR was tried. This was in case only a very small amount of Ft was being transcribed and a nested PCR may be able to pick this up. Nested PCR on the cDNA of clones expected to express the Ft subunits was was used to try and pick up with primers for. Only the positive control, human Ft cDNA, gave positive results on the nested PCR. None of the clones gave any bands from the white and blue clones.

Neural Differentiation of Blue and White Clones

Expression of human Ft subunits may effect differentiation of the mouse ES cells. Both Neural and Glial markers were assessed and compared to non-expressing controls. All four colonies, Blue A and B and White A and B, were differentiated to day 16 in chemically defined media to assess expression of neural, Doublecortin, and glial, GFAP, markers (Figure 4.9). There was no significant difference between expression of GFAP or Doublecortin between the four cell lines at day 16 (Graph 4.1). There is no significant difference in doublecortin expression of Blue A and White A ($t_{3.476}$ =-2.089; p = 0.082) or GFAP expression between the different A or B clones (t_6 =-1.973; p = 0.096, t_6 =-0.382; p = 0.716 respectively). There was a significant decrease in doublecortin expression in White B compared to Blue B (t_7=3.380; p = 0.012).

**GFAP & Doublecortin Expression Levels in Blue and White Cell Lines**

Graph 4.1: Two cell lines, White A and White B, were transfected with a Cre plasmid remove the Stop codon and allow Ftl/Fth transgene expression and their 'parent' unfloxed cell line, Blue A and Blue B, were differentiated down a neural lineage for 16 days and expression levels of Doublecortin and GFAP were compared. Doublecortin expression was significantly decreased in White B compared to Blue B (t_7=3.380; p = 0.012).There is no significant difference in Doublecortin expression of Blue and White A ($t_{3.476}$ =-2.089; p = 0.082) or GFAP between the different A or B clones (t_6 =-1.973; p = 0.096, t_6 =-0.382; p = 0.716 respectively).

Comparing the viability, proliferation and apoptosis rates between the blue and white cells lines

If cells are to be transplanted downstream it is imperative to make sure they do not act differently because of the human Ft expression compared to normal cells. To test this metabolic activity using Wst1 reagent, proliferation rates using propidium iodide and apoptosis rates measuring caspase 3/7 activity was assessed and compared to non-expressing mouse ES cells

Proliferation rate: The proliferation rate was determined using propidium iodide which intercalates with the DNA, determining DNA content. Quantification of DNA concentration allows the cell cycle stage to be determined by flow cytometry. The Watson pragmatic model was applied to the histograms to separate G1 and G2 stages of the cell cycle (Figure 4.10). There was no significant difference in the proliferation rates between the Blue A and White A clones ($t_{2.022}$ =-1.534; p = 0.263) or between the Blue B or White B clones (t_4 =-0.551; p = 0.611) (Graph 4.2).

Proliferation Rate of Floxed and Unfloxed Cell Lines
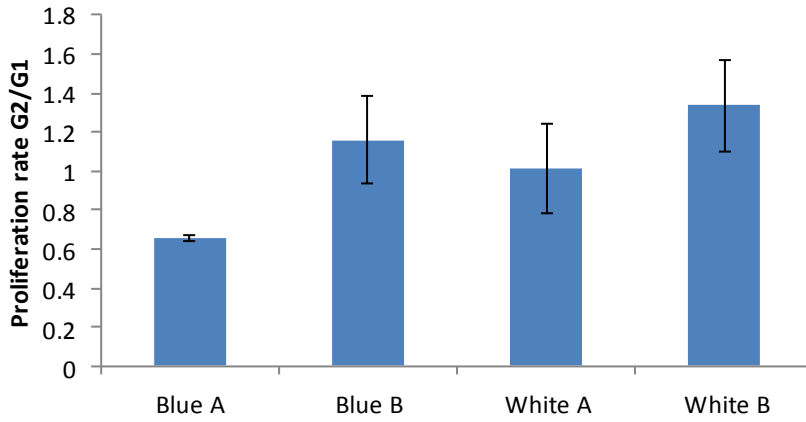
Graph 4.2: Proliferation rate deduced from the cell cycle analysis assessed using Propidium Iodide and flow cytometry, of the unfloxed cell lines, Blue A and Blue B and cell lines treated with Cre, White A and White B. There was no significant difference between group A's ($t_{2.022}$ =-1.534; p = 0.263) or group Bs (t_4 =-0.551; p = 0.611).
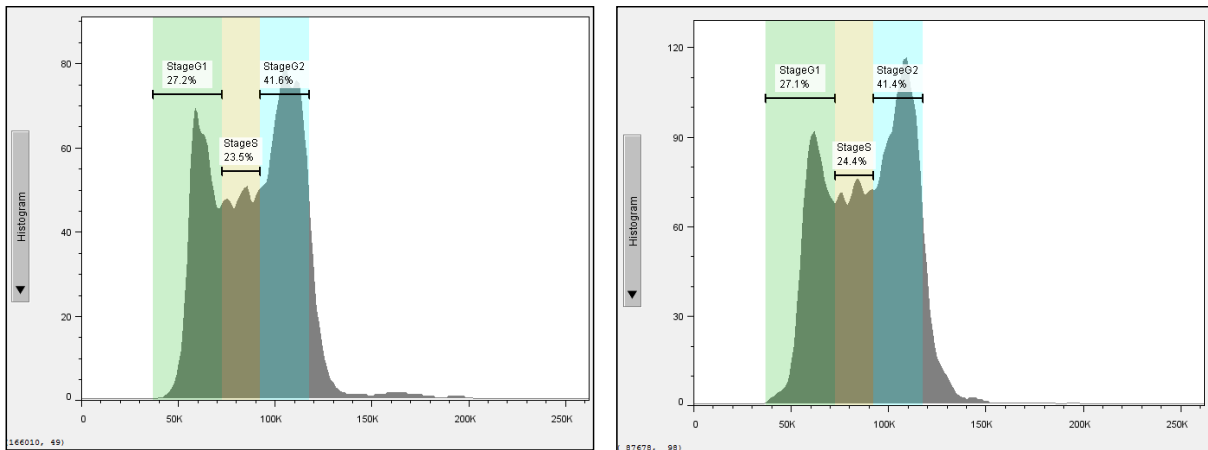

Figure 4.10: Histograms with application of Watson pragmatic model to separate G1 and G2 stages of the cell cycle, of Blue B (left) and White B (right) clones.

Viability test: Wst1 measures metabolic activity of viable cells by reduction of tetrazolium salt (Wst1) to a formazan dye. White B has a significantly higher metabolic activity than Blue B (t_6 =10.386; p = 0.000) and between Blue A and White A there was no significant difference (t_6 =-0.335; p = 0.749) (Graph 4.3).

Apoptosis test: Apoptosis levels were determined by measuring caspase 3 and 7 activity, these caspases play effector roles in apoptosis of mammalian cells. There was no significant difference between apoptosis levels in Blue A compared to White A ($t_{5.118}$ =-0.241; p = 0.819). There is a significant increase in caspase 3/7 activity in white B compared to Blue B ($t_{3.282}$=44.824; p = 0.000) (Graph 4.4).

Wst1 absorbance per cell

Caspase luminescence per cell
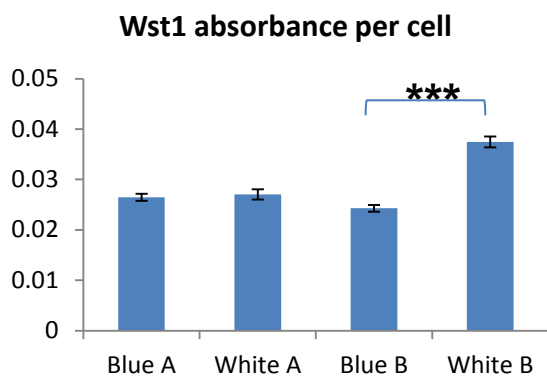
Graph 4.3   Graph 4.4

Graph 4.3: Metabolic activity as determined by Wst1 conversion to formazan, a coloured dye. Metabolic activity is increased in White B compared to Blue B (t_6 =10.386; p = 0.000). There is no significant difference between the Blue parents and the Blue A and White A (t_6 =-0.335; p = 0.749).
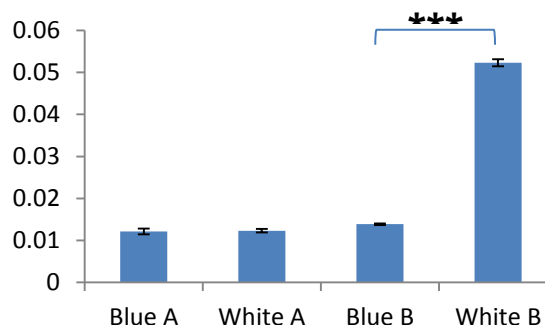
Graph 4.4: Measurement of Caspase 3/7 activity in the four cell lines. White B has a significantly higher caspase activity compared to Blue B ($t_{3.282}$=44.824; p = 0.000). There is no significant difference between the Blue parents and the Blue A and White A ($t_{5.118}$ =-0.241; p = 0.819).

MRI of Ft Expressing clones

To choose the best MRI programme to observe contrast caused by Ft overexpression and test the MRI properties of the White A and White B, the clones were expanded and collected as pellets. The pellets were scanned in the specially crafted MRI eppendorf holder (described in Chapter 5).

MRI analysis of cell pellets in vitro: Optimisation of the MRI programme on *in vitro* samples showed no obvious signal change by eye between the cell types using MSME across the entire range of TEs neither did the FLASH 2D T_2* scans pick up observable contrast under different TR and TE settings (Figure 4.11). However analysis of the MSME scan (Figure 4.12) shows there is a significantly lower T_2 relaxation rate in between White A and Blue A clones (t_6 = -4.35; p<0.01), and White B and Blue A (t_6 =-15.53; p<0.001) (Graph 4.5). White B also has a significantly lower relaxation rate that White A (t_6 =4.34; p<0.01).
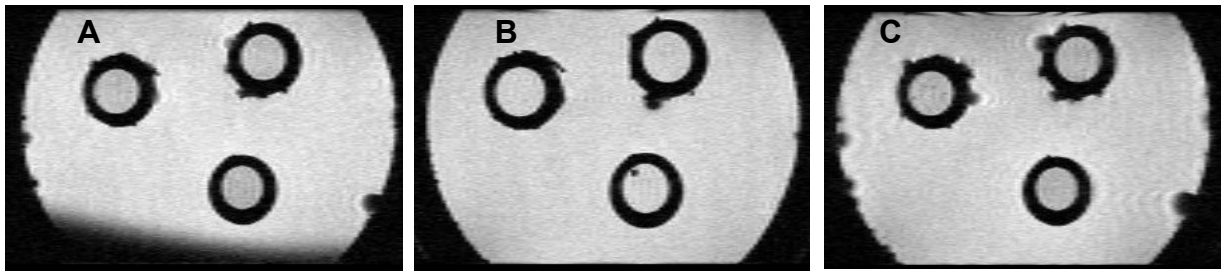
Figure 4.11: MRI of three eppendorfs containing a pellet of cells. The two top samples are the White cell lines (floxed), the bottom is the Blue (unfloxed). Three different FLASH 2D* MRI programmouse ES can be seen (A, B and C) to visualise contrast change resulting from ferritin overexpression. The programmouse ES used were as follows: (A) TR 800ms, TE 8.5ms, (B) TR 800ms, TE 4.5ms (C) TR 1200ms, TE 15ms.
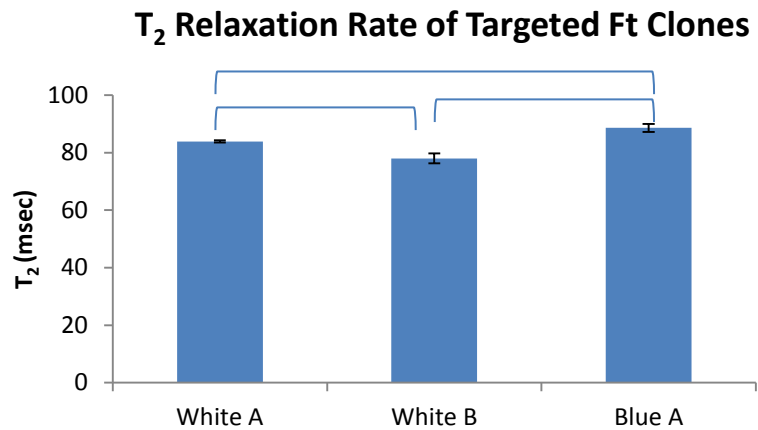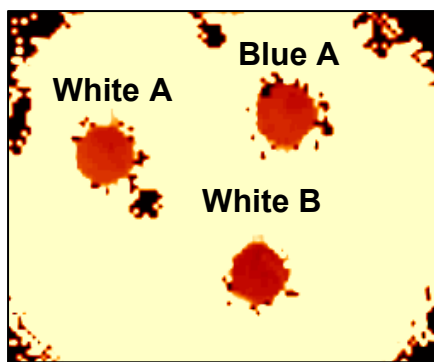

Figure 4.12: Colourmetric T_2 map from a MSME scan of White A, White B and Blue C cell pellets.

Graph 4.5: T_2 relaxation rates of White 1, White 2 and Blue 2 cell pellets. There was a significant difference between the White clones and Blue B in a Students t-test.

Grafting of White and Blue clones into rodent models of HD

The Blue and White clones were grafted into QA lesioned rodent striatum to monitor how the grafts may be affected by human Ft expression compared to control and to check if the graft tissue from White A and White B could be distinguished from host *in vivo* using MRI. While targeting was not confirmed the ubiquitous nature of the expression made continuing down this path a feasible option, until confirmation could be achieved.

To obviate the anomaly of signal drop out from the needletrack the cell lines Blue A, Blue B, White A and White B were injected into the scruff of 129 mice with this intention, unfortunately there was no teratoma formation in any of the 16 animals for unknown reasons.

In vivo MRI analysis of Blue and White cells: To observe what MRI signal from the White clones could be distinguished *in vivo* the grafted animals were scanned with a FLASH 2D T2* programme. This programme was more sensitive to the needle track and due to the small size of the grafts the needle track completely encompassed the grafted area and the graft was not visible using MRI (Figure 4.13).
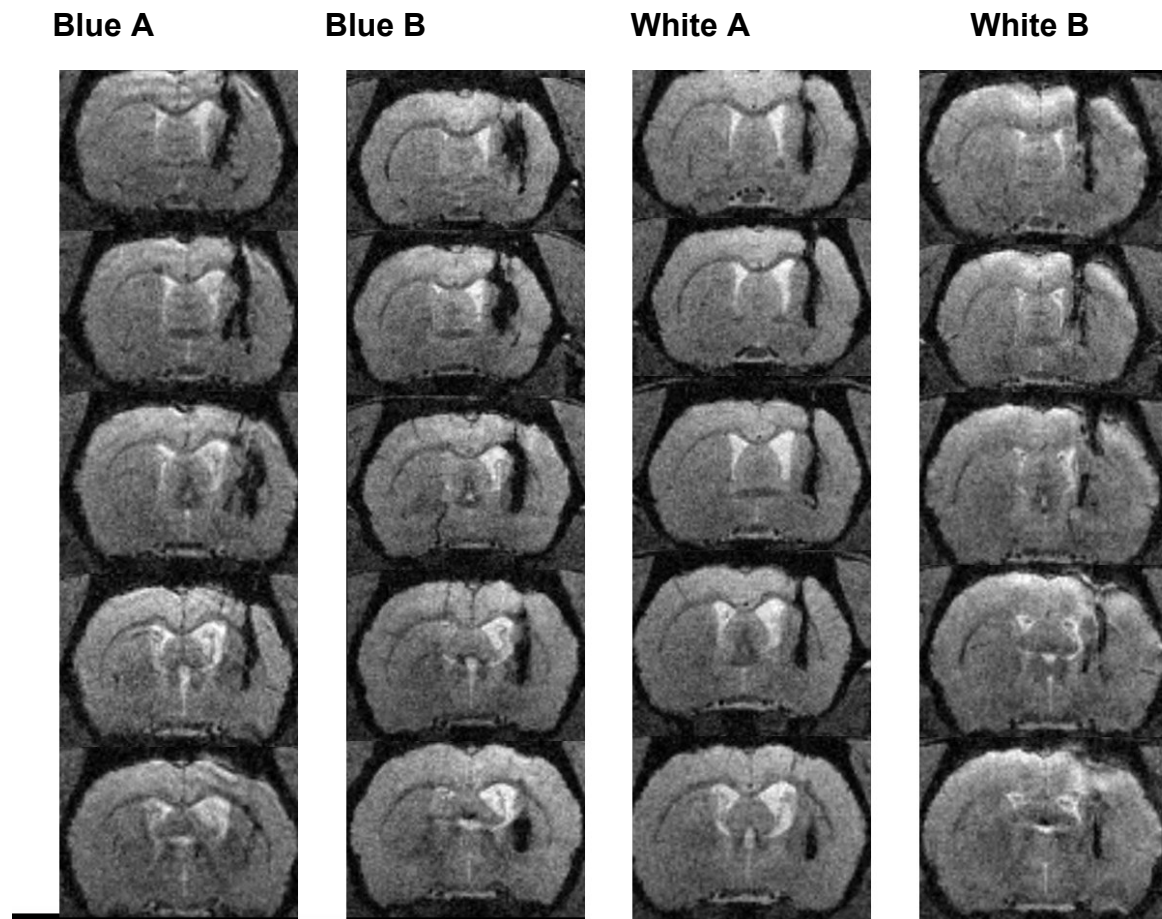

Figure 4.13: Series of slices through four rodent heads, each with a graft into a QA lesioned striatum of the cell lines that have a silent hFtl/Fth transgene, Blue A and Blue B, and two rodents grafted with one of two cell lines that had the Stop codon floxed out to turn on hFtl/Fth expression. FLASH 2D T_2* TR/TE = 1,200/15ms

Histological Analysis of Blue and White Grafts: Blue and White cells were grafted into rodent models of HD and following sacrifice, IHC showed the presence of little to no graft in animals grafted with Blue clones (Figure 4.14), and those grafted with White clones (Figure 4.15) evident in the GFAP and NeuN stains. Graft placement was quite lateral in three of the animals shown (both animals in Figure 4.14 and Figure 4.15 A-D) and more medial in the fourth shown in (Figure 4.15 E-H).

The CV (A and E in both Figure 4.14 and Figure 4.15, low power and A' and E' in both figures, high power) shows increased tissue disorganization and potential graft material in the area of grafting, although this could be microglia and an Ox42 stain would elucidate this. For comparison the CV stain from an ungrafted, unlesioned striatum was included (Figure 4.14.I'). Low power images of Ft (Figure 4.15 D) seem to show some positive staining but on inspection using high power (Figure 4.15 L) the Ft antibody has high background and hemosiderin is quite noticeable in the grafting region with no positive Ft staining.

Blue A
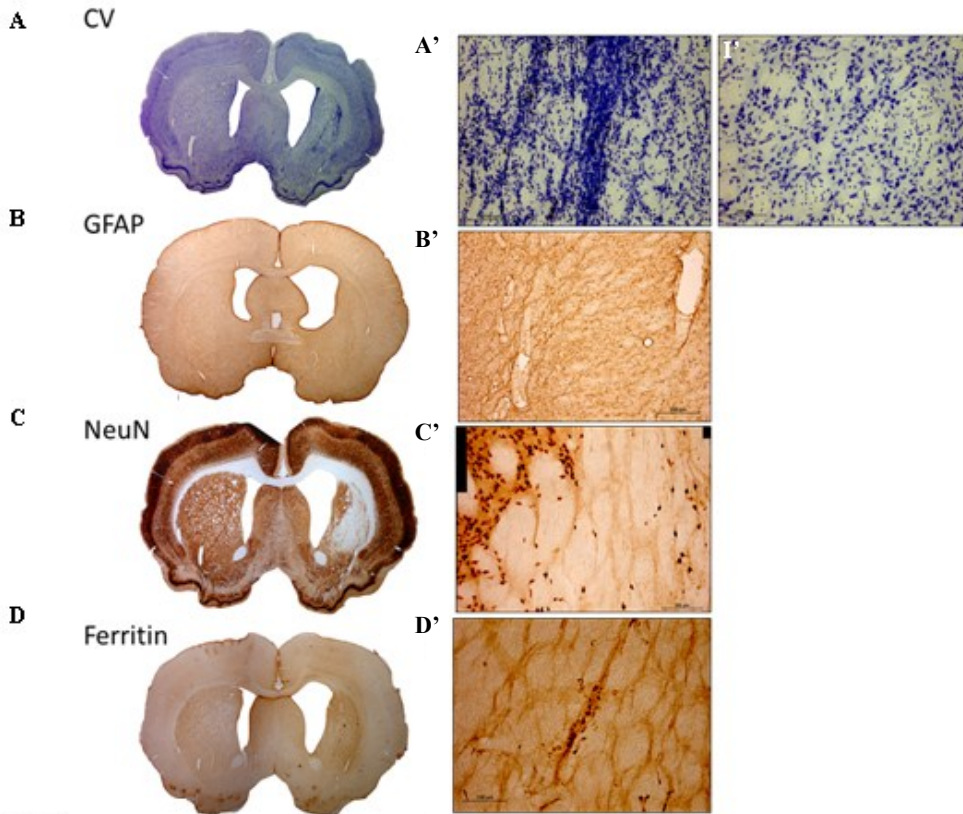
Blue B

Figure 4.14: Histological stains, CV, GFAP, NeuN and Ft, of two animals grafted with Blue A (A-D) and Blue B (E-H). The corresponding high powered images (A'-H') give a closer insight of the graft and I' shows the CV from an ungrafted unlesioned striatum for comparison. Scale Bar is 1mm for whole brain sections, 100µm for high powered images.
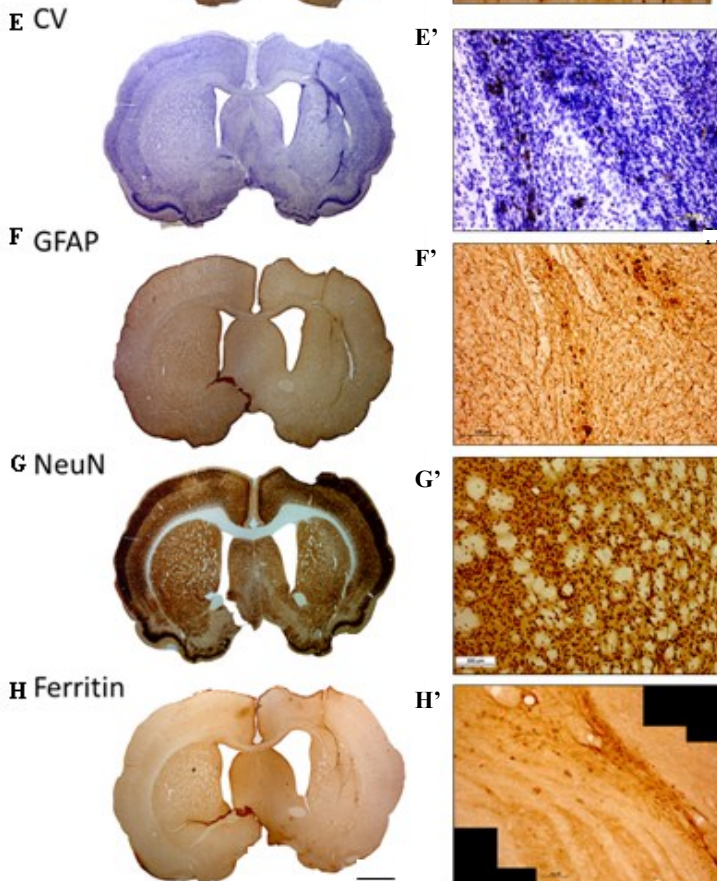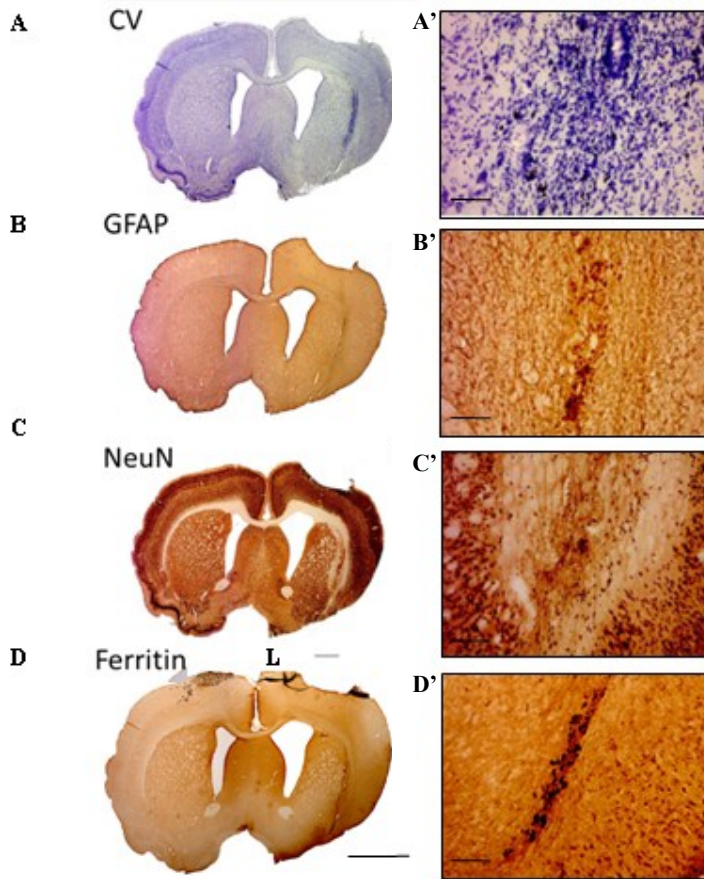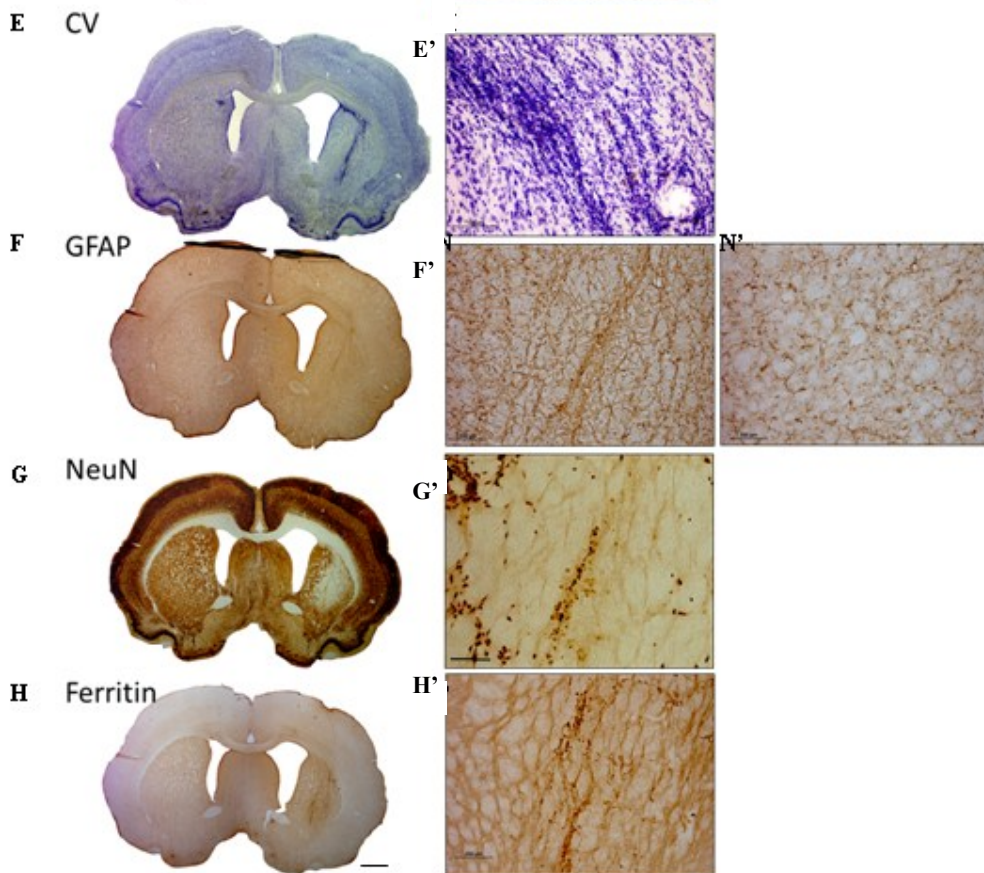
Figure 4.15: Histological stains, CV, GFAP, NeuN and Ft, of two animals grafted with White A (A-D) and White B (E-H). The corresponding high powered images (A'-H') give a closer insight of the graft and N' shows the GFAP from an ungrafted unlesioned striatum for comparison. Scale Bar is 1mm for whole brain sections, 200µm for high powered images.

4.4.1.2 Random Integration of pEC-Ftl/Fth Expression Vector

The pEC-Ftl/Fth vector was transfected into mouse ES cells and HEKs. Observation of cell growth seemed unperturbed in mouse ES cells whereas on expression of the vector in HEK cells the proliferation rate decreased.

PEC-Ftl/Fth transfection into mouse ES cells

E14 ES cells nucleofected with linearized PEC-Ftl/Fth vector showed an efficiency of approximately 25% and using the circular vector an efficiency of 70% was achieved, based on cell counts using bright field and fluorescence microscopy to calculate GFP expression.

Three colonies with the brightest GFP signal were picked and expanded under G418 selection, two of the colonies chosen had been transfected with circular pEC-Ftl/Fth and named Clone A and Clone B. The other GFP positive colony had been transfected with linearized pEC-Ftl/Fth vector and was called Clone C. A G418 resistant colony that did not express GFP was picked and used as a negative control, named Clone D (Figure 4.16).

Name	GFP expression	G418 resistance
Clone A - C	Yes	Yes
Clone D	No	Yes

Western blots confirmed presence of the 2A protein, the Fth and the Ftl in the three GFP positive samples (Clone A, Clone B and Clone C) but not in the G418 resistant, GFP negative sample (Clone D) or the mouse ES cell control protein (Figure 4.17). β-actin was carried out on the same membrane as the Ftl antibody and showed consistent protein levels across all the samples. Protein expression of the Ftl/Fth hybrid gene varied in the three samples, with Clone A having the highest content, followed by Clone C, and Clone B had the lowest. This correlated with GFP expression observed in live cells.
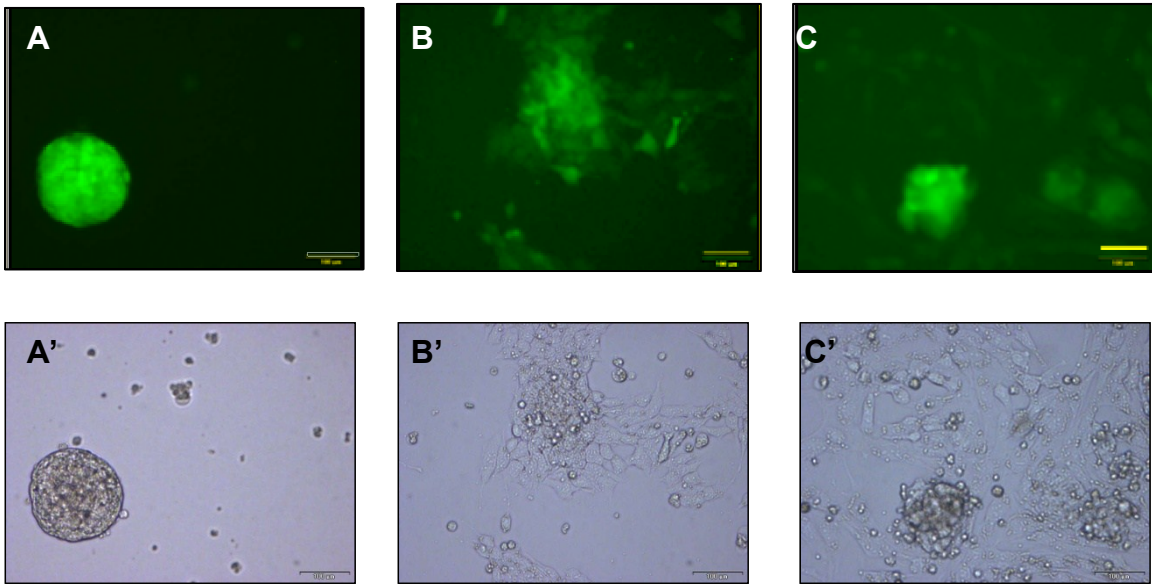
Figure 4.16: Three GFP positive clones were picked after transfection with either the circular PEC-Ftl/Fth plasmid, colonies picked and named Clone A (A) and Clone B (B) or linearized PEC-Ftl/Fth, Clone C (C).
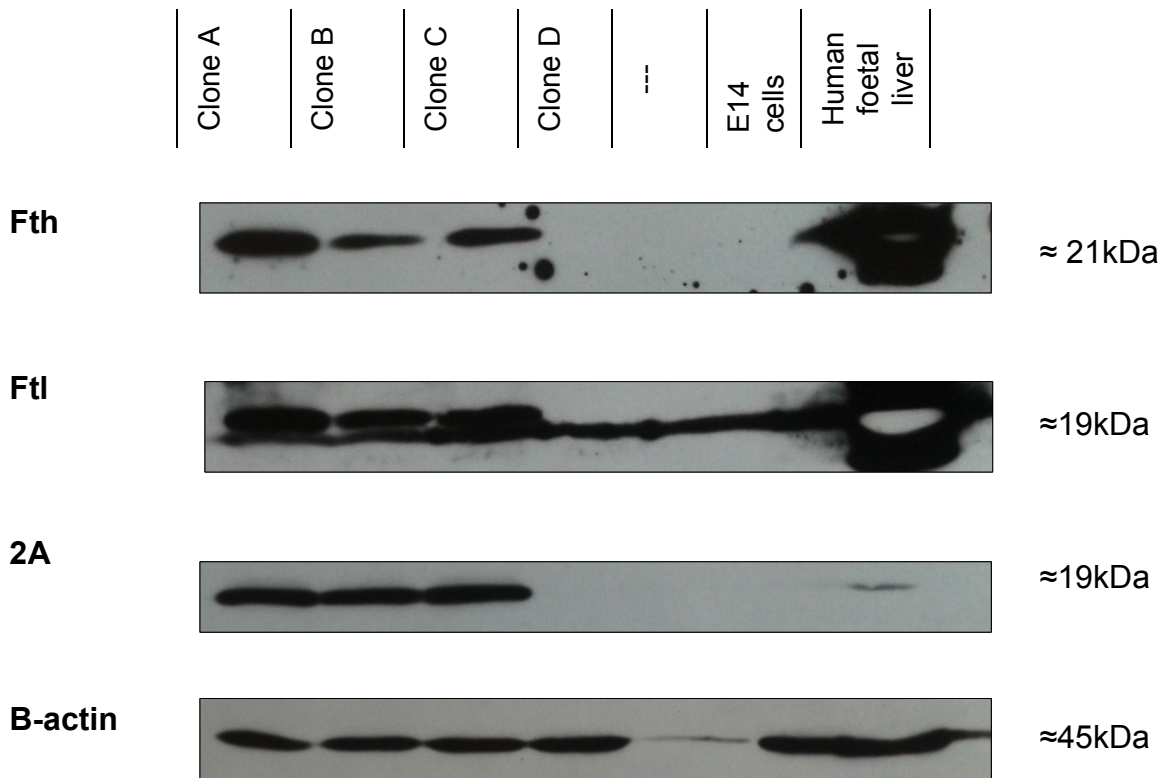
Figure 4.17: E14 cells were transfected with either linearized or circular PEC-Ftl/Fth plasmid, GFP positive and negative colonies picked and tested for expression of Fth, Ftl and the 2A protein. The β-actin demonstrates relative protein levels in each lane. Human foetal liver protein was used as a positive control and the GFP negative colony (Clone D) and E14 ES cell protein was used as a negative control.

MRI Analysis of pEC-Ftl/Fth Expressing mouse ES cells

To assess the MRI properties of the pEC-Ftl/Fth expressing clones they were expanded and MRI scanned as pellets using a number of programmes. The optimal TE for each was determined using a MSME scan and displayed in Figure 4.18. When grown in normal ES cell media Clone A and B had a significantly shorter T_2 relaxation rate than the negative clone, Clone D ($t_{(6)}$=-20.89; $p<0.001$, $t_{(6)}$=11.848; $p<0.001$, respectively). The T_2 relaxation rate of Clone C was not significantly shorter than the control. While there was a significant decrease in T_2 relaxation rate of Clone A, B and C after FACs supplementation compared to normal media (Table 4.1), when the media was supplemented with FACs there was no significant change between the FACs supplemented clones and the decrease seemed independent of Ft overexpression (Graph 4.6).

The FLASH 2D scans did not show an observable difference in contrast *in vitro* between the cell pellets, except those supplemented with FACs, which had increased contrast. The sensitivity of the applied TEs were as expected, with the TR/TE 800/4.5 ms having the lowest contrast difference and the scan with TR/TE 1200/15 ms having the largest difference (Figure 4.19).
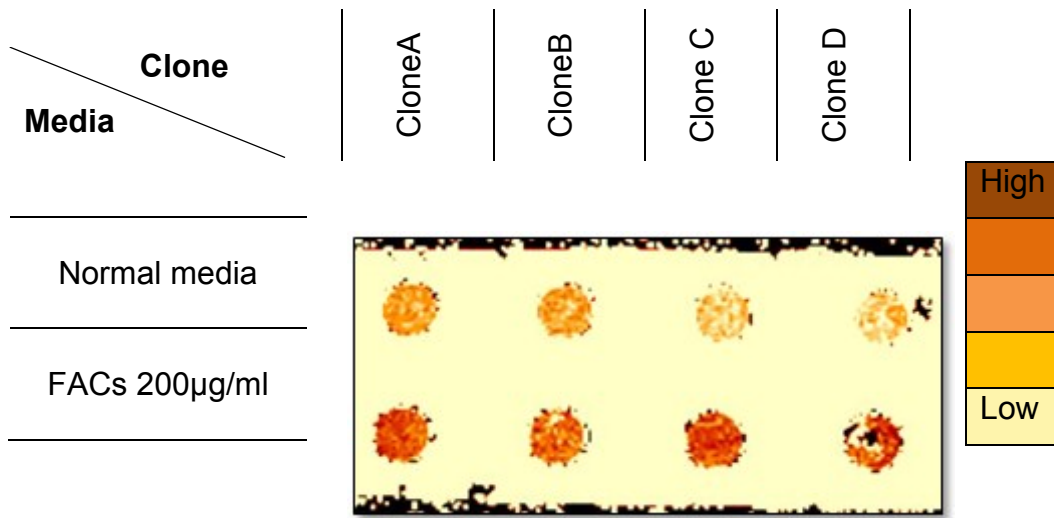
Figure 4.18: T_2 map of calculated MSME results of the Ft expressing pellets (Clones A-C) and control (Clone D) in a modified 96 well plate that were grown in normal ES media or with iron supplement.
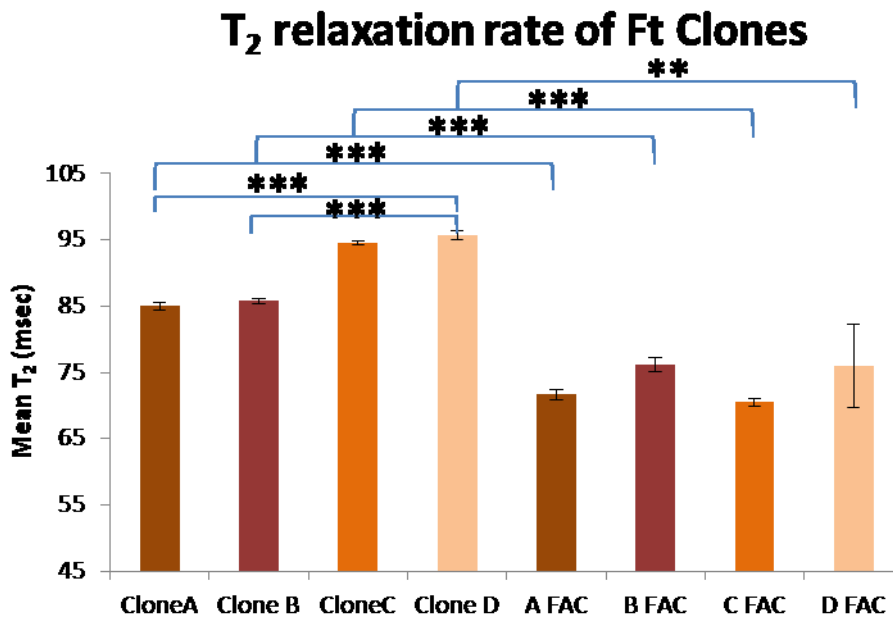
Graph 4.6: T_2 relaxation rates worked out from a MSME scan of overexpressing Ft cell pellets (Clones A-C) and non-expressing mouse ES cells (Clone D) with normal media and when supplemented with FACs.

| Paired Differences | | | | |
Samples	Mean	Std Error Mean	t_6	Sig. (2 tailed)
CloneA – Clone D	-10.69	0.51	**-20.89**	***
Clone D – Clone B	9.87	0.83	**11.85**	***
Clone D – Clone C	1.07	0.58	1.86	
Clone A – Clone A(fac)	13.36	0.77	**17.31**	***
Clone B – Clone B(fac)	9.66	1.09	**8.90**	***
Clone C – Clone C (fac)	24.11	0.54	**44.26**	***
Clone D – Clone D (fac)	19.67	6.21	3.17	*
Clone A (fac) – Clone D (fac)	-4.37	5.78	-0.76	
Clone B (fac) – Clone D (fac)	0.14	5.65	0.03	
Clone C (fac) – Clone D (fac)	-5.51	6.01	-0.92	

Table 4.1: The breakdown of a paired sample t-test comparing the different pEC-FtI/Fth clones against the non-expressing control (Clone D) and against the FAC supplemented media.

Figure 4.19: 2D FLASH T2* with varying TR/TE, from left to right the TR/TE were 800/4.5 ms (A), 800/8.5 ms (B) and 1200/15ms (C). The wells contained from left to right: Clone A, Clone B, Clone C and Clone D and top row media was not supplemented and the bottom row was supplemented with FACs.

4.5 Discussion

The rationale for work in this chapter was to create a vector to permit conditional expression of the Fth and Ftl genes in equimolar concentrations in mouse ES cells and to test t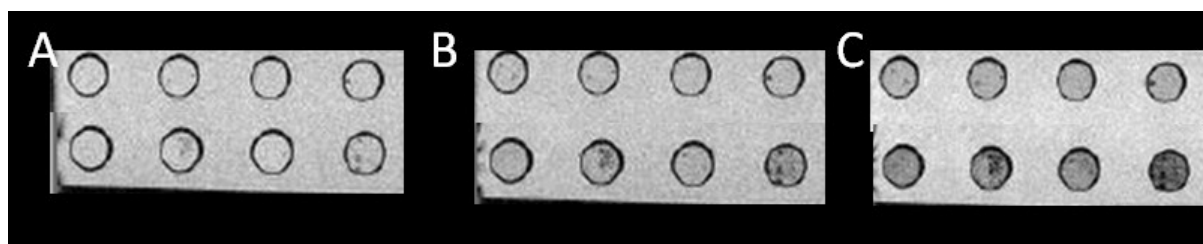he potential the vector to give increased MRI signal compared to either subunit on their own. Furthermore, the targeting of the vector to the ROSA26 locus would ultimately allow comparisons between the effects of Ftl and Fth against other transgene based MRI contrast agents, independent of positional effects, and all using the same system, which has not been done in the literature to date.

The outcomes in this section included construction of the Gateway targeting vector targeting the ROSA26 locus and the successful integration and expression of the vector in mouse ES cells as shown by ubiquitous X-gal staining. Due to the ubiquitous nature of the LacZ expression in clones transfected with the ROSA26-Fth-E2A-Ftl targeting vector, it was decided to take forward these cells to image with MRI, even though the actual targeting to the ROSA26 locus was not confirmed. Interestingly, there was a significant decrease in T_2 relaxation rate in the 'White' floxed clones compared to controls when imaging cell pellets using MSME scans. Floxing out of the lacZ cassette and stop codon by transfection with Cre caused the appropriate loss of X-gal staining, however we could not confirm that this resulted in the expected expression of the Fth/Ftl transgene by detection of human Ft protein on Western Blots. The poor human Ft protein expression could result from ineffective transcription, translation or post-translation cleavage of the chimeric Fth-2A-Ftl protein. To investigate whether the Ft genes could be expressed under alternative promoter control and to assess the effectiveness of the E2A autocleavage peptide the Fth-E2A-Ftl composite gene was cloned into the pEC vector, where the gene was placed under the control of the pCAGGs promoter and was followed by an IRES eGFP reporter. Following transfection and random integration in mouse ES cells Western blot analysis demonstrated the presence of both Ft subunits that were appropriately cleaved by the 2A peptide sequence. Importantly, MRI analysis of stably transfected ES cell pellets confirmed that expression of Ftl and Fth together can be used successfully to produce MRI contrast. The same MSME scan was carried out on cell pellets and there was a significant decrease in T_2 relaxation rate compared to controls. This is more promising than those of Genove's (Genove *et al.* 2005) and Deans' (Deans *et al.* 2006) which did not demonstrate signal contrast *in*

vitro unless the media was iron supplemented. Unlike these works however, there was not a difference between hFt expressing and non-expressing cell clones after iron supplementation with FACs. When media was supplemented for 48 hours prior to MRI the decrease in T_2 relaxation rate was the same across the board. In Genove's study adenoviral transduction of Fth and Ftl subunits and subsequent MRI visualisation of cell pellets did not show an observable difference compared to control until after FACs supplementation, after which a difference between Ft expressing cell pellets and controls was observed (Genove *et al.* 2005). Deans' study only achieved significant MRI contrast in Tfrc and Fth overexpressing cells when there was almost a 10 fold increase in iron content resulting from supplementation using holo-transferrin and iron citrate (Deans *et al.* 2006). It would be interesting to monitor Ft induced MRI signal change of the clones from the pEC Ftl/Fth vector in an *in vivo* environment and see if they fare better than those currently used in the literature.

Determining Iron Content

To further characterise the Ftl/Fth expressing cells and compare them against other combinations of metalloprotein based transgenes in a controlled system it would be prudent to measure iron content. Iron content can be determined by a number of ways including inductively coupled plasma atomic emission spectrometry (Cohen *et al.* 2005; Liu *et al.* 2009b), and scintillation, if the iron supplement is radioactively labelled (Cozzi *et al.* 2000; Genove *et al.* 2005). While not all studies include these tests (Bennett *et al.* 2008; Campan *et al.* 2011) it is important because of the connotations to MRI signal of whether the increased metalloprotein expression is upregulating Trf leading to more effective iron uptake, and which transgene invokes the best uptake. It would also be interesting to confirm if the upregulation is leading to holo- or apo-Fts, this would have connotations in regard to potential toxicity on the cells and whether MRI signal could be further improved. Comparisons with similar MRI contrast agent transgenes need to be carried out under the same parameters as the Ftl/Fth plasmid, including the MRI signal strength.

4.5.1 Targetting Ftl/Fth to the ROSA26 locus

Whilst the results obtained for the pCAGGs-Ft construct provides some proof of principle data for function of the Fth-2A-Ftl chimera as an MRI contrast agent transgene, the goal of targeting its integration to the ROSA26 locus and its conditional regulation was met with a succession of technical difficulties that have not been resolved in the time available.

Difficulties in Generating the Targeting Vector

Considerable, and unexpected, difficulty was encountered in initially cloning the Fth and Ftl genes into the TOPO plasmids. This may be due to an adverse effect on the *E.coli* iron storage system. The structural features of ferritin from mammals to bacteria all have essentially the same architecture regardless of the huge variation in amino acid sequence (Harrison and Arosio 1996). The prokaryote iron storage system does not use both Fth and Ftl, instead *E.coli* has a gene, K12, with sequence similarity to the human Fth (Izuhara, Takamune *et al.* 1991). While human Fth can be overexpressed successfully in *E.coli* with correct structural folding and function (Levi, Cesareni *et al.* 1987), the Fth subunit has been shown to suppress growth in *E.coli* increasing doubling time by almost 2.5 times (Guo *et al.* 1998). Following the initial attempts to clone both subunits into the TOPO vector, to address the possibility of adverse transgene expression in the *E.coli,* I therefore changed to using the pENTR vectors 2B and 4 that contain an rrnb T1 and T2 transcription termination sequence preventing basal expression of the genes following it (Orosz, Boros *et al.* 1991). This successfully allowed the *E.coli* with the Ftl/Fth containing plasmid in to grow unperturbed. Alternatively growing *E.coli* on minimal iron containing media rather than on iron rich LB may be more conducive (Grace *et al.* 2000), the use of minimal media when human Ft is overexpressed results in apoferritin formation, this may avoid the sequestration of iron required for cell growth that otherwise may be detrimentally affecting the cells.

Determining the status of the targeting vector *in vivo*

Following transfection and the successful expression of the lacZ component of the targeting vector, as shown by positive LacZ staining, it was necessary to determine if the vector was correctly targeted to the ROSA26 locus. Two different types of

Southern blot were used, first chemiluminescent and then to increase the sensitivity, radioactive (32P) was used. In each case the probes picked up neither wildtype nor positive control. The Southern Blot can be sensitive to the type of membrane used and trying different brands may yield a better result in future. However, as the western blot and PCRs failed to pick up any expressed human Ft in the samples, coupled with the lack of contrast difference between the MRI samples it was decided that continuing with the Southern blot would be of little to no value at this stage. Even if the ROSA26 locus was correctly targeted the Ft was being expressed at such low levels, if at all, these specific clones would not be strong MRI contrast agent cell lines compared to better expressing cell lines. Due to the lack of evidence that Ftlh was expressed, caution in interpreting data from the *in vitro* and *in vivo* results should be maintained. Nevertheless it is of interest that the comparative MRI tests on the cells showed a decrease in T_2 relaxation rate, which may hint at the presence of low concentrations of Ft.

During routine culturing the cell lines all had a similar turnover rate, however White B had significantly increased metabolic activity compared to Blue B, and an increased caspase 3/7 activity. Proliferation was not affected and while there is no significant difference between Blue B and White B, the variance is large and more replicates may expose the slight increase in proliferation in white B as significant. Following the 16 day differentiation protocol the neuronal or astrocytic yield from the ES cells was similar between clone Blue A and White A, which would be promising if that is the case when Ft is expressed in high concentrations. White B did have significantly lower levels of doublecortin expression compared to Blue B. Whether the change in White B is a result of Ftl/Fth expression remains uncertain and could result from the random integration of the vector.

In vivo monitoring of Blue and White cells

Due to the positive LacZ expression in mouse ES cells transfected with the Ftlh targeting vector, clones selected for ubiquitous lacZ expression were transfected with Cre recombinase to flox out the β-Geo and STOP codon and in parallel to the molecular characterization of the clones both LacZ positive and post Cre recombinase LacZ negative clones were differentiated and tested in vivo by grafting into QA lesioned rats. The grafts were small if present at all and no Ft was picked up

by IHC. Despite the CV showing that some grafted cells may be present the human Fth antibody did not detect grafted tissue. This may be due to the Ft transgenes being expressed at very low levels, if at all. Mouse to rat transplantation typically gives small, pencil like grafts (Kelly *et al.* 2007) but overexpressing Ft in human ES cells would allow grafting into rat models, which can provide much larger grafts for MRI imaging (Aubry *et al.* 2008). Overexpression in human ES cells would be an interesting avenue to follow and fruitful in regard to transplantation studies.

The Problem of Hemosiderin and Imaging Grafts in the Brain

Needle track signal in the MRI scans is most likely to have resulted from hemosiderin. Hemosiderin is an ill-defined mix of proteins, lipids and iron, where the iron is in a less accessible form for cellular use (Koorts and Viljoen 2007a, b). Fth has been implicated in ferritin aggregation and a major constituent in hemosiderin (Miyazaki *et al.* 2002). Hemosiderin along with large Ft clusters result in a quadratic dependence of relaxivity on the magnetic field (Gossuin *et al.* 2007). All of which can contribute to MRI detection. Trying to minimise needle track disruption in the SPIOs chapter by using a glass cannula instead of a thicker metal cannula did not reduce the artefact and more work must be done to try and overcome this (See chapter 3).

The formation of a teratoma would provide a method to visualise MRI contrast from the cell lines without the needle track obfuscation. While teratoma formation is a sine qua non characteristic of pluripotency, the rate of teratoma formation can be site dependent (Prokhorova *et al.* 2009). However, it is doubtful location was the reason the teratomas failed to grow and the reasons remain unknown.

Benefits to the targeting vector yet to be explored

Ideally the luciferase following the IRES would have allowed monitoring of the grafts *in vivo* using the IVIS system. The IVIS system can generate 3D data that can be co-registered with PET or MRI and sensitive enough to pick up Luciferase following an IRES after intra peritoneal injection of D-Luciferine. Luciferase has been successfully used to monitor microglial activation in the rodent olfactory bulb using IVIS (Lalancette-Hebert *et al.* 2009) albeit lower resolution than MRI, the smallest voxel size being 1mm for robust imaging. Bioluminescence provides the ability to image with a depth of up to 7cm tissue penetration using a broad range of *in vivo* imaging

biomarkers such as luciferase, which can image up to 4 fluorophores at a time.

MRI programmes to visualise Ft contrast

The MRI specifications for picking up ferritin vary between studies, some using T_2* weighted 3D gradient echo (TR/TE = 100/9ms) for *in vivo* imaging (Gilissen *et al.* 1998; Kaur *et al.* 2003) and others with a T_2 weighted spin echo (TR/TE = 3,000/55ms) for *in vitro* and T_2-weighted spin-echo (TR/TE = 1,200/35 ms) and T_2*-weighted gradient-echo sequences (TR/TE =1,200/6.7 ms) *in vivo* (Genove *et al.* 2005). The T2* provides increased sensitivity to pick up the Ft signal but at the cost of increasing the MRI tract signal. Here we used a number of T_2 weighted scans and there was no obvious change in intensity apart from with the FACs supplemented cells. The lack of MRI signal difference seen between the negative control and White and Blue cell lines *in vitro* could be the result of the cells not producing a suitable amount of ferritin to be picked up in the first place. The minimal intensity change of the pEC-Ftl/Fth cells could be enhanced in an *in vivo* environment, like that seen in the literature.

In conclusion the Ftl/Fth transgene gives significant MRI contrast compared to control cells *in vitro.* The *in vivo* MRI attributes still need to be confirmed and we have elucidated a number of issues in regard to imaging grafts in the brain that obscure the analysis due to the standard grafting practices used here.

5 CEST as MRI Contrast Agents

5.1 AIMS

This section investigates using artificial genetic contrast agents based on CEST to label and multi label stem cells, to help determine the applicability of monitoring them *in vivo* using MRI. We try and improve CEST scans by shortening scan times without compromising too much on signal loss, so that they will be more appropriate for *in vivo* scanning.

5.2 Introduction

CEST agents have emerged as potential new contrast agents for tracking cells in the last few years. CEST signal is generated by saturation labelling protons of a solute which then exchanges with that of bulk water, resulting in a decrease in the MRI signal from water protons. A rapid exchange rate coupled with a sufficiently long saturation results in a cumulative effect on the water, thus amplifying the original signal meaning even low concentrations of agents should be able to be detected.

While various approaches have been used to take advantage of CEST effects, including endogenous CEST effects in humans, such as gagCEST (Ling *et al.* 2008) and glycoCEST (van Zijl *et al.* 2007), it is the development of diamagnetic contrast agents we are interested in here. There are a number of important benefits specifically associated with CEST signal compared to its adversaries, including the ability to switch the signal on and off at the MRI stage to distinguish artefact from real signal; and dual label a single cell using different promoters, meaning cell type can be determined as well as location. As with other transgene based MRI contrast agents it is biodegradable, allowing differentiation between viable and nonviable cells, and maintains a constant endogenous expression level even following multiple cell divisions.

CEST agents have been imaged as solutions in phantoms and *in vivo* using transgenes that express lysine rich proteins (Gilad *et al.* 2007). Gilad and coworkers constructed a prototype CEST transgene with 200 lysine residues and transfected them into 9L rat glioma cells, which when xenografted into the non-obese diabetic/severe combined immunodeficient mouse brain gave an observable signal

change above baseline (Gilad *et al.* 2007). Intracranial rat 9L gliosarcomas, give increased image contrast due to amide proton transfer (Zhou *et al.* 2003) and the LRP CEST signal intensity difference occurred within an area where the total amide proton pool of 9L rat glioma cells can be affected (2-4ppm). Fortuitously, LRP's CEST effect is more frequency selective and thus distinguishable from the surrounding amide proton pool. In addition to the total proton pool, exchange rate directly determines CEST contrast and the amide proton exchange rate of 22kDa poly L lysine is 403 s^{-1} at pH 7.3, compared to the combined xenograft amide proton's rate of $28s^{-1}$ (Gilad *et al.* 2007). While Gilad et al used an 11.7 T field strength scanner, the detection of endogenous amide protons that provide contrast differences between tumors and edema in a 3T whole body clinical scanner (Jones *et al.* 2006) suggest the approach is extendable to lower field and clinical machines. While the LRP showed no cytotoxic effects in 9L rat glioma cells this needs to be assessed for each application alongside CEST signal intensity when considering its use in other tissues and cell types.

This area of research has grown dramatically over the last few years due to the unique features it possesses over its competitors, but is yet to fully mature. Here we attempt to follow on from Gilad's work on the LRP plasmid to extend into a new cell type and to build on the standard CEST programmes to increase the speed of the scans in order to make it more applicable for *in vivo* studies. In addition to applying the CEST agent in a conditional expression system that allows comparable analyses against other potential MRI contrast agents.

A typical RARE scan with MTC preparation is time consuming and would take up to an hour or more to scan one animal compared to a standard RARE which could typically take a matter of minutes. Typical behavioural studies can use tens of animals per cohort and if scans are required at various time points this becomes time consuming and expensive. Here we consider programmes to shorten the overall CEST scanning time without compromising on signal.

5.3 Methods

5.3.1 Technical CEST MRI Programme Methods

5.3.1.1 Set up for *in vitro* CEST scans

The sample temperature was maintained at approximately 37°C by running the water bed at 75°C and monitored using a temperature probe. CEST imaging is very sensitive to inhomogeneities in B_O and therefore good shimming is very important. To assist in this two MRI suitable sample holders were made, one was constructed by hand in EMRIC and the other was commissioned (Cardiff University workshop), to keep the samples at a reasonable temperature and allow a more homogenous area to be scanned, limiting variation in B_0 (Figure 5.1). The holders were constructed from MRI safe Perspex and made to be water tight.

Two methods were employed to assist with CEST imaging, two versions of 2D RARE and 3D FLASH scans. These would hopefully decrease scan time without diminishing CEST effect.
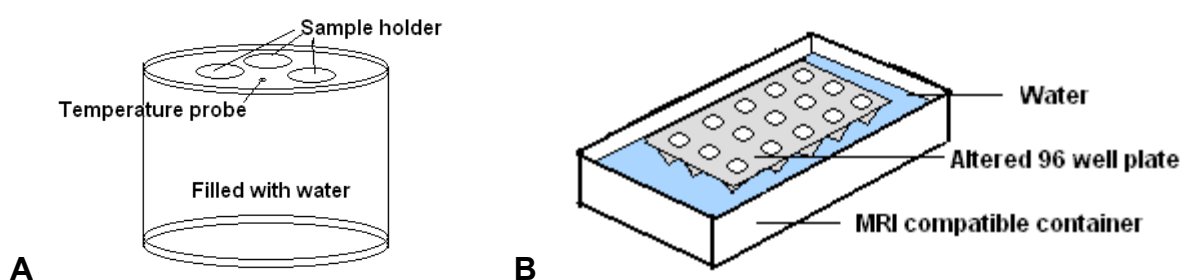
Figure 5.1: Two MRI compatible containers were constructed; one was commissioned by the Cardiff University Workshop (A), the other by hand in EMRIC (B), to improve temperature control and reduce magnetic susceptibility effects when imaging cell pellets or solutions.

5.3.1.2 Preparation of peptides for MRI analysis

PLL and PLR were made up using PLK-hydrobromide (Sigma) or PLR-hydrochloride (Sigma) in concentrations which ranged from 0·98 µM to 1 mM in PBS for the different experiments and PBS on its own was used as a negative control.

5.3.1.3 MRI of CEST solutions and the rat brain

Any chemical exchangeable protons that resonate at the targeted frequency can give contrast when saturated with RF, including some amide protons from natural proteins. However, this background signal should be equivalent across all cells and

should be much lower than the much stronger signal of the CEST poly peptide specifically designed to have a single CEST resonance frequency. To verify the CEST signal is detectable above the natural polypeptide background multiple scans throughout the rat brain were taken while observing if the CEST contrast from solutions were visible.

5.3.1.4 Looking for CEST in vivo

PLK solution (100µM) was stereotactically injected into one hemisphere of the rodent brain to see if the CEST solution could be distinguished from surrounding tissue.

5.3.2 MRI of PLK and PLR *in vitro*

In standard protocols a single MTC preparation module can be applied per slice. The contrast described by Gilad *et al.* (Gilad *et al.* 2007) using PLK requires the slice to be irradiated for 4 seconds, and a repetition time of 8 seconds, making a typical multi-sliced acquisition very slow. To decrease the scan time the programme was modified so the MTC pulse was repositioned in the sequence order to give one MTC preparation per slice pack.

A second modification was based on a 3D FLASH protocol by Dixen *et al.* (Dixon *et al.* 2010), sent to us by Bruker and modified by Pawel Tokarczuk. The additional frequency specific CEST pulses were created by modifying the MTR (magnetisation transfer) preparation module of standard Bruker sequences. This is normally used as a broad short pulse at the start of a sequence.

5.3.2.1 Z spectra

A Z spectrum was constructed to show the optimum irradiation offset frequency for each reporter peptide. The Z was constructed from a series of RARE 2D scans each identical except for the magnetization transfer frequency offset, which ranged from -2000 Hz to +2000 Hz at intervals of 200 Hz. The RF pulse length was 4ms and voxel size was 200µm x 200µm. The coil used was a Quad TX/RX volume coil 1000W Config, Bruker hybrid. The intensity of regions of interest were plotted against the normalized intensity integrals to obtain the optimum offset frequency for each CEST agent. A Z spectrum was constructed from a series of 3D FLASH scans, with an RF pulse length of 6ms and voxel size of 200µm x 200µm x 156µm, using 1mM PLK and 10µM PLR.

5.3.3 Coating Agarose Beads with PLK and PLR

PLK and PLR solutions were made up in concentrations of 1000, 500, 250, 125 and 61.5 µM. Agarose beads (DEAD Affi-Gel, Bio-Rad) were treated either by soaking them in the solutions for one hour and imaging them directly or soaked in the solution for one hour and then washed twice with PBS and imaged. Two samples of beads were soaked for 24 hours in 500 µM PLK or PLR solution prior to being washed with PBS and imaged.

5.3.3.1.1 MRI of CEST loaded Agarose Beads

3D FLASH MTC (200 x 200 x 156 µm resolution) using the Quad 1000W coil. TR/TE 20/3.3ms, FA 10°, FOV 5.12/4.00/1.28 cm. The irradiation offset was applied at a range from -1660 to +1660 at intervals of about 200 Hz. The vials were imaged at the agarose bead level and the solution above the beads.

5.3.4 Cell Culture Strategy with the LRP plasmid

The LRP vector, a gift from Assaf Gilad (Gilad *et al.* 2007), was electroporated into Stbl3 cells (Invitrogen), expanded and purified using an Endofree Maxiprep kit. The vector was transfected into E14 mouse ES cells using electroporation, lipofection and nucleofection (programme A-024). Expression was determined by GFP expression and RT-PCR analysis of GFP positive mouse ES with 'LRP sense' and 'LRP antisense' primers (Table 2.1).

5.4 Results

5.4.1 Technical results

Picking up CEST signal from PLK

To confirm CEST contrast change could be observed in our hands, the 2D RARE programme was tested using 1mM PLK solution using water as a negative control (Figure 5.2). Negative results appear black in the subtracted image, as there is no change in signal after application of an RF pulse. The PLK solution gave CEST contrast most strongly with the 4ms pulse and gave lower contrast difference at an RF pulse of 2ms or 1ms.

A	B	Scan Type
		No RF pulse
		4ms RF pulse on resonance
		4ms RF pulse wrong frequency
		2ms RF pulse
		1ms RF pulse
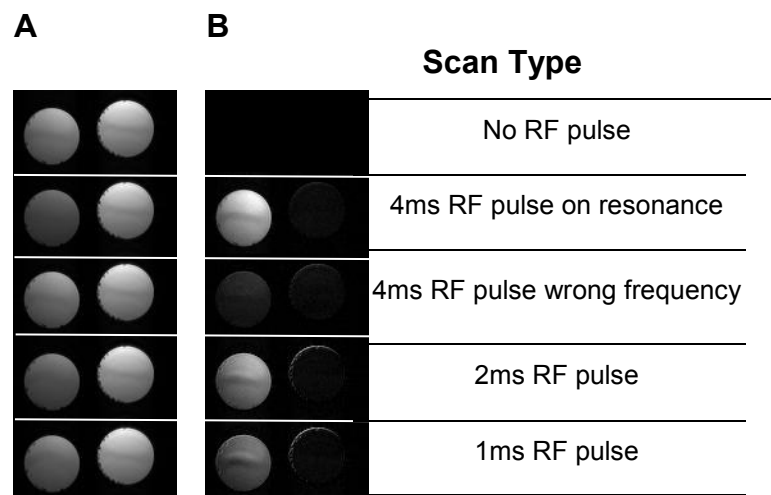
Figure 5.2: Eppendorfs of water (right row of each block) compared to 1mM PLK (left row of each block) at 35°C on application of either no RF pulse or pulses of 4ms either side of the water peak, 2ms and 1ms. Image A shows the scans with no other analyse performed, and Figure B shows images after the initial MRI scan has been subtracted from a second image using an RF pulse. This montage (B) is scaled differently from the first to highlight the relative contrast.

CEST Solution and the Brain

Injecting CEST solutions into the brain: 1mM PLK solution was injected into the brain to see if the scan could distinguish the CEST effect *in vivo* from surrounding tissue. There was little to no CEST contrast observed, and when the threshold was set extremely low background noise increased making it was hard to determine what was significant (Figure 5.3). On further inspection the lack of CEST signal may have

resulted from the needle tract's MRI visible mark causing signal drop out. Upon discovery of this effect the needle track was investigated further (see Chapter 4). Since CEST relies upon the retardation in signal intensity it is impossible to generate a CEST signal from regions of complete signal drop out. The needle track signal is a common problem to all scans at EMRIC and a great deal of effort has been invested in other projects to try and reduce these effects with little success.
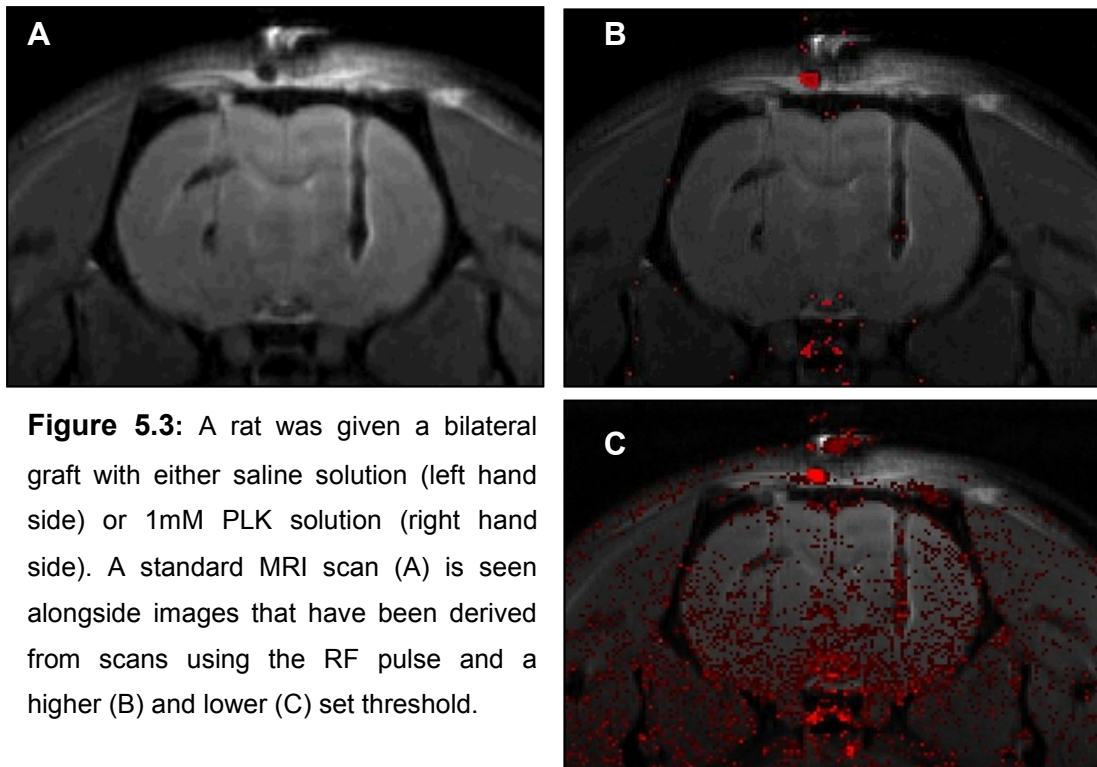
Figure 5.3: A rat was given a bilateral graft with either saline solution (left hand side) or 1mM PLK solution (right hand side). A standard MRI scan (A) is seen alongside images that have been derived from scans using the RF pulse and a higher (B) and lower (C) set threshold.

Imaging Vials of CEST in the Presence of Tissue: Following the inability to view CEST signal from solutions injected into the brain due to the needle track obliterating signal another method was tried. Two vials of PLK, 1mM and 0.1mM, were made up and scanned alongside a rodent brain to see if the CEST signal could be picked up without putting the threshold so low that unrelated CEST signal in the brain section would start to come through. No CEST contrast was visible through various slices of the rat brain or in a vial of PBS, whereas in 1 mM and 0·1 mM PLK vials CEST contrast was observed with the same scan, all CEST contrast was overlaid with red (Figure 5.4). There were some susceptibility artefacts visible at the tissue interfaces, in part explained as the result of magnetic field drift occurring during the scan.

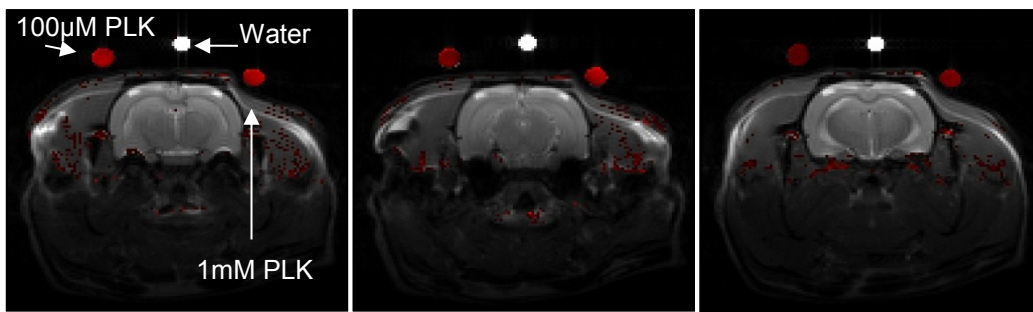**Figure 5.4:** Vials of water and poly L lysine (PLK) solution showing CEST MRI contrast (red) using a custom written IDL programme, through various brain slices, no CEST contrast in the brain.

Modifying RARE to one MTC preparation per Slice Pack

Standard RARE with single scan acquisition can generate large amounts of CEST contrast in phantoms but is slow. The RARE MTC method tested to speed up scan time by applying one MTC per slice pack did not satisfy the requirements. The RARE scan using one MTC preparation per slice pack gave unusual artefacts which were difficult to interpret. After application of the MTC pulse the slices were acquired over a long period in which time the signal was recovering. This could be improved by minimising acquisition time. In addition when the MTC module is switched on the slices are acquired at uniform intervals but when it is switched off they are acquired at different times which could lead to varying amounts of contrast between slices in a uniform sample. Repeating the scan with reproducible timings, whether MTC is applied or not, could improve this.

In summary, acquisition takes time in RARE with TE's of 10s of ms the T1 recovery acts against CEST signal. Increasing the RARE factor to speed up the scan could introduce stronger artefacts caused by T1 recovery from an unusual starting point. FLASH is a quicker technique than RARE and TR can be set to hundreds of ms rather than 8 seconds. FLASH does have lower signal to noise than RARE but the much shorter acquisition times could mean image intensity could be recovered by averaging.

Multi Slice 3D FLASH for CEST

3D FLASH was tried to decrease scan time and make it more applicable for *in vivo* scans and still manage enough sensitivity to pick up CEST contrast. The modified, 'staccato' multi slice FLASH, with a single preparation module per slice pack followed by acquisition from all the slices at once meant a full 3D FLASH image could be completed in 10 minutes. It was possible to distinguish PLR from PLK using this method.

Z spectra of PLK and PLR

To pinpoint the optimum offset frequency for targeting PLK and PLR, Z spectra were obtained using RARE and 3D FLASH.

Z Spectra using RARE: The CEST contrast difference in the wells was overlayed with colour, depicting the PLR as red and PLK as green (Figure 5.5). The lowest concentration visible with PLR was 10µM and for PLK 125µM showed some signal change that was more obvious at 250µM. Looking at the Z spectra of PLK a small difference could be seen at 62.5µM although not visualised in the colour overlay.

Z Spectra using 3D FLASH: Using 1mM PLK a broad peak was observed ranging from 1800 Hz to 100 Hz from the water peak with a maximum of 1450 Hz. PLR had a minor peak at 1700 Hz as expected, representing the amide groups, and a guanidyl peak that covered a larger range, from 1000 Hz to 200 Hz (Figure 5.5). The temperature was maintained at 36.7 - 37.2°C (Figure 5.6).

Poly L arginine Z-spectra
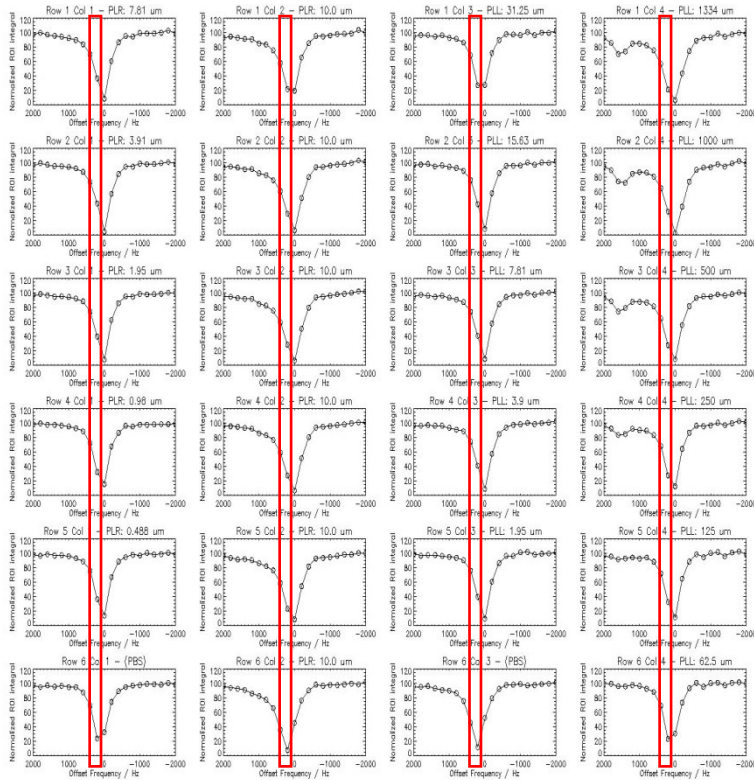
Overlay: diff. contrast/ ref.
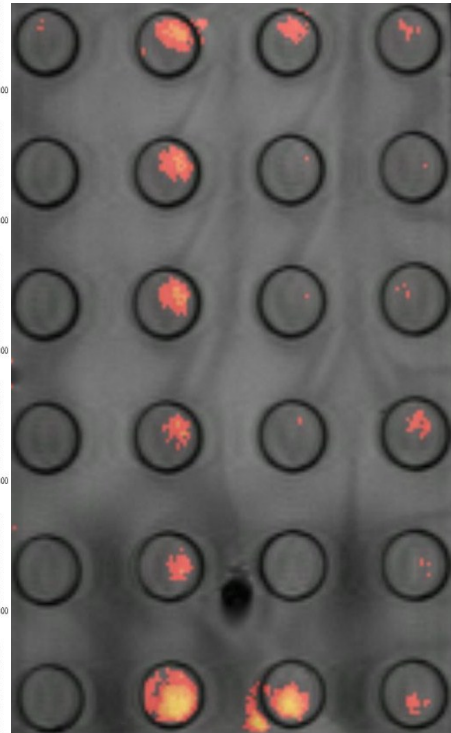
Poly L Lysine Z-spectra
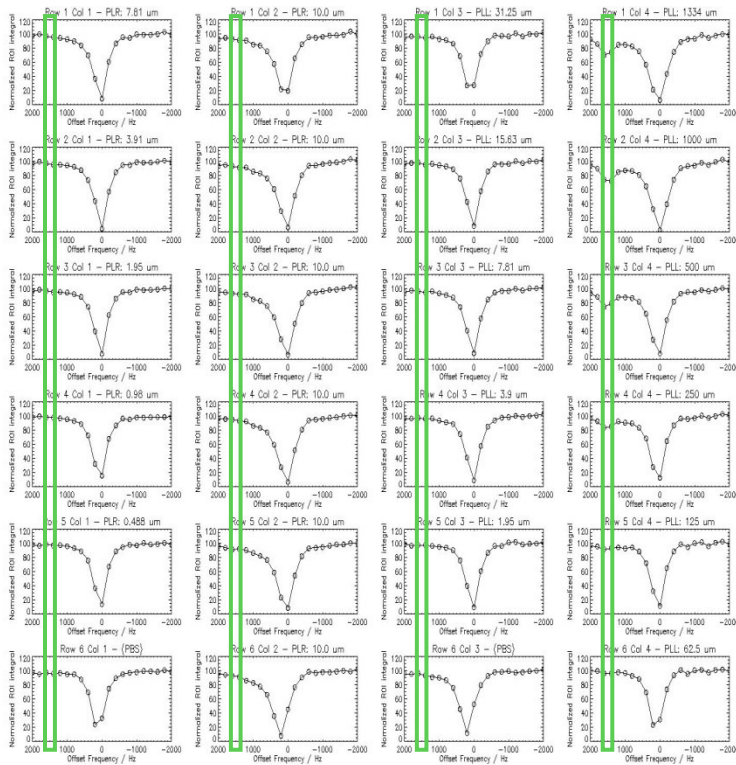
Overlay: diff. contrast/ref.
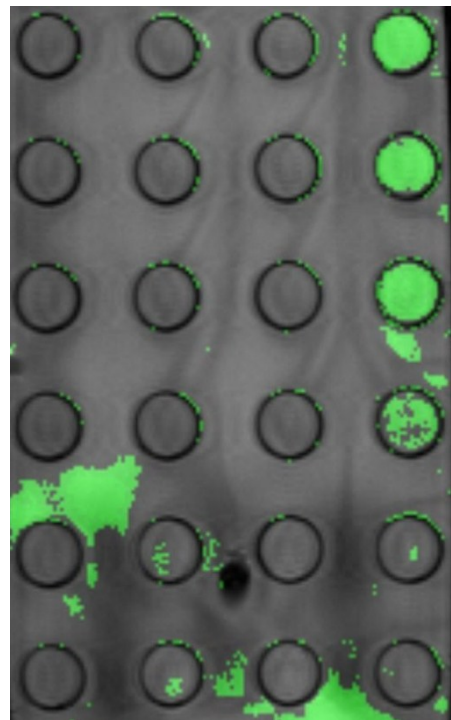
Figure 5.5: Z spectra constructed using RARE scans of PLK and PLR over a range of concentrations (1.95μM-1334μM for PLK and 0.488-10μM for PLR). A colorimetric overlay of the wells is on the right with red assigned to PLR and green assigned to PLK contrast.
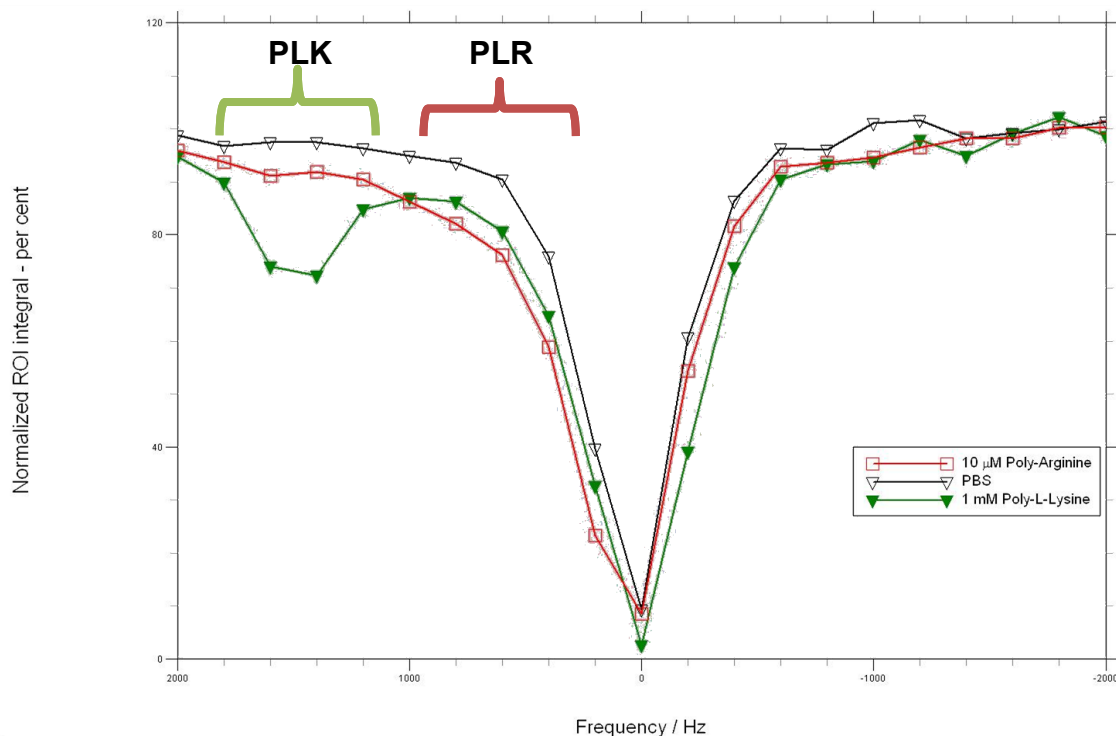
Figure 5.6: The Z spectra were constructed from FLASH scans to determine the optimum frequencies at which PLK and PLR can be targeted with an RF pulse. The peaks are highlighted, a broad peak was observed for PLK (1800 Hz to 100 Hz from the water peak) and for PLR (1000 Hz to 200 Hz) which had a smaller peak resulting from the amide group (1700 Hz).

Loading Agarose Beads with CEST Agents

Agarose beads were labelled with either various concentrations of PLK or PLR to test whether the beads can be used as a method to image CEST agents *in vivo* without the CEST solution dissipating away, causing the signal to become too dilute to observe. The 3D FLASH scan was used because it has the advantage of being a quicker scan, which is important for *in vivo* studies. There was approximately half as much signal change in the beads as in the solution (Figure 5.7). Washing the beads in PBS further reduced the signal of the beads compared to solution. When beads were labelled with CEST agents over 24 hours and the solution changed to PBS all CEST signal was lost (Figure 5.8)
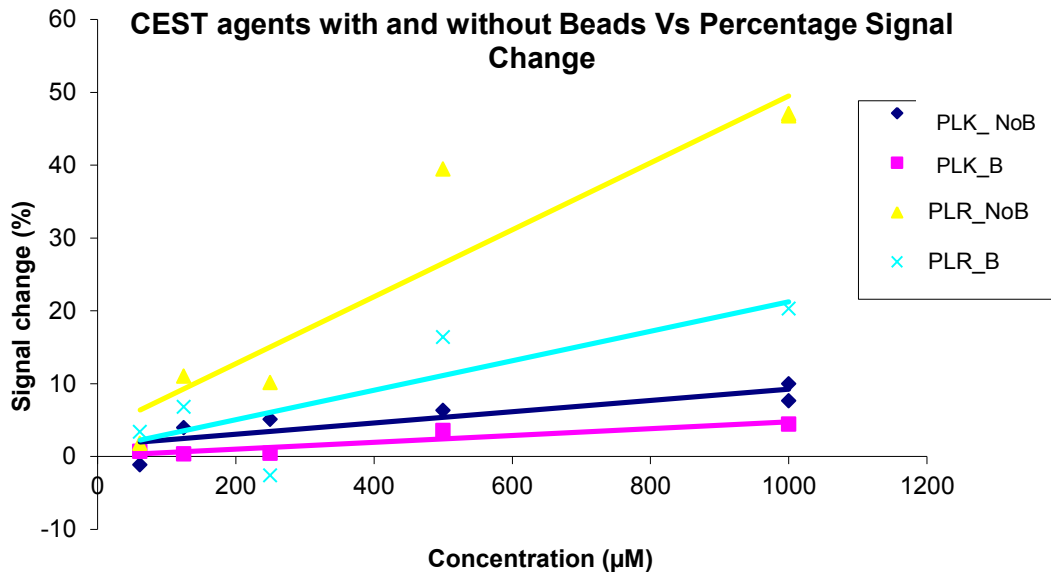
Figure 5.7: A range of solutions from 0 - 1mM of PLK (1440 Hz) and PLR (912 Hz) was imaged either after loading onto agarose beads or in solution. The signal change was recorded after RF pulses of 1440Hz or 912 Hz.
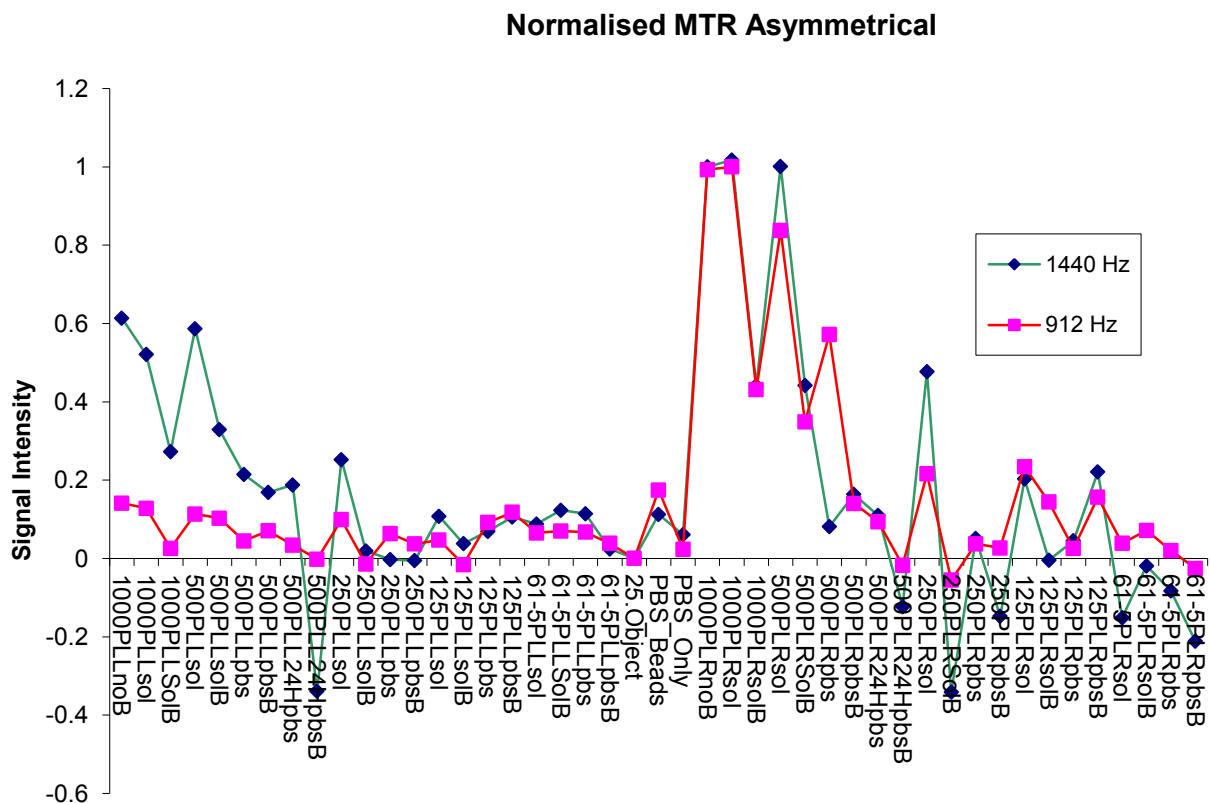
Figure 5.8: A range of solutions from 0 - 1mM of PLK and PLR was imaged either after loading onto agarose beads or in solution. The signal change was recorded after RF pulses of 1440 Hz or 912 Hz. Signal change from the PLR targeted scans at 912 Hz (shown in red) was only visible in PLR samples above 250μM in both beads and solution. While signal from using a PLK targeted RF pulse of 1440

Hz (shown in green) showed contrast change in high concentrations of PLK and PLR as expected. See Key below describing the sample names. Concentration given in µM.

Key to the sample names for Figure 5.10:

noB : Not through the beads section

B : signal intensity through beads

Sol : signal intensity of area above the beads of the PLK or PLR solution

PBS : signal intensity of area above the beads after beads were washed with PBS

PLK and PLR Dilution Series of the Solution above the Beads

The PLK and PLR dilution series set up with the agarose beads was used to indicate the sensitivity of 3D FLASH to decreasing concentrations of CEST *in vitro.* The PLK CEST signal was visible above background at concentrations above 125µM when the RF pulse of 1440 Hz was used (Figure 5.9). There was 44% signal change for concentrations of 1mM PLK. PLR CEST signal was visible from concentrations of 15.83 µM using an RF pulse of 960 Hz, with increasing concentrations signal change also increased, reaching a maximum of 49% at 500µM. The PLK and PLR solutions show the largest signal change when irradiated with 1440 and 960 Hz respectively, and lower signal change when irradiated with the opposite RF pulse (Figure 5.10). The guanidyl NH_2 residues used to confirm the presence of arginine and elucidated through irradiating at 912Hz, are less than 20% of the maximum signal intensity in all concentrations of PLK and, as expected, give strong signal in the solutions of 1000µM with steadily decreasing signal as the concentration lowers. The result is reassuringly reflective of the sample concentrations.
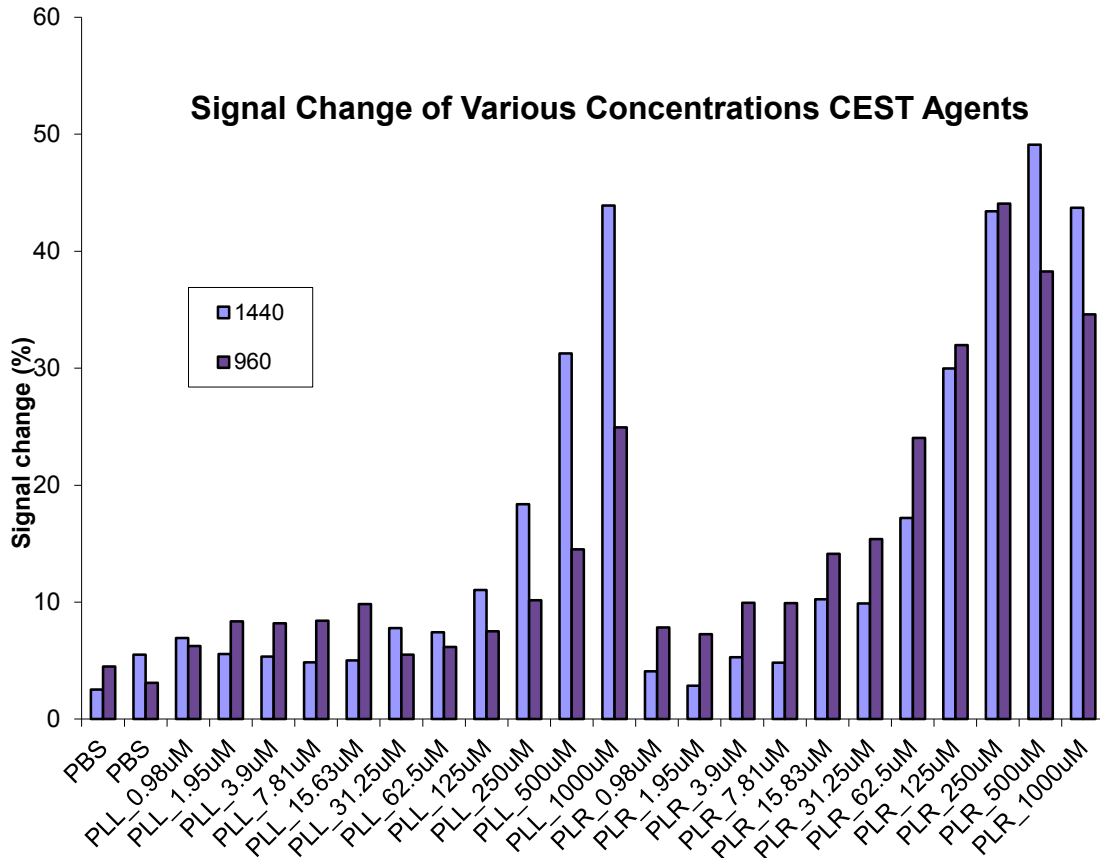
Figure 5.9: A series of PLK and PLR concentrations were imaged with RF pulse of 1440 Hz and 960 Hz and the signal change measured.
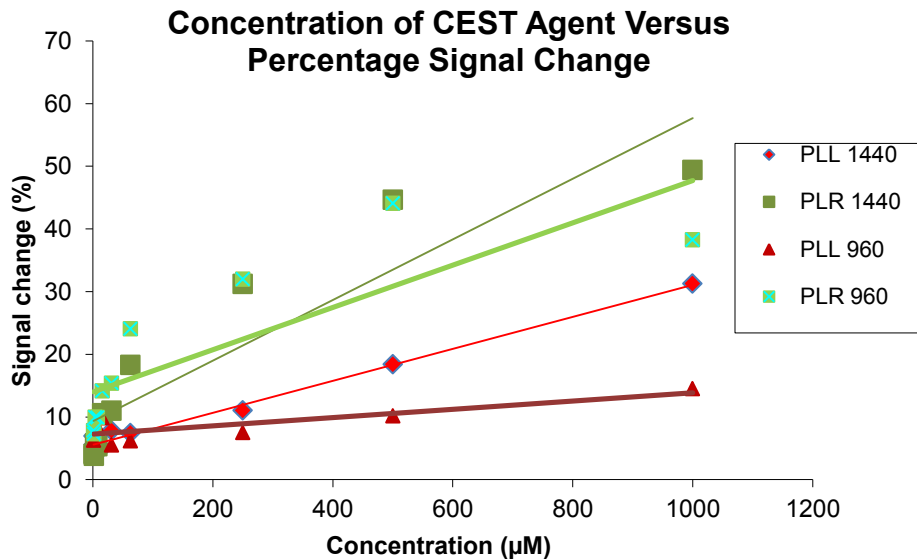
Figure 5.10: The signal change gets greater as the concentration of the CEST agent increases, PLR displays more contrast change when the RF pulse of 960 Hz is applied and PLK has more signal change using 1440 Hz RF pulse.

5.4.2 Cell results

The LRP transgene was received as a gift from Gilad *et al.* (Gilad *et al.* 2007) to test the CEST contrast agent transgene as an MRI marker for tracking mouse ES cells. After carrying out both electroporation and lipofection to get LRP transgenes expressed in E14 cells with little to no GFP expression, nucleofection was tried. After nucleofection the cells expressed the transgene as confirmed by fluorescence microscopy (Figure 5.11) and RT PCR carried out later 48 hours (Figure 5.12). However transgene expression was not stable, after selection with G418 cells survived but lost GFP expression and LRP expression as confirmed by RT PCR.

Positive control   LRP/GFP expressing cells
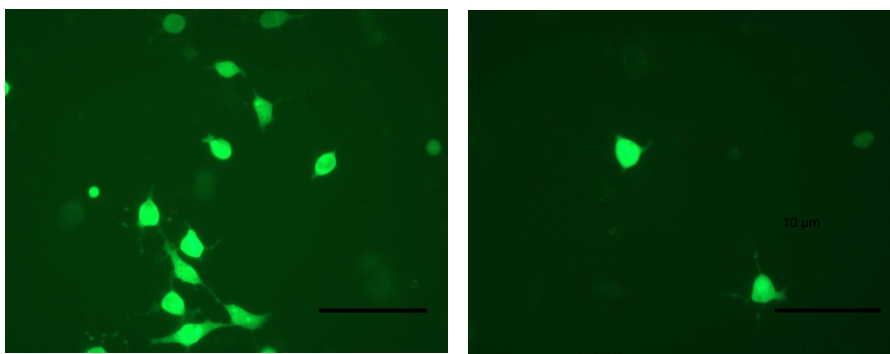
Figure 5.11: Transient GFP expression of LRP is observed after transfection of the LRP plasmid into E14 mouse ES cells. Scale bar 100µm
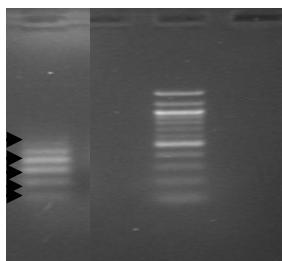
LRP   1kb
Positive   ladder

Figure 5.12: RT PCR: LRP expression was verified using a primer that anneals every 84 bp and a second that anneals only at one site at the 3' end of the gene giving a ladder appearance (Black arrows). Positive LRP expressing sample on left 48 hours after nucleofection and two weeks after nucleofection on right. Ladder NEB 1kb

5.5 Discussion

5.5.1 Technical
Injection of 1mM PLK into the rodent brain

When injecting the PLK solution into the rodent brain observation of the CEST affect was hampered by the needle track. The contrast agent appears to have remained in the needle tack which already has almost total signal drop out. I attempted to address the issue of the needle track MRI signal in chapter 4 by using a glass cannula to decrease the size of the artefact but accumulation of blood in the area is seemingly causing this problem. CEST contrast provided by cells that migrate away from the point of entry may avoid this problem.

Cause of needle tract MRI signal

The needle track's visibility during an MRI scan seems more to do with bleeding caused by the surgery than the cannula. The visibility of the needle tracks plateaued and the track at one week was the same at the second week. We know from historical data that the needle track is evident months after surgery without diminishing and it will be a case of finding methods to ensure it doesn't occur in the first place if we want to image without it. As it seems to be hemosiderin left over from bleeding during and after surgery it may be advisable to use bone wax to seal the drill holes in the skull so that blood can't enter after the skin is stitched back up. Alternatively when carrying out surgery on a rat, when there is typically more bleeding, an absorbable collagen fleece, such as Lyostypt® (BBraun) could be used to stem the blood flow around the drill sites.

Improving RARE for CEST

Since the MRI programming to generate CEST contrast is not a standard protocol on the Bruker scanner it was imperative to get the programme working in our hands and ascertain what CEST signal strengths and *in vivo* capabilities were possible. Quantifying CEST effects is by no means trivial, *in vivo* the effects of MTC, CEST agent and the endogenous signal have to be separated out. Initial proof of concept scans were carried out using the standard 2D RARE protocol with a lengthy (4 second) CEST pulse, at the start of each slice acquisition, whist this gave strong CEST effect *in vitro* it becomes slow and cumbersome to look at multiple slices or

multiple CEST agents as would be required *in vivo*. The 4 second MTC RF pulse required to generate suitable CEST contrast is currently applied once per image slice, the acquisition time could be vastly decreased for multislice images by imaging all the slices in quick succession immediately after the first MTC RF pulse. While this was heavily affected by artefacts, further modifications could avoid this, as detailed in the results section. Also if imaging a live animal the scanner must be triggered by the animal's breathing cycle to avoid motion artefacts appearing in the images. Currently the scan timing is triggered before the 4 second MTC RF pulse (during which time a mouse will go through several full breathing cycles) rendering the triggering ineffective. Since the 4 second MTC RF pulse acts upon the whole sample equally the sequence should be rewritten to include the triggering module after the MTC RF pulse allowing the faster spatially localised parts of the scan sequence to be accurately timed to the breathing cycle of the animal being imaged.

Z Spectra

The optimal radiation frequency was confirmed by obtaining a Z spectrum. A Z spectrum is a curve in which the ratio of the water signal intensities with and without the MT pulse is plotted as a function of frequency offset of the irradiation (relative saturation $S^{\Delta\omega}/S_0$ as a function of saturation frequency). This was acquired with the saturation transfer sequence consisting of a saturation pulse with a variable offset, power B_1 and duration (t_{sat}) followed by spin echo acquisition with radiofrequency pulses centred on water resonance, arbitrarily assigned to 0 ppm. Z spectra for polypeptides PLK and PLR were determined using RARE and FLASH scans, with peaks at the expected positions for both CEST agents.

2D RARE vs 3D FLASH CEST imaging

Standard RARE is slow and the modification in the programme to speed it up met with artefacts that required more work to get around. Instead a 3D FLASH scan was tried based on the literature (Dixon *et al.* 2010). Using the staccato multi slice FLASH (Dixon *et al.* 2010) it was possible to distinguish PLR from PLK. This method provides faster 3D than multislice 2D RARE. However, while 3D Gradient Echo can potentially provide higher resolution and reduced speed, it introduces more noise. Increasing the voxel size could lead to a higher signal to noise ratio, making the CEST signal more pronounced. While gradient echo is a huge improvement in terms

of *in vivo* scanning time it is at the cost of losing sensitivity, although this could be improved by increasing voxel size to try and recover the CEST signal. So we have one method, RARE, which is better for sensitivity and a second, using 3D FLASH, that is better for sample measurements and improved practicality of use.

CEST Imaging of Different Concentrations of PLK and PLR

To determine the concentrations of CEST agent that can be picked up a dilution series of PLK and PLR was made up and imaged. An RF pulse was applied to image the PLK by virtue of their amide groups using a frequency of 1440 Hz, and a pulse of 960 Hz to pick up the gaunidyls on the PLR. The PLR was visible from lower concentrations than the PLK, this is a result of the structure of PLK and PLR (Figure 5.13); there are more protons available for exchange per guanidyl than there are per amide. When irradiating with 1440 Hz signal was also picked up from the PLR solutions at above 62.5µM concentrations because the PLR has both an amide and guanidyl group. As the concentration of PLK increases the peak get broader impinging on the position where you would expect to see PLR signal. This leads to signal change resulting from the 960 Hz RF pulse at concentrations of 500 µM and above. One should be aware of the interference from other channels by looking at the ratio between the signal differences of the two CEST agents used. The background noise seemed to be quite high giving about 10% signal change, if we can reduce the noise which is partially an artefact of voxel size and scan time we would be able to image lower concentrations of CEST agent than we have so far.
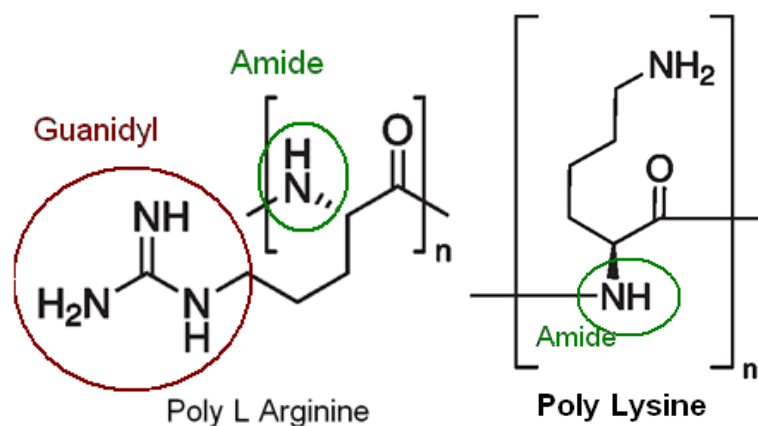
Figure 5.13: Structure of PolyLysine and Poly L arginine with the exchangeable amide and guanidyl protons highlighted

Labelling of Agarose Beads

Following difficulties in imaging CEST reagents *in vivo* on injection of a PLK solution in the rodent brain, CEST labelling of agarose beads was considered. If the agarose beads could be successfully labelled with the PLK/PLR solution, providing CEST contrast at similar levels to the solution, it would be feasible to inject them subcutaneously and determine if it is possible to pick up CEST signal *in vivo.* Allowing the CEST agent to remain in a specific location without the worry of it dissipating that could occur with solution. An MRI scan could then be run to try and distinguish CEST agents in the presence of tissue. During the 3D FLASH scan the temperature was maintained at 37°C and was recorded for each scan. Incubating the beads at room temperature with 500 µM of solution for 24 hours prior to washing and imaging was detrimental to the residues as the signal was completely lost. Imaging the beads soon after labelling would be the only feasible option if using them. While there was still signal from the polypeptides when absorbed onto the agarose beads it was typically half of what it was in the solution without the beads present. This may result from the diluting factor of the beads taking up more area from where the solution would otherwise be or from the way in which the polypeptides become attached which may inhibit proton exchange. Washing the beads with PBS prior to signalling also decreased signal. The beads could be used to look for CEST contrast *in vivo* because the percentage signal change is still higher than background *in vitro.* Labelling the beads for one hour seems sufficient for polypeptides to attach and give a detectable signal. Caution should be taken when labelling for longer as our experiments show proton exchange is affected and signal is lost when labelling for 24 hours. A high concentration would be necessary to account for the associated drop in signal when labelling beads and the polypeptides that may come off the beads in an *in vivo* environment.

The decrease in signal when the polypeptides are attached to the beads may be an effect of the body of the beads taking up room of the voxel and not the polypeptide not penetrating further than the surface and so having an effect of diluting out the CEST agent concentration. Never the less using a high concentration of polypeptide on the beads the signal does not diminish below the threshold and could therefore be seen if imaged directly on injection into a rodent brain, so to test the programme

to see if the agents can be distinguished from amongst endogenous polypeptide residues.

The high signal at 1000 μM PLR is due to the presence of amide groups on the arginine as explained previously. There was a strong CEST effect in percentage signal change but also a large back ground variation masking the effect at lower concentrations. Using the new 3D FLASH method we had very much smaller voxels than the old RARE method meaning there was automatically much less signal to noise, further experiments would be improved by scanning for longer to increase the signal to noise or increasing the voxel size to improve signal to noise in the same scan time.

5.5.2 Cells and CEST

The LRP Plasmid

LRP was expressed in mouse ES cells but only transiently. Cells were later FACs sorted in an attempt to enrich the population of GFP positive cells but the plasmid continued to be turned off. Interdispersing lysine with other amino acids and varying codon usage may make it more tolerable to cells and improve expression, as well as making it easier to manipulate in a molecular biology sense. Repetitive sequences are known to be not well tolerated in cells, and repetitive expansions of certain sequences are associated with a number of diseases.

Imaging cells transfected with LRP showed no contrast using MRI due in part to the small volume of cells and the fact susceptibility artefacts from the plastic vials interfered with image acquisition. It was therefore not possible to tell if cells were expressing PLK using MRI. The susceptibility artefacts that hampered the imaging of transfected cells using MRI, although a problem in plastic vials, would not be an issue in the rodent brain. This is because both graft and brain have the same magnetic properties.

There will need to be careful consideration of which polypeptides can be used as contrast agents, based not just on the MRI properties but also the effects on cells, be they beneficial or detrimental, and worked out on a case by case basis. PLK can have anti proliferative effects of tumours *in vitro* and *in vivo* (Szende *et al.* 2002) but enhance proliferation in glial cells when plated on PLK substratum (Kozlova *et al.*

1993). Studying the biological effects in parallel to the MRI capabilities could save time and money as having a contrast agent with a strong MRI spec won't be useful if it doesn't fulfil its biological remit, after all, we already have SPIO's to that end.

The lysine residues in Gilad's LRP plasmid were followed by an IRES GFP and preceded by a cytomegalovirus (CMV) promoter. The efficiency of the CMV promoter and enhancer has been shown to be susceptible to transcriptional inactivation by methylation *in vitro* (Prosch *et al.,* 1996) and *in vivo* in a rapid and extensive manner (Brooks *et al.,* 2004). This is a major shortcoming for longitudinal studies. A CMV enhancer combined with chicken β-actin promoter (pCAGGs) was shown to have almost 10 fold higher gene expression than a CMV promoter/enhancer alone (Xu *et al.,* 2001) and drives expression widely in the mouse (Okabe *et al.* 1997). A direct comparison of CMV, chicken β actin and pCAGGs promoters in mouse ES cells found the former two unsuitable for sustained transgene expression while pCAGs proved to be stable expressers even during differentiation. In addition transgene expression has been shown to be most effective when under selection, (Alexopoulou**,** Couchman and Whiteford 2008).

Various promoters and methods to label either the proteins or cells expressing the GOI can be created to assist in expression and analysis respectively. The design of optimal expression vectors is an on-going venture with older strategies continually being advanced and replaced by newer models (Chung *et al.,* 2002).

MRI of CEST Solutions and the Rodent Brain

Although there is a potential contribution from protons throughout the brain to add to the CEST contrast of interest, in our scans the analysis of the contrast agent scan, the reference scan and the control scan successfully allowed signal difference captured from the solutions of interest with little to no signal throughout the rodent brain. Therefore any addition of high concentrations of CEST agents should be readily distinguished from the surroundings. Our work was indicative of the fact the contrast agent signal can be viewed above that of endogenous protons as demonstrated in previous studies (Gilad *et al.* 2007) however it also highlighted the biological problems. The system used by Gilad is not conducive to all cell types, in this case mouse ES cells, and a different promoter and targeting system are needed

if the effects of the transgene on the cell are to be determined independent of any effects caused by the random position of integration.

What's Next for CEST?

The technical difficulties of the molecular and MRI aspects are conveyed by the following papers, or rather the lack of *in vivo* papers since the original Gilad paper and a focus on new polypeptides or ironing out the technical difficulties associated with the scans and even the equipment used.

Liu has developed a high throughput method to bulk MRI scan a large number of polypeptides to extrapolate their CEST properties (Liu *et al.* 2010). It is hard to control magnetic fluctuations at the property boundaries and susceptibility artefacts can arise when running a scan of two different materials with different magnetic properties, such as soft tissue and bone. So when imaging CEST agents with multiple holders you introduce the presence of a high density of air/glass/fluid interfaces, resulting in water line broadening and a problem when characterizing CEST agents, particularly when their resonance frequency may be in close proximity to water. Using cost efficient materials Liu was able to extract quantitative information from multiple CEST agents simultaneously without worrying about shimming of B_o. (Liu *et al.* 2010).

Amide protons have the same chemical shift differences as lipid resonances (3.5ppm) but on opposite sides of the water peak which can lead to a lipid artefact. A simple approach to circumvent this is to avoid the unequal suppression of the fat signal through equal suppression of the lipid resonance, regardless of the offset of saturation pulses, with this good quality amide proton transfer images can be achieved (Sun *et al.* 2005). Since the study here began a 3D CEST imaging sequence, allowing Z-spectra construction with 26 different frequencies, of a whole human brain in less than 10 minutes has been achieved (Zhu *et al.* 2011). Zhu et al used a prototype 32 channel phased array coil with a series of four block RF pulses at 200ms each.

CEST contrast is negative which isn't necessarily a limitation because the contrast agents scan is determined relative to the reference scan so the difference image can be displayed as positive, negative or colorized. However, this signal is lost with complete suppression of the background noise. So called Postive CEST (pCEST)

was demonstrated *in vitro* with two PARACEST agents that allows simultaneous total background suppression (Vinogradov *et al.* 2011). While the result of pCEST gives a better dynamic range utilization the sensitivity is lower than standard CEST, and when we consider CEST signal is typically in the order of 5%, it is not always affordable to lose more, especially *in vivo* (Vinogradov *et al.* 2011). Similar attempts have been made to achieve positive contrast in SPIOs in an effort to distinguish SPIO signal loss from native low signal in tissues. In one study the presence of SPIO labelled cells was indicated by hyperintense voxels but also highlighted the importance of proper analysis as haemorrhages also appear hyperintense in these scans (Liu *et al.* 2008).

The latest in a growing line of studies working to achieve more efficient CEST contrast uses a length and offset varied saturation (LOVARS) scheme that improves signal to noise and has decreased sensitivity to B_0 inhomogeneity associated with conventional CEST (Song *et al.* 2012). A number of scans are taken with differing lengths and offset of the saturation pulse and tested in phantoms of PLK and PLR and *in vivo* in 9L rat gliomasarcomas in the mouse brain with the above mentioned results.

The opportunity to dual label cells based on their amide, guanidyl and hydroxyl signatures provides the unique opportunity to follow differentiation and the ratios of different cell types *in vivo* after transplantation. This could provide amazing temporal details of the graft's composition linked to high resolution anatomical information.

Using CEST and T2 based scans it has been possible to image both CEST and SPIOs in the same solution when the SPIOs are less than 5μg/ml and the CEST solution is at 250μM (Gilad *et al.* 2009). The ability to label concurrently with CEST and an iron based contrast agent may be of use when trying to directly analyse the use of CEST as a contrast agent against the current most popular choice, SPIOs. We looked at PLK and PLR as CEST agents in solution here and based on the potential to dual label a CEST agent with an iron based contrast agent one could use ferritin, also considered in this thesis. Since we are looking at labelling cells that will replace those in the brain the choice of CEST agent should be tailored on two counts, one for the cell type and two, the combination of this cell type and any confounding effects with a second contrast agent like ferritin upregulation. For example, glial cells generate significant amounts of toxic superoxide and nitric oxide derived free

radicals from L-arginine. Subsequently these free radicals can release iron from ferritin and nitric oxide can inhibit activity of mitochondrial complex I and II, thereby exacerbating oxidative damage (Yoshida et al, 1995). Bearing such speculation in mind coupling contrast agent could have combined deleterious effects, even if individually the detrimental effect is of an acceptable level.

5.6 Conclusions

Straightforward RARE is too slow due to long TR's and trying to speed things up results in a number of issues. Attempting to speed up the scan using a high RARE factor introduces stronger than normal artefacts caused by T_1 recovery from an unusual start point. Multi slicing after a common MT preparation may be successful but the modulation artefacts introduced in our sequences obstructed any analyses on the scans carried out here. However, with greater technical MRI support it may be possible to overcome these artefacts. In the absence of this expertise we switched our attentions to a published 3D gradient echo sequence which provided the necessary speed up in imaging time and sample coverage but at the expense of a loss of CEST signal strength. Using this sequence we were able to detect and distinguish CEST agents from each other but more optimisation is required to detect the sort of concentrations of agents likely to be produced by cells engineered to produce reporter peptides.

Since the start of this work there has been development of sensitive pulse sequences for rapid acquisition of whole organ images is being undertaken to increase its applicability to human studies (Jones *et al.* 2011). Following these directions there is potential to image increases in specific endogenous polypeptides such as Huntington's polyglutamine aggregates. If the protons in these aggregates are still readily exchangeable with water, MRI could be a useful tool in assessing disease progression of Huntington's disease.

6 General Discussion

There are few methods with which to monitor grafted cells *in vivo,* in longitudinal studies, using whole animal models. Of these methods the ones most often used include labelling with SPIOs, but they are associated with a number of caveats, such as dilution of signal as cells divide and giving a false positive after cells die leaving the SPIOs or they are taken up by macrophages. Given the ease of using SPIOs compared to creating a cell line, which gives relatively low MRI signal, it is no wonder SPIOs are most often used to date. However, SPIO labelling gives but a rough idea of what is going on in the graft. From the work here we see that volumes calculated using MRI are comparable to volumes calculated from stereolgy of histological preparations labelled with cresyl violet or IHC when SPIO labelling mouse ES cells, expanded WGE and primary tissue. Analysis of the graft is difficult when determining what is real signal and when grafting into the striatum the needle track severely impinges on potential MRI signal from the graft. There are a number of technical issues with extracellular SPIOs that are hard to wash off which can affect differentiation as shown in the literature and suggested in this work by the significant decrease in β-tubulin expression in SPIO labelled neurally differentiated mouse ES cells.

As a result this method of monitoring grafts is not routinely carried out and analysis is done almost exclusively by behavioural tests and post mortem analysis. There is a niche to be filled that circumvents the problems associated with SPIOs and provides more robust, dynamic, longitudinal analysis and results in a reduction in animal numbers necessary for each experiment.

Permanent cell marking and lineage tracing can be achieved using genetically encoded reporters. Fth has often been championed among the latest MRI contrast agent based transgenes but gives weak signal compared to the more oft used SPIOs. By expressing Ftl and Fth subunits in equimolar concentrations I tried to improve on that signal through the formation of more holo-Fts than apo-Fts and set up a means with which to determine if expressing both subunits is actually more beneficial to the cell than expression of either subunit alone. Here it was shown that the Ftl/Fth transgene had a significantly lower T_2 relaxation rate than non-expressing cells *in*

vitro without the need for iron supplementation of the media. This is promising for *in vivo* work and gives strong rationale for taking this transgene forward for comparison against other metalloprotein transgenes expressed in the same controlled system.

The needle track once again posed a problem that eclipsed the site of grafting into the striatum. Alternatively, if the injection can be repositioned in an area where the cells will migrate away from this problem could be averted. Iordanova et al showed that while the needle track in the images was still present as cells migrated from the SVZ to the olfactory bulb they were separate from the confounding needle track (Iordanova and Ahrens 2011). Long imaging times are also beneficial when picking up Ft signal, in Iordanova's work the best images were taken *ex vivo* in 16.5 hour long scans although in the shorter 4.5 hour *in vivo* scans Ft chimera cells could still be distinguished from the GFP control. 4.5 hours for one animal is an inordinate and expensive period of time, especially as there are typically many animals in one study. But for basic, initial comparative studies of different transgenes a teratoma model may be more suitable. A teratoma avoids the problems associated with needle track MRI signal and provides a single mass of MRI contrast agent expressing tissue

CEST agents have a number of additional theoretical benefits compared to Ft in terms of MRI signal expression; they can be switched 'on' and 'off' using MRI to distinguish artefacts from real signal and a number of different CEST agents could be used together to dual label cells. It seems CEST agents need to be improved in regard to the transgene sequence choice and the vector constituents (ie the promoter) in terms making them better tolerated by cells. But also the MRI programmes need to be refined to pick up CEST signal change in shorter scan times. What is possible to say from these studies is that while CEST agents can be observed with high sensitivity using 2D RARE scans, the scans are time consuming and not transferrable to *in vivo* studies. We have shown that we can decrease the scan time using 3D FLASH and still observe CEST signal change but with further modifications, discussed in the CEST Chapter 4, this system could be improved further with reduced signal to noise ratio.

The big benefit to MRI contrast agent transgenes that we have considered here is that they can dual label cells, increasing the data acquired from a single MRI scan many fold. The ability to distinguish morphological differences within the graft and changes over time would not only be hugely insightful, increasing the power of the

analysis but also decreases the number of animals necessary for each experiment. The option of using a number of CEST agents to multi-label cells is not restricted to CEST agent alongside CEST agent, not in solution at least (Gilad *et al.,* 2009). While we have seen here that signal loss caused by iron can obliterate any CEST signal at the same location, it has been reported that with low concentrations of SPIOs, less than 5µg/ml, CEST signal from 250µM PLK can still be seen (Gilad *et al.* 2009). As mentioned above SPIO use is riddled with difficulties, however, Gilad *et al*'s study showing that SPIO and CEST signal can co-exist, hints that other forms of superparamagnetic contrast agents, like Ft transgenes, could be imaged simultaneously alongside CEST.

The issues with both Ft and CEST transgenes is the low signal, meaning a large number of cells must be present in close proximity to see contrast change. Increasing the transgenes expression, other than just using a strong promoter like pCAGGs, can be achieved by tagging it onto cellular components, like in the case of the tau-tagged GFP cell line which expresses GFP bound to microtubules (Pratt *et al.* 2000). Theoretically binding Ft to cytoskeletal elements causes aggregation of Ft and increases signal in computer simulations and *in vitro* (Bennett *et al.* 2008). Testing the feasibility of this in cells for both Ft and CEST, after running similar theoretical tests, may well lead to better signal. In the case of CEST especially if the transgenes are modified to be more tolerable *in vivo* with optimised codon usage (McMahon *et al.* 2008) than the original highly repetitive base sequence or 200 lysines as used by Gilad *et al*. (Gilad *et al.* 2007). Certain areas of the genome benefit from lengthy repeats, like centromeres and telomeres, but in many these long repeats are unstable and are affected during replication, repair, transcription and by recombination events. Unusual structures can also form, that are likely to disrupt DNA metabolism (Bowater and Wells 2001). The phenotype of unstable segments in known diseases are progressive and can display anticipation in progeny (Lindblad and Schalling 1996), which could be problematic if creating a CEST mouse strain. Once again highlighting the importance of the conditional loxp flanked STOP codon and the benefits of modifying codon usage will hopefully reduce any detrimental effect to the cells. CEST provides lower signal than SPIOs and of bioluminescence and fluorescence techniques and detection will no doubt be limited to 1,000s of cells in close proximity even after optimisation of the MRI programming. It does, however,

have the advantage of switchable MRI contrast controlled by the RF pulse to avoid artefacts.

Recently both Ft subunits have been expressed in the rodent brain using adenoviral (Vande Velde *et al.* 2011) and lentiviral methods (Vande Velde *et al.* 2012). Hypointensity resulting from Ft expression was observed in the olfactory bulb after injection into the subventricular zone. Injection into the subventricular zone of Ft expressing lentiviruses allowed labelling of neural progenitor cells as they move to the olfactory bulb along the rostral migratory system. Contrast change compared to the contralateral side was observed but visual assessments were subjective, based on the knowledge of where contrast was expected to be seen. On injection into the striatum although needletrack causes signal drop out the Ft expression resulted in a hypointense region. It is difficult to truly compare this contrast to similar studies using metalloprotein transgenes, and it is still uncertain whether expressing both subunits is superior to just using Fth without a more thorough analysis using the rationale in this report.

The conditional expression and targeting system would allow the different MRI contrast agent transgenes to be compared on a level playing field. Once a transgene is targeted to the ROSA26 locus and successfully floxed, the resulting clones could be compared solely based on the effects of transgene expression. Comparisons would be in terms of the effect on cells, including viability and their capacity for differentiation and in terms of MRI contrast. In the literature to date many MRI contrast agent based transgenes have been tried but each uses a different biological system and different instruments and parameters to measure MRI contrast change. Addressing this disparity in the literature by testing them in a standard set up is what I set out to do here. To categorically determine which has the most potential in both an MRI and a biological sense the transgenes should inhabit the same locus, here the ROSA26 locus was chosen for its proven ability to act as a safe harbour to incoming DNA. Secondly if the system is conditional it provides many downstream benefits which are discussed later, but it also means the transgene can be introduced in an 'off' state. This allows the establishment of a cell line, or transgenic animal, in which the transgene, and in this case the human Ft, can be turned on on demand in a variety of ways. The immediate benefits to cell culture are the floxed daughter cell line can be compared with the unfloxed parent, so the control line has

been treated very similarly to the new cell line, as well as other transgenes in the system. When using a LoxP flanked Stop the number of benefits expand in the number of applications downstream, particularly when generating a transgenic mouse.

Generating a mouse using this system has improved simplicity of vector construction and so decreased time taken before the experimental transgenic mice are available than previously done (Srinivas *et al.* 2001). The Cre system can be combined with other regulatable elements such as a tetracycline inducible systems (Belteki *et al.* 2005) or temporal control of Cre governed by tamoxifen (Hayashi and McMahon 2002). So rather than produce a mouse with ubiquitous, constitutive expression, which may cause more detrimental effects than necessary, the mice can be generated with the Ft or CEST transgene turned off and can be crossed with tissue specific Cre recombinase expression mouse lines. There are many hundreds of mouse strains available commercially that express either constitutive or inducible tissue specific Cre recombinase.

The benefits of generating a mouse expressing an MRI reporter gene is that the effects of over expression of the transgene can be assessed long term in the areas of interest. For instance if the CEST contrast agent transgene was required to be on constitutively in grafted cells the Cre system is advantageous in three ways. Firstly, generating mice with CEST activity only 'on' in tissues of the CNS, means the development of the brain, and effects resulting from the CEST expression can be determined separately from the grafting process so one can see how applicable it will be in a particular study, and what contraindications need to be taken into account during graft analysis. Secondly, as we have mentioned before primary foetal tissue grafts are the gold standard by which differentiated ES cell grafts are compared, and this system allows transplantation of ready labelled primary tissue. Foetal tissue from transgenic mice with the MRI contrast agent either in an 'on' or 'off' state can be dissected and transplanted directly without disruptive labelling prior to grafting. The third benefit is that the grafted cells can either be turned 'on' to express the MRI contrast agent prior to grafting, on differentiation down a specific lineage or at the researcher's discretion by inducing expression, for example through tetracycline or tamoxifen inducible Cre recombinase systems.

It is extremely important to take into account the method by which the cells will be grafted when carrying out MRI analysis. As we have seen when grafting directly into the striatum a region of the graft is often obscured by hemosiderin in the needle track. This makes both labelling with SPIOs and Ft and CEST transgenes problematic. When labelling with cells expressing the Ft transgene, the type of contrast will be much lower than the needle track, and if the graft volume is large, with the assumption that the cells will also inhabit the middle of the graft not just the periphery, the outer areas of contrast could be measured. However, the background contrast surrounding the needle track mark may also be contributed to by reactive microglia for which Ft is a marker (Kaneko *et al.* 1989), so a contrast over and above this would need to be produced. Because CEST agents give a different signal type to both SPIOs and metalloprotein transgenes, while the CEST contrast would not be visible in the areas of complete signal drop out of the needle track, the signal change in the periphery could be confirmed as a result of CEST labelled cells or not. When imaging cells far from the point of injection contrast change would be more obvious. When optimising and comparing MRI contrast agents it would be useful to use a model that doesn't suffer the compounding effects of the needle track, either through experimental teratoma formation by injection of ES cells to ectopic sites or a position where cells are expected to migrate from.

If imaging far from the needletrack it would be possible to calculate iron concentration using MRI (Bartzokis *et al.* 1993). The FDRI has been shown to correlate with published brain iron levels and *in vitro* experiments in phantoms showed that significant field dependence was only observed for ferritin and not for apo-Ft, transferrin or apotransferrin. Calculating Ft bound iron content using field dependent R2 increase (FDRI) has not been used for imaging Ft based contrast agents, probably due to the requirement of two field strengths, but the ability to accurately calculate iron concentration would be useful in relation to use of Ft as a contrast agent, as a means of measuring graft density. The necessity to form iron loaded Fts rather than apoFt is important for this type of measurement and expression of both Ft subunits could be more beneficial if wanting to carry out these quantitative studies as a means to determine graft density.

Transferring any contrast agents to the clinic for grafting studies is still a long way off and requires strong, long term toxicology studies. The thought of introducing

transgenes into the human body is not what it once was, and with the advent of gene therapy, the medical community and society are more receptive to such technology. There has to be a measure of low risk to high value, with clearly defined results regarding the detriment to the graft and consequence to the host. Transgenes may be more suited to this direction because it is likely any problems will be confined to the grafted cells, whereas SPIOs and similar exogenous agents can affect host tissue following apoptosis or necrosis of labelled cells. Transgenes may even be found which not only give high contrast but also provide benefits to the cell. Equally long term monitoring of human subjects can take place over the course of decades and a transgene can better monitor this without dilution of signal associated with SPIOs.

There is potential for MRI contrast agent transgenes to become the method of choice when monitoring cells *in vivo* and, as has been specified in this work, increased MRI contrast signal is one of the major areas to be improved. These include both expression levels and reducing the detrimental effects on cells. There also needs to be improvements in the MRI programming with regards to CEST to make it more applicable to *in vivo* studies, where these transgenes could be most beneficial. They do negate many of the issues associated with other methods like PET, but because of the increased signal quality and reduced costs of PET, it may be a case of accepting the limitations of PET agents to monitor cells *in vivo* until a better method comes along. The benefits of a reliable *in vivo* monitoring method are too important to just suffice with SPIOs, but there is not yet a clear front runner in the transgene stakes. It is likely different contrast agents will be more equipped for different experiments and researching down different avenues is necessary.

Conclusions

Monitoring and tracking of cells *in vivo* after transplantation is a much sought after technique that would provide increased power to longitudinal analyses. Three different MRI contrast agents were explored here, SPIOs and two transgenes based on CEST and ferritin gene expression.

CEST is an attractive option but its use in routine analysis is still many years off. As we have seen there are a number of issues that need to be overcome, from development of new peptide sequences that are tolerated by living cells, to improved MRI programmes. While 2D RARE scans were successfully used here to distinguish different CEST polypeptides in solution, 3D FLASH scans were developed that are faster and have provided us with usable Z spectra over a whole sample in a reasonable time frame. The poly-lysine LRP transgene developed by Gilad (Gilad *et al.* 2007) as a CEST probe was tested *in vivo* in mouse ES cells, however, expression was lost even under antibiotic selection. New polypeptides based on a wider range of codon usage are likely to be more tolerable as well as easier to manipulate when generating vectors.

SPIO's successfully labelled mouse ES-derived neural stem cells, expanded whole ganglionic eminence and rat ventral mesencephalon. After grafting, volumetric MRI data corresponded to volumes that were determined through stereology on immunohistological sections. There was high variability between the graft sizes that larger numbers of animals and more reliable grafts could overcome. Problems were discovered in reference to the needle track leaving an MRI visible track that eclipsed the area of graft deposition, and while SPIOs did not seem to hamper graft survival *in vivo*, only large grafts extending out from the needle track could be reliably measured. Extracellular SPIOs are very hard to wash out from cell preparations and can not only adversely affect differentiation but could also be taken up by other host cells *in vivo. In vitro* analysis of SPIO labelled mouse ES-derived neural stem cells hinted that continued differentiation down the neural lineage was being affected, but this will have to be confirmed with further analysis.

Constitutive over expression of the Ferritin heavy and light subunit genes, randomly integrated into mouse ES cells, showed a T_2 contrast change significantly different

from control lines using the MSME programme. Comparison with the ferritin chimeric genes and the individual heavy and light chain genes would be an interesting next step.

For future studies the problem of small and variable grafts found here could be circumvented using other techniques to assess the transgene function. For example employing recombinant viruses that spread out from the area of the needle track would provide a good model system, or the larger grafts observed when grafting into 6-OHDA lesioned animals would also have the benefit of not having the MRI contrast disturbance caused by a lesion into the striatum using QA.

There are many potential contrast agents on the horizon each with different attributes and it will be a matter of working out the best cost/benefit ratios for their use. Cost, in terms of the affect it will have on the cells and host tissue, and benefits in terms of the contrast level and any contrast agent specific traits, such as the ability to turn off the signal or dual label cells. It is unlikely that there will be one contrast agent that will fit all applications and the choice of contrast agent will depend on the type of study. Work in this thesis contributes some understanding towards the promises and pitfalls of three MRI contrast agents, two of which may ultimately be used more routinely for cell tracking in the future.

7 Bibliography

Abt, A. C. and Meucci, O. (2011). Regulation of Neuronal Ferritin Heavy Chain, A New Player in Opiate-Induced Chemokine Dysfunction. *J Neuroimmune Pharmacol* **6:**466-476.

Aguilar-Martinez, P., Biron, C., Masmejean, C., Jeanjean, P. and Schved, J. F. (1996). A novel mutation in the iron responsive element of ferritin L-subunit gene as a cause for hereditary hyperferritinemia-cataract syndrome. *Blood* **88:**1895.

Aime, S., Carrera, C., Delli Castelli, D., Geninatti Crich, S. and Terreno, E. (2005). Tunable imaging of cells labeled with MRI-PARACEST agents. *Angew Chem Int Ed Engl* **44:**1813-1815.

Allkemper, T., Bremer, C., Matuszewski, L., Ebert, W. and Reimer, P. (2002). Contrast-enhanced blood-pool MR angiography with optimized iron oxides: effect of size and dose on vascular contrast enhancement in rabbits. *Radiology* **223:**432-438.

Amit, M., Carpenter, M. K., Inokuma, M. S., Chiu, C. P., Harris, C. P., Waknitz, M. A., Itskovitz-Eldor, J. *et al.* (2000). Clonally derived human embryonic stem cell lines maintain pluripotency and proliferative potential for prolonged periods of culture. *Dev Biol* **227:**271-278.

Anderson, S. A., Shukaliak-Quandt, J., Jordan, E. K., Arbab, A. S., Martin, R., McFarland, H. and Frank, J. A. (2004). Magnetic resonance imaging of labeled T-cells in a mouse model of multiple sclerosis. *Ann Neurol* **55:**654-659.

Andreini, C., Bertini, I. and Rosato, A. (2009). Metalloproteomes: a bioinformatic approach. *Acc Chem Res* **42:**1471-1479.

Andrews, N. C. (1999). Disorders of iron metabolism. *N Engl J Med* **341:**1986-1995.

Anzai, Y., Blackwell, K. E., Hirschowitz, S. L., Rogers, J. W., Sato, Y., Yuh, W. T., Runge, V. M. *et al.* (1994). Initial clinical experience with dextran-coated superparamagnetic iron oxide for detection of lymph node metastases in patients with head and neck cancer. *Radiology* **192:**709-715.

Arbab, A. S., Yocum, G. T., Kalish, H., Jordan, E. K., Anderson, S. A., Khakoo, A. Y., Read, E. J. *et al.* (2004a). Efficient magnetic cell labeling with protamine sulfate complexed to ferumoxides for cellular MRI. *Blood* **104:**1217-1223.

Arbab, A. S., Yocum, G. T., Kalish, H., Jordan, E. K., Anderson, S. A., Khakoo, A. Y., Read, E. J. *et al.* (2004b). Ferumoxide-protamine sulfate labeling does not alter differentiation of mesenchymal stem cells. *Blood* **104:**3410.

Arbab, A. S., Yocum, G. T., Rad, A. M., Khakoo, A. Y., Fellowes, V., Read, E. J. and Frank, J. A. (2005). Labeling of cells with ferumoxides-protamine sulfate complexes does not inhibit function or differentiation capacity of hematopoietic or mesenchymal stem cells. *NMR Biomed* **18:**553-559.

Arbab, A. S., Yocum, G. T., Wilson, L. B., Parwana, A., Jordan, E. K., Kalish, H. and Frank, J. A. (2004c). Comparison of transfection agents in forming complexes with ferumoxides, cell labeling efficiency, and cellular viability. *Mol Imaging* **3:**24-32.

Arnold, P., Ward, J., Wilson, D., Ashley Guthrie, J. and Robinson, P. J. (2003). Superparamagnetic iron oxide (SPIO) enhancement in the cirrhotic liver: a comparison of two doses of ferumoxides in patients with advanced disease. *Magn Reson Imaging* **21:**695-700.

Arosio, P. and Levi, S. (2002). Ferritin, iron homeostasis, and oxidative damage. *Free Radic Biol Med* **33:**457-463.

Arredondo, M. and Nunez, M. T. (2005). Iron and copper metabolism. *Mol Aspects Med* **26:**313-327.

Aubry, L., Bugi, A., Lefort, N., Rousseau, F., Peschanski, M. and Perrier, A. L. (2008). Striatal progenitors derived from human ES cells mature into DARPP32 neurons in vitro and in quinolinic acid-lesioned rats. *Proc Natl Acad Sci U S A* **105:**16707-16712.

Bachoud-Levi, A. C., Remy, P., Nguyen, J. P., Brugieres, P., Lefaucheur, J. P., Bourdet, C., Baudic, S. *et al.* (2000). Motor and cognitive improvements in patients with Huntington's disease after neural transplantation. *Lancet* **356:**1975-1979.

Bain, G., Kitchens, D., Yao, M., Huettner, J. E. and Gottlieb, D. I. (1995). Embryonic stem cells express neuronal properties in vitro. *Dev Biol* **168:**342-357.

Bartzokis, G., Aravagiri, M., Oldendorf, W. H., Mintz, J. and Marder, S. R. (1993). Field dependent transverse relaxation rate increase may be a specific measure of tissue iron stores. *Magn Reson Med* **29:**459-464.

Bartzokis, G., Beckson, M., Hance, D. B., Marx, P., Foster, J. A. and Marder, S. R. (1997). MR evaluation of age-related increase of brain iron in young adult and older normal males. *Magn Reson Imaging* **15:**29-35.

Bartzokis, G., Cummings, J. L., Markham, C. H., Marmarelis, P. Z., Treciokas, L. J., Tishler, T. A., Marder, S. R. *et al.* (1999). MRI evaluation of brain iron in earlier- and later-onset Parkinson's disease and normal subjects. *Magn Reson Imaging* **17:**213-222.

Bartzokis, G. and Tishler, T. A. (2000). MRI evaluation of basal ganglia ferritin iron and neurotoxicity in Alzheimer's and Huntingon's disease. *Cell Mol Biol (Noisy-le-grand)* **46:**821-833.

Battersby, A., Jones, R. D., Lilley, K. S., McFarlane, R. J., Braig, H. R., Allen, N. D. and Wakeman, J. A. (2007). Comparative proteomic analysis reveals differential expression of Hsp25 following the directed differentiation of mouse embryonic stem cells. *Biochim Biophys Acta* **1773:**147-156.

Beal, M. F. and Martin, J. B. (1986). Neuropeptides in neurological disease. *Ann Neurol* **20:**547-565.

Beard, J. L., Wiesinger, J. A. and Connor, J. R. (2003). Pre- and postweaning iron deficiency alters myelination in Sprague-Dawley rats. *Dev Neurosci* **25:**308-315.

Beaumont, C., Dugast, I., Renaudie, F., Souroujon, M. and Grandchamp, B. (1989). Transcriptional regulation of ferritin H and L subunits in adult erythroid and liver cells from the mouse. Unambiguous identification of mouse ferritin subunits and in vitro formation of the ferritin shells. *J Biol Chem* **264:**7498-7504.

Belteki, G., Haigh, J. J., Kabacs, N., Haigh, K., Sison, K., Constantini, F., Whitsett, J. *et al.* (2005). Conditional and inducible transgene expression in mice through the combinatorial use of Cre-mediated recombination and tetracycline induction. *Nucl. Acids Res.* **33:**e51.

Bennett, K. M., Shapiro, E. M., Sotak, C. H. and Koretsky, A. P. (2008). Controlled aggregation of ferritin to modulate MRI relaxivity. *Biophys J* **95:**342-351.

Berman, S. C., Galpoththawela, C., Gilad, A. A., Bulte, J. W. and Walczak, P. (2011). Long-term MR cell tracking of neural stem cells grafted in immunocompetent versus immunodeficient mice reveals distinct differences in contrast between live and dead cells. *Magn Reson Med* **65:**564-574.

Berry, C. C., Wells, S., Charles, S., Aitchison, G. and Curtis, A. S. (2004). Cell response to dextran-derivatised iron oxide nanoparticles post internalisation. *Biomaterials* **25:**5405-5413.

Bizzi, A., Brooks, R. A., Brunetti, A., Hill, J. M., Alger, J. R., Miletich, R. S., Francavilla, T. L. *et al.* (1990). Role of iron and ferritin in MR imaging of the brain: a study in primates at different field strengths. *Radiology* **177:**59-65.

Bjornerud, A. and Johansson, L. (2004). The utility of superparamagnetic contrast agents in MRI: theoretical consideration and applications in the cardiovascular system. *NMR Biomed* **17:**465-477.

Blasberg, R. (2002). PET imaging of gene expression. *Eur J Cancer* **38:**2137-2146.

Blomer, U., Naldini, L., Kafri, T., Trono, D., Verma, I. M. and Gage, F. H. (1997). Highly efficient and sustained gene transfer in adult neurons with a lentivirus vector. *J Virol* **71:**6641-6649.

Bothwell, T. H. (1995). Overview and mechanisms of iron regulation. *Nutr Rev* **53:**237-245.

Bouhon, I. A., Kato, H., Chandran, S. and Allen, N. D. (2005). Neural differentiation of mouse embryonic stem cells in chemically defined medium. *Brain Res Bull* **68:**62-75.

Bowater, R. P. and Wells, R. D. (2001). The intrinsically unstable life of DNA triplet repeats associated with human hereditary disorders. *Prog Nucleic Acid Res Mol Biol* **66:**159-202.

Boyd, D., Vecoli, C., Belcher, D. M., Jain, S. K. and Drysdale, J. W. (1985). Structural and functional relationships of human ferritin H and L chains deduced from cDNA clones. *J Biol Chem* **260:**11755-11761.

Bresgen, N., Ohlenschlager, I., Fiedler, B., Wacht, N., Zach, S., Dunkelmann, B., Arosio, P. *et al.* (2007). Ferritin--a mediator of apoptosis? *J Cell Physiol* **212:**157-164.

Brons, I. G., Smithers, L. E., Trotter, M. W., Rugg-Gunn, P., Sun, B., Chuva de Sousa Lopes, S. M., Howlett, S. K. *et al.* (2007). Derivation of pluripotent epiblast stem cells from mammalian embryos. *Nature* **448:**191-195.

Bulte, J. W., de Cuyper, M., Despres, D. and Frank, J. A. (1999). Short- vs. long-circulating magnetoliposomes as bone marrow-seeking MR contrast agents. *J Magn Reson Imaging* **9:**329-335.

Bulte, J. W., Douglas, T., Witwer, B., Zhang, S. C., Strable, E., Lewis, B. K., Zywicke, H. *et al.* (2001). Magnetodendrimers allow endosomal magnetic labeling and in vivo tracking of stem cells. *Nat Biotechnol* **19:**1141-1147.

Bulte, J. W., Kraitchman, D. L., Mackay, A. M. and Pittenger, M. F. (2004). Chondrogenic differentiation of mesenchymal stem cells is inhibited after magnetic labeling with ferumoxides. *Blood* **104:**3410-3412; author reply 3412-3413.

Campan, M., Lionetti, V., Aquaro, G. D., Forini, F., Matteucci, M., Vannucci, L., Chiuppesi, F. *et al.* (2011). Ferritin as a reporter gene for in vivo tracking of stem cells by 1.5-T cardiac MRI in a rat model of myocardial infarction. *Am J Physiol Heart Circ Physiol* **300:**H2238-2250.

Carter, D. E. (1995). Oxidation-reduction reactions of metal ions. *Environ Health Perspect* **103 Suppl 1:**17-19.

Chalela, J. A., Kidwell, C. S., Nentwich, L. M., Luby, M., Butman, J. A., Demchuk, A. M., Hill, M. D. *et al.* (2007). Magnetic resonance imaging and computed tomography in emergency assessment of patients with suspected acute stroke: a prospective comparison. *Lancet* **369:**293-298.

Chalfie, M., Tu, Y., Euskirchen, G., Ward, W. W. and Prasher, D. C. (1994). Green fluorescent protein as a marker for gene expression. *Science* **263:**802-805.

Chambon, C., Clement, O., Le Blanche, A., Schouman-Claeys, E. and Frija, G. (1993). Superparamagnetic iron oxides as positive MR contrast agents: in vitro and in vivo evidence. *Magn Reson Imaging* **11:**509-519.

Choi, H. S., Liu, W., Misra, P., Tanaka, E., Zimmer, J. P., Itty Ipe, B., Bawendi, M. G. *et al.* (2007). Renal clearance of quantum dots. *Nat Biotechnol* **25:**1165-1170.

Chu, S. C., Xu, Y., Balschi, J. A. and Springer, C. S., Jr. (1990). Bulk magnetic susceptibility shifts in NMR studies of compartmentalized samples: use of paramagnetic reagents. *Magn Reson Med* **13:**239-262.

Cicchetti, F., Saporta, S., Hauser, R. A., Parent, M., Saint-Pierre, M., Sanberg, P. R., Li, X. J. *et al.* (2009). Neural transplants in patients with Huntington's disease undergo disease-like neuronal degeneration. *Proc Natl Acad Sci U S A* **106:**12483-12488.

Cohen, B., Dafni, H., Meir, G., Harmelin, A. and Neeman, M. (2005). Ferritin as an endogenous MRI reporter for noninvasive imaging of gene expression in C6 glioma tumors. *Neoplasia* **7:**109-117.

Cohen, M. E., Muja, N., Fainstein, N., Bulte, J. W. and Ben-Hur, T. (2010). Conserved fate and function of ferumoxides-labeled neural precursor cells in vitro and in vivo. *J Neurosci Res* **88:**936-944.

Cole, E. S. and Glass, J. (1983). Transferrin binding and iron uptake in mouse hepatocytes. *Biochim Biophys Acta* **762:**102-110.

Connor, J. R., Menzies, S. L., Burdo, J. R. and Boyer, P. J. (2001). Iron and iron management proteins in neurobiology. *Pediatr Neurol* **25:**118-129.

Cosentino U, Pitea D, Moro G, Saracino GA, Villa A. (2009) Conformational behaviour determines the low-relaxivity state of a conditional MRI contrast agent. *Phys Chem Chem Phys* **11(20)**:3943-50.

Cowley, J. M., Janney, D. E., Gerkin, R. C. and Buseck, P. R. (2000). The structure of ferritin cores determined by electron nanodiffraction. *J Struct Biol* **131:**210-216.

Cozzi, A., Corsi, B., Levi, S., Santambrogio, P., Albertini, A. and Arosio, P. (2000). Overexpression of wild type and mutated human ferritin H-chain in HeLa cells: in vivo role of ferritin ferroxidase activity. *J Biol Chem* **275:**25122-25129.

Cromer Berman, S. M., Kshitiz, Wang, C. J., Orukari, I., Levchenko, A., Bulte, J. W. and Walczak, P. (2012). Cell motility of neural stem cells is reduced after SPIO-labeling, which is mitigated after exocytosis. *Magn Reson Med*.

Curtin, J. F., Donovan, M. and Cotter, T. G. (2002). Regulation and measurement of oxidative stress in apoptosis. *J Immunol Methods* **265:**49-72.

Curtis, A. R., Fey, C., Morris, C. M., Bindoff, L. A., Ince, P. G., Chinnery, P. F., Coulthard, A. *et al.* (2001). Mutation in the gene encoding ferritin light polypeptide causes dominant adult-onset basal ganglia disease. *Nat Genet* **28:**350-354.

Dagher, A. P., Aletras, A., Choyke, P. and Balaban, R. S. (2000). Imaging of urea using chemical exchange-dependent saturation transfer at 1.5T. *J Magn Reson Imaging* **12:**745-748.

Daldrup-Link, H. E., Rudelius, M., Oostendorp, R. A., Settles, M., Piontek, G., Metz, S., Rosenbrock, H. *et al.* (2003). Targeting of hematopoietic progenitor cells with MR contrast agents. *Radiology* **228:**760-767.

Das, R. H., Jahr, H., Verhaar, J. A., van der Linden, J. C., van Osch, G. J. and Weinans, H. (2008). In vitro expansion affects the response of chondrocytes to mechanical stimulation. *Osteoarthritis Cartilage* **16:**385-391.

De Jong, W. H., Hagens, W. I., Krystek, P., Burger, M. C., Sips, A. J. and Geertsma, R. E. (2008). Particle size-dependent organ distribution of gold nanoparticles after intravenous administration. *Biomaterials* **29:**1912-1919.

de Vries, I. J., Lesterhuis, W. J., Barentsz, J. O., Verdijk, P., van Krieken, J. H., Boerman, O. C., Oyen, W. J. *et al.* (2005). Magnetic resonance tracking of dendritic cells in melanoma patients for monitoring of cellular therapy. *Nat Biotechnol* **23:**1407-1413.

Deans, A. E., Wadghiri, Y. Z., Bernas, L. M., Yu, X., Rutt, B. K. and Turnbull, D. H. (2006). Cellular MRI contrast via coexpression of transferrin receptor and ferritin. *Magn Reson Med* **56:**51-59.

Dexheimer, V., Frank, S. and Richter, W. (2012) Proliferation as a Requirement for In Vitro Chondrogenesis of Human Mesenchymal Stem Cells. *Stem Cells Dev*.

Dixon, W. T., Hancu, I., Ratnakar, S. J., Sherry, A. D., Lenkinski, R. E. and Alsop, D. C. (2010). A multislice gradient echo pulse sequence for CEST imaging. *Magn Reson Med* **63:**253-256.

Doetsch, F., Caille, I., Lim, D. A., Garcia-Verdugo, J. M. and Alvarez-Buylla, A. (1999). Subventricular zone astrocytes are neural stem cells in the adult mammalian brain. *Cell* **97:**703-716.

Donahue, K. M., Weisskoff, R. M. and Burstein, D. (1997). Water diffusion and exchange as they influence contrast enhancement. *J Magn Reson Imaging* **7:**102-110.

Donaldson, K., Stone, V., Clouter, A., Renwick, L. and MacNee, W. (2001). Ultrafine particles. *Occup Environ Med* **58:**211-216, 199.

Drysdale, J., Arosio, P., Invernizzi, R., Cazzola, M., Volz, A., Corsi, B., Biasiotto, G. *et al.* (2002). Mitochondrial ferritin: a new player in iron metabolism. *Blood Cells Mol Dis* **29:**376-383.

Dunnett, S. B., Bjorkland, A. and Lindvall, O. (2001). Cell therapy in Parkinson's disease - stop or go? *Nat Rev Neurosci* **2:**365-369.

Einstein, A., Fürth, R. and D., t. b. C. A. (1926). On the Movement of Small Particles Suspended in a Stationary Liquid Demanded by the Molecular-Kinetic Theory of Heat. *Investigations on the Theory of the Brownian Movement* **Dover Pulblications**.

Ekonomou A, Kazanis I, Malas S, Wood H, Alifragis P, Denaxa M, Karagogeos D, Constanti A, Lovell-Badge R, and Episkopou V (2005) Neuronal Migration and Ventral Subtype Identity in the Telencephalon Depend on SOX1 *PLoS Biol* **3(6):** e186.

Epsztejn, S., Glickstein, H., Picard, V., Slotki, I. N., Breuer, W., Beaumont, C. and Cabantchik, Z. I. (1999). H-ferritin subunit overexpression in erythroid cells reduces the oxidative stress response and induces multidrug resistance properties. *Blood* **94:**3593-3603.

Eriksson, P. S., Perfilieva, E., Bjork-Eriksson, T., Alborn, A. M., Nordborg, C., Peterson, D. A. and Gage, F. H. (1998). Neurogenesis in the adult human hippocampus. *Nat Med* **4:**1313-1317.

Evans, M. J. and Kaufman, M. H. (1981). Establishment in culture of pluripotential cells from mouse embryos. *Nature* **292:**154-156.

Feder, J. N., Gnirke, A., Thomas, W., Tsuchihashi, Z., Ruddy, D. A., Basava, A., Dormishian, F. *et al.* (1996). A novel MHC class I-like gene is mutated in patients with hereditary haemochromatosis. *Nat Genet* **13:**399-408.

Feng, Y., Liu, Q., Zhu, J., Xie, F. and Li, L. (2012). Efficiency of Ferritin as an MRI Reporter Gene in NPC Cells Is Enhanced by Iron Supplementation. *J Biomed Biotechnol* **2012:**434878.

Fernandez-Gomez, F. J., Galindo, M. F., Gomez-Lazaro, M., Yuste, V. J., Comella, J. X., Aguirre, N. and Jordan, J. (2005). Malonate induces cell death via mitochondrial potential collapse and delayed swelling through an ROS-dependent pathway. *Br J Pharmacol* **144:**528-537.

Ferreira, C., Bucchini, D., Martin, M. E., Levi, S., Arosio, P., Grandchamp, B. and Beaumont, C. (2000). Early embryonic lethality of H ferritin gene deletion in mice. *J Biol Chem* **275:**3021-3024.

Fisher, M., French, S., Ji, P. and Kim, R. C. Cerebral microbleeds in the elderly: a pathological analysis. *Stroke* **41:**2782-2785.

Fleige, G., Nolte, C., Synowitz, M., Seeberger, F., Kettenmann, H. and Zimmer, C. (2001). Magnetic labeling of activated microglia in experimental gliomas. *Neoplasia* **3:**489-499.

Forsén, S. and Hoffman, R. (1963). Study of moderately rapid chemical exchange reactions by means of nuclear magnetic double resonance. *J chem phys* **39:**2892-2901.

Foster-Gareau, P., Heyn, C., Alejski, A. and Rutt, B. K. (2003). Imaging single mammalian cells with a 1.5 T clinical MRI scanner. *Magn Reson Med* **49:**968-971.

Frank, J. A., Anderson, S. A., Kalsih, H., Jordan, E. K., Lewis, B. K., Yocum, G. T. and Arbab, A. S. (2004). Methods for magnetically labeling stem and other cells for detection by in vivo magnetic resonance imaging. *Cytotherapy* **6:**621-625.

Frank, J. A., Miller, B. R., Arbab, A. S., Zywicke, H. A., Jordan, E. K., Lewis, B. K., Bryant, L. H., Jr. *et al.* (2003). Clinically applicable labeling of mammalian and stem

cells by combining superparamagnetic iron oxides and transfection agents. *Radiology* **228:**480-487.

Freed, C. R., Greene, P. E., Breeze, R. E., Tsai, W. Y., DuMouchel, W., Kao, R., Dillon, S. *et al.* (2001). Transplantation of embryonic dopamine neurons for severe Parkinson's disease. *N Engl J Med* **344:**710-719.

Freeman, T. B., Cicchetti, F., Hauser, R. A., Deacon, T. W., Li, X. J., Hersch, S. M., Nauert, G. M. *et al.* (2000). Transplanted fetal striatum in Huntington's disease: phenotypic development and lack of pathology. *Proc Natl Acad Sci U S A* **97:**13877-13882.

Friedrich, G. and Soriano, P. (1991). Promoter traps in embryonic stem cells: a genetic screen to identify and mutate developmental genes in mice. *Genes Dev* **5:**1513-1523.

Fujita, T., Nishikawa, M., Ohtsubo, Y., Ohno, J., Takakura, Y., Sezaki, H. and Hashida, M. (1994). Control of in vivo fate of albumin derivatives utilizing combined chemical modification. *J Drug Target* **2:**157-165.

Gambhir, S. S., Bauer, E., Black, M. E., Liang, Q., Kokoris, M. S., Barrio, J. R., Iyer, M. *et al.* (2000). A mutant herpes simplex virus type 1 thymidine kinase reporter gene shows improved sensitivity for imaging reporter gene expression with positron emission tomography. *Proc Natl Acad Sci U S A* **97:**2785-2790.

Garcia, M., Vanhoutte, P., Pages, C., Besson, M. J., Brouillet, E. and Caboche, J. (2002). The mitochondrial toxin 3-nitropropionic acid induces striatal neurodegeneration via a c-Jun N-terminal kinase/c-Jun module. *J Neurosci* **22:**2174-2184.

Gaura, V., Bachoud-Levi, A. C., Ribeiro, M. J., Nguyen, J. P., Frouin, V., Baudic, S., Brugieres, P. *et al.* (2004). Striatal neural grafting improves cortical metabolism in Huntington's disease patients. *Brain* **127:**65-72.

Genove, G., DeMarco, U., Xu, H., Goins, W. F. and Ahrens, E. T. (2005). A new transgene reporter for in vivo magnetic resonance imaging. *Nat Med* **11:**450-454.

Gerfen, C. R. (1992). The neostriatal mosaic: multiple levels of compartmental organization. *Trends Neurosci* **15:**133-139.

Gilad, A. A., McMahon, M. T., Walczak, P., Winnard, P. T., Jr., Raman, V., van Laarhoven, H. W., Skoglund, C. M. *et al.* (2007). Artificial reporter gene providing MRI contrast based on proton exchange. *Nat Biotechnol* **25:**217-219.

Gilad, A. A., van Laarhoven, H. W., Michael T. McMahon, Piotr Walczak, Arend Heerschap, Michal Neeman, Peter C.M. van Zijl *et al.* (2009). Feasibility of concurrent dual contrast enhancement using CEST contrast agents and superparamagnetic iron oxide particles. *Magnetic Resonance in Medicine* **61:**970-974.

Gilchrist, R. K., Medal, R., Shorey, W. D., Hanselman, R. C., Parrott, J. C. and Taylor, C. B. (1957). Selective inductive heating of lymph nodes. *Ann Surg* **146:**596-606.

Gilissen, E. P., Ghosh, P., Jacobs, R. E. and Allman, J. M. (1998). Topographical localization of iron in brains of the aged fat-tailed dwarf lemur (Cheirogaleus medius) and gray lesser mouse lemur (Microcebus murinus). *Am J Primatol* **45:**291-299.

Gillies, R. J. and Gatenby, R. A. (2007). Hypoxia and adaptive landscapes in the evolution of carcinogenesis. *Cancer Metastasis Rev* **26:**311-317.

Gillis, P. and Koenig, S. H. (1987). Transverse relaxation of solvent protons induced by magnetized spheres: application to ferritin, erythrocytes, and magnetite. *Magn Reson Med* **5:**323-345.

Gillis, P., Moiny, F. and Brooks, R. A. (2002). On T(2)-shortening by strongly magnetized spheres: a partial refocusing model. *Magn Reson Med* **47:**257-263.

Girelli, D., Olivieri, O., De Franceschi, L., Corrocher, R., Bergamaschi, G. and Cazzola, M. (1995). A linkage between hereditary hyperferritinaemia not related to iron overload and autosomal dominant congenital cataract. *Br J Haematol* **90:**931-934.

Gossuin, Y., Gillis, P., Hocq, A., Vuong, Q. L. and Roch, A. (2009). Magnetic resonance relaxation properties of superparamagnetic particles. *Wiley Interdiscip Rev Nanomed Nanobiotechnol* **1:**299-310.

Gossuin, Y., Gillis, P., Muller, R. N. and Hocq, A. (2007). Relaxation by clustered ferritin: a model for ferritin-induced relaxation in vivo. *NMR Biomed* **20:**749-756.

Gossuin, Y., Muller, R. N. and Gillis, P. (2004). Relaxation induced by ferritin: a better understanding for an improved MRI iron quantification. *NMR Biomed* **17:**427-432.

Gottesfeld, Z. and Neeman, M. (1996). Ferritin effect on the transverse relaxation of water: NMR microscopy at 9.4 T. *Magn Reson Med* **35:**514-520.

Grace, J. E., Jr., Van Eden, M. E. and Aust, S. D. (2000). Production of recombinant human apoferritin heteromers. *Arch Biochem Biophys* **384:**116-122.

Gray, C. P., Franco, A. V., Arosio, P. and Hersey, P. (2001). Immunosuppressive effects of melanoma-derived heavy-chain ferritin are dependent on stimulation of IL-10 production. *Int J Cancer* **92:**843-850.

Greer LF 3rd, Szalay AA. (2002) Imaging of light emission from the expression of luciferases in living cells and organisms: a review. *Luminescence* **17(1)**:43-74.

Grundemann, D. and Schomig, E. (1996). Protection of DNA during preparative agarose gel electrophoresis against damage induced by ultraviolet light. *Biotechniques* **21:**898-903.

Guo, J. H., Juan, S. H. and Aust, S. D. (1998). Suppression of cell growth by heavy chain ferritin. *Biochem Biophys Res Commun* **242:**39-45.

Guzman, R., Uchida, N., Bliss, T. M., He, D., Christopherson, K. K., Stellwagen, D., Capela, A. *et al.* (2007). Long-term monitoring of transplanted human neural stem cells in developmental and pathological contexts with MRI. *Proc Natl Acad Sci U S A* **104:**10211-10216.

Haacke, E. M., Cheng, N. Y., House, M. J., Liu, Q., Neelavalli, J., Ogg, R. J., Khan, A. *et al.* (2005). Imaging iron stores in the brain using magnetic resonance imaging. *Magn Reson Imaging* **23:**1-25.

Hagell, P., Piccini, P., Bjorklund, A., Brundin, P., Rehncrona, S., Widner, H., Crabb, L. *et al.* (2002). Dyskinesias following neural transplantation in Parkinson's disease. *Nat Neurosci* **5:**627-628.

Halliwell, B. (2001). Role of free radicals in the neurodegenerative diseases: therapeutic implications for antioxidant treatment. *Drugs Aging* **18:**685-716.

Hamm, B., Staks, T., Taupitz, M., Maibauer, R., Speidel, A., Huppertz, A., Frenzel, T. *et al.* (1994). Contrast-enhanced MR imaging of liver and spleen: first experience in humans with a new superparamagnetic iron oxide. *J Magn Reson Imaging* **4:**659-668.

Handley, O. J., Naji, J. J., Dunnett, S. B. and Rosser, A. E. (2006). Pharmaceutical, cellular and genetic therapies for Huntington's disease. *Clin Sci (Lond)* **110:**73-88.

Harper, P. S. (1992). The epidemiology of Huntington's disease. *Hum Genet* **89:**365-376.

Harris, R. (1986). Nuclear Magnetic Resonance Spectroscopy-a Physicochemical View. London: Longman Scientific and Technical.

Harrison, P. M. and Arosio, P. (1996). The ferritins: molecular properties, iron storage function and cellular regulation. *Biochim Biophys Acta* **1275:**161-203.

Hartley, J. L., Temple, G. F. and Brasch, M. A. (2000). DNA cloning using in vitro site-specific recombination. *Genome Res* **10:**1788-1795.

Hauser, R. A., Furtado, S., Cimino, C. R., Delgado, H., Eichler, S., Schwartz, S., Scott, D. *et al.* (2002). Bilateral human fetal striatal transplantation in Huntington's disease. *Neurology* **58:**687-695.

Hawrylak, N., Ghosh, P., Broadus, J., Schlueter, C., Greenough, W. T. and Lauterbur, P. C. (1993). Nuclear magnetic resonance (NMR) imaging of iron oxide-labeled neural transplants. *Exp Neurol* **121:**181-192.

Hayashi, S. and McMahon, A. P. (2002). Efficient recombination in diverse tissues by a tamoxifen-inducible form of Cre: a tool for temporally regulated gene activation/inactivation in the mouse. *Dev Biol* **244:**305-318.

Heuer, A., Smith, G. A., Lelos, M. J., Lane, E. L. and Dunnett, S. B. (2012). Unilateral nigrostriatal 6-hydroxydopamine lesions in mice I: motor impairments identify extent of dopamine depletion at three different lesion sites. *Behav Brain Res* **228:**30-43.

Heyn, C., Bowen, C. V., Rutt, B. K. and Foster, P. J. (2005). Detection threshold of single SPIO-labeled cells with FIESTA. *Magn Reson Med* **53:**312-320.

Himes, N., Min, J. Y., Lee, R., Brown, C., Shea, J., Huang, X., Xiao, Y. F. *et al.* (2004). In vivo MRI of embryonic stem cells in a mouse model of myocardial infarction. *Magn Reson Med* **52:**1214-1219.

Hinds, K. A., Hill, J. M., Shapiro, E. M., Laukkanen, M. O., Silva, A. C., Combs, C. A., Varney, T. R. *et al.* (2003). Highly efficient endosomal labeling of progenitor and stem cells with large magnetic particles allows magnetic resonance imaging of single cells. *Blood* **102:**867-872.

Hoehn, M., Kustermann, E., Blunk, J., Wiedermann, D., Trapp, T., Wecker, S., Focking, M. *et al.* (2002). Monitoring of implanted stem cell migration in vivo: a highly resolved in vivo magnetic resonance imaging investigation of experimental stroke in rat. *Proc Natl Acad Sci U S A* **99:**16267-16272.

Hooper, M., Hardy, K., Handyside, A., Hunter, S. and Monk, M. (1987). HPRT-deficient (Lesch-Nyhan) mouse embryos derived from germline colonization by cultured cells. *Nature* **326:**292-295.

Horowitz, J. M., Nikolaidis, P., Chen, Z. M., Siegelman, E., Garg, A., Feng, C. and Miller, F. H. Iron deposition surrounding the hepatic veins of cirrhotic patients on MRI. *J Magn Reson Imaging* **33:**598-602.

Hsiao, J. K., Tai, M. F., Chu, H. H., Chen, S. T., Li, H., Lai, D. M., Hsieh, S. T. *et al.* (2007). Magnetic nanoparticle labeling of mesenchymal stem cells without transfection agent: cellular behavior and capability of detection with clinical 1.5 T magnetic resonance at the single cell level. *Magn Reson Med* **58:**717-724.

Huang, L. S., Sun, G., Cobessi, D., Wang, A. C., Shen, J. T., Tung, E. Y., Anderson, V. E. *et al.* (2006). 3-nitropropionic acid is a suicide inhibitor of mitochondrial respiration that, upon oxidation by complex II, forms a covalent adduct with a catalytic base arginine in the active site of the enzyme. *J Biol Chem* **281:**5965-5972.

Hume, S. P., Myers, R., Bloomfield, P. M., Opacka-Juffry, J., Cremer, J. E., Ahier, R. G., Luthra, S. K. *et al.* (1992). Quantitation of Carbon-11-labeled raclopride in rat striatum using positron emission tomography. *Synapse* **12:**47-54.

Huntington, G. (2003). On chorea. George Huntington, M.D. *J Neuropsychiatry Clin Neurosci* **15:**109-112.

Hurelbrink, C. B., Armstrong, R. J., Dunnett, S. B., Rosser, A. E. and Barker, R. A. (2002). Neural cells from primary human striatal xenografts migrate extensively in the adult rat CNS. *Eur J Neurosci* **15:**1255-1266.

Hurelbrink, C. B. and Barker, R. A. (2005). Migration of cells from primary transplants of allo- and xenografted foetal striatal tissue in the adult rat brain. *Eur J Neurosci* **21:**1503-1510.

Ill, A. M., Mitchell, T. R., Neely, E. B. and Connor, J. R. (2006). Metabolic analysis of mouse brains that have compromised iron storage. *Metab Brain Dis* **21:**77-87.

Ingrassia, R., Gerardi, G., Biasiotto, G. and Arosio, P. (2006). Mutations of ferritin H chain C-terminus produced by nucleotide insertions have altered stability and functional properties. *J Biochem* **139:**881-885.

Iordanova, B. and Ahrens, E. T. (2011). In vivo magnetic resonance imaging of ferritin-based reporter visualizes native neuroblast migration. *Neuroimage* **59:**1004-1012.

Iordanova, B., Robison, C. S. and Ahrens, E. T. (2010). Design and characterization of a chimeric ferritin with enhanced iron loading and transverse NMR relaxation rate. *J Biol Inorg Chem* **15:**957-965.

Iordanova, B., Robison, C. S., Goins, W. F. and Ahrens, E. T. (2010a). Single chain ferritin chimera as an improved MRI gene reporter. *Prilozi* **31:**151-155.

Ishibashi K, Ishii K, Oda K, Mizusawa H, Ishiwata K. (2010) Competition between 11C-raclopride and endogenous dopamine in Parkinson's disease. *Nucl Med Commun* **31(2)**:159-66

Jackson, J., Chapon, C., Jones, W., Hirani, E., Qassim, A. and Bhakoo, K. (2009). In vivo multimodal imaging of stem cell transplantation in a rodent model of Parkinson's disease. *J Neurosci Methods*.

Janic, B., Iskander, A. S., Rad, A. M., Soltanian-Zadeh, H. and Arbab, A. S. (2008). Effects of ferumoxides-protamine sulfate labeling on immunomodulatory characteristics of macrophage-like THP-1 cells. *PLoS One* **3:**e2499.

Jendelova, P., Herynek, V., DeCroos, J., Glogarova, K., Andersson, B., Hajek, M. and Sykova, E. (2003). Imaging the fate of implanted bone marrow stromal cells labeled with superparamagnetic nanoparticles. *Magn Reson Med* **50:**767-776.

Jendelova, P., Herynek, V., Urdzikova, L., Glogarova, K., Kroupova, J., Andersson, B., Bryja, V. *et al.* (2004). Magnetic resonance tracking of transplanted bone marrow and embryonic stem cells labeled by iron oxide nanoparticles in rat brain and spinal cord. *J Neurosci Res* **76:**232-243.

Johnson, W. K., Stoupis, C., Torres, G. M., Rosenberg, E. B. and Ros, P. R. (1996). Superparamagnetic iron oxide (SPIO) as an oral contrast agent in gastrointestinal (GI) magnetic resonance imaging (MRI): comparison with state-of-the-art computed tomography (CT). *Magn Reson Imaging* **14:**43-49.

Jones, C. K., Polders, D., Hua, J., Zhu, H., Hoogduin, H. J., Zhou, J., Luijten, P. *et al.* (2011). In vivo three-dimensional whole-brain pulsed steady-state chemical exchange saturation transfer at 7 T. *Magn Reson Med*.

Jones, C. K., Schlosser, M. J., van Zijl, P. C., Pomper, M. G., Golay, X. and Zhou, J. (2006). Amide proton transfer imaging of human brain tumors at 3T. *Magn Reson Med* **56:**585-592.

Kaneko, Y., Kitamoto, T., Tateishi, J. and Yamaguchi, K. (1989). Ferritin immunohistochemistry as a marker for microglia. *Acta Neuropathol* **79:**129-136.

Kaur, D., Rajagopalan, S. and Andersen, J. K. (2009). Chronic expression of H-ferritin in dopaminergic midbrain neurons results in an age-related expansion of the labile iron pool and subsequent neurodegeneration: implications for Parkinson's disease. *Brain Res* **1297:**17-22.

Kaur, D., Rajagopalan, S., Chinta, S., Kumar, J., Di Monte, D., Cherny, R. A. and Andersen, J. K. (2007). Chronic ferritin expression within murine dopaminergic midbrain neurons results in a progressive age-related neurodegeneration. *Brain Res* **1140:**188-194.

Kaur, D., Yantiri, F., Rajagopalan, S., Kumar, J., Mo, J. Q., Boonplueang, R., Viswanath, V. *et al.* (2003). Genetic or pharmacological iron chelation prevents MPTP-induced neurotoxicity in vivo: a novel therapy for Parkinson's disease. *Neuron* **37:**899-909.

Keene, C. D., Chang, R. C., Leverenz, J. B., Kopyov, O., Perlman, S., Hevner, R. F., Born, D. E. *et al.* (2009). A patient with Huntington's disease and long-surviving fetal neural transplants that developed mass lesions. *Acta Neuropathol* **117:**329-338.

Kelly, C. M., Precious, S. V., Penketh, R., Amso, N., Dunnett, S. B. and Rosser, A. E. (2007). Striatal graft projections are influenced by donor cell type and not the immunogenic background. *Brain* **130:**1317-1329.

Kelly, C. M., Precious, S. V., Scherf, C., Penketh, R., Amso, N. N., Battersby, A., Allen, N. D. *et al.* (2009a). Neonatal desensitization allows long-term survival of neural xenotransplants without immunosuppression. *Nat Methods* **6:**271-273.

Kelly, C. M., Precious, S. V., Torres, E. M., Harrison, A. W., Williams, D., Scherf, C., Weyrauch, U. M. *et al.* (2011). Medical terminations of pregnancy: a viable source of tissue for cell replacement therapy for neurodegenerative disorders. *Cell Transplant* **20:**503-513.

Kemp, J. M. and Powell, T. P. (1971). The structure of the caudate nucleus of the cat: light and electron microscopy. *Philos Trans R Soc Lond B Biol Sci* **262:**383-401.

Kim, J. S., Yoon, T. J., Yu, K. N., Kim, B. G., Park, S. J., Kim, H. W., Lee, K. H. *et al.* (2006). Toxicity and tissue distribution of magnetic nanoparticles in mice. *Toxicol Sci* **89:**338-347.

Klein, A., Metz, G. A., Papazoglou, A. and Nikkhah, G. (2007). Differential effects on forelimb grasping behavior induced by fetal dopaminergic grafts in hemiparkinsonian rats. *Neurobiol Dis* **27:**24-35.

Knobel, Y., Glei, M., Osswald, K. and Pool-Zobel, B. L. (2006). Ferric iron increases ROS formation, modulates cell growth and enhances genotoxic damage by 4-hydroxynonenal in human colon tumor cells. *Toxicol In Vitro* **20:**793-800.

Köhler, C., Hall, H., Ogren, S. O. and Gawell, L. (1985). Specific in vitro and in vivo binding of 3H-raclopride. A potent substituted benzamide drug with high affinity for dopamine D-2 receptors in the rat brain. *Biochem Pharmacol* **34:**2251-2259.

Koorts, A. M. and Viljoen, M. (2007a). Ferritin and ferritin isoforms I: Structure-function relationships, synthesis, degradation and secretion. *Arch Physiol Biochem* **113:**30-54.

Koorts, A. M. and Viljoen, M. (2007b). Ferritin and ferritin isoforms II: protection against uncontrolled cellular proliferation, oxidative damage and inflammatory processes. *Arch Physiol Biochem* **113:**55-64.

Kopyov, O. V., Jacques, S., Lieberman, A., Duma, C. M. and Eagle, K. S. (1998). Safety of intrastriatal neurotransplantation for Huntington's disease patients. *Exp Neurol* **149:**97-108.

Kordower, J. H., Freeman, T. B., Snow, B. J., Vingerhoets, F. J., Mufson, E. J., Sanberg, P. R., Hauser, R. A. *et al.* (1995). Neuropathological evidence of graft survival and striatal reinnervation after the transplantation of fetal mesencephalic tissue in a patient with Parkinson's disease. *N Engl J Med* **332:**1118-1124.

Koretsky, A. P., Brosnan, M. J., Chen, L. H., Chen, J. D. and Van Dyke, T. (1990). NMR detection of creatine kinase expressed in liver of transgenic mice: determination of free ADP levels. *Proc Natl Acad Sci U S A* **87:**3112-3116.

Kostura, L., Kraitchman, D. L., Mackay, A. M., Pittenger, M. F. and Bulte, J. W. (2004). Feridex labeling of mesenchymal stem cells inhibits chondrogenesis but not adipogenesis or osteogenesis. *NMR Biomed* **17:**513-517.

Kotamraju, S., Chitambar, C. R., Kalivendi, S. V., Joseph, J. and Kalyanaraman, B. (2002). Transferrin receptor-dependent iron uptake is responsible for doxorubicin-mediated apoptosis in endothelial cells: role of oxidant-induced iron signaling in apoptosis. *J Biol Chem* **277:**17179-17187.

Kozlova, M., Kentroti, S. and Vernadakis, A. (1993). Influence of culture substrata on the differentiation of advanced passage glial cells in cultures from aged mouse cerebral hemispheres. *Int J Dev Neurosci* **11:**513-519.

Kraitchman, D. L., Heldman, A. W., Atalar, E., Amado, L. C., Martin, B. J., Pittenger, M. F., Hare, J. M. *et al.* (2003). In vivo magnetic resonance imaging of mesenchymal stem cells in myocardial infarction. *Circulation* **107:**2290-2293.

Kreft, B. P., Tanimoto, A., Leffler, S., Finn, J. P., Oksendal, A. N. and Stark, D. D. (1994). Contrast-enhanced MR imaging of diffuse and focal splenic disease with use of magnetic starch microspheres. *J Magn Reson Imaging* **4:**373-379.

Krejci, J., Pachernik, J., Hampl, A. and Dvorak, P. (2008). In vitro labelling of mouse embryonic stem cells with SPIO nanoparticles. *Gen Physiol Biophys* **27:**164-173.

Lalancette-Hebert, M., Phaneuf, D., Soucy, G., Weng, Y. C. and Kriz, J. (2009). Live imaging of Toll-like receptor 2 response in cerebral ischaemia reveals a role of olfactory bulb microglia as modulators of inflammation. *Brain* **132:**940-954.

Lee, J., Kim, S. W., Kim, Y. H. and Ahn, J. Y. (2002). Active human ferritin H/L-hybrid and sequence effect on folding efficiency in Escherichia coli. *Biochem Biophys Res Commun* **298:**225-229.

Leibold, E. A. and Munro, H. N. (1988). Cytoplasmic protein binds in vitro to a highly conserved sequence in the 5' untranslated region of ferritin heavy- and light-subunit mRNAs. *Proc Natl Acad Sci U S A* **85:**2171-2175.

Lepore, A. C., Walczak, P., Rao, M. S., Fischer, I. and Bulte, J. W. (2006). MR imaging of lineage-restricted neural precursors following transplantation into the adult spinal cord. *Exp Neurol* **201:**49-59.

Levi, S., Corsi, B., Bosisio, M., Invernizzi, R., Volz, A., Sanford, D., Arosio, P. *et al.* (2001). A human mitochondrial ferritin encoded by an intronless gene. *J Biol Chem* **276:**24437-24440.

Levi, S., Corsi, B., Rovida, E., Cozzi, A., Santambrogio, P., Albertini, A. and Arosio, P. (1994a). Construction of a ferroxidase center in human ferritin L-chain. *J Biol Chem* **269:**30334-30339.

Levi, S., Santambrogio, P., Cozzi, A., Rovida, E., Corsi, B., Tamborini, E., Spada, S. *et al.* (1994b). The role of the L-chain in ferritin iron incorporation. Studies of homo and heteropolymers. *J Mol Biol* **238:**649-654.

Levi, S., Yewdall, S. J., Harrison, P. M., Santambrogio, P., Cozzi, A., Rovida, E., Albertini, A. *et al.* (1992). Evidence of H- and L-chains have co-operative roles in the iron-uptake mechanism of human ferritin. *Biochem J* **288 (Pt 2):**591-596.

Lewin, M., Carlesso, N., Tung, C. H., Tang, X. W., Cory, D., Scadden, D. T. and Weissleder, R. (2000). Tat peptide-derivatized magnetic nanoparticles allow in vivo tracking and recovery of progenitor cells. *Nat Biotechnol* **18:**410-414.

Li, A. X., Wojciechowski, F., Suchy, M., Jones, C. K., Hudson, R. H., Menon, R. S. and Bartha, R. (2008). A sensitive PARACEST contrast agent for temperature MRI: Eu3+-DOTAM-glycine (Gly)-phenylalanine (Phe). *Magn Reson Med* **59:**374-381.

Li, R., Luo, C., Mines, M., Zhang, J. and Fan, G. H. (2006). Chemokine CXCL12 induces binding of ferritin heavy chain to the chemokine receptor CXCR4, alters CXCR4 signaling, and induces phosphorylation and nuclear translocation of ferritin heavy chain. *J Biol Chem* **281:**37616-37627.

Li, Y., Chi, X. C., Li, X. X. and Xu, J. C. (2008b). Multipotency of human neural stem cells from fetal striatum. *Neuroreport* **19:**1679-1683.

Lin, H. and Schagat, T. (1997). Neuroblasts: a model for the asymmetric division of stem cells. *Trends Genet* **13:**33-39.

Lindblad, K. and Schalling, M. (1996). Clinical implications of unstable DNA repeat sequences. *Acta Paediatr* **85:**265-271.

Lindvall, O., Backlund, E. O., Farde, L., Sedvall, G., Freedman, R., Hoffer, B., Nobin, A. *et al.* (1987). Transplantation in Parkinson's disease: two cases of adrenal medullary grafts to the putamen. *Ann Neurol* **22:**457-468.

Lindvall, O., Brundin, P., Widner, H., Rehncrona, S., Gustavii, B., Frackowiak, R., Leenders, K. L. *et al.* (1990). Grafts of fetal dopamine neurons survive and improve motor function in Parkinson's disease. *Science* **247:**574-577.

Lindvall, O., Sawle, G., Widner, H., Rothwell, J. C., Bjorklund, A., Brooks, D., Brundin, P. *et al.* (1994). Evidence for long-term survival and function of dopaminergic grafts in progressive Parkinson's disease. *Ann Neurol* **35:**172-180.

Ling, W., Regatte, R. R., Navon, G. and Jerschow, A. (2008). Assessment of glycosaminoglycan concentration in vivo by chemical exchange-dependent saturation transfer (gagCEST). *Proc Natl Acad Sci U S A* **105:**2266-2270.

Liu, G., Gilad, A. A., Bulte, J. W., van Zijl, P. C. and McMahon, M. T. (2010). High-throughput screening of chemical exchange saturation transfer MR contrast agents. *Contrast Media Mol Imaging* **5:**162-170.

Liu, J., Cheng, E. C., Long Jr, R. C., Yang, S. H., Wang, L., Cheng, P. H., Yang, J. J. *et al.* (2009b). Noninvasive Monitoring of Embryonic Stem Cells in vivo with MRI Transgene Reporter. *Tissue Eng Part C Methods*.

Liu, J., Zhang, Z., Liu, Y., Guo, C., Gong, Y., Yang, S., Ma, M. *et al.* (2012) Generation, Characterization and Potential Therapeutic Applications of Cardiomyocytes from Various Stem Cells. *Stem Cells Dev*.

Liu, W., Dahnke, H., Jordan, E. K., Schaeffter, T. and Frank, J. A. (2008). In vivo MRI using positive-contrast techniques in detection of cells labeled with superparamagnetic iron oxide nanoparticles. *NMR Biomed* **21:**242-250.

Livet, J., Weissman, T. A., Kang, H., Draft, R. W., Lu, J., Bennis, R. A., Sanes, J. R. *et al.* (2007). Transgenic strategies for combinatorial expression of fluorescent proteins in the nervous system. *Nature* **450:**56-62.

Maeda, H., Wu, J., Sawa, T., Matsumura, Y. and Hori, K. (2000). Tumor vascular permeability and the EPR effect in macromolecular therapeutics: a review. *J Control Release* **65:**271-284.

Magnitsky, S., Walton, R. M., Wolfe, J. H. and Poptani, H. (2008). Magnetic resonance imaging detects differences in migration between primary and immortalized neural stem cells. *Acad Radiol* **15:**1269-1281.

Majumdar, S., Zoghbi, S. S. and Gore, J. C. (1989). The influence of pulse sequence on the relaxation effects of superparamagnetic iron oxide contrast agents. *Magn Reson Med* **10:**289-301.

Mangiarini, L., Sathasivam, K., Seller, M., Cozens, B., Harper, A., Hetherington, C., Lawton, M. *et al.* (1996). Exon 1 of the HD gene with an expanded CAG repeat is sufficient to cause a progressive neurological phenotype in transgenic mice. *Cell* **87:**493-506.

Martin, G. R. (1981). Isolation of a pluripotent cell line from early mouse embryos cultured in medium conditioned by teratocarcinoma stem cells. *Proc Natl Acad Sci U S A* **78:**7634-7638.

Marx, J. J. (2002). Iron and infection: competition between host and microbes for a precious element. *Best Pract Res Clin Haematol* **15:**411-426.

Matuszewski, L., Persigehl, T., Wall, A., Schwindt, W., Tombach, B., Fobker, M., Poremba, C. *et al.* (2005). Cell tagging with clinically approved iron oxides: feasibility and effect of lipofection, particle size, and surface coating on labeling efficiency. *Radiology* **235:**155-161.

McBain, S. C., Yiu, H. H. and Dobson, J. (2008). Magnetic nanoparticles for gene and drug delivery. *Int J Nanomedicine* **3:**169-180.

McConnell, H. M. and Thompson, D. D. (1959). Molecular transfer of nonequilibrium nuclear spin magnetization. *J. Chem. Phys.* 85–88.

McGill, J. R., Naylor, S. L., Sakaguchi, A. Y., Moore, C. M., Boyd, D., Barrett, K. J., Shows, T. B. *et al.* (1987). Human ferritin H and L sequences lie on ten different chromosomes. *Hum Genet* **76:**66-72.

McMahon, M. T., Gilad, A. A., DeLiso, M. A., Berman, S. M., Bulte, J. W. and van Zijl, P. C. (2008). New "multicolor" polypeptide diamagnetic chemical exchange saturation transfer (DIACEST) contrast agents for MRI. *Magn Reson Med* **60:**803-812.

Melancon, M., Lu, W. and Li, C. (2009). Gold-Based Magneto/Optical Nanostructures: Challenges for In Vivo Applications in Cancer Diagnostics and Therapy. *Mater Res Bull* **34:**415-421.

Miyazaki, E., Kato, J., Kobune, M., Okumura, K., Sasaki, K., Shintani, N., Arosio, P. *et al.* (2002). Denatured H-ferritin subunit is a major constituent of haemosiderin in the liver of patients with iron overload. *Gut* **50:**413-419.

Moghimi, S. M., Hunter, A. C. and Murray, J. C. (2001). Long-circulating and target-specific nanoparticles: theory to practice. *Pharmacol Rev* **53:**283-318.

Montet-Abou, K., Montet, X., Weissleder, R. and Josephson, L. (2005). Transfection agent induced nanoparticle cell loading. *Mol Imaging* **4:**165-171.

Mora, B., Narasimhan, P. T., Ross, B. D., Allman, J. and Barker, P. B. (1991). 31P saturation transfer and phosphocreatine imaging in the monkey brain. *Proc Natl Acad Sci U S A* **88:**8372-8376.

Moroz, C., Traub, L., Maymon, R. and Zahalka, M. A. (2002). PLIF, a novel human ferritin subunit from placenta with immunosuppressive activity. *J Biol Chem* **277:**12901-12905.

Munoz, A., Lopez, A., Caruncho, H. J., Guerra, M. J. and Labandeira-Garcia, J. L. (2001). Long-term cortical atrophy after excitotoxic striatal lesion: effects of intrastriatal fetal-striatum grafts and implications for Huntington disease. *J Neuropathol Exp Neurol* **60:**786-797.

Murray, B. M., Paller, M. S. and Ferris, T. F. (1985). Effect of cyclosporine administration on renal hemodynamics in conscious rats. *Kidney Int* **28:**767-774.

Neri, M., Maderna, C., Cavazzin, C., Deidda-Vigoriti, V., Politi, L. S., Scotti, G., Marzola, P. *et al.* (2008). Efficient in vitro labeling of human neural precursor cells with superparamagnetic iron oxide particles: relevance for in vivo cell tracking. *Stem Cells* **26:**505-516.

Neuberger, T., Schöpf, B. and Hofmann H, H. M., von Rechenberg B. (2005). Superparamagnetic nanoparticles for biomedical applications: Possibilities and limitations of a new drug delivery system. *J Magn Magn Mater* **1:**483–496.

Nikkhah, G., Olsson, M., Eberhard, J., Bentlage, C., Cunningham, M. G. and Bjorklund, A. (1994). A microtransplantation approach for cell suspension grafting in the rat Parkinson model: a detailed account of the methodology. *Neuroscience* **63:**57-72.

Norman, A. B., Thomas, S. R., Pratt, R. G., Lu, S. Y. and Norgren, R. B. (1992). Magnetic resonance imaging of neural transplants in rat brain using a superparamagnetic contrast agent. *Brain Res* **594:**279-283.

Nyabi, O., Naessens, M., Haigh, K., Gembarska, A., Goossens, S., Maetens, M., De Clercq, S. *et al.* (2009). Efficient mouse transgenesis using Gateway-compatible ROSA26 locus targeting vectors and F1 hybrid ES cells. *Nucleic Acids Res* **37:**e55.

O'Malley, C. D. and Sounders, J. B. d. C. M. (1952). Leonardo on the Human Body: The Anatomical, Physiological, and Embryological Drawings of Leonardo da Vinci. With Translations, Emendations and a Biographical Introduction. . *Henry Schuman, New York.*

Oberdorster, G., Oberdorster, E. and Oberdorster, J. (2005). Nanotoxicology: an emerging discipline evolving from studies of ultrafine particles. *Environ Health Perspect* **113:**823-839.

Ogris, M., Steinlein, P., Kursa, M., Mechtler, K., Kircheis, R. and Wagner, E. (1998). The size of DNA/transferrin-PEI complexes is an important factor for gene expression in cultured cells. *Gene Ther* **5:**1425-1433.

Okabe, M., Ikawa, M., Kominami, K., Nakanishi, T. and Nishimune, Y. (1997). 'Green mice' as a source of ubiquitous green cells. *FEBS Lett* **407:**313-319.

Olanow, C. W., Goetz, C. G., Kordower, J. H., Stoessl, A. J., Sossi, V., Brin, M. F., Shannon, K. M. *et al.* (2003). A double-blind controlled trial of bilateral fetal nigral transplantation in Parkinson's disease. *Ann Neurol* **54:**403-414.

Olson, L. and Seiger, A. (1975). Brain tissue transplanted to the anterior chanber of the eye: 2. Fluorescence histochemistry of immature catecholamine- and 5-hydroxytryptamine neurons innervating the rat vas deferens. *Cell Tissue Res* **158:**141-150.

Pankhurst, Q. A., Connolly, J., Jones, S. K. and Dobson, J. (2003). Applications of magnetic nanoparticles in biomedicine. *JOURNAL OF PHYSICS D: APPLIED PHYSICS* **36:**R167-R181.

Papadakis, E. D., Nicklin, S. A., Baker, A. H. and White, S. J. (2004). Promoters and control elements: designing expression cassettes for gene therapy. *Curr Gene Ther* **4:**89-113.

Pawelczyk, E., Arbab, A. S., Chaudhry, A., Balakumaran, A., Robey, P. G. and Frank, J. A. (2008). In vitro model of bromodeoxyuridine or iron oxide nanoparticle uptake by activated macrophages from labeled stem cells: implications for cellular therapy. *Stem Cells* **26:**1366-1375.

Paxinos G. and Franklin K. (1997) The Mouse Brain in Stereotaxic Coordinates Second Edition *Academic Press, Inc. San Diego, New York, Boston, London Sydney, Tokyo, Toronto*

Paxinos G. and Watson C. (1986) The Rat Brain in Stereotaxic Coordinates Second Edition *Academic Press, Inc. San Diego, New York, Boston, London Sydney, Tokyo, Toronto*

Perlow, M. J., Freed, W. J., Hoffer, B. J., Seiger, A., Olson, L. and Wyatt, R. J. (1979). Brain grafts reduce motor abnormalities produced by destruction of nigrostriatal dopamine system. *Science* **204:**643-647.

Pham, C. G., Bubici, C., Zazzeroni, F., Papa, S., Jones, J., Alvarez, K., Jayawardena, S. *et al.* (2004). Ferritin heavy chain upregulation by NF-kappaB inhibits TNFalpha-induced apoptosis by suppressing reactive oxygen species. *Cell* **119:**529-542.

Picard, V., Renaudie, F., Porcher, C., Hentze, M. W., Grandchamp, B. and Beaumont, C. (1996). Overexpression of the ferritin H subunit in cultured erythroid cells changes the intracellular iron distribution. *Blood* **87:**2057-2064.

Piccini, P., Lindvall, O., Bjorklund, A., Brundin, P., Hagell, P., Ceravolo, R., Oertel, W. *et al.* (2000). Delayed recovery of movement-related cortical function in Parkinson's disease after striatal dopaminergic grafts. *Ann Neurol* **48:**689-695.

Pisanic, T. R., 2nd, Blackwell, J. D., Shubayev, V. I., Finones, R. R. and Jin, S. (2007). Nanotoxicity of iron oxide nanoparticle internalization in growing neurons. *Biomaterials* **28:**2572-2581.

Potrykus, J., Jonna, V. R. and Dopson, M. (2010). Iron homeostasis and responses to iron limitation in extreme acidophiles from the Ferroplasma genus. *Proteomics* **11:**52-63.

Pratt, T., Sharp, L., Nichols, J., Price, D. J. and Mason, J. O. (2000). Embryonic stem cells and transgenic mice ubiquitously expressing a tau-tagged green fluorescent protein. *Dev Biol* **228:**19-28.

Prokhorova, T. A., Harkness, L. M., Frandsen, U., Ditzel, N., Schroder, H. D., Burns, J. S. and Kassem, M. (2009). Teratoma formation by human embryonic stem cells is site dependent and enhanced by the presence of Matrigel. *Stem Cells Dev* **18:**47-54.

Ramaswamy, S., Schornack, P. A., Smelko, A. G., Boronyak, S. M., Ivanova, J., Mayer, J. E., Jr. and Sacks, M. S. (2012). Superparamagnetic iron oxide (SPIO) labeling efficiency and subsequent MRI tracking of native cell populations pertinent to pulmonary heart valve tissue engineering studies. *NMR Biomed* **25:**410-417.

Ramírez-Solis, R., Rivera-Pérez, J., Wallace, J. D., Wims, M., Zheng, H. and Bradley, A. (1992). Genomic DNA microextraction: a method to screen numerous samples. *Anal Biochem.* **201:**331-335.

Remy, P., Samson, Y., Hantraye, P., Fontaine, A., Defer, G., Mangin, J. F., Fenelon, G. *et al.* (1995). Clinical correlates of [18F]fluorodopa uptake in five grafted parkinsonian patients. *Ann Neurol* **38:**580-588.

Reubinoff, B. E., Pera, M. F., Fong, C. Y., Trounson, A. and Bongso, A. (2000). Embryonic stem cell lines from human blastocysts: somatic differentiation in vitro. *Nat Biotechnol* **18:**399-404.

Reuter, I., Tai, Y. F., Pavese, N., Chaudhuri, K. R., Mason, S., Polkey, C. E., Clough, C. *et al.* (2008). Long-term clinical and positron emission tomography outcome of fetal striatal transplantation in Huntington's disease. *J Neurol Neurosurg Psychiatry* **79:**948-951.

Rice, B. W., Cable, M. D. and Nelson, M. B. (2001). In vivo imaging of light-emitting probes. *J Biomed Opt* **6:**432-440.

Ross, C. A. and Margolis, R. L. (2001). Huntington's Disease. . *Clinical Neuroscience Research* **1:**142-152.

Rosser, A. E., Kelly, C. and Dunnett, S. B. (2011a). Cell transplantation for Huntington's disease: Practical and clinical considerations. *Future Neurology* **6:**45-62.

Rosser, A. E., Kelly, C. and Dunnett, S. B. (2011b). Cell transplantation for Huntington's disease: practical and clinical considerations. *Future Neurology* **6:**45–62.

Rossi, F. and Cattaneo, E. (2002). Opinion: neural stem cell therapy for neurological diseases: dreams and reality. *Nat Rev Neurosci* **3:**401-409.

Rucker, P., Torti, F. M. and Torti, S. V. (1996). Role of H and L subunits in mouse ferritin. *J Biol Chem* **271:**33352-33357.

Ruehm, S. G., Corot, C., Vogt, P., Kolb, S. and Debatin, J. F. (2001). Magnetic resonance imaging of atherosclerotic plaque with ultrasmall superparamagnetic particles of iron oxide in hyperlipidemic rabbits. *Circulation* **103:**415-422.

Sadan, O., Shemesh, N., Barzilay, R., Bahat-Stromza, M., Melamed, E., Cohen, Y. and Offen, D. (2008). Migration of neurotrophic factors-secreting mesenchymal stem cells toward a quinolinic acid lesion as viewed by magnetic resonance imaging. *Stem Cells* **26:**2542-2551.

Sambrook, J., Fritsch, E. F. and Maniatis, T. (1989). Molecular Cloning. A Laboratory Manual. Second Edition. *Cold Spring Harbor Laboratory Press* Southern Blots p9.31-39.57, Alkaline Lysis Miniprep p31.25-31.28, B.22, STETL p31.29, 31.34, Competent cells 31.82-31.84, Western Blots 18.60-18.75.

Santambrogio, P., Levi, S., Arosio, P., Palagi, L., Vecchio, G., Lawson, D. M., Yewdall, S. J. *et al.* (1992). Evidence that a salt bridge in the light chain contributes to the physical stability difference between heavy and light human ferritins. *J Biol Chem* **267:**14077-14083.

Schoepf, U., Marecos, E. M., Melder, R. J., Jain, R. K. and Weissleder, R. (1998). Intracellular magnetic labeling of lymphocytes for in vivo trafficking studies. *Biotechniques* **24:**642-646, 648-651.

Schuldiner, M., Itskovitz-Eldor, J. and Benvenisty, N. (2003). Selective ablation of human embryonic stem cells expressing a "suicide" gene. *Stem Cells* **21:**257-265.

Selkoe, D. J., Salazar, F. J., Abraham, C. and Kosik, K. S. (1982). Huntington's disease: changes in striatal proteins reflect astrocytic gliosis. *Brain Res* **245:**117-125.

Sengupta, R., Burbassi, S., Shimizu, S., Cappello, S., Vallee, R. B., Rubin, J. B. and Meucci, O. (2009). Morphine increases brain levels of ferritin heavy chain leading to inhibition of CXCR4-mediated survival signaling in neurons. *J Neurosci* **29:**2534-2544.

Shan, L. (2004). Bimodal lentiviral vector encoding myc-tagged human ferritin heavy chain and green fluorescent protein (GFP).

Shaner, N. C., Campbell, R. E., Steinbach, P. A., Giepmans, B. N., Palmer, A. E. and Tsien, R. Y. (2004). Improved monomeric red, orange and yellow fluorescent proteins derived from Discosoma sp. red fluorescent protein. *Nat Biotechnol* **22:**1567-1572.

Shaner, N. C., Patterson, G. H. and Davidson, M. W. (2007). Advances in fluorescent protein technology. *J Cell Sci* **120:**4247-4260.

Shapiro, E. M., Sharer, K., Skrtic, S. and Koretsky, A. P. (2006). In vivo detection of single cells by MRI. *Magn Reson Med* **55:**242-249.

Shapiro, E. M., Skrtic, S., Sharer, K., Hill, J. M., Dunbar, C. E. and Koretsky, A. P. (2004). MRI detection of single particles for cellular imaging. *Proc Natl Acad Sci U S A* **101:**10901-10906.

Shen, T., Weissleder, R., Papisov, M., Bogdanov, A., Jr. and Brady, T. J. (1993). Monocrystalline iron oxide nanocompounds (MION): physicochemical properties. *Magn Reson Med* **29:**599-604.

Sheth, V. R., Li, Y., Chen, L. Q., Howison, C. M., Flask, C. A. and Pagel, M. D. (2011). Measuring in vivo tumor pHe with CEST-FISP MRI. *Magn Reson Med*.

Shimomura, O. (2009). Discovery of green fluorescent protein (GFP) (Nobel Lecture). *Angew Chem Int Ed Engl* **48:**5590-5602.

Shterman, N., Kupfer, B. and Moroz, C. (1989). Expression of messenger RNA species coding for a Mr 43,000 peptide associated with ferritin in human leukemia-K562 cells and its down regulation during differentiation. *Cancer Res* **49:**5033-5036.

Silva, J. and Smith, A. (2008). Capturing pluripotency. *Cell* **132:**532-536.

Smith-Arica, J. R., Morelli, A. E., Larregina, A. T., Smith, J., Lowenstein, P. R. and Castro, M. G. (2000). Cell-type-specific and regulatable transgenesis in the adult brain: adenovirus-encoded combined transcriptional targeting and inducible transgene expression. *Mol Ther* **2:**579-587.

Smith, B. R., Heverhagen, J., Knopp, M., Schmalbrock, P., Shapiro, J., Shiomi, M., Moldovan, N. I. *et al.* (2007). Localization to atherosclerotic plaque and biodistribution of biochemically derivatized superparamagnetic iron oxide nanoparticles (SPIONs) contrast particles for magnetic resonance imaging (MRI). *Biomed Microdevices* **9:**719-727.

Soenen, S. J., Himmelreich, U., Nuytten, N. and De Cuyper, M. (2010). Cytotoxic effects of iron oxide nanoparticles and implications for safety in cell labelling. *Biomaterials* **32:**195-205.

Soenen, S. J., Nuytten, N., De Meyer, S. F., De Smedt, S. C. and De Cuyper, M. (2010a). High intracellular iron oxide nanoparticle concentrations affect cellular cytoskeleton and focal adhesion kinase-mediated signaling. *Small* **6:**832-842.

Song, X., Gilad, A. A., Joel, S., Liu, G., Bar-Shir, A., Liang, Y., Gorelik, M. *et al.* (2012). CEST phase mapping using a length and offset varied saturation (LOVARS) scheme. *Magn Reson Med*.

Sorgi, F. L., Bhattacharya, S. and Huang, L. (1997). Protamine sulfate enhances lipid-mediated gene transfer. *Gene Ther* **4:**961-968.

Spinney, L. (2010). Uncovering the true prevalence of Huntington's disease. *Lancet Neurol* **9:**760-761.

Srinivas, S., Watanabe, T., Lin, C., William, C. M., Tanabe, Y., Jessell, T. M. and Constantini, F. (2001). Cre reporter strains produced by targeted insertion of EYFP and ECFP into the ROSA26 locus. *BMC Dev Biol* **1**.

Stroh, A., Faber, C., Neuberger, T., Lorenz, P., Sieland, K., Jakob, P. M., Webb, A. *et al.* (2005). In vivo detection limits of magnetically labeled embryonic stem cells in the rat brain using high-field (17.6 T) magnetic resonance imaging. *Neuroimage* **24:**635-645.

Sun, J. H., Zhang, Y. L., Qian, S. P., Yu, X. B., Xie, H. Y., Zhou, L. and Zheng, S. S. (2012). Assessment of biological characteristics of mesenchymal stem cells labeled with superparamagnetic iron oxide particles in vitro. *Mol Med Report* **5:**317-320.

Sun, P. Z., Farrar, C. T. and Sorensen, A. G. (2007). Correction for artefacts induced by B(0) and B(1) field inhomogeneities in pH-sensitive chemical exchange saturation transfer (CEST) imaging. *Magn Reson Med* **58:**1207-1215.

Sun, P. Z. and Sorensen, A. G. (2008). Imaging pH using the chemical exchange saturation transfer (CEST) MRI: Correction of concomitant RF irradiation effects to quantify CEST MRI for chemical exchange rate and pH. *Magn Reson Med* **60:**390-397.

Sun, P. Z., Zhou, J., Sun, W., Huang, J. and van Zijl, P. C. (2005). Suppression of lipid artefacts in amide proton transfer imaging. *Magn Reson Med* **54:**222-225.

Swinkels, D. W., Janssen, M. C., Bergmans, J. and Marx, J. J. (2006). Hereditary hemochromatosis: genetic complexity and new diagnostic approaches. *Clin Chem* **52:**950-968.

Symons and Gutteridge. (1998). Free radicals and iron: Chemistry, biology, and medicine. *Oxford University Press (Oxford and New York)*.

Szende, B., Szokan, G., Tyiha, E., Pal, K., Gaborjanyi, R., Almas, M. and Khlafulla, A. R. (2002). Antitumor effect of lysine-isopeptides. *Cancer Cell Int* **2:**4.

Tanoura, T., Bernas, M., Darkazanli, A., Elam, E., Unger, E., Witte, M. H. and Green, A. (1992). MR lymphography with iron oxide compound AMI-227: studies in ferrets with filariasis. *AJR Am J Roentgenol* **159:**875-881.

Terrovitis, J., Stuber, M., Youssef, A., Preece, S., Leppo, M., Kizana, E., Schar, M. *et al.* (2008). Magnetic resonance imaging overestimates ferumoxide-labeled stem cell survival after transplantation in the heart. *Circulation* **117:**1555-1562.

Tesar, P. J., Chenoweth, J. G., Brook, F. A., Davies, T. J., Evans, E. P., Mack, D. L., Gardner, R. L. *et al.* (2007). New cell lines from mouse epiblast share defining features with human embryonic stem cells. *Nature* **448:**196-199.

Thompson, K., Menzies, S., Muckenthaler, M., Torti, F. M., Wood, T., Torti, S. V., Hentze, M. W. *et al.* (2003). Mouse brains deficient in H-ferritin have normal iron concentration but a protein profile of iron deficiency and increased evidence of oxidative stress. *J Neurosci Res* **71:**46-63.

Thomson, J. A., Itskovitz-Eldor, J., Shapiro, S. S., Waknitz, M. A., Swiergiel, J. J., Marshall, V. S. and Jones, J. M. (1998). Embryonic stem cell lines derived from human blastocysts. *Science* **282:**1145-1147.

Torti, S. V., Kwak, E. L., Miller, S. C., Miller, L. L., Ringold, G. M., Myambo, K. B., Young, A. P. *et al.* (1988). The molecular cloning and characterization of murine ferritin heavy chain, a tumor necrosis factor-inducible gene. *J Biol Chem* **263:**12638-12644.

Trichas, G., Begbie, J. and Srinivas, S. (2008). Use of the viral 2A peptide for bicistronic expression in transgenic mice. *BMC Biol* **6:**40.

Troy, T., Jekic-McMullen, D., Sambucetti, L. and Rice, B. (2004). Quantitative comparison of the sensitivity of detection of fluorescent and bioluminescent reporters in animal models. *Mol Imaging* **3:**9-23.

Urbanczyk-Pearson, L. M. and Meade, T. J. (2008). Preparation of magnetic resonance contrast agents activated by beta-galactosidase. *Nat Protoc* **3:**341-350.

Vallier, L., Touboul, T., Chng, Z., Brimpari, M., Hannan, N., Millan, E., Smithers, L. E. *et al.* (2009). Early cell fate decisions of human embryonic stem cells and mouse epiblast stem cells are controlled by the same signalling pathways. *PLoS One* **4:**e6082.

van Buul, G. M., Farrell, E., Kops, N., van Tiel, S. T., Bos, P. K., Weinans, H., Krestin, G. P. *et al.* (2009). Ferumoxides-protamine sulfate is more effective than ferucarbotran for cell labeling: implications for clinically applicable cell tracking using MRI. *Contrast Media Mol Imaging* **4:**230-236.

van Zijl, P. C., Jones, C. K., Ren, J., Malloy, C. R. and Sherry, A. D. (2007). MRI detection of glycogen in vivo by using chemical exchange saturation transfer imaging (glycoCEST). *Proc Natl Acad Sci U S A* **104:**4359-4364.

Vande Velde, G., Raman Rangarajan, J., Vreys, R., Guglielmetti, C., Dresselaers, T., Verhoye, M., Van der Linden, A. *et al.* (2012). Quantitative evaluation of MRI-based tracking of ferritin-labeled endogenous neural stem cell progeny in rodent brain. *Neuroimage* **62:**367-380.

Vande Velde, G., Rangarajan, J. R., Toelen, J., Dresselaers, T., Ibrahimi, A., Krylychkina, O., Vreys, R. *et al.* (2011). Evaluation of the specificity and sensitivity of ferritin as an MRI reporter gene in the mouse brain using lentiviral and adeno-associated viral vectors. *Gene Ther* **18:**594-605.

Vargas, M., Kashefi, K., Blunt-Harris, E. L. and Lovley, D. R. (1998). Microbiological evidence for Fe(III) reduction on early Earth. *Nature* **395:**65-67.

Verdijk, P., Scheenen, T. W., Lesterhuis, W. J., Gambarota, G., Veltien, A. A., Walczak, P., Scharenborg, N. M. *et al.* (2007). Sensitivity of magnetic resonance imaging of dendritic cells for in vivo tracking of cellular cancer vaccines. *Int J Cancer* **120:**978-984.

Verma, A. and Stellacci, F. (2010). Effect of surface properties on nanoparticle-cell interactions. *Small* **6:**12-21.

Vinogradov, E., Soesbe, T. C., Balschi, J. A., Dean Sherry, A. and Lenkinski, R. E. (2011). pCEST: Positive contrast using Chemical Exchange Saturation Transfer. *J Magn Reson*.

Vreys, R., Soenen, S. J., De Cuyper, M. and Van der Linden, A. (2010). Background migration of USPIO/MLs is a major drawback for in situ labeling of endogenous neural progenitor cells. *Contrast Media Mol Imaging* **6:**1-6.

Vymazal, J., Brooks, R. A., Baumgarner, C., Tran, V., Katz, D., Bulte, J. W., Bauminger, R. *et al.* (1996). The relation between brain iron and NMR relaxation times: an in vitro study. *Magn Reson Med* **35:**56-61.

Vymazal, J., Brooks, R. A., Zak, O., McRill, C., Shen, C. and Di Chiro, G. (1992). T1 and T2 of ferritin at different field strengths: effect on MRI. *Magn Reson Med* **27:**368-374.

Walczak, P., Kedziorek, D. A., Gilad, A. A., Barnett, B. P. and Bulte, J. W. (2007). Applicability and limitations of MR tracking of neural stem cells with asymmetric cell division and rapid turnover: the case of the shiverer dysmyelinated mouse brain. *Magn Reson Med* **58:**261-269.

Walczak, P., Kedziorek, D. A., Gilad, A. A., Lin, S. and Bulte, J. W. (2005). Instant MR labeling of stem cells using magnetoelectroporation. *Magn Reson Med* **54:**769-774.

Ward, K. M., Aletras, A. H. and Balaban, R. S. (2000). A new class of contrast agents for MRI based on proton chemical exchange dependent saturation transfer (CEST). *J Magn Reson* **143:**79-87.

Weissleder, R., Cheng, H. C., Bogdanova, A. and Bogdanov, A., Jr. (1997). Magnetically labeled cells can be detected by MR imaging. *J Magn Reson Imaging* **7:**258-263.

Weissleder, R., Elizondo, G., Wittenberg, J., Rabito, C. A., Bengele, H. H. and Josephson, L. (1990). Ultrasmall superparamagnetic iron oxide: characterization of a new class of contrast agents for MR imaging. *Radiology* **175:**489-493.

Weissleder, R., Stark, D. D., Engelstad, B. L., Bacon, B. R., Compton, C. C., White, D. L., Jacobs, P. *et al.* (1989). Superparamagnetic iron oxide: pharmacokinetics and toxicity. *AJR Am J Roentgenol* **152:**167-173.

Wenning, G. K., Odin, P., Morrish, P., Rehncrona, S., Widner, H., Brundin, P., Rothwell, J. C. *et al.* (1997). Short- and long-term survival and function of unilateral intrastriatal dopaminergic grafts in Parkinson's disease. *Ann Neurol* **42:**95-107.

Wernig, M., Tucker, K. L., Gornik, V., Schneiders, A., Buschwald, R., Wiestler, O. D., Barde, Y. A. *et al.* (2002). Tau EGFP embryonic stem cells: an efficient tool for neuronal lineage selection and transplantation. *J Neurosci Res* **69:**918-924.

Wilson, C., Bellen, H. J. and Gehring, W. J. (1990). Position effects on eukaryotic gene expression. *Annu Rev Cell Biol* **6:**679-714.

Wood, H. B. and Episkopou, V. (1999). Comparative expression of the mouse Sox1, Sox2 and Sox3 genes from pre-gastrulation to early somite stages. *Mech Dev* **86:**197-201.

Yang, J., Liu, J., Niu, G., Chan, K. C., Wang, R., Liu, Y. and Wu, E. X. (2009). In vivo MRI of endogenous stem/progenitor cell migration from subventricular zone in normal and injured developing brains. *Neuroimage* **48:**319-328.

Yang, S. H., Cheng, P. H., Banta, H., Piotrowska-Nitsche, K., Yang, J. J., Cheng, E. C., Snyder, B. *et al.* (2008). Towards a transgenic model of Huntington's disease in a non-human primate. *Nature* **453:**921-924.

Yeh, T. C., Zhang, W., Ildstad, S. T. and Ho, C. (1995). In vivo dynamic MRI tracking of rat T-cells labeled with superparamagnetic iron-oxide particles. *Magn Reson Med* **33:**200-208.

Ying, Q. L., Stavridis, M., Griffiths, D., Li, M. and Smith, A. (2003). Conversion of embryonic stem cells into neuroectodermal precursors in adherent monoculture. *Nat Biotechnol* **21:**183-186.

Zamani, F., Razmjou, S., Akhlaghpoor, S., Eslami, S. M., Azarkeivan, A. and Amiri, A. T2* magnetic resonance imaging of the liver in thalassemic patients in Iran. *World J Gastroenterol* **17:**522-525.

Zambrowicz, B. P., Imamoto, A., Fiering, S., Herzenberg, L. A., Kerr, W. G. and Soriano, P. (1997). Disruption of overlapping transcripts in the ROSA beta geo 26 gene trap strain leads to widespread expression of beta-galactosidase in mouse embryos and hematopoietic cells. *Proc Natl Acad Sci U S A* **94:**3789-3794.

Zecca, L., Youdim, M. B., Riederer, P., Connor, J. R. and Crichton, R. R. (2004). Iron, brain ageing and neurodegenerative disorders. *Nat Rev Neurosci* **5:**863-873.

Zhang, R. L., Zhang, L., Zhang, Z. G., Morris, D., Jiang, Q., Wang, L., Zhang, L. J. *et al.* (2003a). Migration and differentiation of adult rat subventricular zone progenitor cells transplanted into the adult rat striatum. *Neuroscience* **116:**373-382.

Zhang, S., Malloy, C. R. and Sherry, A. D. (2005). MRI thermometry based on PARACEST agents. *J Am Chem Soc* **127:**17572-17573.

Zhang, S., Merritt, M., Woessner, D. E., Lenkinski, R. E. and Sherry, A. D. (2003b). PARACEST agents: modulating MRI contrast via water proton exchange. *Acc Chem Res* **36:**783-790.

Zhang, W., Zhou, D., Yang, W., Yin, G. and Ou, J. (2007). A novel europium doped apatite/wollastonite porous magnetic bioactive glass ceramic. *Sheng Wu Yi Xue Gong Cheng Xue Za Zhi* **24:**785-789.

Zhang, Z., Jiang, Q., Jiang, F., Ding, G., Zhang, R., Wang, L., Zhang, L. *et al.* (2004). In vivo magnetic resonance imaging tracks adult neural progenitor cell targeting of brain tumor. *Neuroimage* **23:**281-287.

Zhao, S., Maxwell, S., Jimenez-Beristain, A., Vives, J., Kuehner, E., Zhao, J., O'Brien, C. *et al.* (2004). Generation of embryonic stem cells and transgenic mice expressing green fluorescence protein in midbrain dopaminergic neurons. *Eur J Neurosci* **19:**1133-1140.

Zhou, J., Lal, B., Wilson, D. A., Laterra, J. and van Zijl, P. C. (2003). Amide proton transfer (APT) contrast for imaging of brain tumors. *Magn Reson Med* **50:**1120-1126.

Zhu, H., Jones, C. K., van Zijl, P. C., Barker, P. B. and Zhou, J. (2011). Fast 3D chemical exchange saturation transfer (CEST) imaging of the human brain. *Magn Reson Med* **64:**638-644.

Zhu, W., Li, X., Tang, Z., Zhu, S., Qi, J., Wei, L. and Lei, H. (2007). Superparamagnetic iron oxide labeling of neural stem cells and 4.7T MRI tracking in vivo and in vitro. *J Huazhong Univ Sci Technolog Med Sci* **27:**107-110.

Ziv, K., Meir, G., Harmelin, A., Shimoni, E., Klein, E. and Neeman, M. (2010). Ferritin as a reporter gene for MRI: chronic liver over expression of h-ferritin during dietary iron supplementation and aging. *NMR Biomed*.